A TIME DOMAIN BEM INVERSE METHOD FOR IDENTIFICATION OF LAUNCHERS ACOUSTIC SOURCES

S.Alestra[1], I.Terrasse[1], B.Troclet[2]

[1] Simulation Systems and Information Technology Department, EADS CRC

(European Aeronautic Defence and Space Company Corporate Research Center)

92150 Suresnes, France, stephane.alestra@eads.net

[2] Missile Structural Analysis Department, EADS Space Transportation , 78133 Les Mureaux, France

Keywords: BEM, Time Domain, Inverse Source Method, Acoustics, Overpressure, Lift-Off,Dynamic responses, Adjoint, Gradient, Optimisation

Abstract.

At lift-off, launch vehicles are subjected to a very severe overpressure, which can induce loads acting on payloads in the low frequency domain. The overpressure starts at ignition of solid rocket motors. For a numerical prediction of the overpressure environment, EADS has developed an inverse method via a Time Domain Boundary Integral Equations approach using an optimal control method, with direct and adjoint equations and Quasi Newton optimizer. The corresponding discrete schemes are highly accurate and unconditionally stable. As an industrial application, the identification of overpressure sources is shown, on the lift-off acoustic environment of ARIANE V

Introduction

During the lift-off phase, the launch vehicles, such as the ARIANE 5 launcher, are subjected to severe loads: the overpressure loads, which appear at ignition of solid rocket motors. The overpressure loads are among the most severe loads that a launcher can encounter during flight. The initial cause of the overpressure is the rocket-exhausts and their interactions with the launch pad. The overpressure is composed of the Ignition OverPressure (IOP), which originates from the launch table, and the Duct OverPressure (DOP), which originates from the launch ducts. Figure 1 illustrates this point with a picture of ARIANE 5 launch pad with the ducts.The overpressure is a deterministic load having discrete spikes at certain particular frequencies, with significant levels for frequencies lower than 40 Hz [1][2].This low frequency excitation excites the launch vehicle and induces Quasi Static Loads (QSL) at the payload/launcher interface, which the payload has to endure. Consequently, it is important to predict these loads before launches.

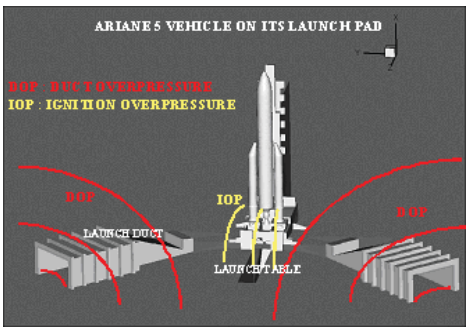

Fig 1 : Ignition and Duct OverPressure definition

To achieve this goal, an inverse method using an optimal control method (direct and adjoint equations), with a Time Domain Boundary Integral Equations approach, has been progressing for several years at EADS Common Research Center CRC, in collaboration with EADS Space Transportation [3] The corresponding discrete schemes are high accurate quality and unconditionally stable.
Having localized the overpressure sources from ARIANE 5 in-flight measurements, it will be easy to rebuild the unsteady pressure field and to estimate the pressure levels at any point of the vehicle for other flights. By integrating the unsteady pressures over all surfaces of the launchers, the loads created by the overpressure can be estimated. Consequently, the response of the launcher to this load case during the lift-off phase can be analyzed in the temporal domain by using any FEM software

Inverse Source Problem with BEM (Boundary Element Method) in Time domain

We wish to identify time domain acoustic source, emitted at point source x_0 parameterized by a real function p for each sampling time, which will be the control parameter variable used for the optimal control inverse method.
($p = \left(p_1; \cdots, p_p, \cdots, p_N \right)$ stands for parameter, N is the number of Time sampling for solving direct problem).
We associate the discrete emission function and the corresponding incident field $O_{inc}(p)$ to this parameter.

$$f_p(t) = \begin{pmatrix} p_1 = f(\Delta t) \\ \vdots \\ p_N = f(N\Delta t) \end{pmatrix} \qquad O_{inc}(p)(x,t) = \frac{f_p\left(t - |x - x_0|/c\right)}{4\pi |x - x_0|}$$

We consider the scattering problem of transient acoustic waves in a fluid medium by a submerged rigid object.
Let Ω^i be a three-dimensional object with a regular (without tip) bounded surface $\Gamma = \partial\Omega^i$.
Let $\Omega^e = R^3 \backslash \Omega^i$ denote the exterior domain occupied by the fluid medium.. We denote by O^e_{diff} the scattered acoustic pressure created in the fluid medium by an incident field $O_{inc}(p)$ (the wave propagating without the obstacle), which is the contribution of a time domain point source.
Therefore, we have the following initial boundary value problem:

$$\begin{cases} \dfrac{1}{c^2}\dfrac{\partial O^e_{diff}(x,t)}{\partial t^2} - \Delta O^e_{diff}(x,t) = 0 & \text{in } \Omega^e \times R^+, \\ O^e_{diff}(x,0) = \dfrac{\partial O^e_{diff}}{\partial t}(x,0) = 0 & \text{in } \Omega^e, \\ \dfrac{\partial O^e_{diff}}{\partial n} = -\dfrac{\partial O_{inc}}{\partial n}(p)(x,t) & \text{on } \Gamma \times \mathrm{R}^+. \end{cases}$$

where n denotes the unit normal vector to Γ, oriented from domain Ω^I to Ω^{e}. c is the speed of sound in the medium. We associate to the *exterior* problem an appropriate *interior* problem with O^i_{diff} in Ω^I . It is well-known that the scattered field O^e_{diff} has the following representation formula, using the Near Field Scattered operator Q :

$$O^e_{diff}(x,t) = QU = -\frac{1}{4\pi}\int_\Gamma n_y . \nabla_x \frac{U\left(y, t - |x-y|/c\right)}{|x-y|} dy \qquad \forall x \in \Omega^i \cup \Omega^e$$

where: $U = O^{i}_{diff} - O^{e}_{diff}$ is the jump O^{e}_{diff} crossing Γ, and τ= t-|x-y| is the *retarded time*. Using formula to compute the traces of O^{e}_{diff} ΓxR^{+}, as a function of *U*, and introducing the boundary conditions, one obtains the *Boundary Integral Equation* for the unknown function *U* :

$$RU(x,t)) = S(p)(x,t) \quad \forall (x,t) \in \Gamma$$

with the surface operator *R*, a Double layer Integral Operator coming from the variationnal formulation with function *U* in$H^2(R+,H^{1/2}(\Gamma))$, such that, for all Ψ in the same space:

$$RU(x,t) = \int_{\mathbb{R}} \int_{\Gamma\times\Gamma} \frac{\vec{n}(x)\vec{n}(y)}{4\pi|x-y|} \frac{\partial^2 U}{\partial t^2}\left(y, t-\frac{|x-y|}{c}\right) \frac{\partial \Psi}{\partial t}(x,t)\,dx\,dy\,dt$$
$$+c^2 \int_{\mathbb{R}} \int_{\Gamma\times\Gamma} \frac{curl U}{4\pi|x-y|}\left(y, t-\frac{|x-y|}{c}\right) curl \frac{\partial \Psi}{\partial t}(x,t)\,dx\,dy\,dt$$

$$S(p)(x,t) = \int_{\mathbb{R}} \int_{\Gamma} \left(\frac{\partial O_{inc}}{\partial n}(p)(x,t)\right) \frac{\partial \Psi}{\partial t}(x,t)\,dx\,dt$$

The equation is solved in space by a P1 surface finite element method. The boundary Γ of the object is meshed with triangular elements.

Finally, the direct problem consists in two main steps:
1) Computation of the pressure jump U by the Integral Equation operator R, and the excitation S
2) The radiating post-treatment equation to compute the acoustic pressure O by the scattered operator Q added with the Oinc incident field contribution :

$$1) \quad RU = S(p)$$
$$2) \quad O = QU + O_{inc}(p)$$

The quadratic error or cost function j(p), depending on the source parameters p, is defined by

$$J(O(p)) = j(p) = \min_{q \in X} j(q) = \frac{1}{2}\left\| O(q) - O_{mes} \right\|^2$$

Then after some derivations, we obtain

- The Adjoint Equations

$$\begin{cases} O^* = -\dfrac{dJ(O)}{dO} = -(O(p) - O_{mes}) \\ RU^* = Q^T O^* \end{cases}$$

- The Gradients Formula for multiparameter p

$$\frac{\nabla j}{\nabla p} = - < U^*, \frac{\partial S(p)}{\partial p} > - < O^*, \frac{\partial O_{inc}(p)}{\partial p} >$$

The expression of the gradients is now completely established. Starting with an initial guess for the estimated parameter p_0, a Quasi-Newton optimizer is used to update the parameter value *p* and to find the optimal p_{opt} which causes the gradients to vanish.

Some recent progresses :

- We can reduce the computation times by decomposing the sources parameters vector into a base of unitary sources (multilinear process): the time computation is then reduced by a factor 10.
- We have completed the identification of sources by optimizing on p and Δp (differences of pressures between opposite points; (The launcher is excited by the differences of pressures in the low frequency domain),
- We have introduced physical sources constraints in the optimization process

Numerical Results

For identifying the overpressure sources, the flight of concern is the 511 ARIANE 5 flight. Indeed, pressure measurements have been mounted on the lower (9 available measurements) and on the upper part of the launcher (4 available measurements).
The locations of sources are defined a priori from previous experience. 10 sources have been identified:

- one per EAP solid rocket booster and its image with regards to the mast, which was not modelled,
- one per solid rocket booster at launch duct exit and its image with regards to the mast,
- one source for the Vulcain engine.

After identification of the overpressure source locations, a direct problem is solved to compute simulated pressure levels and compare them with the real measured values on the same sensors. The comparisons were made on the pressures and the differences of pressure measured at diametrically opposite points. Indeed, this quantity is the adequate parameter for the calculations of low frequency dynamic response of the launch vehicle.

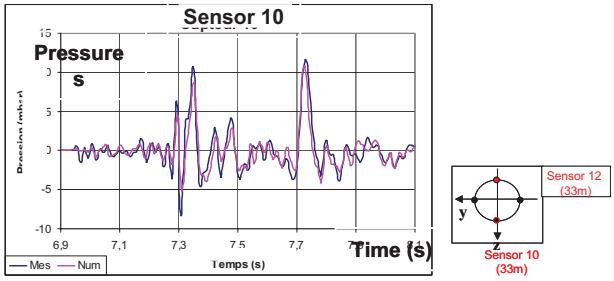

Fig 2 : Comparison of the measured and computed data (Sensor 10, FAIRING)

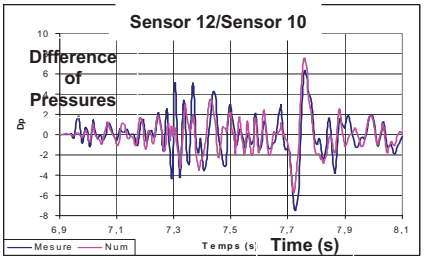

Fig 3 : Comparison of the measured and computed differences of pressure data (Sensor 10, 12 FAIRING)

Good correlations are observed between the measured and calculated pressures. Also, the comparisons on the rebuilt and measured diametrically opposite pressures are good.
A deep robustness analysis of the method has then been performed, as follows,

- A calculation of the field of pressures on a number of necessary points was achieved, in order to check the physical character of the calculated pressures.
- The study of the robustness of the method with regards to the number of measurements
- The comparison between the measured propulsion parameters and the evolution of the identified sources versus time, to check the physical meaning of the identified sources.

Summary

A robust and accurate time domain integral equation for wave propagation was developed. The time marching scheme for the direct acoustic source problem is unconditionally stable (no CFL conditions). This allows a classical optimization approach for the inverse problem.

Direct and adjoint codes have exactly the same properties. Prior knowledge of the localization of sources and power parallel computers allow the industrial application of such an inverse problem.

We demonstrate the interest of the method on some examples of source reconstructions in low frequency acoustics for the ARIANE 5 overpressure source identification on the data from 511 ARIANE 5 flight: initial results are very promising and show a good identification of the multiparameter sources in the 0- 40 Hz frequency domain

For future launches from the same launch pad, that the one used for the identification, and having the same characteristics in terms of propulsion, the complete pressure field in the time domain can be estimated.

The dynamic response of the launcher will be investigated.

References

[1] Troclet B, Chemoul.B, P. Roux, D. Gely and G. Elias.

"*Synthesis of Vibroacoustic Studies performed during ARIANE 5 Program", In Launch Vehicle Vibrations, Toulouse*, pages 201, 210, 1999

[2] H.Ikawa F.Laspesa

Ignition/Duct Overpressue Induced by Space Shuttle Solid Rocket Motor Ignition», Journal of Spacecraft, pages 4841- 488, Vol 22, n°4, July- August 1985

[3] S.Alestra, I.Terrasse, B.Troclet,

Inverse Method for Identification of Acoustic Sources at Launch Vehicle Lift-off", AIAA JOURNAL, Vol 41, Number 10, Octobre 2003

Analysis of Plates with Stiffeners by The Boundary Element Method with Condensation of Variables

Wilson Wesley Wutzow[1], João Batista de Paiva[2]

[1]São Carlos Engineering School, University of São Paulo
Structures Engineering Department, Av. Trabalhador Sãocarlense, 400
13566-590 São Carlos-SP, Brazil
wwesleyw@sc.usp.br

[2]São Carlos Engineering School, University of São Paulo
Structures Engineering Department, Av. Trabalhador Sãocarlense, 400
13566-590 São Carlos-SP, Brazil
paiva@sc.usp.br

Key-words: *Boundary Element Method, plates, stiffeners*

Abstract. In this paper a formulation for representation of stiffeners in plane stress by the BEM (Boundary Elements Method) with linear approach of variable and in linear analysis is presented. The strategy is to adopt approaches for the displacements in the central line of the stiffener. With this approach the spurious for oscillations in the stress along stiffeners with small thickness is prevented. Worked examples are analyzed to show the efficiency of these techniques, especially in the insertion of very narrow sub-regions, in which quasi-singular integrals are calculated, with stiffeners that are much stiffer than the main domain. The results obtained with this formulation are very close to those obtained with other formulations.

1. INTRODUCTION

The boundary elements method (BEM) has proved a valuable tool for the resolution of a wide range of problems in structural engineering, including 2D and 3D elastic problems. The first direct applications of the boundary integral equation method were published by Rizzo [1] and Cruse [2], the former dealing with 2D problems and the latter extending the analysis to three dimensions. In addition, we should recall the work of Lachat [3] and Lachat & Watson [4], who pioneered the generalization of the method. Following these, many other researchers have refined and adapted the BEM formulation, demonstrating how to apply it in diverse fields of engineering.

It is a very common situation in engineering problems that elastic domains need to be embedded in structures. Such domains may be relatively stiff or flexible, thin (narrow) or thick (wide) in the context of the domain in which they are inserted. In particular, these sub-domains are often included in models of domains stiffened with fibres, which may endow the structure with anisotropic properties.

The standard BEM formulation used in the analysis of domains stiffened with bars or fibres is derived by coupling BEM to the finite element method (FEM), BEM being employed to discretize the main structural domain while the stiffening elements inserted in it are modeled by FEM. The coupling is achieved by ensuring the compatibility of the displacements and establishing equilibrium between the forces acting at the interface of the main domain with the sub-domains. The practical use of BEM/FEM combinations in the modeling of stress distribution in engineering problems can be found, for example, in the work of Beer [5], Coda & Venturini [6,7], Coda *et al.* [8] and Coda [9].

In general, BEM/FEM coupling leads to good results. However, when employed to solve problems in which stiffeners are composed of materials with different properties from those of the main structure, much worse results are obtained, usually showing spurious oscillations in space (see the recommendations concerning Dirichlet boundary conditions in Babuska [10], Brezzi [11] and Bathe [12]). When the inserted stiffener is made stiffer, these oscillations become even more pronounced, although the resultant forces are always correct.

In this paper we demonstrate an alternative way of handling the stiffeners, using a form of BEM/BEM coupling known as the sub-region technique, which is employed here in two forms. The first is the classic sub-region technique of Venturini [13], in which the boundary integrals are all solved analytically,

whether or not they include singularities. In the second form of this technique, the unknowns at the boundaries of the stiffeners are condensed on to their central axes, in an approach similar to that used by Leite *et al.* [14] .

Worked examples are analyzed to show the efficiency of these techniques, especially in the insertion of very narrow sub-regions, in which quasi-singular integrals are calculated, with stiffeners that are much stiffer than the main domain.

2. INTEGRAL EQUATION

In this study, the Somigliana equation for displacements in planar domains was used:

$$u_i(s) = -\int_{\Gamma} P_{ij}^*(s,q)u_j(q)d\Gamma + \int_{\Gamma} u_{ij}^*(s,q)P_j(q)d\Gamma + \int_{\Omega} b_j(q)u_{ij}^*(s,q)d\Omega \qquad (1)$$

Ignoring the last term, which represents the parts of the loads applied to the domain of the problem being analyzed, this equation can be written in the algebraic form as follows:

$$[c]\{u\}^p + \sum_{j=1}^{ne}\left(\int_{\Gamma_j}[p^*]\{u\}\,d\Gamma_j\right) = \sum_{j=1}^{ne}\left(\int_{\Gamma_j}[u^*]\{p\}\,d\Gamma_j\right) \qquad (2)$$

Boundary elements were adopted with a linear isoparametric approximation and boundary integrals were all calculated analytically

3. STIFFENERS

The stiffeners are, as a rule, linear elements, nearly always of negligible thickness. They are commonly introduced into BEM analyses *via* BEM/FEM coupling, the BEM being used to model the continuous elastic medium and the FEM to represent the rigid linear elements used to stiffen it (this is just one among several applications of BEM/FEM coupling).

With improved methods of integrating Kelvin's fundamental solution, by analytical treatment of both singular and non-singular integrands and by the introduction of the sub-region technique, it is now feasible to model stiffeners uniform as uniform sub-regions. The quality of the equations is ensured by the use of analytical integration and the values at the interface boundaries are smoothed by a least-squares technique. Moreover, the unknown values that should be calculated at the boundary may be transformed into unknowns on the central line, with or without a reduction in their number. In the work presented here, the sub-region technique was used with analytical integration and the boundary unknowns were condensed on to the central axis of the stiffener, without reducing their number.

3.2. **Sub-regions**

By means of the sub-regions technique, problems can be resolved whose domains contain several sub-domains composed of different materials with contrasting properties. To model such a problem, each homogeneous sub-domain, Ω_i, is separately discretized. The mathematical specification is completed by imposing equilibrium between the forces and compatible displacements at all points along the sub-region interfaces.

Taking the surfaces forces and displacements of points on the interface as unknown values, the equations are assembled into a single system consisting of blocks of zeroes and non-zeroes, which form a sparse matrix. This system can be resolved by a computer routine that handle sparse matrices, which employs Gauss-Jordan elimination with full pivoting.

To illustrate this technique, a system composed of two sub-regions, sketched in Figure 1, will be analyzed.

Before considering the equilibrium of surface forces and compatibility of displacements at the interface between the sub-regions the systems of equations for each domain are written down separately. By imposing the force equilibrium ($\{P\}^{1i} + \{P\}^{2i} = 0$) and displacement compatibility ($\{P\}^{1i} + \{P\}^{2i} = 0$) and the boundary conditions, the two systems are united:

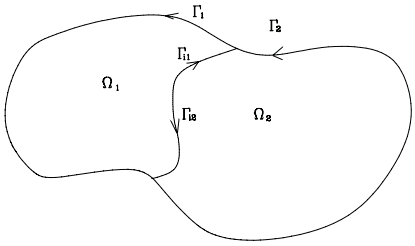

Figure 1. Two sub-regions.

$$\begin{bmatrix} [H]^1_{11} & [H]^1_{1i} & -[G]^1_{1i} & [0] \\ [H]^1_{i1} & [H]^1_{ii} & -[G]^1_{ii} & [0] \\ [0] & [H]^2_{ii} & [G]^2_{ii} & [H]^2_{i2} \\ [0] & [H]^2_{2i} & [G]^2_{2i} & [H]^2_{22} \end{bmatrix} \begin{Bmatrix} \{U\}^1 \\ \{U\}^{1i} \\ \{P\}^{1i} \\ \{U\}^2 \end{Bmatrix} = \begin{bmatrix} [G]^1_{11} & [0] \\ [G]^1_{i1} & [0] \\ [0] & [G]^2_{i2} \\ [0] & [G]^2_{22} \end{bmatrix} \begin{Bmatrix} \{P\}^1 \\ \{P\}^2 \end{Bmatrix} \tag{3}$$

Simplifying:

$$[A]\{X\} = [C]\{D\} \tag{4}$$

The elements of product [C] {D} are known, so the system may be further simplified to:

$$[A]\{X\} = \{B\} \tag{5}$$

The vector {X} contains all the unknowns which, as (5) is a linear system, can be found by applying a routine that solves sparse linear systems of equations.

3.3. Reduction of unknowns at the boundary of the stiffener

The sub-region representing a stiffener, Figure 2, is generally narrow compared to its length and the surrounding region. Hence, it is possible to approximate the normal and tangential displacements along its boundary by displacements on its median line, and their partial derivatives, while the surface forces can be substituted by the load acting on a beam equivalent to the stiffener (represented now by the median line).

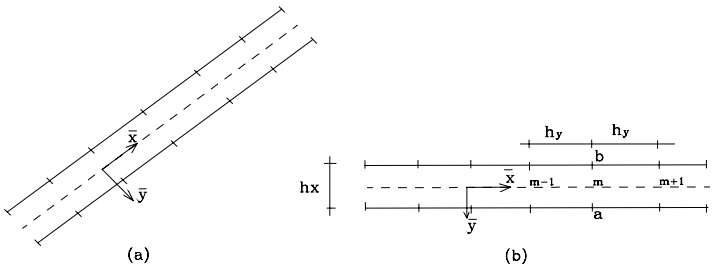

Figure 2. (a) Stiffener with local axes $\bar{x}$ e $\bar{y}$, (b) central nodes that receive the results of integration on the boundary.

For the axes shown, a linear approximation for the displacements gives:

$$u = f(\bar{x}) = a\bar{x} + b \tag{6}$$

while their derivatives with respect to $\bar{x}$ are written:

$$\frac{\partial u_{\bar{x}}}{\partial \bar{x}} = \theta^m_{\bar{x}} \qquad and \qquad \frac{\partial u_{\bar{y}}}{\partial \bar{x}} = \theta^m_{\bar{y}} \tag{7}$$

Then, for the geometry in Figure 2:

$$u_x^a = u_x^m + \theta_x^m \frac{h_x}{2} \quad , \quad u_y^a = u_y^m + \theta_y^m \frac{h_x}{2} \quad , \quad u_x^b = u_x^m - \theta_x^m \frac{h_x}{2} \quad , \quad u_y^b = u_y^m - \theta_y^m \frac{h_x}{2} \tag{8}$$

Using (8), the unknown displacements u_x^a, u_y^a, u_x^b *and* u_y^b on the boundary can be replaced by u_x^m, u_y^m, θ_x^m *and* θ_y^m on the median line of the stiffener, as in Figure 3 (a).

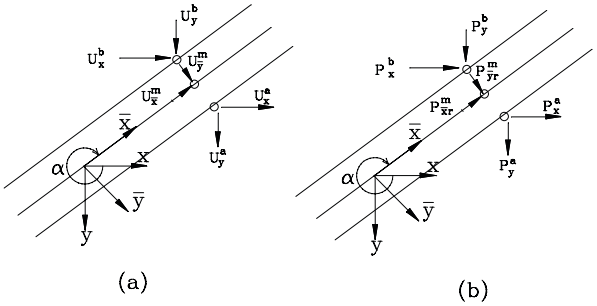

Figure 3. Transformations of unknowns at the boundary into central unknowns: (a) displacements, (b) forces.

Similarly, for the forces, we can write:

$$p_x^a = p_x^m + \frac{\Delta p_x}{2} \quad , \quad p_y^a = p_y^m + \frac{\Delta p_y}{2} \quad , \quad p_x^b = p_x^m - \frac{\Delta p_x}{2} \quad , \quad p_y^b = p_y^m - \frac{\Delta p_y}{2} \tag{9}$$

Thus, equations (9) could be used to substitute the the boundary unknowns p_x^a, p_y^a, p_x^b *and* p_y^b for central values p_x^m, p_y^m, Δp_x *and* Δp_y. In this case, the unknown variables on the median line would be the means of the forces at the boundaries and not the resultant forces acting on the stiffener. Alternatively, the unknown forces could be transformed as follows:

$$p_x^a = \frac{p_{xr}^m}{2} + \frac{\Delta p_x}{2} \quad , \quad p_y^a = \frac{p_{yr}^m}{2} + \frac{M_r}{h_x} \quad , \quad p_x^b = \frac{p_{xr}^m}{2} - \frac{\Delta p_x}{2} \quad , \quad p_y^b = \frac{p_{yr}^m}{2} - \frac{M_r}{h_x} \tag{10}$$

Using (10), the central unknowns are now p_{xr}^m, p_{yr}^m, M_r *e* Δp_x, where p_{xr}^m and p_{yr}^m are resultant loads acting on the stiffener in the directions $\bar{x}$ and $\bar{y}$, M_r is the resultant bending moment on the stiffener and Δp_x is the change in load across the section (see Figure 3 (b)).

With the help of Hookes law, the deformation-displacement relation, and using finite differences, the unknowns Δp_x and Δp_y, or M_r and Δp_x, could be expressed as functions of u_x^m, u_y^m, θ_x^m *and* θ_y^m, so that the total number of unknowns would be reduced, without greatly affecting the accuracy of the results in the case of thin stiffeners.

4. Example: Beam fixed at each end reinforced with a stiffener in its lower face and submitted to a load uniformly distributed over the upper face.

In this example, a horizontal fixed beam submitted to a uniform load across its upper surface, with a stiffener inside its lower region is analyzed. This example is designed simply to show the differences in the results obtained by the sub-region and variable-reduction techniques. The geometric and physical details of this case, as well as the boundary conditions, are shown in Figure 4. The boundary of the beam is divided into 110 elements and the stiffener into 50 elements.

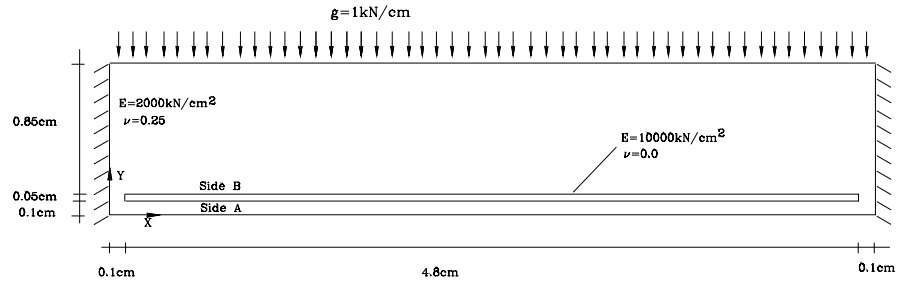

Figure 4. Physical data, geometry and boundary conditions of Example 2.

The results generated for this case by the two techniques are displayed in Figure 5, the displacements of the stiffener and in Figure 6, the bending moment and the normal force difference.

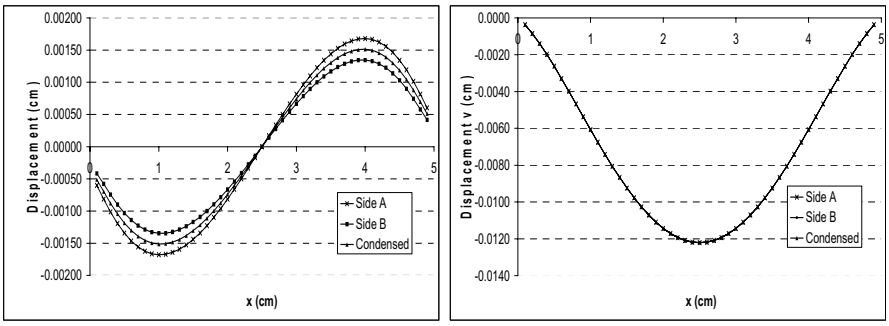

(a) (b)

Figure 5. Displacements of the stiffener (a) in x-direction, (b) in y-direction.

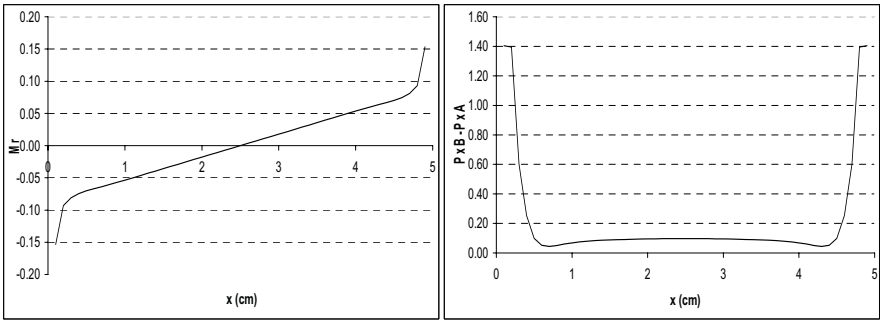

(a) (b)

Figure 6. Graphs showing (a) bending moment (b) normal force difference between upper and lower faces, along the stiffener.

The vertical displacement of point A, at the centre of the stiffener (Figure 4), was calculated by the BEM, using the sub-region and reduction techniques, and by the FEM, using Shell93 in the program Ansys with a fine mesh of 2500 finite elements. The three estimates are compared in Table 1. The two BEM techniques gave the same result, which was similar to the Ansys solution.

Table 1. Displacements in the center of the stiffener in y direction.

Method of calculation	Displacement y (cm)
Sub-region	-0.012211
Reduction	-0.012211
SHELL 93 (ANSYS)	-0.012368

4. CONCLUSIONS

As foreseen, the application of the technique of reduction of variables to the modeling of narrow stiffening elements led to good simulations, smoothing out the distortions that arise in the surface-force results for very thin elements. We should not forget, however, that the use of analytical integration, both for singular and quasi-singular cases, made a significant contribution to the viability of this technique, owing to improvements in calculating the integrals. In nonlinear problems or inverse analysis, the smoothing of such oscillations is crucial to obtaining good results.

Several kinds of reduction can be employed, but it is important to keep in mind the specific problem being analyzed, so as to avoid simplifications that change its essential nature. Although the present treatment of this technique did not involve any reduction in the degrees of freedom of the system, such a reduction could be achieved if we transformed the variables representing the bending moment and the difference between the normal forces at the faces of the stiffener into mean deformations and displacements of the stiffener, by applying Hooke's Law, the deformation-displacement relation and finite differences. We should, however, be aware of the fact that by using finite differences in this approximation we risk losing much of its precision and thus spoiling the results.

REFERENCES

[1] Rizzo PJ, 1967. An integral equation approach to boundary value problems of classical elastostatics. Q Appl Math ;25:83–95.

[2] Cruse TA, 1969. Numerical solutions in three-dimensional elastostatics. Int J Solids Struct ;5:1259–74.

[3] Lachat JC, 1975.Afurther development of the boundary integral technique for elastostatics.PhDThesis. Southampton University, Southampton.

[4] Lachat JC, Watson JO, 1976. Effective numerical treatment of boundary integral equations: a formulation for three-dimensional elastostatics. Int J Numer Meth Engng;10:991–1005.

[5] Beer G, Watson JO, 1992. Introduction to finite and boundary element methods for engineers. New York: Wiley.

[6] Coda HB, Venturini WS, 1995. Three-dimensional transient BEM analysis. Comput Struct ;56(5):751–68.

[7] Coda HB, Venturini WS, 1999. On the coupling of 3D BEM and FEM frame model applied to elastodynamic analysis. Int J Solids Struct; 36(31/32):4789–804.

[8] Coda HB, Venturini WS, Aliabadi MH, 1999. A general 3D BEM/FEM coupling applied to elastodynamic continua/frame structures interaction analysis. Int J Numer Meth Engng ;46(5):695–712.

[9] Coda HB, 2001. Dynamic and static non-linear analysis of reinforced media: a BEM/FEM coupling approach. Comput Struct;79:2751–65.

[10] Babuska I, Aziz AK, 1972. Survey lectures on the mathematical foundations of the finite element methods. In: Aziz AK, editor. The mathematical foundations of finite elements with applications to partial differential equations. New York: Academic Press. p. 5–359.

[11] Brezzi F, 1974. On the existence, uniqueness and approximation of saddlepoint problems arising from Lagrange multipliers. Revue Francaise d'automatique informatique et recherche operationnelle;8-R2: 129–51.

[12] Bathe KJ. (1996). Finite element procedures. Englewood Cliffs: Prentice-Hall

[13] Venturini WS, 1992. Alternative formulations of the boundary element method for potential and elastic zoned problems. Engng Anal;

[14] Leite, L.G.S.; Coda, H.B.; Venturini, W.S, 2003. Two-dimensional solids reinforced by thin bars using the boundary element method. Engineering analysis with boundary elements, v. 27, pp. 193-201.

Boundary element method for magneto-electro-elastic laminates

A. Milazzo[1], I. Benedetti[2] and C. Orlando[3]

[1]Dipartimento di Ingegneria Aeronautica e dei Trasporti, Università di Palermo, Viale delle Scienze, Edificio 8, 90128, Palermo, Italy, milazzo@diat.unipa.it

[2]Dipartimento di Ingegneria Aerospaziale, Università di Pisa, Via Diotisalvi 2, 56126, Pisa, Italy, benedetti@diat.unipa.it

[3] Dipartimento di Ingegneria Aeronautica e dei Trasporti, Università di Palermo, Viale delle Scienze, Edificio 8, 90128, Palermo, Italy, orlando@diat.unipa.it

Keywords: Magneto-electro-elastic materials; Boundary element method; Laminates.

Abstract. A boundary integral formulation and its numerical implementation are presented for the analysis of magneto-electro-elastic media. The problem is formulated by using a suitable set of generalized variables. The governing boundary integral equation is obtained by generalizing the reciprocity theorem to the magneto-electro-elasticity. The fundamental solutions are calculated through a modified Lekhnitskii's approach, reformulated in terms of generalized magneto-electro-elastic displacements. To assess the reliability and effectiveness of the formulation, some numerical analyses have been carried out and the convergence of the method has been studied. The multidomain approach has been developed for the analysis of multilayered structures. Obtained numerical results show good agreement with those found in the literature.

Introduction. The new class of magneto-electro-elastic materials has recently emerged in the field of smart structures and materials by virtue of their features, namely the ability to convert energy into three different forms, magnetic, electric and mechanical. This makes these materials potentially superior to other materials for the construction of smart devices, such as sensors, actuators or trasducers. Magneto-electro-elastic media can fundamentally be of two kinds: a) particulate composites having a 0-3 connectivity; b) composites having a 2-2 connectivity [1]. The optimal exploitation of these materials relies upon the correct analysis of their coupled response to external stimula. While the inherent coupling of the three fields makes them particularly attractive in the framework of intelligent systems, on the other hand it makes the mathematical modelling of their behavior more complex. Indeed, analytical solutions to the governing differential equations are rather rare and either devoted to the treatment of infinite domain problems or limited to special configurations. Example could be found in the works of Wang and Shen [3], Hou et al. [4], Ding and Jiang [5], Guan et He [6], Hou et al. [7], Pan [8], Pan et Heyliger, [9, 10], Heyliger et al. [11], Pan and Han [12], Wang et al. [13] and Chen et al [14]. While some numerical models, both FEM and BEM, was proposed by Bhangale and Ganesan [15], Buchanan [2, 16], Lage et al. [17], Ding and Jiang [5], Ding et al. [18]. In the present paper a multidomain boundary element model for 2D magneto-electro-elastic laminates is developed. The formulation is expressed in terms of suitably defined generalized variables, namely generalized displacements and tractions. By using these variables the magneto-electro-elastic governing equations can be recast in a form that resembles the governing equations of classical elasticity and allows the straightforward extension of classical methods to the magneto-electro-elastic analysis. The boundary integral representation is deduced by generalizing the reciprocity theorem. The fundamental solutions are determined by using a generalized displacement based modified Lekhnitskii's approach [19]. Finally, the numerical solution of the formulation is obtained by the boundary element method. A multidomain approach, obtained by enforcing suitable continuity and equilibrium conditions between adiacent layers, has been used to model laminate configurations. Some numerical results are presented to evaluate the effectiveness and the reliability of the proposed model.

Basic equations. The formulation will be developed for two-dimensional magneto-electro-elastic domains Ω with boundary $\partial\Omega$ lying in the x_1x_2 plane. It is assumed that the magneto-electro-elastic response does not vary along the x_3 direction, so that the analysis leads to a generalized plane strain elasticity problem and an in-plane magneto-electrostatic problem. To maintain a compact and efficient matrix notation the strain component γ_{33}, the electric field component E_3 and the magnetic field component H_3, which are trivially zero due to the assumption of generalized plane strain and in-plane electrostatics and magnetostatics, are kept in the formulation and the generalized in-plane behaviour will be expressed by suitable differential operators. The elastic state of the body is described in terms of mechanical displacements **u**, elastic strains $\boldsymbol{\gamma}$ and stresses $\boldsymbol{\sigma}$. The electric state is defined by the electric potential φ, the electric field **E** and the electric displacement field **D**. Assuming that there is no external current density in the domain, the magnetic field variables are the scalar magnetic potential ψ, the magnetic field **H** and the magnetic induction field **B**. All these variables are linked by the following constitutive equations for magneto-electro-elastic materials

$$\begin{bmatrix} \boldsymbol{\sigma} \\ \mathbf{D} \\ \mathbf{B} \end{bmatrix} = \begin{bmatrix} \mathbf{C} & \mathbf{e}^T & \mathbf{d}^T \\ \mathbf{e} & -\boldsymbol{\varepsilon} & -\mathbf{g} \\ \mathbf{d} & -\mathbf{g} & -\boldsymbol{\mu} \end{bmatrix} \cdot \begin{bmatrix} \boldsymbol{\gamma} \\ -\mathbf{E} \\ -\mathbf{H} \end{bmatrix} \tag{1}$$

where **C** is the elasticity matrix, $\boldsymbol{\varepsilon}$ and $\boldsymbol{\mu}$ are the matrices of dielectric constants and magnetic permeability respectively, **e** and **d** are the matrices of piezoelectric and piezomagnetic constants and **g** is the matrix describing the direct magneto-electric coupling. Moreover, the form of the strain-displacement relations and of the irrotationality conditions of electric and magnetic fields, and that of the classical elastic indefinite equilibrium equations and of the Maxwell's equations for electrostatic and magnetostatic suggests the extension to the general magneto-electro-elastic problem of the Barnett and Lothe's [20] formalism for piezoelectrics. Opportunely definig the generalized displacements **U**, generalized body forces **F**, generalized strains $\boldsymbol{\Gamma}$, generalized stresses $\boldsymbol{\Sigma}$ and the generalized compatibility oprator $\mathfrak{D}$ as in Davì and Milazzo [23], the generalized strain-displacement relationship, the generalized indefinite equilibrium equations and the generalized constitutive link can be written in compact matrix forms as

$$\boldsymbol{\Gamma} = \mathfrak{D}\,\mathbf{U}, \quad \mathfrak{D}^T\boldsymbol{\Sigma} + \mathbf{F} = \mathbf{0}, \quad \boldsymbol{\Sigma} = \mathbf{R}\boldsymbol{\Gamma} \tag{2}$$

where **R** is the generalized constitutive matrix; now, by combining the last set of equations the generalized governing equations are obtained

$$\mathfrak{D}^T\mathbf{R}\mathfrak{D}\,\mathbf{U} + \mathbf{F} = \mathbf{0} \tag{3}$$

The generalized boundary conditions associated with the above equation can be then expressed by

$$\begin{aligned} \mathbf{U} &= \bar{\mathbf{U}} && on\ \partial\Omega_1 \\ \mathbf{T} = \mathfrak{D}_n^T\mathbf{R}\mathfrak{D}\,\mathbf{U} &= \bar{\mathbf{T}} && on\ \partial\Omega_2 \end{aligned} \tag{4}$$

where $\mathbf{T} = \begin{bmatrix} t_1 & t_2 & t_3 & D_n & B_n \end{bmatrix}^T$ is the generalized tractions vector and $\mathfrak{D}_n$ is the generalized traction operator, obtained by substituting the derivatives with the corresponding boundary outer normal direction cosines in the generalized compatibility operator $\mathfrak{D}$ [21].

Boundary integral representation. Let U_j and F_j be system of generalized displacements and forces which satisfies eq (3), and let T_j be the corresponding generalized tractions. If $\mathbf{F}_j = \mathbf{c}_j\delta(P - P_0)$, where the $\mathbf{c}_j$ is the load intensity and $\delta(P - P_0)$ is the Dirac's delta function and

U_j and T_j represent the problem fundamental solution, extending the reciprocity theorem to the generalized magneto-electro-elastic problem, the following equation can be written [22]

$$\mathbf{c}_j^T\mathbf{U}(P_0)+\int_{\partial\Omega}\left(\mathbf{T}_j^T\mathbf{U}-\mathbf{U}_j^T\mathbf{T}\right)d\partial\Omega=\int_{\Omega}\mathbf{U}_j^T\mathbf{F}\,d\Omega \tag{5},$$

which is the analogous of the classical Somigliana's identity of elasticity and constitutes the boundary integral representation of the magneto-electro-mechanical problem. By using five independent fundamental solutions associated with the concentrated point load directed along the three axes, with a concentrated charge and with a concentrated current, the generalized displacements at the generic point P_0 can be expressed in terms of generalized displacements and generalized tractions on the boundary. In compact matrix notation one writes

$$\mathbf{c}^*\mathbf{U}(P_0)+\int_{\partial\Omega}\left(\mathbf{T}^*\mathbf{U}-\mathbf{U}^*\mathbf{T}\right)d\partial\Omega=\mathbf{0} \tag{6}$$

where the hypothesis of null body forces has been assumed. The kernel terms U_{ij}^* and T_{ij}^* and the matrix $\mathbf{c}^*$ are opportunely defined for magneto-electro-elastic problems as explained in Davì and Milazzo [23] for the piezoelectric case. When collocated at the boundary, eq (6) provides the boundary integral equations which, coupled with the essential and natural conditions (4), allows the determination of the unknowns on the boundary.

Fundamental solutions. The formulation of the boundary integral equations relies the magneto-electro-elastic fundamental solution, which is governed by the following equation

$$\mathfrak{D}^T\mathbf{R}\,\mathfrak{D}\,\mathbf{U}_j+\mathbf{c}_j\delta(P-P_0)=\mathbf{0} \tag{7}$$

in the infinite domain Ω_∞, it is deduced by extending to magneto-electro-elastic materials a modified Lekhnitskii's approach previously used for piezoelectric materials [23]. In this framework, the solution of eq (7) is sought of the form

$$\mathbf{U}=\lambda\,\mathbf{a}\ln(X_1+\alpha X_2) \tag{8}$$

where $X_i=x_i(P)-x_i(P_0)$ with $(i=1,2)$, and $\mathbf{a}$ and α are complex constants to be determined feeding the expression (8) into eq (7) and solving the produced generalized eigenvalue problem. The solution of the eigenvalue problem gives ten eigenvalues α_k with the associated eigenvectors $\mathbf{a}_k$, which form conjugate pairs for non degenerate materials. In the case of distinct eigenvalues the fundamental solution is then expressed as superposition of functions of the form (8), associated with the calculated eigenvalues α_k. By selecting the eigenvalues with positive imaginary parts, $\mathrm{Im}(\alpha_k)>0$, the generalized fundamental solution and the corresponding tractions can be expressed as

$$\mathbf{U}_j=2\sum_{k=1}^{5}\mathrm{Re}\left[\lambda_{jk}\mathbf{a}_k\ln(X_1+\alpha_k X_2)\right]\quad\text{and}\quad\mathbf{T}_j=2\sum_{k=1}^{5}\mathrm{Re}\left[\lambda_{jk}\mathfrak{D}_n^T\mathbf{R}\,\mathfrak{D}_{\alpha_k}\mathbf{a}_k\frac{1}{X_1+\alpha_k X_2}\right] \tag{9}$$

where the matrix $\mathfrak{D}_{\alpha_k}$ is opportunely defined as just done by Davì and Milazzo [23] for piezoelectric problem. Finally, the complex constants λ_{jk} are determined by enforcing the compatibility and equilibrium conditions on the Gauss plane. It is worth noting that, by virtue of the generalized formalism used, the present fundamental solution has been derived in compact matrix notation, which has proved to be very practical and advantageous for computer implementation.

Numerical results. The boundary integral formulation has been numerically implemented by using the classical BEM [24], and expressing the generalized boundary variables **U** and **T** in terms of their nodal values via linear shape functions. In the present application, the magneto-electro-elastic behavior of

the two layer composite laminate shown in Fig. 1 has been studied. The analysis is carried out under cylindrical bending conditions and generalized plain strain hypothesis. The plate dimensions are $b = 0.01\ m$ and $h = 0.001\ m$. The generalized boundary conditions are summarized in Table 1,while the material properties of the piezoelectric and piezomagnetic layers have been extracted from Heyliger et al. [11].

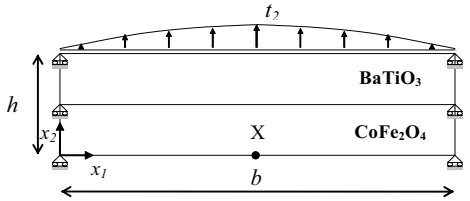

Fig. 1 *Two layers magneto-electro-elastic laminates scheme.*

Boundary	Boundary conditions			
$x_1 = 0, b$	$t_1 = 0$	$u_2 = 0$	$\varphi = 0$	$\psi = 0$
$x_2 = 0$	$t_1 = 0$	$t_2 = 0$	$D_2 = 0$	$B_2 = 0$
$x_2 = h$	$t_1 = 0$	$t_2 = sin(\pi x_1 / b)$	$D_2 = 0$	$B_2 = 0$

Table 1*Boundary conditions for the magneto-electro-elastic simply-supported laminate*

In Table 2 the transverse displacement, the electric potential and the magnetic scalar potential, computed by using 427 linear elements, are listed for three selected points. The values in parentheses are the exact solutions as extracted from Heyliger et al. [11]. The convergence analysis for the transverse displacement and the electric and magnetic potential at the point X≡(b/2,0) has been carried out showing that the magnetic scalar potential exhibits the slowest convergence.

x_1	x_2	$u_2\ [m]$	$\varphi\ [V]$	$\psi\ [A]$
		7.9190e-12	2.1345e-4	-1.5767e-7
	0	(7.9832e-12)	(2.141e-4)	(-1.6977e-7)
		7.9730e-12	2.1572e-4	-2.3101e-7
b/2	h/2	(8.0377e-12)	(2.1637e-4)	(-2.4008e-7)
		7.9353e-12	1.228e-4	-2.296e-7
	h	(7.9997e-12)	(1.2268e-4)	(-2.386e-7)

Table 2 *Transverse displacement and electric and magnetic scalar potantials at three points for the $CoFe_2O_4/BaTiO_3$ laminate.*

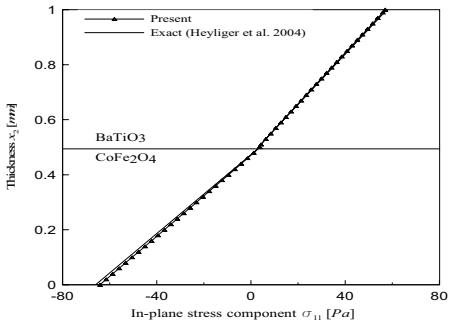

Fig. 2 *Through thickness distribution of the in-plane normal stress σ_{11}.*

Fig. 2 to Fig. 8 show the components of the generalized traction as functions of the plate thickness. Fig. 2 shows the presence of a small discontinuity, both in terms of intensity and inclination, in the distribution of the stress component σ_{11} at the interface between the two layers, due to the different material properties, as also pointed out by Heyliger et al. [11], while the stress components σ_{22} and σ_{12}, shown in Fig. 3 and Fig. 4 respectively, are continuous through the interface.

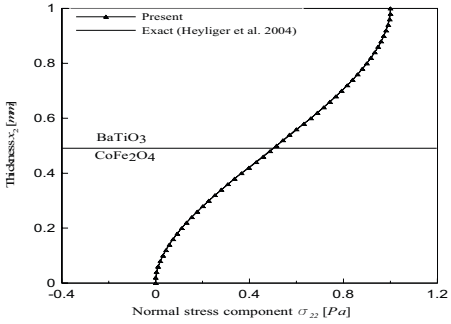

Fig. 3 *Through thickness distribution of transverse normal stress σ_{22}.*

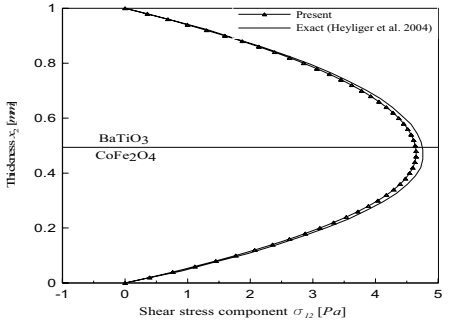

Fig. 4 *Through thickness distribution of the transverse shear stress σ_{12}.*

The electric displacement components D_1 and D_2 and the magnetic induction components B_1 and B_2, shown in Fig. 5 to Fig. 8, present a more relevant discontinuity crossing the interface, both in the intensity (B_1 and D_1) and in the slope (B_2 and D_2), due to the transition from a piezoelectric to a piezomagnetic layer; moreover they show a characteristic behavior, also depicted by Heyliger et al. [11]: the through thickness electric displacement distribution is linear in the magnetostrictive layer and non-linear in the piezoelectric one, while the through thickness magnetic induction distribution is linear in the piezoelectric medium and non-linear in the magnetostrictive one.
In all the studied cases, the agreement between previous results and those calculated through the developed formulation appears fully satisfying.

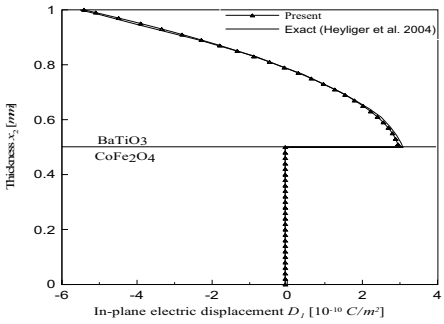

Fig. 5 *Through thickness distributionof the in-plane electric displacement component D_1.*

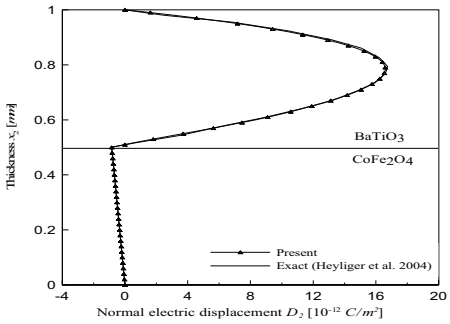

Fig. 6 *Through thickness distribution of the normal electric displacement component D_2.*

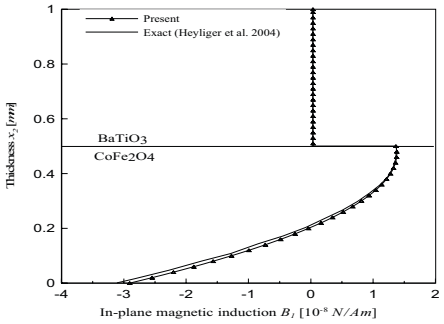

Fig. 7 *Through thickness distributionof the in-plane magnetic induction component B_1.*

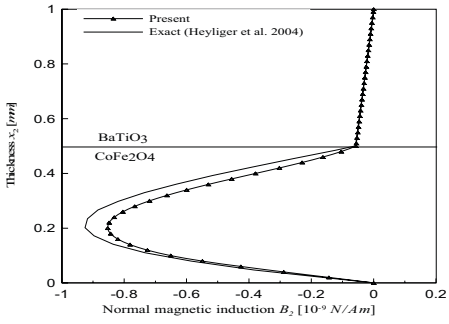

Fig. 8 *Through thickness distributionof the in-plane magnetic induction component B_2.*

Conclusions. In this work a multidomain boundary element approach for the analysis of general magneto-electro-elastic laminates has been developed. The model is entirely expressed in terms of generalized magneto-electro-elastic variables, which allow the extension of anisotropic elasticity techniques to the more general magneto-electro-elastic problem. In particular, the Somigliana's identity is rewritten in the extended notation and the boundary integral representation is then directly deduced. The fundamental solutions are calculated generalizing a modified Lekhnitskii's approach and are expressed in a very compact matrix notation. The analysis of some configuration has been carried out and the results showed good agreement with those found in the literature. These analyses have also evidenced some characteristic features of magneto-electro-elastic laminates.

References

[1] Ryu, J., Priya, S., Uchino, K., Kim, H.E., Magnetoelectric Effect in Composites of Magnetostrictive and Piezoelectric Materials, *Journal of Electroceramics*, 8 (2002), 107-119.

[2] Buchanan G. R., Layered versus multiphase magneto-electro-elastic composites, *Composites: Part B* 35 (2004) 413–420.

[3] Wang Xu, Shen Y., The general solution of three-dimensional problems in magneto-electro-elastic media, *International Journal of Engineering Science,* 40 (2002) 1069-1080.

[4] Hou, P., Leung Y.T. A., Ding H.J., The elliptical Hertzian contact of transversely isotropic magnetoelctroelastic bodies, *International Journal of Solids and Structures,* 40 (2003), 2833-2850.

[5] Ding, H., Jiang, A., A boundary integral formulation and solution for 2D problems in magneto-electro-elastic media, *Computers & Structures,* 82 (2004) 1599-1607.

[6] Guan, Q., He, S.R., Two-dimansional analysis of piezoelectric/piezomagnetic and elastic media, *Composite Structures,* 69 (2005) 229-237.

[7] Hou, P.F., Ding, H.J., Chen, J.Y., Green's function for transversely isotropic magneto-electro-elastic media, *International Journal of Engineerig Science,* 43 (2005) 826-858.

[8] Pan, E., Exact Solution for Simply Supported and Multilayered Magneto-Electro-Elastic Plates, *Journal of Applied Mechanics,* 68 (2001) 608-618.

[9] Pan, E., Heyliger, P.R., Free vibrations of simply supported and multilayered magneto-electro-elastic plates, *Journal of Sound and Vibration* 252(3) (2002), 429-442.

[10] Pan, E., Heyliger, P.R., Exact solutions for magneto-electro-elastic laminates in cylindrical bending, *International Journal of Solids and Structures*, 40 (2003), 6859-6876.

[11] Heyliger, P.R., Ramirez, F., Pan, E., Two-dimensional Static Fields in Magnetoelectroelastic Laminates, *Journal of Intelligent Material Systems and Structures,* 15 (2004) 689-709.

[12] Pan, E., Han, F., Exact solution for functionally graded and layered magneto-electro-elastic plates, *International Journal of Engineering Science*, 43 (2005), 321-339.

[13] Wang, J.G., Chen, L.F., Fang, S., State vector approach to analysis of multilayered magneto-electro-elastic plates, *International Journal of Solids and Structures*, 40 (2003), 1669-1680.

[14] Chen, W.Q., Lee, K.Y., Ding, H.J., On free vibrations of non-homogeneous transversely isotropic magneto-electro-elastic plates, *Journal of Sound and Vibration*, 279 (2005), 237-251.

[15] Bhangale, R.K., Ganesan, N., Free vibration studies of simply supported nonhomogeneous functionally graded magneto-electro-elastic finite cylindrical shell, *Journal of Sound and Vibration*, 288 (2005), 412-422.

[16] Buchanan, G.R., Free vibration of an infinite magneto-electro-elastic cylinder, *Journal of Sound and Vibration*, 268 (2003), 413-426.

[17] Lage, R.G., Mota Soares, C.M., Mota Soares, C.A., Reddy, J.N., Layerwise partial mixed finite element analysis of magneto-electro-elastic plates, *Computers and Structures*, 82 (2004), 12931301.

[18] Ding, H.J., Jiang,A.M., Hou, P.F., Chen, W.Q., Green's functions for two-phase transversely isotropic magneto-electro-elastic media, *Engineering Analysis with Boundary Elements*, 29 (2005), 551-561.

[19] Lekhnitskii, S.G., *Theory of elasticity of an anisotropic body*, Holden-Day, San Francisco (1963).

[20] Barnett D.M., Lothe J., Dislocations and line charges in anisotropic piezoelectric insulators, *Physics State Solid* (b), 67 (1975),105-111.

[21] Davì G., Milazzo A., Boundary element solution for the free edge stresses in composite laminates, *Journal of Applied Mechanics,* 64 (3) (1997), 877-884.

[22] Aliabadi, M. H., *The Boundary Element Method*, *Vol.2*, Wiley, (2002)

[23] Davì G., Milazzo A., Multidomain boundary integral formulation for piezoelectric materials fracture mechanics, *International Journal of Solids and Structures,* 38 (2001), 7065-7078.

[24] Banerjiee, P.K., Butterfield, R., *Boundary Element Methods in Engineering Science*, McGraw-Hill, (1981).

BEM based solution for an inverse problem in MRI by the Tikhonov regularization method

L. Marin[1,*], H. Power[1], R.W. Bowtell[2], C. Cobos Sanchez[2], A.A. Becker[1], P. Glover[2] and I.A. Jones[1]

[1]School of Mechanical, Materials and Manufacturing Engineering, The University of Nottingham, University Park, Nottingham NG7 2RD, UK, *liviu.marin@nottingham.ac.uk

[2]Sir Peter Mansfield Magnetic Resonance Centre, School of Physics and Astronomy, The University of Nottingham, Nottingham Park, Nottingham NG7 2RD, UK

Keywords: Inverse problem; Regularization; Divergence-free BEM; Magnetic resonance imaging (MRI)

Abstract. We investigate the reconstruction of a divergence-free surface current distribution from knowledge of the magnetic flux density in a prescribed region of interest in the framework of static electromagnetism. This inverse problem is approached by employing the Tikhonov regularization method, in conjunction with a novel BEM which satisfies the continuity equation for the current density.

Mathematical Formulation

Magnetic resonance imaging (MRI) is a non-invasive technique for imaging the human body, which has revolutionised the field of diagnostic medicine. MRI relies on the generation of highly controlled magnetic fields that are essential to the process of image production. In particular, an extremely homogeneous, strong, static field is required to polarize the sample and provide a uniform frequency of precession, while pure field gradients are needed to encode the spatial origin of signals. The field gradients are generated by carefully arranged wire distributions generally placed on cylindrical surfaces surrounding the imaging subject, known as gradient coils [1-3].

In a non-magnetic material, as is the case of biological tissue, the magnetic flux density $\mathbf{B} = (\mathrm{B_x}, \mathrm{B_y}, \mathrm{B_z})^{\mathrm{T}}$ satisfies the following system of partial differential equations [4]:

$$\nabla \times \mathbf{B}(\mathbf{x}) = \mu_0 \mathbf{J}(\mathbf{x}), \qquad \nabla \cdot \mathbf{B}(\mathbf{x}) = 0, \qquad \mathbf{x} = (\mathrm{x}, \mathrm{y}, \mathrm{z})^{\mathrm{T}} \in \mathbb{R}^3. \tag{1}$$

Here $\mu_0 = 4\pi \times 10^{-7}\,\mathrm{N/A^2}$ is the permeability of the free-space and $\mathbf{J} = (\mathrm{J_x}, \mathrm{J_y}, \mathrm{J_z})^{\mathrm{T}}$ is the current density which is defined as a surface current density $\mathbf{J}^{\mathrm{coil}} = (\mathrm{J_x^{coil}}, \mathrm{J_y^{coil}}, \mathrm{J_z^{coil}})^{\mathrm{T}}$, i.e.

$$\mathbf{J}(\mathbf{x}) = \mathbf{J}^{\mathrm{coil}}(\mathbf{x}')\,\delta(\mathbf{x}', \mathbf{x}), \qquad \mathbf{x} \in \mathbb{R}^3, \quad \mathbf{x}' \in \Gamma_{\mathrm{coil}}, \tag{2}$$

where $\Gamma_{\mathrm{coil}} \subset \mathbb{R}^3$ is the coil surface and $\delta(\mathbf{x}', \mathbf{x})$ is the Kronecker delta function, such that

$$\nabla \cdot \mathbf{J}^{\mathrm{coil}}(\mathbf{x}) = 0, \qquad \mathbf{J}^{\mathrm{coil}}(\mathbf{x}) \cdot \boldsymbol{\nu}(\mathbf{x}) = 0, \qquad \mathbf{x} \in \Gamma_{\mathrm{coil}}. \tag{3}$$

with $\boldsymbol{\nu}$ the outward unit vector normal to the coil surface Γ_{coil}.

If the vector potential $\mathbf{A} = (\mathrm{A_x}, \mathrm{A_y}, \mathrm{A_z})^{\mathrm{T}}$ is introduced as:

$$\mathbf{B}(\mathbf{x}) = \nabla \times \mathbf{A}(\mathbf{x}), \qquad \mathbf{x} \in \mathbb{R}^3, \tag{4}$$

then the system of partial differential equations (1) reduces to the following Poisson equation for the vector potential $\mathbf{A}$:

$$\nabla^2 \mathbf{A}(\mathbf{x}) = \mu_0 \mathbf{J}(\mathbf{x}), \qquad \mathbf{x} \in \mathbb{R}^3. \tag{5}$$

In the *direct problem* formulation, the current density $\mathbf{J}^{\mathrm{coil}}$ is known on the coil surface Γ_{coil} and satisfies condition (3), whilst the vector potential $\mathbf{A}$ is determined from the Poisson equation (5) by employing its integral representation, namely

$$\mathbf{A}(\mathbf{x}) = \frac{\mu_0}{4\pi} \int_{\mathbb{R}^3} \frac{\mathbf{J}(\mathbf{x}')}{|\mathbf{x} - \mathbf{x}'|} \mathrm{d}\mathbf{x}' = \frac{\mu_0}{4\pi} \int_{\Gamma_{\mathrm{coil}}} \frac{\mathbf{J}^{\mathrm{coil}}(\mathbf{x}')}{|\mathbf{x} - \mathbf{x}'|} \mathrm{d}\Gamma(\mathbf{x}'), \qquad \mathbf{x} \in \mathbb{R}^3. \tag{6}$$

On using eqns. (4) and (6), the magnetic flux density may be recast as

$$\mathbf{B}(\mathbf{x}) = \frac{\mu_0}{4\pi} \int_{\Gamma_{\text{coil}}} \frac{-(\mathbf{x}-\mathbf{x}') \times \mathbf{J}^{\text{coil}}(\mathbf{x}')}{|\mathbf{x}-\mathbf{x}'|^3} \mathrm{d}\Gamma(\mathbf{x}'), \qquad \mathbf{x} \in \mathbb{R}^3. \tag{7}$$

Motivated by the design of gradient coils used in MRI, we investigate the reconstruction of the divergence-free surface current distribution $\mathbf{J}^{\text{coil}}$ from knowledge of one component of the magnetic flux density $\mathbf{B}$ in a prescribed region of interest $\Omega \subset \mathbb{R}^3$, i.e. we focus on the following *inverse problem*:

$$\begin{array}{l} \text{Given } \ \widetilde{\mathrm{B}}_{\mathrm{z}}(\mathbf{x}),\, \mathbf{x} \in \Omega, \ \text{ find } \ \mathbf{J}^{\text{coil}}(\mathbf{x}),\, \mathbf{x} \in \Gamma_{\text{coil}}, \ \text{ such that:} \\ \mathrm{B}_{\mathrm{z}}(\mathbf{x}) = \widetilde{\mathrm{B}}_{\mathrm{z}}(\mathbf{x}),\, \mathbf{x} \in \Omega, \ \text{ and } \ \nabla \cdot \mathbf{J}^{\text{coil}}(\mathbf{x}) = 0,\, \mathbf{J}^{\text{coil}}(\mathbf{x}) \cdot \boldsymbol{\nu}(\mathbf{x}) = 0,\, \mathbf{x} \in \Gamma_{\text{coil}}. \end{array} \tag{8}$$

Divergence-Free BEM

Assume that the coil surface Γ_{coil} is approximated as $\Gamma_{\text{coil}} \approx \bigcup_{\mathrm{n}=1}^{\mathrm{N}} \Gamma_{\mathrm{n}}$, where Γ_{n}, $1 \le \mathrm{n} \le \mathrm{N}$, are triangular boundary elements (not necessarily flat). In the sequel, we use the following notation:

- $\Gamma_{\mathrm{n}} := \triangle \mathbf{x}^{\mathrm{n}1}\mathbf{x}^{\mathrm{n}2}\mathbf{x}^{\mathrm{n}3}$, $1 \le \mathrm{n} \le \mathrm{N}$, triangular boundary elements;
- $\mathbf{x}^{\mathrm{nj}}$, $1 \le \mathrm{j} \le \mathrm{N_e}$, local nodes corresponding to the triangular boundary element Γ_{n}, e.g. $\mathrm{N_e} = 3$, $\mathrm{N_e} = 6$ and $\mathrm{N_e} = 10$ for linear, quadratic and cubic triangular boundary elements, respectively;
- $\mathbf{x}^{\mathrm{nj}}$, $1 \le \mathrm{j} \le 3$, vertices of the triangular boundary element Γ_{n};
- Γ_{nj}, $1 \le \mathrm{j} \le 3$, the edge of the triangular boundary element Γ_{n} opposite to the vertex $\mathbf{x}^{\mathrm{nj}}$;
- N the number of triangular boundary elements;
- M the number of global nodes on the coil surface Γ_{coil};
- $\mathrm{N_e}$ the number of local nodes corresponding to each triangular boundary element Γ_{n}.

Geometry of the BEM. The parametrization of the triangular boundary elements is given by

$$(\xi,\eta) \in \Big\{ (\xi,\eta)\,|\xi \ge 0, \eta \ge 0, \xi+\eta \le 1 \Big\} \longmapsto \mathbf{x}(\xi,\eta) \in \Gamma_{\mathrm{n}}, \quad \mathbf{x}(\xi,\eta) = \sum_{\mathrm{j}=1}^{\mathrm{N_e}} \mathrm{N_j}(\xi,\eta)\, \mathbf{x}^{\mathrm{nj}}\,, \tag{9}$$

where $\mathrm{N_j}(\xi,\eta)$, $1 \le \mathrm{j} \le \mathrm{N_e}$, are given geometrical shape functions [5]. Consequently, the derivatives in the $\xi-$ and $\eta-$directions may be recast as:

$$\begin{cases} \boldsymbol{\tau}^{\mathrm{n}\xi}(\xi,\eta) := \boldsymbol{\tau}^{\mathrm{n}\xi}\left(\mathbf{x}(\xi,\eta)\right) = \dfrac{\partial \mathbf{x}(\xi,\eta)}{\partial \xi} = \displaystyle\sum_{\mathrm{j}=1}^{\mathrm{N_e}} \frac{\partial \mathrm{N_j}(\xi,\eta)}{\partial \xi}\, \mathbf{x}^{\mathrm{nj}} \\ \boldsymbol{\tau}^{\mathrm{n}\eta}(\xi,\eta) := \boldsymbol{\tau}^{\mathrm{n}\eta}\left(\mathbf{x}(\xi,\eta)\right) = \dfrac{\partial \mathbf{x}(\xi,\eta)}{\partial \eta} = \displaystyle\sum_{\mathrm{j}=1}^{\mathrm{N_e}} \frac{\partial \mathrm{N_j}(\xi,\eta)}{\partial \eta}\, \mathbf{x}^{\mathrm{nj}}. \end{cases} \tag{10}$$

Then the surface metric (Jacobian) J^{n} and the outward unit normal $\boldsymbol{\nu}^{\mathrm{n}}$ to the triangular boundary element Γ_{n} are given by:

$$\mathrm{J}^{\mathrm{n}}(\xi,\eta) := \mathrm{J}^{\mathrm{n}}\left(\mathbf{x}(\xi,\eta)\right) = |\boldsymbol{\tau}^{\mathrm{n}\xi}(\xi,\eta) \times \boldsymbol{\tau}^{\mathrm{n}\eta}(\xi,\eta)| \tag{11}$$

and

$$\boldsymbol{\nu}^{\mathrm{n}}(\xi,\eta) := \boldsymbol{\nu}^{\mathrm{n}}\left(\mathbf{x}(\xi,\eta)\right) = \frac{1}{\mathrm{J}^{\mathrm{n}}(\xi,\eta)} \boldsymbol{\tau}^{\mathrm{n}\xi}(\xi,\eta) \times \boldsymbol{\tau}^{\mathrm{n}\eta}(\xi,\eta). \tag{12}$$

Basis Functions. On every triangular boundary element $\Gamma_{\rm n}$, we define the following vectors:

$$\left\{\begin{array}{l} \mathbf{v}^{\rm n1}(\xi,\eta) := \mathbf{v}^{\rm n1}\left(\mathbf{x}(\xi,\eta)\right) = -\dfrac{1}{\mathrm{J}^{\rm n}(\xi,\eta)}\,\boldsymbol{\tau}^{\rm n\eta}(\xi,\eta) \\ \mathbf{v}^{\rm n2}(\xi,\eta) := \mathbf{v}^{\rm n2}\left(\mathbf{x}(\xi,\eta)\right) = \dfrac{1}{\mathrm{J}^{\rm n}(\xi,\eta)}\,\boldsymbol{\tau}^{\rm n\xi}(\xi,\eta) \\ \mathbf{v}^{\rm n3}(\xi,\eta) := \mathbf{v}^{\rm n3}\left(\mathbf{x}(\xi,\eta)\right) = \dfrac{1}{\mathrm{J}^{\rm n}(\xi,\eta)}\,\left[-\boldsymbol{\tau}^{\rm n\xi}(\xi,\eta) + \boldsymbol{\tau}^{\rm n\eta}(\xi,\eta)\right]. \end{array}\right. \tag{13}$$

From definition (13), it follows that the vectors $\mathbf{v}^{\rm ni}(\xi,\eta)$ satisfy the identity:

$$\sum_{\rm i=1}^{3} \mathbf{v}^{\rm ni}(\xi,\eta) = 0, \quad \mathbf{x} = \mathbf{x}(\xi,\eta) \in \Gamma_{\rm n}. \tag{14}$$

Next, we define the incidence function i as follows:

$$\begin{array}{l} i(\cdot,\cdot) : \{1,2,\ldots,\mathrm{M}\} \times \{1,2,\ldots,\mathrm{N}\} \longrightarrow \{0,1,2,3\} \\ (\mathrm{m},\mathrm{n}) \longmapsto i(\mathrm{m},\mathrm{n}) = \left\{\begin{array}{ll} 0 & \text{if } \mathbf{x}^{\rm m} \neq \mathbf{x}^{\rm nj},\ \forall\,\mathrm{j} \in \{1,2,3\} \\ \mathrm{j} & \text{if } \exists\,\mathrm{j} \in \{1,2,3\} : \mathbf{x}^{\rm m} = \mathbf{x}^{\rm nj}. \end{array}\right. \end{array} \tag{15}$$

For every global node $\mathbf{x}^{\rm m}$, $1 \leq \mathrm{m} \leq \mathrm{M}$, we define the set $\mathrm{C_m} \subset \Gamma_{\rm coil}$ of triangular boundary elements $\Gamma_{\rm n}$, $1 \leq \mathrm{n} \leq \mathrm{N}$, adjacent to $\mathbf{x}^{\rm m}$, i.e.

$$\mathrm{C_m} := \bigcup_{i(\mathrm{m},\,\mathrm{n}) \,\overline{=}\, 1}^{\mathrm{N}} \Gamma_{\rm n}, \qquad 1 \leq \mathrm{m} \leq \mathrm{M}. \tag{16}$$

The vector basis function $\mathbf{f}^{\rm m}$ associated to the global node $\mathbf{x}^{\rm m}$ is defined by

$$\mathbf{f}^{\rm m}(\cdot) : \Gamma_{\rm coil} \longrightarrow \mathbb{R}^3, \qquad \mathbf{f}^{\rm m}(\mathbf{x}) = \left\{\begin{array}{ll} \mathbf{v}^{{\rm n},i({\rm m},{\rm n})}(\mathbf{x}) & \text{if } \mathbf{x} \in \mathrm{C_m} \\ \mathbf{0} & \text{if } \mathbf{x} \notin \mathrm{C_m} \end{array}\right. \tag{17}$$

and, clearly, its support is a subset of $\mathrm{C_m}$, i.e. $\{\mathbf{x} \in \Gamma_{\rm coil}\,|\mathbf{f}^{\rm m}(\mathbf{x}) \neq \mathbf{0}\} \subset \mathrm{C_m}$.

Surface Current Density. The current density $\mathbf{J}^{\rm coil}$ on the coil surface $\Gamma_{\rm coil}$ is then approximated by

$$\mathbf{J}^{\rm coil}(\mathbf{x}) \approx \sum_{\rm m=1}^{\mathrm{M}} \mathrm{I_m}\mathbf{f}^{\rm m}(\mathbf{x}) = \sum_{\rm m=1}^{\mathrm{M}} \mathrm{I_m} \sum_{i(\mathrm{m},\,\mathrm{n}) \,\overline{=}\, 1}^{\mathrm{N}} \mathbf{v}^{{\rm n},i({\rm m},{\rm n})}(\mathbf{x}), \quad \mathbf{x} \in \Gamma_{\rm coil}, \tag{18}$$

where $\mathrm{I_m} \in \mathbb{R}$, $1 \leq \mathrm{m} \leq \mathrm{M}$, are unknown coefficients that correspond to the stream function intensities. For direct problems, the stream function intensities are determined from appropriate boundary conditions, while in the case of inverse problems, they are obtained by solving a minimisation problem.

It should be noted that the degree of the approximation (18) for the surface current density $\mathbf{J}^{\rm coil}$ is one unit less than the degree of the triangular boundary elements $\Gamma_{\rm n}$, $1 \leq \mathrm{n} \leq \mathrm{N}$, since the vectors $\mathbf{v}^{\rm ni}(\xi,\eta)$, $1 \leq \mathrm{i} \leq 3$, are related to the derivatives of the geometrical shape functions $\mathrm{N_i}(\xi,\eta)$, $1 \leq \mathrm{i} \leq \mathrm{N_e}$, associated with the triangular boundary element $\Gamma_{\rm n}$, see eqns. $(9)-(13)$. More precisely, linear, quadratic and cubic triangular boundary elements provide constant, linear and quadratic approximations for the surface current density, respectively. From eqns. (12) and (13) it follows that for every triangular boundary element $\Gamma_{\rm n}$ the vectors $\mathbf{v}^{\rm ni}(\xi,\eta)$, $1 \leq \mathrm{i} \leq 3$, and the outward unit normal vector $\boldsymbol{\nu}^{\rm n}(\xi,\eta)$ are orthogonal and hence expression (18) enforces the approximated current density $\mathbf{J}^{\rm coil}$ to lie in the plane tangent to the coil surface $\Gamma_{\rm coil}$, i.e. condition (3_2) is satisfied. Furthermore, the interpolation given by eqn. (18) is divergence-free pointwise, i.e. condition (3_1) is satisfied, since $\nabla \cdot \dfrac{\partial \mathbf{x}}{\partial \xi} = \dfrac{\partial}{\partial \xi}\left(\nabla \cdot \mathbf{x}\right) = 0$ and $\nabla \cdot \dfrac{\partial \mathbf{x}}{\partial \eta} = \dfrac{\partial}{\partial \eta}\left(\nabla \cdot \mathbf{x}\right) = 0$.

Magnetic Vector Potential and Magnetic Flux Density. According to eqns. (6), (7) and (18), the magnetic vector potential $\mathbf{A}$ and magnetic flux density $\mathbf{B}$ are approximated by

$$\mathbf{A}(\mathbf{x}) \approx \frac{\mu_0}{4\pi} \sum_{\mathrm{m}=1}^{\mathrm{M}} \mathrm{I_m} \sum_{\substack{\mathrm{n}=1 \\ i(\mathrm{m},\mathrm{n}) \neq 0}}^{\mathrm{N}} \int_{\Gamma_\mathrm{n}} \frac{\mathbf{v}^{\mathrm{n},i(\mathrm{m},\mathrm{n})}(\mathbf{x}')}{|\mathbf{x}-\mathbf{x}'|} \, \mathrm{d}\Gamma(\mathbf{x}'), \qquad \mathbf{x} \in \mathbb{R}^3 \tag{19}$$

and

$$\mathbf{B}(\mathbf{x}) \approx \frac{\mu_0}{4\pi} \sum_{\mathrm{m}=1}^{\mathrm{M}} \mathrm{I_m} \sum_{\substack{\mathrm{n}=1 \\ i(\mathrm{m},\mathrm{n}) \neq 0}}^{\mathrm{N}} \int_{\Gamma_\mathrm{n}} \frac{-(\mathbf{x}-\mathbf{x}') \times \mathbf{v}^{\mathrm{n},i(\mathrm{m},\mathrm{n})}(\mathbf{x}')}{|\mathbf{x}-\mathbf{x}'|^3} \, \mathrm{d}\Gamma(\mathbf{x}'), \qquad \mathbf{x} \in \mathbb{R}^3. \tag{20}$$

Description of the Algorithm

If the z−component of the magnetic flux density $\mathbf{B}$ is known at L points in the region of interest Ω then the BEM discretisation of the inverse problem (8) yields the following system of linear algebraic equations

$$\mathbf{H}\,\mathbf{I} = \widetilde{\mathbf{B}}_\mathrm{z}. \tag{21}$$

Here $\mathbf{H} \in \mathbb{R}^{\mathrm{L}\times\mathrm{M}}$ is the BEM matrix used for computing the z−component of the magnetic flux density $\mathbf{B}$ given by eqn. (20) calculated at L points in the region of interest Ω, $\widetilde{\mathbf{B}}_\mathrm{z} = (\widetilde{\mathrm{B}}_\mathrm{z}^1, \ldots, \widetilde{\mathrm{B}}_\mathrm{z}^\mathrm{L})^\mathrm{T} \in \mathbb{R}^\mathrm{L}$ is a vector containing the z−component of the magnetic flux density at L points in the region of interest Ω and $\mathbf{I} \in \mathbb{R}^\mathrm{M}$ is a vector containing the unknown values of the stream function $\mathrm{I_m}$, $1 \leq \mathrm{m} \leq \mathrm{M}$, at the global nodes.

The system of linear algebraic equations (21) cannot be solved by direct methods, such as the least-squares method, since such an approach would produce an inaccurate and/or physically meaningless solution due to the large value of the condition number of the system matrix $\mathbf{H}$ which increases dramatically as the BEM mesh is refined. Several regularization procedures have been developed to solve such ill-conditioned systems [6, 7]. In the sequel, we only consider the Tikhonov regularization method and for further details on this method, we refer the reader to [6].

Magnetic Energy and Regularization. The magnetic energy W defined by

$$\mathrm{W} = \frac{1}{2} \int_{\Gamma_\mathrm{coil}} \mathbf{J}^\mathrm{coil}(\mathbf{x}) \cdot \mathbf{A}(\mathbf{x}) \, \mathrm{d}\Gamma(\mathbf{x}) \tag{22}$$

is approximated, according to eqns. (18) and (19), as

$$\mathrm{W} \approx \frac{1}{2} \sum_{\mathrm{m}=1}^{\mathrm{M}} \sum_{\mathrm{n}=1}^{\mathrm{M}} \mathrm{L_{mn}}\, \mathrm{I_n}\, \mathrm{I_m}, \tag{23}$$

where the components of the inductance matrix $\mathbf{L} = [\mathrm{L_{mn}}] \in \mathbb{R}^{\mathrm{M}\times\mathrm{M}}$ are given by

$$\mathrm{L_{mn}} := \frac{\mu_0}{4\pi} \sum_{\substack{\mathrm{m}'=1 \\ i(\mathrm{m},\mathrm{m}') \neq 0}}^{\mathrm{N}} \sum_{\substack{\mathrm{n}'=1 \\ i(\mathrm{n},\mathrm{n}') \neq 0}}^{\mathrm{N}} \int_{\Gamma_{\mathrm{m}'}} \int_{\Gamma_{\mathrm{n}'}} \frac{\mathbf{v}^{\mathrm{m}',i(\mathrm{m},\mathrm{m}')}(\mathbf{x}) \cdot \mathbf{v}^{\mathrm{n}',i(\mathrm{n},\mathrm{n}')}(\mathbf{x}')}{|\mathbf{x}-\mathbf{x}'|} \, \mathrm{d}\Gamma(\mathbf{x}') \, \mathrm{d}\Gamma(\mathbf{x}). \tag{24}$$

The approximated magnetic energy W given by eqn. (23) is a quadratic and positive definite form which induces the following discrete energy norm:

$$\|\mathbf{I}\|_\mathrm{W}^2 := \|\widetilde{\mathbf{L}}\mathbf{I}\|^2 = \sum_{\mathrm{m}=1}^{\mathrm{M}} \sum_{\mathrm{n}=1}^{\mathrm{M}} \mathrm{L_{mn}}\, \mathrm{I_n}\, \mathrm{I_m} = 2\mathrm{W}, \tag{25}$$

where $\widetilde{\mathbf{L}} \in \mathbb{R}^{\mathrm{M}\times\mathrm{M}}$ such that $\widetilde{\mathbf{L}}^\mathrm{T} = \widetilde{\mathbf{L}}$ and $\mathbf{L} = \widetilde{\mathbf{L}}^\mathrm{T}\widetilde{\mathbf{L}}$.

The Tikhonov regularized solution $\mathbf{I}_\lambda$ to the inverse problem (8) is sought as [5]

$$\mathbf{I}_\lambda \in \mathbb{R}^\mathrm{M} : \quad \mathcal{F}_\lambda(\mathbf{I}_\lambda) = \min_{\mathbf{I}\in\mathbb{R}^\mathrm{M}} \mathcal{F}_\lambda(\mathbf{I}), \tag{26}$$

where $\mathcal{F}_\lambda$ is the Tikhonov functional given by

$$\mathcal{F}_\lambda(\cdot) : \mathbb{R}^{\mathrm{M}} \longrightarrow [0,\infty), \quad \mathcal{F}_\lambda(\mathbf{I}) = \tfrac{1}{2}\|\mathbf{H}\,\mathbf{I} - \widetilde{\mathbf{B}}_{\mathrm{z}}\|^2 + \tfrac{1}{2}\lambda\|\mathbf{I}\|^2_{\mathrm{W}}, \tag{27}$$

with $\lambda > 0$ the regularization parameter to be chosen. Formally, the Tikhonov regularized solution $\mathbf{I}_\lambda$ of the minimisation problem (26) is given by the solution of the regularized normal equation [6]

$$\left(\mathbf{H}^{\mathrm{T}}\mathbf{H} + \lambda\widetilde{\mathbf{L}}^{\mathrm{T}}\widetilde{\mathbf{L}}\right)\mathbf{I}_\lambda = \mathbf{H}^{\mathrm{T}}\,\widetilde{\mathbf{B}}_{\mathrm{z}}. \tag{28}$$

Numerical Results

In order to present the performance of the proposed method, we solve the inverse problem (8) for a hemispherical coil $\Gamma_{\mathrm{coil}} = \partial\mathrm{B}\,(\mathbf{0},\mathrm{R}) \cap \{\mathrm{z} \geq 0\}$, where $\mathrm{R} = 0.175\,\mathrm{m}$, whilst the region of interest is a sphere of radius $\mathrm{r} = 0.065\,\mathrm{m}$ and centered at $\mathbf{x}^{\mathrm{c}} = (0,0,0.081)$, i.e. $\Omega = \mathrm{B}\,(\mathbf{x}^{\mathrm{c}},\mathrm{r})$. Since the geometry of the coil considered in this paper is symmetrical with respect to the z−axis, it is sufficient to investigate only the design of x− and z−gradients, i.e. $\widetilde{\mathrm{B}}_{\mathrm{z}}\,(\mathbf{x}) = \mathrm{G}_{\mathrm{x}}\,\mathrm{x}$, $\mathbf{x} \in \Omega$ and $\widetilde{\mathrm{B}}_{\mathrm{z}}\,(\mathbf{x}) = \mathrm{G}_{\mathrm{z}}\,\mathrm{z}$, $\mathbf{x} \in \Omega$, where $\mathrm{G}_{\mathrm{x}} = \mathrm{G}_{\mathrm{z}} = 1.0\,\mathrm{T\,m^{-1}}$.

The choice of the regularization parameter λ in the minimisation process of the Tikhonov functional (27) is crucial for obtaining a stable, accurate and physically correct numerical solution $\mathbf{I}_\lambda$. The optimal value λ_{opt} of the regularization parameter λ should be chosen such that a trade-off between the two quantities $\|\mathbf{H}\,\mathbf{I} - \widetilde{\mathbf{B}}_{\mathrm{z}}\|$ and $\|\mathbf{I}\|_{\mathrm{W}} = \|\widetilde{\mathbf{L}}\mathbf{I}\|$ involved in the minimisation of the functional (27) is attained. To do so, we introduce a global measure for error that relates the computed and desired z−components of the magnetic flux density in the region of interest Ω, namely the maximum relative percentage error

$$\mathrm{Err}\,(\mathrm{B_z};\lambda) = \max_{\mathbf{x}\in\Omega} \frac{|\mathrm{B}^{\lambda}_{\mathrm{z}}(\mathbf{x}) - \widetilde{\mathrm{B}}_{\mathrm{z}}(\mathbf{x})|}{|\widetilde{\mathrm{B}}_{\mathrm{z}}(\mathbf{x})|} \times 100 \tag{29}$$

where $\mathrm{B}^{\lambda}_{\mathrm{z}}(\mathbf{x})$ is the numerical z−component of the magnetic flux density calculated at the point $\mathbf{x}$ in the region of interest Ω, for a given regularization parameter λ, by employing the proposed BEM-based algorithm. On assuming that a deviation $\epsilon > 0$ from the desired z−component of the magnetic flux density $\widetilde{\mathrm{B}}_{\mathrm{z}}$ is admissible in Ω, such that

$$\widetilde{\mathrm{B}}^{\epsilon}_{\mathrm{z}}(\mathbf{x}) := \widetilde{\mathrm{B}}_{\mathrm{z}}(\mathbf{x})\,(1 \pm \epsilon)\,, \qquad \mathbf{x} \in \Omega, \tag{30}$$

then the choice of the optimal regularization parameter λ_{opt} is made by employing the maximum relative percentage error given by eqn. (29) and the admissible level of noise in $\mathrm{B_z}|_\Omega$ defined by relation (30), namely

$$\lambda_{\mathrm{opt}} = \max\left\{\lambda > 0 \middle| \mathrm{Err}\,(\mathrm{B_z};\lambda) \leq \epsilon\right\}. \tag{31}$$

The numerical solution $\mathbf{I}_\lambda$ of the regularized system of normal equations (28), with $\lambda = \lambda_{\mathrm{opt}}$ given by eqn. (31), provides only a discrete distribution of the stream function at the global nodes of the BEM mesh employed. However, these discrete values should be extended to a continuous distribution of the numerical stream function over the entire coil surface Γ_{coil} and this is achieved by employing the contours of the stream function using its discrete distribution and the Matlab (The Mathworks, Inc., Natick, MD, USA) contouring function. Hence, in the sequel, the numerically retrieved solutions of the inverse problem given by eqn. (8) are presented in terms of the contours of the stream function as described above.

Figures 1(a) and (b) present the contours of the stream function in the so-called Lambert cylindrical equal-area projection, i.e. the $\theta - \cos\phi$ plane, corresponding to the hemispherical x− and z−gradient coils, respectively, obtained using the optimal regularization parameter λ_{opt} given by eqn. (31), $\mathrm{L} = 351$ internal points in the region of interest and $\mathrm{N} = 2840$ linear, quadratic and cubic triangular boundary elements. From these figures it can be seen that, for the examples investigated in this study, the numerical results retrieved using linear boundary elements are more inaccurate than those obtained by employing higher-order boundary elements, with the mention that there are no major quantitative differences between the contours of the stream function corresponding to quadratic and

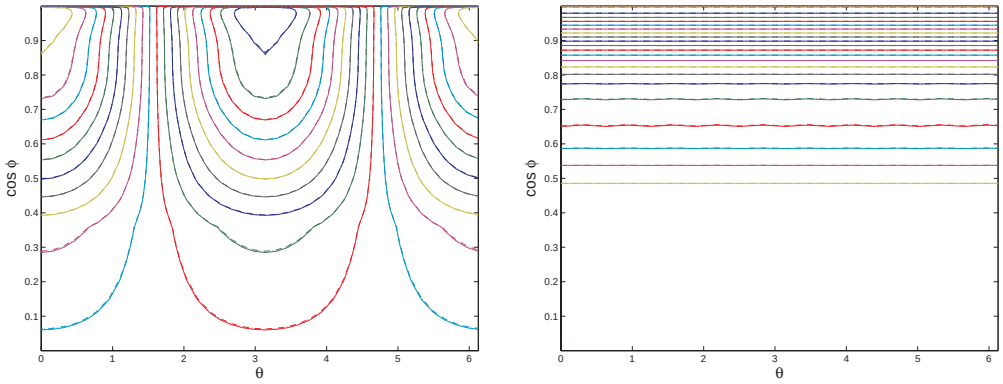

(a) (b)

Figure 1: The contours of the stream function corresponding to the hemispherical (a) x−, and (b) z−gradient coils, obtained using $\lambda = \lambda_{\text{opt}}$, L = 351 internal points in Ω and N = 2840 linear (——), quadratic (− −) and cubic ($\cdots$) triangular boundary elements.

cubic triangular elements.

Although not presented here, it is reported that the Tikhonov regularization method, in conjunction with the proposed divergence-free BEM, is also convergent with respect to increasing the number of boundary elements used to discretise the coil surface Γ_{coil}. Furthermore, the finer the BEM mesh size is then the smoother contours of the stream function corresponding to the hemispherical x− and z−gradient coils. It should be noted that similar results have been obtained for other coil geometries.

Conclusions

In this paper, we have investigated the design of MRI hemispherical gradient coils by considering the reconstruction of a divergence-free surface current distribution from knowledge of the magnetic flux density in a prescribed region of interest. This inverse problem was formulated in the framework of static electromagnetism using its corresponding integral representation according to potential theory. In order to retrieve an accurate and physically correct numerical solution of this inverse problem, a minimisation problem for the Tikhonov functional was solved, in conjunction with a novel higher-order BEM which satisfies the continuity equation for the current density. The numerical solutions were presented in terms of the contours of the stream function and using various types of boundary elements. For the examples analysed, it was proved the efficiency of the proposed method, as well as an improvement in the accuracy of the numerical solutions in the case of higher-order elements. However, there are no major quantitative differences between the contours of the stream function corresponding to quadratic and cubic triangular elements.

References

[1] R. Turner, *Magnetic Resonance Imaging*, **11**, 903-920 (1993).
[2] J. Leggett, S. Crosier, S. Blackband and R.W. Bowtell, *Concepts in Magnetic Resonance B: Magnetic Resonance Engineering*, **16**, 38-46 (2003).
[3] D. Green, J. Leggett, and R.W. Bowtell, *Magnetic Resonance in Medicine*, **54**, 656-668 (2005).
[4] J.D. Jackson, *Classical Electrodynamics*, John Wiley & Sons (1962).
[5] C.A. Brebbia, J.F.C. Telles, and L.C. Wrobel, *Boundary Element Techniques*, Springer-Verlag (1984).
[6] A.N. Tiknonov, and V.Y. Arsenin, *Methods for Solving Ill-Posed Problems*, Nauka (1986).
[7] P.C. Hansen, *Rank-Deficient and Discrete Ill-Posed Problems: Numerical Aspects of Inversion*, SIAM (1998).

The Green Element Method Applied to Plate Bending

Akpofure E. Taigbenu[1] **& Alex Elvin**[2]
School of Civil and Environmental Engineering, University of the Witwatersrand. P. Bag 3, Johannesburg, WITS 2050. South Africa.
[1]*Email: aetaigbenu@civil.wits.ac.za*
[2]*Email: elvin@civil.wits.ac.za*

Abstract
The biharmonic equation that describes plate deflections under transverse loading is formulated as two coupled harmonic equations. Using the logarithmic fundamental solution and implementing the integral equations obtained from applying Green's identity in an element-by-element fashion, the deflections, moments and their normal slopes can be obtained at each node. By adopting this method, exceptionally high accuracy is achieved in the primary variables and their normal derivatives that are calculated directly by the same order of Lagrange-type interpolation functions. The compatibility conditions for the normal derivatives of deflection and moments at internal nodes are prescribed in a novel manner that avoids any numerical artefacts. Numerical examples are used to demonstrate the accuracy of the current formulation.

Keywords: *Plate bending, Biharmonic equation, Poisson equation, Green element method.*

1 Introduction

The biharmonic equation which governs flexural deflection of thin plates (commonly referred to as Kirchhoff plates) is solved as two coupled harmonic equations of the Poisson type. This approach of considering the biharmonic as two Poisson-type equation had been adopted by quite a number of investigators in boundary integral circles in the past [1, 2, 3, 4], but what is unique in the current formulation is the solution methodology of the coupled Poisson-type equations. The integral equations from applying Green's identity are solved element-by-element so that the solution space comprises the deflection, moment, rotation and shear force in the normal direction to the boundary of each element. In essence, the solution in each element is complete, and solution information at any point other than grid points of the elements is obtained by implementing the integral equations only in those elements in which the point is located. This represents tremendous savings in computing resources. Furthermore, the current formulation, referred to as the flux-based Green element formulation, achieves exceptionally high accuracy with coarse discretization because it directly calculates the rotations and shear forces in the normal direction to the boundary of the elements. This is demonstrated with an example in which less than 10% of the nodal points of the indirect radial basis function network (IRBFN) collocation formulation of [3] are used in GEM to achieve comparable accuracy.

The novelty of the current formulation in applying the compatibility conditions in the normal directional rotations and shear forces at internal nodes is also worth mentioning. The universality of this compatibility condition makes it equally applicable to the rotations and the shear forces. That condition states that the integration of the normal directional rotations and the shear forces about the internal node equals zero. Three examples are used to demonstrate the accuracy of the current formulation for plate bending problems.

2 Governing Equations

The deflection of thin isotropic and homogeneous plates under transverse loads is given by

$$D\nabla^4 w = p \tag{1}$$

where w is the transverse deflection of the plate, $p \equiv p(x, y)$ is the load distribution, ∇ is the gradient operator in two dimensions and D is the stiffness of the plate given by

$$D = \frac{Eh^3}{12(1-\upsilon^2)} \tag{2}$$

where E is the Young's modulus of elasticity, h is the thickness of plate, and υ is the Posson's ratio. Eq (1) is converted to two harmonic Poisson-type equations given by

$$\nabla^2 w = M \tag{3}$$

and

$$\nabla^2 M = p / D = f \tag{4}$$

where the moment $M = (M_x + M_y)/(1+\upsilon)$ is expressed in the terms of the moments in the x and y directions and the Posson ratio. Two broad types of boundary conditions are addressed. The first is the case when one condition is specified for each of the equations and the second is when equation (3) is over specified with two boundary conditions for the deflection w and its normal derivative or the rotation in the normal direction. The first type of conditions makes for a much easier solution of eqs (3) and (4); in fact both equations can be decoupled and solved independently with eq (4) being solved first, and the results for M are then the input for eq (3). The second type of conditions requires that both equations be solved in a coupled manner as there are no conditions for eq (4). The approach which is used here solves the two equations in a coupled manner irrespective of the boundary data type. The solutions to eqs (3) and (4) are achieved in a Green element sense by transforming the differential equations into integral equations using Green's second identity and the free-space Green's function for the Laplace operator and implementing those integral equations in an element-by-element fashion.

3 Green element formulation

The free-space Green's function $G = \ln(r - r_i)$ that is derived from Laplace equation $\nabla^2 G = \partial(r - r_i)$ for the infinite space $\{r = (x, y) : x, y \in (-\infty, \infty)\}$ is used to derive integral equations within a spatial element Ω^e with closed boundary Γ^e that constitutes one of the elements used to discretize the entire computational region Ω. The integral equations are given by [5]

$$-\lambda w_i + \int_{\Gamma^e} \left(w \nabla G \cdot \mathbf{n} - G \nabla w \cdot \mathbf{n} \right) ds + \iint_{\Omega^e} G\, M\, dA = 0 \tag{5}$$

$$-\lambda M_i + \int_{\Gamma^e} \left(M \nabla G \cdot \mathbf{n} - G \nabla M \cdot \mathbf{n} \right) ds + \iint_{\Omega^e} G\, f\, dA \tag{6}$$

where λ is the nodal angle at the source point $r_i = (x_i, y_i)$ that is obtained from integrating the dependent variable with the Dirac delta function in a Cauchy sense and $\mathbf{n}$ is the outward pointing normal on the elemental boundary. It should be noted that in arriving at eqs (5) and (6), no approximation has been introduced despite the fact that the integrations are carried out element by element. It is in interpolating for the primary variables w and M and their normal derivatives, namely the rotation $\theta = \nabla w \cdot \mathbf{n}$ and the shear force $V = \nabla M \cdot \mathbf{n}$, that approximations are introduced into the formulation. Essentially, it is how well the unknown quantities are approximated that determines the accuracy of the numerical calculations. The Lagrange-type interpolation functions are used. The 4-node linear and the 8-node quadratic rectangular elements have been used in this paper. Introducing these interpolations into eqs (5) and (6) and carrying out the integrations results in the matrix equations

$$R_{ij} w_j - L_{ij} \theta_j + S_{ij} M_j = 0 \tag{7}$$

$$R_{ij} M_j - L_{ij} V_j + S_{ij} f_j = 0 \tag{8}$$

where

$$R_{ij} = \int_{\Gamma^e} N_j \nabla G(r, r_i) \cdot \mathbf{n}\, ds - \delta_{ij}\lambda, \qquad L_{ij} = \int_{\Gamma^e} N_j G(r, r_i)\, ds, \qquad S_{ij} = \iint_{\Omega^e} N_j G(r, r_i)\, dA \tag{9}$$

It is worth pointing out the similarity in the element matrices R_{ij}, L_{ij} and S_{ij} in the two equations (7) and (8). This is exploited during the coding of the formulation in order to enhance computational efficiency. Furthermore, there are four unknowns at each node, namely the deflection w, the moment M, the rotation θ in the normal direction at the boundaries of the element and the shear force V also in the normal direction. The formulation calculates all these quantities in a novel way that is subsequently described. In eq (9), the interpolation functions have been denoted as N_j with respect to the grid point

or node j. All the integrations in eq (9) are done analytically because the logarithmic Green's function in combination with polynomial functions is readily integratable. That further preserves the high level of accuracy that characterizes this formulation. Eqs (7) and (8) are now aggregated for all elements used in discretizing the computational domain and simplified to

$$\mathbf{Rw} - \mathbf{L\theta} + \mathbf{SM} = 0 \tag{10}$$

$$\mathbf{RM} - \mathbf{LV} + \mathbf{Sf} = 0 \tag{11}$$

4 Compatibility and equilibrium conditions at internal nodes

Whatever boundary data set is available, eqs (10) and (11) are not sufficient to produce the solutions for all the degrees of freedom. At an internal node, there are $(C+1)\times 2$ unknowns to be calculated, where C is the number of elements meeting at the internal node or the number of elements shared by the internal node. Taking the case shown in Fig. 1, the value of C is 5. However, the number of equations generated for the internal node taken as the source node by carrying the element integrations as dictated by eqs (7) and (8) is $C\times 2$. This means that at an internal node there are two more unknown degrees of freedom than the number of equations. This is not the case with the external nodes where the two prescribed boundary conditions give the two extra equations/conditions required. This is the closure problem that has been recognized in boundary element circles. In the past, the closure problem made it unattractive to carry out direct calculations of the normal derivatives of the primary variable within internal boundaries in singular boundary integral formulations. Those calculations were done only on external boundaries where the closure problem was eliminated by the prescribed boundary conditions. Previous Green element formulations replaced these normal derivatives at internal boundaries by with their difference expressions in terms of the primary variable [6, 7]. In certain boundary element codes, this closure problem was resolved by artificially creating additional internal nodes and relocating them by small distances from their original location of the internal node along the internal segments [8]. Such an approach is a numerical artefact that usually reconfigures the geometry at the internal nodes to suit the numerical formulation.

Here we resolve the closure problem in a novel manner by generating two additional equations which are the compatibility conditions for the rotation θ and equilibrium condition for the shear force V in the normal directions on the sides of the elements that meet at the internal node. The derivation of this compatibility and equilibrium relationships is presented in detail in manuscripts that are being prepared. The relationship is the same for θ and V, making it have a universal appeal. It is sufficient to mention here that the proof of the compatibility equilibrium relationships is based on integrating the normal derivative of the primary (dependent) variable around a circle of small radius ε centred at the internal node. In the limit as the radius tends to zero, the integral equals the value of discontinuity of the primary variable at the internal point. Where no discontinuity exists, the integral equals zero. This can be stated as

$$\oint \nabla w \cdot \mathbf{n}\, dn = \oint \frac{\partial w}{\partial n}\, dn = w^{(\beta=2\pi)} - w^{(\beta=0)} = 0 \tag{12}$$

To implement eqn (12) numerically,

$$\oint \frac{\partial w}{\partial n} dn = \underset{\varepsilon\to 0}{Limit}\, 2\pi \int_0^{2\pi} \theta\, d\beta \approx \sum_{i=1}^{C} \theta_i \Delta\beta_i = 0 \tag{13}$$

See Fig. 1. Eq (12) is the same for the shear force in the normal direction. When rectangular elements are used to discretize the computational domain, the included angles $\Delta\beta_i$ have a uniform value of $\pi/2$ for each of the four elements meeting at the internal node. In that case, eq (13) becomes

$$\oint \frac{\partial w}{\partial n} dn = \underset{\varepsilon\to 0}{Limit}\, 2\pi \int_0^{2\pi} \theta\, d\beta \approx \sum_{i=1}^{4} \theta_i \Delta\beta_i = \frac{\pi}{2} \sum_{i=1}^{4} \theta_i = \sum_{i=1}^{4} \theta_i = 0 \tag{14}$$

The additional equations generated by the compatibility condition for θ and V along the line of eq (13) are then used to resolve the closure problem at internal nodes.

The boundary conditions at external boundaries are introduced into eqs (10) and (11), and both equations are solved in a coupled manner. The equations are assembled into a matrix form

$$\mathbf{A\,z} = \mathbf{B} \tag{15}$$

where the matrix $\mathbf{A}$ contains elements from matrices $\mathbf{R}$ and $\mathbf{L}$, while the known right-hand-side vector $\mathbf{B}$ accounts from the boundary and load data, and the vector $\mathbf{z}$ comprise the unknowns

$$\mathbf{z} = \begin{Bmatrix} \mathbf{w} \\ \mathbf{M} \\ \boldsymbol{\theta} \\ \mathbf{V} \end{Bmatrix} \tag{16}$$

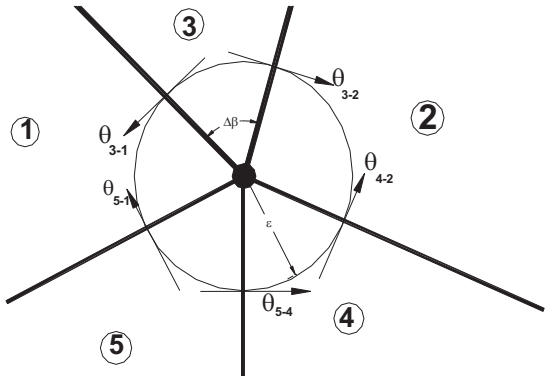

Figure 1: Normal directional rotations at an internal node.

Two unique features of the current Green element formulation, which we shall refer to as a flux-based GEM because of the retention of the normal derivatives of the primary variable (surrogate for normal fluxes) at every node, are (a) the attainment of high solution accuracy with coarse discretization and (b) the provision of the complete solution information for each element. The first feature is due to the fact that the only approximation in the formulation comes from the interpolation of the unknown quantities. Thus, the escalation in the number of degrees of freedom due to the evaluation of the primary variable and their normal derivatives at every node is ameliorated by the coarse grid required to generate accurate solutions. The second feature allows the calculations of the solution at any point other than the grid points to involve only integrations within the element in which the point is located. No reference is made to other elements in the computational region. That represents enormous computational savings when solutions are required at points of interest other than grid points. Thus, the elemental solutions are complete.

5 Numerical Examples

Example 1. The first example is a classical case that has been used by other investigators to validate their numerical schemes [3, 9]. It belongs to the first type boundary data in which one boundary condition exist for each of eqs (3) and (4). The computational region is a square plate of unit length, $p = 0$, and the boundary conditions for the deflection and moments are obtained from the analytical solution:

$$w = \frac{1}{2}\left[x \sin x \cosh y - x \cos x \sinh y\right];\ M = \cos x \cosh y + \sin x \sinh y\ ;\ x \in [0,1], y \in [0,1] \tag{17}$$

The Green element calculations are carried out with 16 quadratic rectangular elements comprising a total of 65 nodes, which is less than 10% of the 727 nodal points used by Mai-Duy and Tang-Cong [3] in their indirect radial basis function network (IRBFN) collocation formulation. The solutions for w, M, rotation in the x and y directions ($\theta_x = \partial w/\partial x$ and $\theta_y = \partial w/\partial y$) and the shear force in the x and y directions ($V_x = \partial M/\partial x$ and $V_y = \partial M/\partial y$) are presented along the lines that go through the centre of the domain, that is $x = 0.5$ and $y = 0.5$. The results for the exact and GEM solutions are presented in Figs. 2 through 5. There is excellent agreement between the GEM and exact solutions. Typical values of the

mean deviations between the two solutions are 1.4×10^{-5} for the deflections, 2.3×10^{-5} for the moments, 1.2×10^{-4} for the rotations and 1.4×10^{-4}. It is significant to observe the level of accuracy of this formulation with a coarse grid not only in calculating the deflections and moments, as most other numerical methods achieve, but also in the rotations and shear forces.

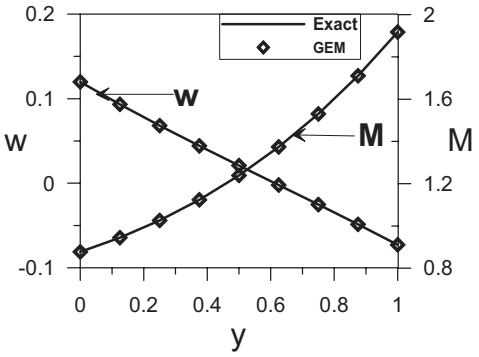

Figure 2: GEM and exact solutions for w and M of example 1 along $x = 0.5$.

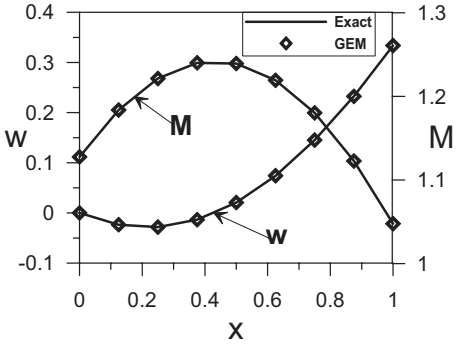

Figure 3: GEM and exact solutions for w and M of example 1 along $y = 0.5$.

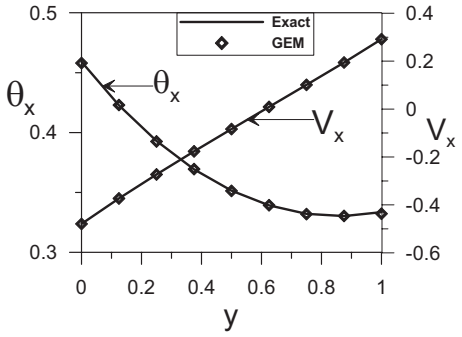

Figure 4: GEM and exact solutions for θ_x and V_x of example 1 along $x = 0.5$.

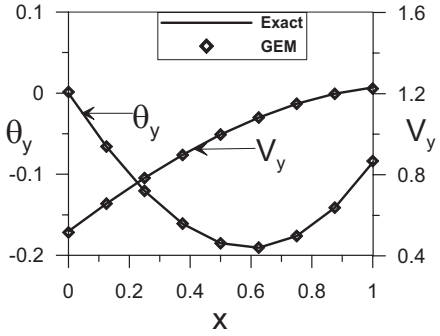

Figure 5: GEM and exact solutions for θ_y and V_y of example 1 along $y = 0.5$.

Example 2. The second example is another classical problem of a rectangular plate that is simply supported on all sides and subjected to a uniform transverse loading q. This example belongs to the first type of boundary data because the deflection and moments are specified on the boundary. The GEM calculations are carried with four sets of discretizations: 2 × 2 and 4 × 4 quadratic rectangular elements and 4 × 4 and 8 × 8 linear rectangular elements. The numerical results are compared with the Fourier series solutions presented in [10] for the maximum deflections and moments at the centre of the plate (Table 1) and the maximum shear force in the x direction at $(a, b/2)$ and in the y direction at $(a/2, 0)$ (Table 2) for plate dimensions: $b/a = 1, 1.5, 2$. The results have been achieved by taking unit values of a and q, and $\upsilon = 0.3$. Taking into account the computational difficulties with correct reproduction of the boundary conditions at the corners, the GEM solutions, particularly with quadratic elements, are excellent.

Example 3. The third example is a problem of a rectangular plate that is clamped on all sides and subjected to a uniform transverse loading q. This example belongs to the second type of boundary conditions in which the conditions for eq (3) are fully specified while eq (4) is under-specified. The

deflections and rotations are zero on the all external boundaries. The GEM formulation carries out the calculations in one sweep without iterations. The presence of the moment in both equations allows for the coupling. Using unit values for a and q, the Green element solutions with quadratic and linear rectangular elements, and the Fourier series solutions from [10] are presented for the deflection and moments at the centre of the plate in Table 3. As expected the results obtained with the 4 × 4 quadratic rectangular element are most accurate, and they have good agreement (lees than 2%) with the Fourier series analytical solution.

Solutions for $w_{\max}$							
$\frac{b}{a}$	Analytic	Quadratic			Linear		
		Grid	GEM	Rel. Error %	Grid	GEM	Rel. Error %
1	0.00406	2 × 2	0.00391	3.7	4 × 4	0.00366	9.9
		4 × 4	0.00406	0.0	8 × 8	0.00384	5.4
1.5	0.00772	2 × 2	0.00748	3.1	4 × 4	0.00703	8.9
		4 × 4	0.00772	0.0	8 × 8	0.00739	4.3
2.0	0.01013	2 × 2	0.00990	2.3	4 × 4	0.00940	7.2
		4 × 4	0.01014	0.1	8 × 8	0.00972	4.1
Solutions for $M_{\max}$							
$\frac{b}{a}$	Analytic	Quadratic			Linear		
		Grid	GEM	Rel. Error %	Grid	GEM	Rel. Error %
1	0.0737	2 × 2	0.0736	0.1	4 × 4	0.0734	0.4
		4 × 4	0.0737	0.0	8 × 8	0.0724	1.8
1.5	0.1008	2 × 2	0.1006	0.2	4 × 4	0.1008	0.0
		4 × 4	0.1009	0.1	8 × 8	0.1000	0.8
2.0	0.1139	2 × 2	0.1133	0.5	4 × 4	0.1145	0.5
		4 × 4	0.1140	0.1	8 × 8	0.1128	1.0

Table 1: GEM and Fourier series solution of example 2 for $w_{\max}$ and $M_{\max}$

Solutions for $(V_x)_{\max}$							
$\frac{b}{a}$	Analytic	Quadratic			Linear		
		Grid	GEM	Rel. Error %	Grid	GEM	Rel. Error %
1.0	0.338	2 × 2	0.330	2.4	4 × 4	0.336	0.6
		4 × 4	0.338	0.0	8 × 8	0.333	1.5
1.5	0.424	2 × 2	0.410	3.3	4 × 4	0.422	0.5
		4 × 4	0.423	0.2	8 × 8	0.419	1.2
2.0	0.465	2 × 2	0.446	4.1	4 × 4	0.464	0.2
		4 × 4	0.464	0.2	8 × 8	0.462	0.7
Solutions for $(V_y)_{\max}$							
$\frac{b}{a}$	Analytic	Quadratic			Linear		
		Grid	GEM	Rel. Error %	Grid	GEM	Rel. Error %
1	0.338	2 × 2	0.330	0.4	4 × 4	0.336	0.6
		4 × 4	0.338	0.0	8 × 8	0.333	1.5
1.5	0.363	2 × 2	0.363	0.0	4 × 4	0.364	0.3
		4 × 4	0.367	1.1	8 × 8	0.358	1.4
2.0	0.370	2 × 2	0.380	2.7	4 × 4	0.374	1.1
		4 × 4	0.376	1.6	8 × 8	0.363	1.9

Table 2: GEM and Fourier series solution of example 2 for $(V_x)_{\max}$ and $(V_y)_{\max}$

Solutions for $w_{\max}$							
$\frac{b}{a}$	Analytic	Quadratic			Linear		
		Grid	GEM	Rel. Error %	Grid	GEM	Rel. Error %
1	0.00126	2 × 2	0.00139	10.3	4 × 4	0.00127	0.8
		4 × 4	0.00128	1.6	8 × 8	0.00124	1.6
2.0	0.00254	2 × 2	0.00281	10.6	4 × 4	0.00264	3.9
		4 × 4	0.00256	0.8	8 × 8	0.00253	0.4
Solutions for $(M)_{x=0,y=0}$							
$\frac{b}{a}$	Analytic	Quadratic			Linear		
		Grid	GEM	Rel. Error %	Grid	GEM	Rel. Error %
1.0	0.0355	2 × 2	0.0383	7.9	4 × 4	0.0412	16.1
		4 × 4	0.0359	1.1	8 × 8	0.0362	2.0
2.0	0.0442	2 × 2	0.0457	3.4	4 × 4	0.0505	14.2
		4 × 4	0.0442	0	8 × 8	0.0453	2.5

Table 3: GEM and Fourier series solution of example 3 for w and M the centre of the plate.

6 Conclusion

The biharmonic equation which governs flexural plate problems under transverse loading has been solved as coupled harmonic equations with a novel Green element formulation that calculates the deflections, moments, rotations and shear forces at every node. High level of accuracy is achieved by the formulation using coarse grid due to the fact that all unknown quantities are calculated directly. The accuracies for all the quantities therefore depend on the order of the polynomial used in approximating them. The increased number of degrees of freedom at each node is compensated for by requiring only a coarse grid to achieve high accuracy. The novel feature of the current Green element formulation is that the elemental solution is complete in the sense that the solution at any point in an element is obtained by carrying out the boundary and domain integrations within that element. No reference is made to other elements in the discretized the region. The solutions at points other than the grid points are second-order accurate; the same order of accuracy as the solutions at the nodal points.

7 References

[1] F. París and S. De León. Simply supported plates by the boundary integral equation method, *Int. J. Num. Engrg*., 23, 173-191 (1986).

[2] A. Zeb, L. Elliott, D.B. Ingham and D. Lesnic. A comparison of different methods to solve inverse biharmonic boundary value problems, *Int. J. Num. Engrg*., 45, 1791-1806 (1999).

[3] N. Mai-Duy and T. Tran-Cong. Solving biharmonic problems with scattered-point discretization using indirect radial-basis-function networks, *EABE*, 30, 77-87 (2006).

[4] J. Sladek, V. Sladek and H.A. Mang. Meshless formulations for simply supported and clamped plate problems, *Int. J. Num. Engrg*., 55, 359-375 (2002).

[5] Taigbenu, A.E. *The Green Element Method*, Kluwer, USA (1999).

[6] A.E. Taigbenu. Green element calculations of nonlinear heat conduction with a time-dependent fundamental solution, *EABE*, **28**(1), 53-60 (2004).

[7] A.E. Taigbenu. The Green Element Method, *Int. J. Num. Engrg*., **38** 2241-2263 (1995).

[8] J.A. Liggett, & P.L-F. Liu, *The boundary Integral Equation Method for Porous Media Flow*, George Allen & Unwin (1983).

[9] N. Mai-Duy and R.I. Tanner. An effective high order interpolation scheme in BIEM for biharmonic boundary value problems, *EABE*, **29**, 210-223 (2005).

[10] S. Timoshenko and S. Woinowsky-Krieger. *Theory of Plates and Shells*, McGraw-Hill (1959).

A Boundary Element Approach for Topology Optimization Problem Using the Level Set Method

Kazuhisa Abe[1], Shunsuke Kazama[2] and Kazuhiro Koro[3]
[1] Department of Civil Engineering and Architecture, Niigata University
8050 Igarashi 2-Nocho, Niigata 950-2181, JAPAN, abe@eng.niigata-u.ac.jp
[2] Graduate School of Science and Technology, Niigata University
8050 Igarashi 2-Nocho, Niigata 950-2181, JAPAN
[3] Department of Civil Engineering and Architecture, Niigata University
8050 Igarashi 2-Nocho, Niigata 950-2181, JAPAN

Keywords: BEM, Topology optimization, Level set method, Design sensitivity analysis

Introduction

In contrast to the success of the boundary element method (BEM) in the shape design problem, the application of BEM to the topology optimization has still some difficulties. So far, the freedom in the topological change has suffered substantial restrictions. For example, in existing method the fusion and fission of holes are not allowed during the optimization process[1]. Though the genetic algorithms make it easy to change the topology, the shape of holes is strongly restricted[2].

On the other hand, various finite element based topology optimization methods have successfully developed since the innovative approach of Bendsøe and Kikuchi[3]. The employment of the Eulerian description enables to reduce the topology design to the sizing problem. In addition to these methods, the application of the level set method[4] was also proposed. This method realizes the optimum topology by finding an optimum level set function distributed in a design domain. Here the level set function is defined as the signed distance from the boundary. Therefore the change of the shape can be achieved by the convection of the level set function governed by a Hamilton-Jacobi equation. One of the advantages of this method is that the boundary contour can be defined distinctly. It implies the applicability of the method to the BE topology design.

In this study the development of a BE topology optimization method is attempted by utilizing the level set approach. The proposed method is applied to a compliance problem within the framework of the two-dimensional plane strain linear elasticity, and the feasibility of the method is demonstrated.

Design Sensitivity Analysis

An objective function J defined by the following equation is considered,

$$J = F(\mathbf{U}, \mathbf{P}, \mathbf{x}_G) + \boldsymbol{\lambda}^T\{\mathbf{HU} - \mathbf{GP}\} + \lambda_+(V - V_{max}), \tag{1}$$

where F is a cost function, $\boldsymbol{\lambda}$ is a vector of the Lagrange multiplier, $\mathbf{H}$ and $\mathbf{G}$ are boundary element matrices, $\mathbf{U}$ and $\mathbf{P}$ are displacement and traction vectors, $\lambda_+ \geq 0$ is a Lagrange multiplier, V is the volume of body and V_{max} is a volume constraint. $\mathbf{x}_G$ is a set of nodal coordinates given by the boundary element junctions.

The variation ΔJ with respect to the geometrical change $\Delta\mathbf{x}_G$ is given by

$$\Delta J = \frac{\partial F}{\partial \mathbf{x}_G}\Delta\mathbf{x}_G + \boldsymbol{\lambda}^T[\frac{\partial H}{\partial \mathbf{x}_G}\mathbf{U} - \frac{\partial G}{\partial \mathbf{x}_G}\mathbf{P}]\Delta\mathbf{x}_G + \lambda_+\frac{\partial V}{\partial \mathbf{x}_G}\Delta\mathbf{x}_G, \tag{2}$$

were $\partial/\partial\mathbf{x}_G$ stands for the Fréchet derivative, and $\boldsymbol{\lambda}$ is determined so that it satisfies the adjoint equation :

$$\frac{\partial F}{\partial \mathbf{U}}\mathbf{Z}_U + \frac{\partial F}{\partial \mathbf{P}}\mathbf{Z}_P + \boldsymbol{\lambda}^T\{\mathbf{HZ}_U - \mathbf{GZ}_P\} = 0, \quad \text{for } {}^\forall\mathbf{Z}_U, \mathbf{Z}_P, \tag{3}$$

here $\mathbf{Z}_U$ and $\mathbf{Z}_P$ are arbitrary vectors sufficing $\mathbf{Z}_U = 0$ and $\mathbf{Z}_P = 0$ on the Dirichlet and Neumann subboundaries, respectively.

In this study the motion of the geometrical points $\Delta\mathbf{x}_G$ is specified by the normal velocity vector derived from eq(2).

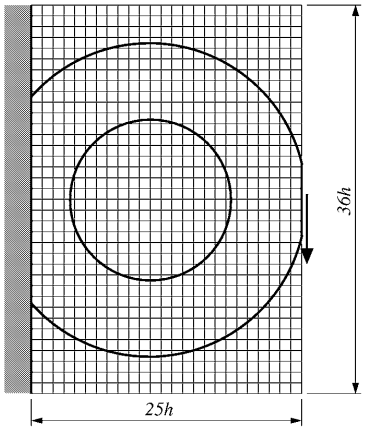

Fig.1 Initial topology and analytical conditions.

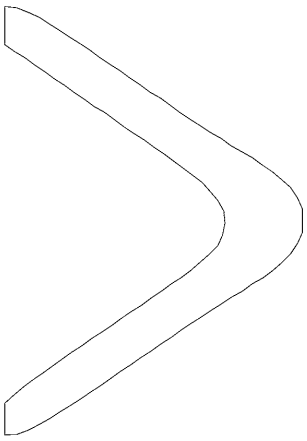

Fig.2 Final topology.

Level Set Method

The level set function is assigned at each fixed grid point embedded in the design domain irrespective of the topology. The boundary is implicitly defined by the zero contour of the level set function. Once the contour line is drawn on the background grid, the boundary element discretization can be developed along the contour. Since the level set function is used to represent the zero level set, it is sufficient to assign the nodal values only in the neighborhood of the contour. These nodal values are given by a signed distance function from the contour. The change of the shape and the topology arises from the convective motion of the level set function governed by the Hamilton-Jacobi equation. The normal velocity along the boundary is determined by the shape sensitivity analysis.

Numerical Example

An application to the minimum compliance problem of linear elastic body is demonstrated. The background grid and initial topology are shown in Fig.1 together with the boundary conditions. In the analysis the elastic problem is non-dimensionalized by the grid size h and Young's modulus with Poisson's ratio of 0.3. Two boundary elements subjected to the vertical load are fixed. As shown in Fig.1 the initial topology has a circular hole. The whole boundary is discretized by piecewise constant elements with the length of about h. Fig.2 shows the final topology for the volume restriction of $V_{max} = 0.5V_0$, where V_0 is the initial volume. The optimum topology has a two-bar truss-like structure that is identical with the results obtained by existing methods. During the design process, the hole has been merged into the external boundary. Although more than 250 steps were required for the convergence, the developed method successfully captured the topological change.

References

[1] K.Tai and R.T.Fenner *Int. J. Solids Struct.*, **36**, 2021-2040 (1999).
[2] J.Lee, S.Wang and A.Dikec *J. Sound Vibr.*, **276**, 899-918 (2004).
[3] M.P.Bendsøe and N.Kikuchi *Comput. Meth. Appl. Mech. Eng.*, **71**, 197-224 (1988).
[4] G.Allaire, F.Jouve and A-M.Toader *C. R. Acad. Sci. Paris*, **Ser.I 334**, 1125-1130 (2002).

High performance preconditioners and solvers for the fast multipole methods

G.Alléon, G.Sylvand[a], Luc Giraud[b]
[a] EADS CRC, Centre de Toulouse, 4 Avenue Daurat, 31700 Blagnac, France
[b] ENSEEIHT, 2 rue Camichel, 31071 Toulouse Cedex, France.

At the sight of the results achieved during the ten last years, one can affirm that the contribution of the fast multipole method (FMM) to wave propagation modelling is comparable with the one of the Fast Fourier Transform (FFT) for signal processing!
In this paper, we will describe the numerical techniques that enable fast multipole methods to be very efficient while the problem is known to be numerically difficult for iterative solvers. These techniques are basically of two different classes. The first class of techniques is iterative solvers and especially accelerating technique for multiple right hand sides linear systems. A comparison of single right hand side like GMRES, QMR with additional strategies to take into account several right hand sides and block solvers that natively take into account multiple right hand sides (BGMRES, …) will be presented. The second class of methods consider accelerating techniques such as preconditioners. The design of robust preconditioners for boundary integral equations can be challenging. Simple parallel preconditioners like the diagonal of A, diagonal blocks, or a band can be effective only when the coefficient matrix has some degree of diagonal dominance depending on the integral formulation. Incomplete factorizations have been successfully used on non-symmetric dense systems and hybrid integral formulations, but on the EFIE the triangular factors computed by the factorization are often very ill-conditioned due to the indefiniteness of A. This makes the triangular solves highly unstable and the preconditioner ineffective. Approximate inverse methods are generally less prone to instabilities on indefinite systems, and systems, and several pre-conditioners of this type have been proposed in electromagnetism and their efficiency in acoustics has been proven. A complete review of these techniques will be considered and their efficiency will be assessed on electromagnetics and acoustics multipole boundary element solvers developed by EADS.

Influence of the soil profile randomness on the seismic response of multilayered soils with a rigid inclusion

M. Badaoui[1,2], M.K. Berrah[3] and A. Mebarki[1]

[1] Laboratoire de Mécanique, Université de Marne-la-Vallée, 5 bd Descartes 77454, Marne-la-Vallée, Cedex 2, France

Email: m_badaoui@yahoo.fr, Tel.: 33 1 60 95 77 83, Fax: 33 1 60 95 77 99.

[2] LBE, Faculty of Civil Engineering, USTHB, BP 32 El-Alia Bab-Ezzouar 16111, Algiers Algeria.

[3] Ecole Nationale Polytechnique, 10 Avenue Hassan Badi El-Harrach, Algiers, Algeria.

Abstract. This paper deals with the response of a multilayered soil under seismic excitation. It focuses on the influence of the uncertainty that affects the soil height. The soil under study is composed by a superposition of layers extending horizontally to infinity. A tunnel, located inside the soil, is supposed to behave as a rigid inclusion. It represents the Algiers subway (under construction) under the effect the Boumerdes earthquake, May 21st 2003 (magnitude M_w=6.5). The accelerations are collected from Keddara station (12 km from the epicenter) as it is located directly on the bedrock. As the study is restricted herein to SH wave propagation, the accelerations under study correspond to one horizontal direction (EW).
The soil height below the tunnel is assumed to be a random variable. For this purpose, a lognormal distribution is adopted. The probabilistic seismic response of the soil, in time and frequency domains, is therefore investigated. The tunnel displacement as well as the mean and standard deviation of both the extreme ground acceleration and the transfer function are analyzed.
The present analysis is based on the boundary element method, which is adequate for the case of systems with infinite boundaries, while the Greens functions are calculated using the Thin Layer Method.

Keywords: Uncertainty, height, layered soil, tunnel, seismic acceleration, BEM, lognormal.

Seismic excitations produce waves that are transmitted through the surrounding soil. These waves have mechanical influence on the structures and buildings that are located at their neighborhood (Pais 1988 and Von Estorff et al. 1991). For structures buried in layered soil, the analysis of the seismic response has to face many difficulties due to structures features and soil characteristics. Another complexity rises from the randomness of the geological and mechanical characteristics. Therefore, the use of probabilistic methods, generally based on simulation techniques, is required.

The present paper, a tunnel (Algiers subway under construction) in multi-layered soil subjected to seismic excitation is considered: case of Boumerdes earthquake (Algeria, May 21st 2003, magnitude M_w=6.5). The input acceleration corresponds to the in situ data collected at Keddara station (12 km from Boumerdes) as it is located directly on the bedrock. The considered accelerations correspond to a horizontal direction (EW) and the analysis focuses on the SH wave propagation. The height of the bottom layer is supposed to be uncertain and log-normally distributed (Badaoui et al. 2004, 2005). Monte Carlo simulations are thus ran: 100 samples are considered to calculate the mean and the standard deviation of the ground surface and tunnel displacements, as well as the transfer function in order to investigate the probabilistic uncertainty effect on the seismic response in time and frequency domains (Badaoui et al. 2004, 2005).

When a soil contains several horizontal layers, the modelization of such system as a homogeneous half-space may be inadequate. The presence of structures, as inclusions, represents an additional difficulty.

In the case of soils represented by a pilling of distinct horizontal layers, extending to infinity at their lateral boundaries, and in the presence of underground structures as inclusions, the BEM appears as the most powerful approach for infinite media. This method requires the use of the Green's functions, which are, in general, very difficult to obtain and are analytically known only for some simple geometry cases. In the present case, these functions are obtained by using the Thin Layer Method (Kausel and Roësset 1981, Kausel and Peek 1982).

The maximum of the mean displacement corresponds approximately to the fundamental frequency of the excitation and is observed at the lateral borders of the tunnel. The standard deviation of the displacements is important for the low fundamental frequencies. However, the response frequency content is less sensitive.
The mean value of the tunnel displacement is important at the fundamental frequencies of the soil-tunnel system. The standard deviation has approximately the same shape than the mean value and is important for fundamental frequencies.

The maximum values of the transfer function correspond approximately to the same frequencies that those of the tunnel displacement and are located at the lateral extremity of the tunnel. The standard deviation is important for low frequencies. This shows that the heterogeneity causes a decrease of the transfer function for low eigen frequencies whereas it leads to an increase for high eigen frequencies.

The heterogeneity leads to a transfer function amplitude decrease but extends the frequency content. Furthermore, the standard deviation follows the same shape than the mean curve but is important for frequencies around 10 Hz .

References

M. Badaoui, A. Nour, A. Slimani and M.K. Berrah, “Stochastic seismic investigation of the heterogeneous soil profile having uncertainty depth”, *Proceedings of the Fourth International Conference on Engineering Computational Technology (ECT2004)*, paper 114, B. H. V. Topping and C. A. Mota Soares (Editors),Civil-Comp Press, Stirling, UK, Lisbon, Portugal, (2004).
M. Badaoui and M.K. Berrah , “Influence of the soil profile uncertainty on the tunnel – layered soil interaction subjected to seismic acceleration”, *Proceedings of the Tenth International Conference on Civil, Structural and Environmental Engineering Computing (CC2005)*, paper 226, B. H. V. Topping (Editor), Civil-Comp Press, Stirling, UK, Rome, Italy, (2005).
E. Kausel and J.M. *Roësset Stiffness matrices for layered soils,* Bulletin of Seismological Society of America, 71 (6), 1743-1761 (1981).
E. Kausel and R. Peek *Dynamic loads in the interior of layered stratum: an explicit solution,* Bulletin of Seismological Society of America, 72 (5), 1459-1481 (1982).
A.L. Pais *Dynamic coupling of multiple structures through soi*, Ph.D. Thesis, Department of civil engineering, MIT, Boston (1988).
O. Von Estorff, AA Stamos, DE Beskos and H. Antes (Eds) *Dynamic interaction effects in underground traffic systems*, Engineering Analysis with Boundary Elements, 8 (4), 167-175 (1991).

A Fundamental-Solution-Less Boundary Element Method for Exterior Wave Problems

Chongmin Song and Mohammad H. Bazyar

School of Civil and Environmental Engineering, University of New South Wales, Sydney, NSW 2052, Australia.

E-mail: c.song@unsw.edu.au; mhbazyar@student.unsw.edu.au

Keywords: Scaled boundary finite-element method; Absorbing boundary; Transmitting boundary; Unbounded domain; Wave propagation.

Abstract

Boundary element method [1] is an attracting technique for solving exterior wave problems. In this method, only the boundary is divided into elements yielding a reduction of the spatial dimension by one. The radiation condition at infinity and the governing differential equations for waves are satisfied automatically by a fundamental solution. However, difficulties are encountered in applying the boundary element method to many practical engineering problems owing to its reliance on the fundamental solution. When the material is general anisotropic, the complexity of the fundamental solution increases dramatically. As the boundary element formulation is spatially and temporally global, it becomes prohibitively expensive for large-scale problems or long-time calculations.

A fundamental-solution-less boundary element method, the scaled boundary finite-element method [2,3], has been developed recently as a novel numerical technique that not only combines many advantages of the finite element and boundary element methods but also presents appealing features of its own. In this method, only the boundary is discretised yielding a reduction of the spatial dimension by one. After applying the Galerkin weighted residual technique along the circumferential directions parallel to the boundary, the governing partial differential equations are transformed to ordinary differential equations for displacement functions. No singular integrals are evaluated in computing the coefficient matrices. The scaled boundary finite-element equation in the dynamic-stiffness matrix of the unbounded domain is a system of ordinary differential equations in frequency. The radiation condition is easily enforced in the solution for the ordinary differential equations. No fundamental solution as required in standard boundary element method is necessary. General anisotropic materials can be analysed without additional efforts. The solution for the dynamic stiffness matrix is symmetric. Seamless coupling with standard finite elements is straightforward.

The original scaled boundary finite-element formulation, as a rigorous method like the standard boundary element method, is spatially and temporally global. This paper exploits the new possibilities opened up by reformulating the governing partial differential equations as ordinary differential equations to significantly increase the computational efficiency for large-scale exterior wave problems. A technique of reduced set of weighted orthogonal base functions similar to the method of separation of variables is developed. It significantly reduces the number of degrees of freedom while maintaining sufficient accuracy of the results [4]. Exploiting the sparsity of the coefficient matrix, the base functions are obtained by a partial Schur decomposition together with an iterative scheme. This approach greatly reduces the computer time and storage requirement for large-scale unbounded domains. The scaled boundary finite-element equation in dynamic stiffness

for the reduced set is a system of ordinary differential equations with the excitation frequency as the independent variable. The solution for the dynamic stiffness is expressed as a Padé series in frequency. The coefficient matrices of the Padé series are determined based on the high frequency behaviour. Numerical results demonstrate that accurate results over the whole frequency range can be obtained at a relative small order (≤10). The dynamic stiffness at a specified frequency is evaluated directly. The Padé series solution can be extended to construct a temporally local boundary condition for time domain analysis.

A rigid hemispherical footing (Fig. 1a) is addressed as a numerical example. It has a radius of the r_0 and is embedded in a half-space with shear modulus G, Poisson's ratio $\nu = 0.3$ and mass density ρ. The boundary is discretized with 300 9-node surface elements with 1241 nodes. A reduced set of 84 base functions is constructed. The vertical dynamic stiffness coefficient obtained with an order $M = 6$ Padé series is plotted in Fig. 1b as a function of the dimensionless frequency $a_0 = \omega r_0 / c_s$ ($c_s = \sqrt{G/\rho}$). It agrees very well with the converged axisymmetric solution. The computational time is recorded on a laptop computer with a Pentium M 2GHz CPU and 1GB of RAM. The total time to obtain the continued fraction is 32s including 28s for the partial Schur decomposition and 0.2s for the coefficient matrices of the Padé series. This example demonstrates that the scaled boundary finite-element method can be applied to solve large-scale problems. It is worth mentioning that the computational effort remains the same for waves propagating in anisotropic materials.

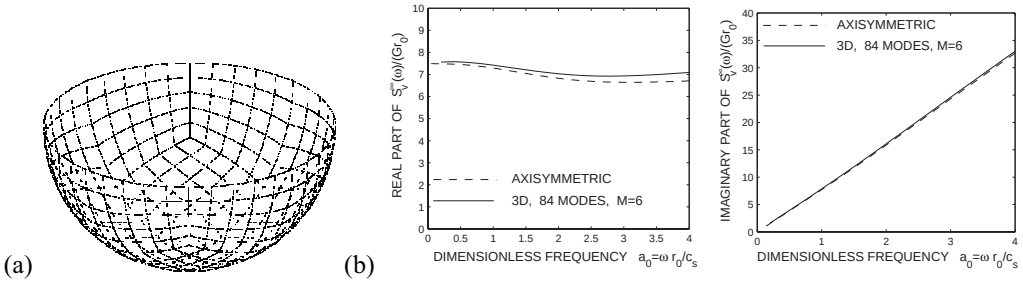

Figure 1: Rigid hemispherical footing embedded in half-space

References

[1] W.S. Hall and G. Oliveto (Eds) *Boundary Element Methods for Soil-Structure Interaction*;. Kluwer Academic, Publishers, (2003).

[2] J.P. Wolf and Ch. Song *Computers & Structures*, **78**, 191-210, (2000).

[3] Ch. Song and J.P. Wolf *Computers & Structures*, **78**, 211-225, (2000).

[4] Song, Ch. *Computer Methods in Applied Mechanics and Engineering,* **195**, *4075-4094*, (2006).

Performance analysis of parallel Krylov methods for solving boundary integral equations in electromagnetism

B. Carpentieri*

The simulation of high-frequency scattering of electrically large objects is very demanding in terms of computer resources and requires the use of fast numerical methods with reduced computational and memory complexity. The underlying physical issue is the detection of the electromagnetic radiation that is scattered back by an object that is illuminated by an in-going incident radiation. Two distinct approaches can be followed for the numerical solution, one based on differential equation methods, the other on integral methods. Using the equivalence principle, Maxwell's equations can be recast in the form of a set of integral equations which relate the electric and magnetic fields to the equivalent electric and magnetic currents on the surface of the object. For homogeneous or layered homogeneous dielectric bodies, the Galerkin method discretizes integral equations on the surface of the object and at the discontinuous interfaces between two different materials. The discretization gives rise to dense and complex linear systems of equations whose unknowns are associated with the vectorial flux across an edge in the mesh. The number of unknowns increases proportionately to the dimension of the object and quadratically with the frequency of the problem. The right-hand side depends on the frequency and on the direction of the illuminating wave.

With the advent of high-performance parallel computers, boundary integral methods have received an increasing interest for the solution of high-frequency electromagnetic scattering problems. Although efficient out-of-core direct solvers have been developed for this problem class, the huge storage requirement is often a severe limit to the viability of integral equation methods for solving realistic applications in electromagnetism. In this work, we present experiments with iterative solution strategies based on Krylov methods and combined with the Fast Multipole Method (FMM) for the matrix-vector products. The FMM algorithm, introduced by Greengard and Rokhlin in the 80's, enables us to perform approximate matrix-vector products with boundary integral operators in $\mathcal{O}(n \log n)$ arithmetic operations and $\mathcal{O}(n \log n)$ memory storage. In the numerical experiments, we consider the parallel multilevel implementation of the FMM developed by Guillaume Sylvand (EADS-CCR Toulouse, see [1]).

Amongst integral formulations, we concentrate on the Electric Field Integral Equation (EFIE) that is widely used in realistic simulations in industrial environment because it is applicable to arbitrary geometries. The condition number of the coefficient matrices arising from the discretization of the EFIE formulation can grow like $p^{1/2}$, where p denotes the size of the scatterer in terms of the wavelength, and linearly with the number of points per wavelength. For a correct representation of the oscillation of the field and the singularities of the scatterer, the edge length has to be of the order of $\lambda/10$, where λ denotes the wavelength of the physical problem. As a result, Krylov methods scale as $\mathcal{O}(n^{0.5})$ and preconditioning is a crucial component of the iterative process. The design of robust preconditioners can be a tough problem. Basic preconditioners like diagonal scaling, diagonal blocks, or a band can be effective when the coefficient matrix has some degree of diagonal dominance but are unreliable at high frequencies when the coefficient matrices become poorly diagonally dominant. Incomplete factorizations have been successfully

*Karl-Franzens University, Institute for Mathematics and Scientific Computing
Heinrichstraße 36, A-8010 Graz, Austria.
Email : bruno.carpentieri@uni-graz.at

used on nonsymmetric integral equations and hybrid formulations, but on the EFIE the triangular factors computed by the factorization are often very ill-conditioned and the preconditioner is useless. In this work we analyse the performance of parallel iterative solution schemes based on an approximate inverse preconditioner. The approximate inverse is computed as the matrix M that minimizes the Frobenius-norm of the error matrix $\|I - \tilde{A}M\|_F$ (we denote $\tilde{A}$ a sparse approximation of the coefficient matrix), subject to certain sparsity constraints. The pattern of M and $\tilde{A}$ is computed in advance using graph information from the mesh, by selecting for the jth column of the approximate inverse edge j and its qth level nearest-neighbors. Both the construction and the application of M are embarrassingly parallel.

We present results with an embedded iterative solution scheme based on the GMRES method and implemented using different levels of accuracy for the matrix-vector products in the inner and outer loop. We report on experiments on test problems arising from realistic electromagnetic simulations in industry to illustrate the potential of the proposed method for solving large-scale applications in electromagnetism. More extensive results and algorithmic details are found in [2, 3]. Most of the reported experiments require a huge amount of computation and storage; such simulations are feasible thanks to the use of iterative methods and can be integrated in the design processes where nowadays the bottleneck moves from the simulation to the pre and post-processing phase of the results as the tools are not yet available to easily manipulate meshes with millions of degrees of freedom.

This is a joint collaboration between CERFACS (Toulouse), EADS-CCR (Toulouse), INRIA-CERMICS (Sophia Antipolis).

References

[1] G. Sylvand. *La Méthode Multipôle Rapide en Electromagnétisme : Performances, Parallélisation, Applications*. PhD thesis, Ecole Nationale des Ponts et Chaussées, 2002.

[2] B. Carpentieri. *Sparse preconditioners for dense linear systems from electromagnetic applications*. PhD thesis, CERFACS, Toulouse, France, 2002.

[3] B. Carpentieri, I. S. Duff, L. Giraud, and G. Sylvand. Combining fast multipole techniques and an approximate inverse preconditioner for large electromagnetism calculations. *SIAM J. Scientific Computing*, 27(3):774–792, 2005.

Topology Optimization of 2D Potential Problems Using Boundary Elements

Adrián P. Cisilino

Welding and Fracture Division, Faculty of Engineering, University of Mar del Plata
Av. Juan B. Justo 4302
7600 Mar del Plata, Argentina
email: cisilino@fi.mdp.edu.ar

Keywords: topology optimization, topological derivative, boundary elements, potential problems

Introduction

A classical problem in engineering design consists in finding the optimum geometric configuration of a body that maximizes or minimizes a given cost function while it satisfies the problem boundary conditions. The most general approach to tackle these problems is by means of topological optimization tools, which allow not only to change the shape of the body but its topology via the creation of internal holes. Topological optimization tools are capable of deliver optimal designs with an "a priori" poor information on the optimal shape of the body.

Homogenization methods are possibly the most used approach for topology optimization [1], but they present the limitation of producing designs with infinitesimal pores that make the structure not manufacturable. An alternative approach aiming to solve the aforementioned limitation of homogenization methods is the Topological Derivative (DT) method [2]. The basic idea behind the DT is the evaluation of cost function sensitivity to the creation of a hole. Wherever this sensitivity is low enough (or high enough depending on the nature of the problem) the material can be progressively eliminated.

Problem Formulation

A numerical approach for the topological optimization of 2D potential problems using Boundary Elements is presented in this work. The formulation of the problem is based on some recent results by Novotny et al. [2] which allow computing the topological derivative using potential and flux results. The Boundary Element analysis is done using a standard direct formulation. Models are discretized using linear elements and a periodic distribution of internal points over the domain. The total potential energy is selected as cost function. Afterwards, material is removed from the model by deleting the internal points and boundary nodes with the lowest (or highest) values of the topological derivate. The new geometry is remeshed using an Extended Delaunay Tessellation algorithm [3] capable of detecting "holes" at those positions where internal points and nodes have been removed. The procedure is repeated until a given stopping criteria is satisfied.

Results and Conclusions

The proposed strategy proved to be flexible and robust. A number of examples are solved and results are compared to those available in the literature.

A typical example is illustrated next. It consists in a heat exchanger with prescribed temperature in the top and piecewise periodic flux prescribed in the bottom. The objective of the optimization is to open cooling holes with prescribed Robin boundary conditions in order to minimize the temperature in the device (see Figure 1). Figure 2 depicts the initial and final temperature maps, while Figure 3 shows the evolution of the maximum temperature during the optimization process.

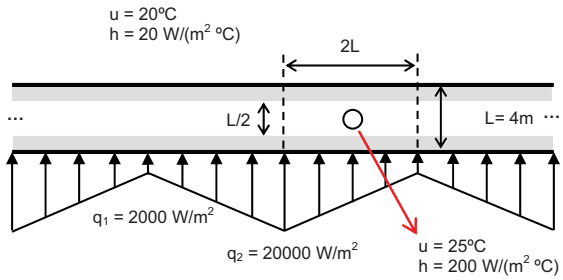

Figure 1: problem geometry and boundary conditions

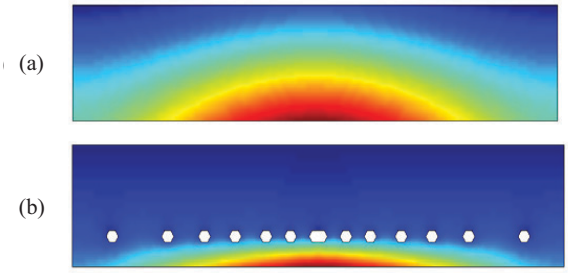

Figure 2: (a) Initial and (b) optimized temperature maps.

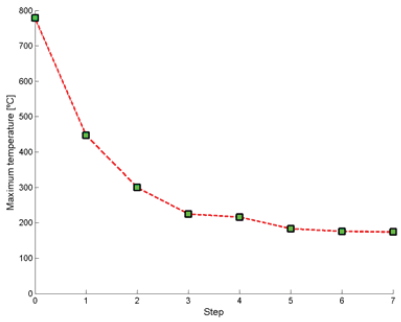

Figure 3: Evolution of the maximum temperature value.

References

[1] Bensoe, M.P. and Kikuchi N.Generating optimal topologies in structural design using a homogenization method. *Comput. Methods Appl. Mech. Engrg*, 71, 197-224 (1988)

[2] Novotny A.A, Feijoo R.A., Taroco E. and Padra C. C. Topological-shape sensitivity analysis. *Mathematical Models and Methods in Applied Sciences*, 192, 803–829 (2003)

[3] Calvo N, Idelsohn S.R. and Oñate E. The Extended Delaunay Tessellation. *Engineering Computations*, 20/5-6.(2003)

An Alternative BEM for Fracture Mechanics

Giuseppe Davì[1] and Alberto Milazzo[1]

[1] Dipartimento di Tecnologie e Infrastrutture Aeronautiche
Università di Palermo, Viale delle Scienze, 90128 Palermo – Italy. E-mail: davi@unipa.it

Keywords: Fracture mechanics, stress function, stress intensity factor

Abstract. An alternative single domain boundary element formulation and its numerical implementation are presented for the analysis of two-dimensional cracked bodies. The problem is formulated employing the classical displacement boundary integral representation and a novel integral equation based on the stress or Airy's function. This integral equation written on the crack provides the relations needed to determine the problem solution in the framework of linear elastic fracture mechanics. Results are presented for typical problems in terms of stress intensity factors and they show the accuracy and efficiency of the approach.

The Boundary Element Method for Fracture Mechanics

The Somigliana identity is the fundamental relation giving the boundary integral representation of the elastic response in the elastic domain Ω having contour Γ. Indeed it links the displacements at the point P_0 to the displacements **u** and tractions **p** on the boundary through a fictitious elastic system due to a concentrated body force acting at the point P_0. Denoting by $\mathbf{u}_j$ and $\mathbf{p}_j$ the displacements and tractions of the fictitious system, respectively, The Somigliana identity is written [3, 4]

$$\mathbf{u}(P_0) = \int_\Gamma \left(\mathbf{u}_j^T \mathbf{p} - \mathbf{p}_j^T \mathbf{u} \right) d\Gamma + \int_\Omega \mathbf{u}_j^T \mathbf{f}\, d\Omega \tag{1}$$

where f are the body forces applied in the domain. The eq (1) is the boundary integral representation of the displacement field inside the continuum Ω. If the point P_0 belongs to the boundary Γ, by a suitable limit procedure [3], one obtains the boundary integral equation which, taking the prescribed boundary conditions into account, allows the solution of the elastic problem in terms of displacements and tractions on the boundary [3, 4]. One has

$$\mathbf{c}\,\mathbf{u}(P_0) = \int_\Gamma \left(\mathbf{u}_j^T \mathbf{p} - \mathbf{p}_j^T \mathbf{u} \right) d\Gamma + \int_\Omega \mathbf{u}_j^T \mathbf{f}\, d\Omega \tag{2}$$

where the coefficient matrix **c** is given by

$$\mathbf{c} = -\int_\Gamma \mathbf{p}_j^T\, d\Gamma \tag{3}$$

The eq (2) is the basis for the numerical solution of the problem by the Boundary Element Method; However, in the framework of Fracture Mechanics when cracks are located in the domain, the eq (2) needs to be revised by taking the unknowns relative displacements along the cracks into account; the eq (2) becomes [5, 6, 12]

$$\mathbf{c}\,\mathbf{u}(P_0) = \int_\Gamma \left(\mathbf{u}_j^T \mathbf{p} - \mathbf{p}_j^T \mathbf{u} \right) d\Gamma - \int_{\Gamma_f} \mathbf{p}_j^T\, \Delta\mathbf{u}\, d\Gamma + \int_\Omega \mathbf{u}_j^T \mathbf{f}\, d\Omega \tag{4}$$

where Γ_f is the boundary representative of the crack and $\Delta\mathbf{u}$ are the relative displacements along it. It straight away appears that eq (4) in its numerical application originates a system with more unknowns than equations. To overcome this drawback many approaches have been proposed among which there are the Green's function, the multidomain method and the Dual Boundary Element Method (DBEM) [6]. The Green's function method even is very accurate is limited to very simple problems [12], whereas the other two approaches are general and therefore they are the most employed. The multidomain method requires a partition of the investigated domain into suitable subregions so that each face of the cracks belongs to the boundary of distinct subregions. Restoring the continuity conditions between the considered subregions the number of integral equations written is equal to the number of unknowns and the problem can be modelled

without limitations [8, 9]. Nevertheless the resolving system arising from the multidomain approach has higher order than that strictly needed to solve the problem with the consequent higher computational effort required. On the other hand the Dual Boundary Element Method (DBEM) does not require any partition of the investigated domain [10]; it recovers the further equations for the problem solution by expressing the tractions acting on the crack faces by means of the relative boundary integral representations. The main difficulty of this single domain approach is due to the hypersingular kernels occurring in the traction integral equation which need particular care in their numerical integration [11].

Stress function approach

For an homogeneous, isotropic two-dimensional body the stress field can be derived from a single function, the so-called stress function or Airy function $\Phi = \Phi(x, y)$, so that the equilibrium equations are trivially fulfilled; in the absence of body forces one has [13]

$$\boldsymbol{\sigma} = \begin{bmatrix} \sigma_{xx} & \sigma_{yy} & \sigma_{xy} \end{bmatrix}^T = \mathbf{C}\Phi \tag{5}$$

where

$$\mathbf{C}^T = \begin{bmatrix} \dfrac{\partial^2}{\partial y^2} & \dfrac{\partial^2}{\partial x^2} & -\dfrac{\partial^2}{\partial x \partial y} \end{bmatrix} \tag{6}$$

Besides, the compatibility conditions requires that the stress function Φ satisfies the following governing equation

$$\mathbf{C}^T \mathbf{E}^{-1} \mathbf{C} \Phi = 0 \tag{7}$$

where **E** denotes the elasticity matrix. From eq (7) one deduces that the stress function Φ is biharmonic. Once the stress function is introduced the displacement field can be expressed by

$$\mathbf{u} = \mathbf{v} - \frac{1}{2G}\mathbf{S}\Phi \tag{8}$$

where $\mathbf{S} = \begin{bmatrix} \partial/\partial x & \partial/\partial y \end{bmatrix}^T$ is the gradient operator; G is the shear modulus and **v** is a vector, whose components v_1 and v_2 are conjugate harmonic functions. The boundary tractions **p** are expressed by the following relationship

$$\mathbf{p} = \frac{\partial}{\partial s}\mathbf{H}\mathbf{S}\Phi \tag{9}$$

where $\partial/\partial s$ indicates the tangent derivative, whereas the matrix **H** is defined by

$$\mathbf{H} = \begin{bmatrix} 0 & 1 \\ -1 & 0 \end{bmatrix} \tag{10}$$

In terms of stress function the integral equation (4) becomes

$$\mathbf{c}\,\mathbf{v}(P_0) - \frac{1}{2G}\mathbf{c}\mathbf{S}\Phi(P_0) = \int_\Gamma \left(\mathbf{u}_j^T \mathbf{p} - \mathbf{p}_j^T \mathbf{u}\right) d\Gamma - \int_{\Gamma_f} \mathbf{p}_j^T \Delta\mathbf{u}\, d\Gamma \tag{11}$$

Given that the components of **v** are harmonic functions, applying the Green theorem one has

$$\mathbf{c}\,\mathbf{v}(P_0) = \int_\Gamma \left(\varphi \frac{\partial \mathbf{v}}{\partial n} - \frac{\partial \varphi}{\partial n}\mathbf{v} \right) d\Gamma \tag{12}$$

where

$$\varphi = \ln r(P, P_0) \tag{13}$$

and $r(P, P_0)$ is the distance between the domain point P and the point P_0. Remembering that v_1 and v_2 are conjugate and taking eq (8) into account, eq (12) becomes

$$\mathbf{c}\,\mathbf{v}(P_0) = \int_\Gamma \left(\mathbf{u}^*\,\mathbf{p} - \mathbf{p}^*\,\mathbf{u}\right) d\Gamma - \frac{1}{2G}\int_\Gamma \mathbf{S}\Phi \frac{\partial \varphi}{\partial n} d\Gamma \tag{14}$$

where

$$\mathbf{u}^* = \frac{1}{2G}\begin{bmatrix} \varphi & 0 \\ 0 & \varphi \end{bmatrix} \tag{15}$$

$$\mathbf{p}^* = \begin{bmatrix} \dfrac{\partial \varphi}{\partial n} & -\dfrac{\partial \varphi}{\partial s} \\ \dfrac{\partial \varphi}{\partial s} & \dfrac{\partial \varphi}{\partial n} \end{bmatrix} \tag{16}$$

Finally, by using eq (14), the integral equation (11) is written as

$$\begin{aligned} \frac{1}{2G}\mathbf{c}\mathbf{S}\Phi(P_0) = {} & \int_\Gamma \left(\mathbf{p}_j^T\,\mathbf{u} - \mathbf{u}_j^T\,\mathbf{p}\right) d\Gamma + \int_{\Gamma_f} \mathbf{p}_j^T\,\Delta\mathbf{u}\, d\Gamma + \\ & + \int_\Gamma \left(\mathbf{u}^*\,\mathbf{p} - \mathbf{p}^*\,\mathbf{u}\right) d\Gamma - \int_{\Gamma_f} \mathbf{p}^*\,\Delta\mathbf{u}\, d\Gamma - \frac{1}{2G}\int_\Gamma \mathbf{S}\Phi \frac{\partial \varphi}{\partial n} d\Gamma \end{aligned} \tag{17}$$

Recalling that the components of the resultant of the tractions applied between the point P_0 and a generic point P_A are defined as

$$\mathbf{R} = \int_{P_0}^{P_A} \mathbf{p}\, d\Gamma \tag{18}$$

by integration of the eq (9) one obtains

$$\mathbf{S}\Phi = \mathbf{H}^{-1}\,\mathbf{R} + \mathbf{k} \tag{19}$$

where **k** is a vector whose components are arbitrary constants. For a point P_0 belonging to the crack line the integral equation (17) becomes

$$\begin{aligned} \frac{1}{G}\mathbf{c}\mathbf{k} = {} & \int_\Gamma \left(\mathbf{p}_j^T\,\mathbf{u} - \mathbf{u}_j^T\,\mathbf{p}\right) d\Gamma + \int_{\Gamma_f} \mathbf{p}_j^T\,\Delta\mathbf{u}\, d\Gamma + \\ & + \int_\Gamma \left(\mathbf{u}^*\,\mathbf{p} - \mathbf{p}^*\,\mathbf{u}\right) d\Gamma - \int_{\Gamma_f} \mathbf{p}^*\,\Delta\mathbf{u}\, d\Gamma - \frac{\mathbf{H}^{-1}}{2G}\int_\Gamma \mathbf{R} \frac{\partial \varphi}{\partial n} d\Gamma \end{aligned} \tag{20}$$

This equation allows the problem solution through the boundary element method. After the discretization by boundary elements of the boundaries Γ and Γ_f [5], one obtains the resolving system by collocating the Eq. (4) at the nodes on the boundary Γ and the Eq. (20) at the points belonging to Γ_f. Once the displacements **u** and the tractions **p** on the boundary Γ and the relative displacements $\Delta\mathbf{u}$ along Γ_f are determined, the Fracture Mechanics parameters, specifically the stress intensity factor, can be calculated by standard procedures [5, 8, 14].

Applications

To validate the proposed approach and prove its efficacy and potentiality some numerical results are presented for classical Fracture Mechanics problems. The first application deals with the computation of the stress intensity factors for a crack of length 2*a* embedded in an infinite domain. The results for horizontal and 45° inclined crack are shown in Table 1 where the comparison with the analytical solution is also presented. This comparison clearly shows the accuracy of the proposed approach to compute the stress intensity factor. In the second example a rectangular panel having $h/w = 2$ with a central crack inclined of 45° is analysed. The results obtained in terms of stress intensity factor for different crack length are given in Tables 2 and 3. Again the comparison of the present results with those found in the literature shows the accuracy and efficiency of the proposed method. Finally a finite rectangular plate $h/w = 0.5$ with an edge crack of length *a* has been analyzed. The calculated stress intensity factors are given in Table 4. Once again the comparison

between the present results and those found in the literature confirms the soundness of the method for both its accuracy and efficiency.

	Stress Intensity Factor (SIF)		
	SIF	Present	Analytic
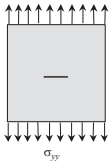	$K_I/\sigma_{yy}\sqrt{\pi a}$	1.00	1.00
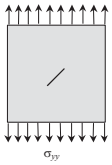	$K_I/\sigma_{yy}\sqrt{\pi a}$	0.50	0.50
	$K_{II}/\sigma_{yy}\sqrt{\pi a}$	0.50	0.50

Table 1. SIFs for horizontal and 45° inclined crack in an infinite domain

a/w	Present	Ref. [5]	Ref. [15]
0.2	0.51	0.53	0.52
0.3	0.52	0.55	0.54
0.4	0.56	0.59	0.57
0.5	0.60	0.63	0.61
0.6	0.65	0.69	0.66

Table 2. $K_I/\left(\sigma_{yy}/\sqrt{\pi a}\right)$ for a 45° central crack in a finite rectangular plate with $h/w=2$

a/w	Present	Ref. [5]	Ref. [15]
0.2	0.49	0.52	0.51
0.3	0.50	0.53	0.52
0.4	0.52	0.54	0.53
0.5	0.54	0.56	0.55
0.6	0.56	0.58	0.57

Table 3. $K_{II}/\left(\sigma_{yy}/\sqrt{\pi a}\right)$ for a 45° central crack in a finite rectangular plate with $h/w=2$

a/w	Present	Ref. [5]	Ref. [15]
0.2	1.48	1.57	1.49
0.3	1.86	1.96	1.85
0.4	2.34	2.23	2.32
0.5	3.04	3.27	3.01

Table 4. $K_I \Big/ \left(\sigma_{yy} \Big/ \sqrt{\pi a} \right)$ for finite rectangular plate having $h/w = 0.5$ with edge crack.

Conclusions

A single domain boundary element method for two dimensional elastic solids has been presented with the aim of overcoming the computational drawbacks of classical BEM approaches for fracture mechanics. The method rests on the use of additional integral equations deduced in terms of stress function which collocated on the crack provide the relations needed to determine the solution. These integral equations do not involve hypersingular integrals with the resulting simplification in numerical implementation. The numerical results obtained show the accuracy, efficiency and usefulness of the proposed approach to determine the characteristic parameters of fracture mechanics

References

[1] A.R.Ingraffea and P.A.Wawrzynek *Comprehensive Structural Integrity. Vol 3. Numerical and Computational Methods.* Elsevier Science Ltd, 1-88 (2003).

[2] T.H.H. Pian Crack Elements *Proceedings of World Congress on Finite Element Methods in Structural Mechanics*, S F.1-F.39, Bournemouth (1975).

[3] B.Banerjee and P.K. Butterfield *Boundary element methods in engineering science*. McGraw-Hill, Maidenhead (1981).

[4] H.Hong and J.Chen *Journal Engineering Mechanics*; **114**, 1028-1044 (1988).

[5] M.H.Aliabadi The *Boundary Element method, Volume 2, Applications in Solids and Structures*. Wiley (2002).

[6] M.H.Aliabadi *Applied Mechanics Review*, **50,** 83-96 (1997).

[7] M.H.Aliabadi *Comprehensive Structural Integrity. Vol 3. Numerical and Computational Methods.* Elsevier Science Ltd, 89-125 (2003).

[8] G.E.Blandford, A.R.Ingraffea and J.A. Ligget, *International Journal for Numerical Methods in Engineering*, **17**, 387-404 (1981).

[9] G.Davì and A.Milazzo *International Journal of Solids and Structures*, **38,** 7065-7078 (2001).

[10] A.Portela, M.H.Aliabadi and D.P.Rooke *International Journal Numerical Methods Engineering*, **33,** 1269-1287 (1992).

[11] L.J.Gray, L.F.Martha and A.R.Ingraffea *International Journal Numerical Methods Engineering*, **29**, 1135-1158 (1990).

[12] M.D.Snyder, T.A.Cruse. *International Journal Fracture Mechanics*, **11,** 315-328 (1975).

[13] P.G.Chou and N.J.Pagano *Elasticity tensor, dyadic and engineering approach*, Dover Publications Inc., New York (1992).

[14] T.A.Cruse, *Surface cracks: Physical problems and computational solutions.* ASME: New York, 153-170 (1972).

[15] M.B.Civelek and F.Erdogan, *International Journal of Fracture*, **19,** 139-159 (1982).

Integrated Numerical Approach to Surface Reconstruction from Noisy Data

Peter Dabnichki[1] and Angel Zhivkov[2]

[1] Department of Engineering, Queen Mary, University of London

Mile End Road, London E1 4NS, UK, p.dabnichki@qmul.ac.uk

[2] Faculty of Mathematics and Informatics, Sofia University,

Boul. J. Bourchier 5, 1164 Sofia, Bulgaria, zhivkov@fmi.uni-sofia.bg

Keywords: Elliptic Functions, Biology, Noisy Data, Filtering, theta functions.

Abstract. The work represents a new approach that is designed to automatically reconstruct the boundary biological objects and simultaneously remove the noise from the image data. This is achieved through an integrated approach that allows a global reconstruction of the object with built-in filtering technique based on Fourier analysis.

Introduction. Unlike traditional engineering applications biological analysis need to use input data that is contaminated with noise due to physical phenomena such as light refraction, error due to insufficient accuracy i.e. low resolution and more frequently with biased error introduced by the image processing software. As shown in earlier works [1,2] theta functions and the related elliptic functions possess properties that render them appropriate for use in reconstruction of biological functions. However, the more traditionally established applications [3,4] allowed to further enhancement of the method

Integrated geometric reconstruction and data filtering. Traditionally noisy data have been used using some types of piece-wise reconstruction based on some approximation criteria. The main reason for avoiding data interpolation the is the introduction of noise due to errors in measurements. Furthermore the

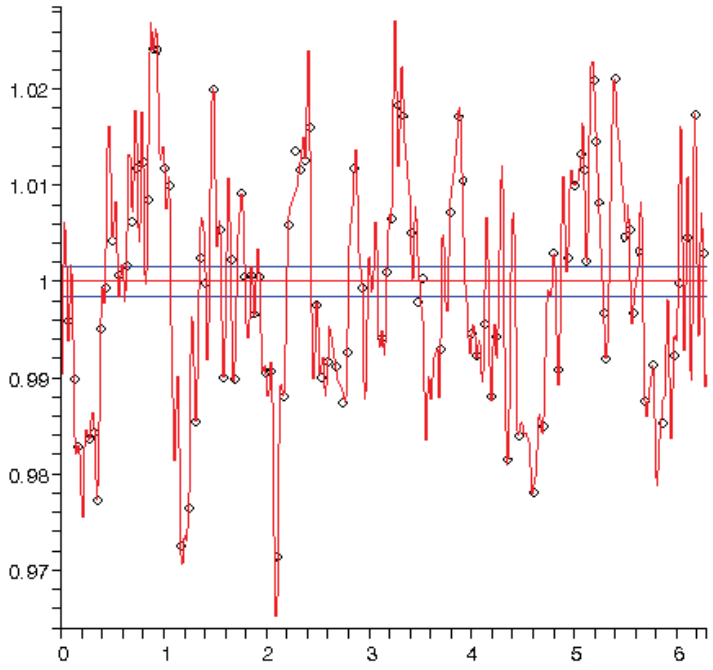

Figure 1 Error distribution as % with respect to the elliptical parameter *t*.

modern systems and devices tend to use built-in data processing routines that add systematic error.

As a standard filtering procedures are devised to remove "white noise" from the data. However, as illustrated in fig. 1, this is seldom if ever the case. In general there are broadly two types of strategies known as time and frequency domain filters. Each of them has its shortcomings that could be summarised that either geometric accuracy is sacrificed in order to select a cut-off frequency in the case of frequency domain or in order to improve the approximation artificial high frequency noise is introduced.

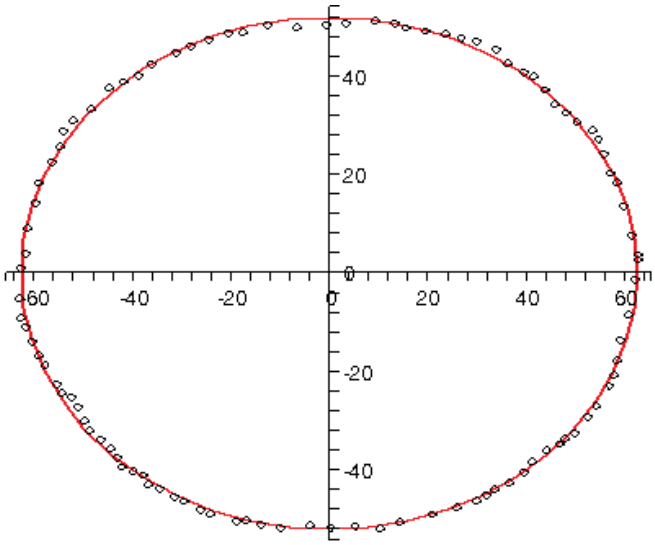

Figure 2 Pseudo-ellipse and the approximation f the noisy data.

The importance of the earlier developed method based on theta functions lies in the fact that they could be used for geometric reconstruction of pseudo-rotational bodies of random shape including irregular bodies with holes in the structure [1, 2, 5]. Theta functions or more accurately elliptic functions allow to use a hybrid approach that allows to control both the geometric accuracy and the number of harmonics (equivalent to frequency domain analysis) without setting a cut-off frequency. It further allows the use of global characteristics such as curvature to be introduced in the approximation criteria.

Fig.2 illustrates a reconstruction of cell image from "noisy" digital data. As can be seen the data are quite close to the proposed approximation but this lead to unwarranted increase in the number of "harmonics" which is not adequate with the characteristics of the structure. The best fit was achieved with the use of three harmonics only. However the actual geometric configuration was analysed including important issue like inclusion of clusters versus solitary points. The method is automatic and this is important if one considers that biology related applications require analysis of objects with a degree of variation in both initial shape and responses that is not the case in traditional engineering applications.

References

[1] Dabnichki P and Zhivkov, In Selvadurai APS, Tan, CL and Aliabadi MH Eds, *Proceedings of VIth International BEM Conferences*, pp.261-267 (2005)

[2] Dabnichki P. and Zhivkov A. *Computers, Media and Structures,* **2**(2), 97-104 (2005)

[3] Gavrilov, L and Zhivkov, A. The complex geometry of Lagrange top. *L'Enseignement Mathematique*, **44**, 133-170 (1998).

[4] Wiles, A. *Annals of Mathematics*, **141**(3), 443-551 (1995).

A hybrid Laplace transform/finite difference boundary element method for diffusion problems

A. J. Davies[1], D. Crann[1] , S. J. Kane[1] and C-H. Lai[2]

[1] School of Physics, Astronomy and Mathematics,

University of Hertfordshire, Hatfield, Herts. AL10 9AB, U.K.
{a.j.davies,d.crann,s.j.kane}@herts.ac.uk

[2] School of Computing and Mathematical Sciences,

University of Greenwich, London SE10 9LS, U.K. c.h.lai@gre.ac.uk

Keywords: Boundary element method, finite difference method, diffusion problem

Extended Abstract.

We consider an approach to the numerical solution of the diffusion problem in which the 'space variation' is developed using a boundary element approach and the 'time development' is obtained in a hybrid Laplace transform/finite difference manner. The motivation for this study is the proposal of a time domain-decomposition procedure which has the potential for exploitation in a parallel computing environment. Such procedures have been considered before in a purely finite difference context in terms of the so-called *parareal algorithm* and this proposed approach is as follows: Decompose the time integration into coarse-grained time slabs and find the solution at the start of each time slab. Now use this coarse solution as an initial-value for a fine-grained solution over each slab. The fine-grained solution can then be used to recalculate the coarse solution and the process repeated. The coarse solution is sequential whereas the fine-grained solutions can be developed in parallel. There is also a potential data-distribution difficulty in the updating of the coarse solution as initial-values for the fine-grained solutions. This difficulty would be overcome if the coarse solution could also be developed in parallel.

A numerical Laplace transform approach using Stehfest's method provides just such an approach since the solution at any specific time can be obtained independently of those at any other times.The space solution at each time value could be obtained by any suitable solver. The most commonly used approach is that using finite differences. In our approach we shall use a boundary element technique in space incorporating the dual reciprocity method. This has been used extensively by the authors in both Laplace transform and finite difference time-decompositions.

We take as our test problem

$$\nabla^2 u = \frac{1}{\alpha}\frac{\partial u}{\partial t} + h(x,y,t) \quad \text{in} \quad \Omega$$

subject to suitable boundary and initial conditions.

We seek the solution $u(x,y,t)$ for $(x,y)\in\Omega$ and $0<t\le T$.

The coarse-grained approach is obtained by taking the Laplace transform of the initial boundary-value problem to obtain

$$\nabla^2 \overline{u} = \frac{1}{\alpha}\left(\lambda\overline{u} - u_0\right) + \overline{h} \quad \text{in } \Omega$$

subject to the transformed boundary conditions.

This non-homogeneous equation my be written in the form

$$\nabla^2 \overline{u} = b(x,y,\overline{u};\lambda)$$

and the corresponding boundary integral equation is

$$c_i\overline{u}_i + \int_\Gamma q^* \overline{u}_i d\Gamma - \int_\Gamma u^* \overline{q}_i d\Gamma + \int_\Omega b_i u^* d\Omega = 0$$

with a similar form for the value of $\overline{u}_i$ at internal points.

In these forms we can apply the dual reciprocity approach in which we expand the domain term in the form

$$b_i = \sum_{j=1}^{M} \alpha_j f_j(R_i)$$

where $\{f_j(R)\}$ is a set of linearly independent basis functions.

With this expansion we can approximate the boundary integral equation by the system of equations

$$\mathbf{H}\bar{\mathbf{U}} - \mathbf{G}\bar{\mathbf{Q}} = \mathbf{Sb}(\bar{\mathbf{U}})$$

where $\bar{\mathbf{U}}$ and $\bar{\mathbf{Q}}$ include N values on the boundary and L internal values.

The Stehfest method then yields the inverse transforms as follows:

$$U_r = \frac{\ln 2}{\tau} \sum_{j=1}^{m} w_j \bar{U}_{rj} \quad \text{and} \quad U_r^I = \frac{\ln 2}{\tau} \sum_{j=1}^{m} w_j \bar{U}_{rj}$$

where $r = 1,\ldots,N$ for boundary points and $r = 1,\ldots,L$ for internal points.

If we define the time slabs as

$$0 = \tau_0 \le t < \tau_1,\ \tau_1 \le t < \tau_2, \ldots, \tau_{p-1} \le t < \tau_p = T$$

then the fine-grained approach is applied in each time slab $\tau_i \le t < \tau_{i+1}$ $i = 0,1,\ldots,p-1$ and we could use any suitable finite difference time integration scheme. We use the Euler method to illustrate the process and set up the time-marching scheme

$$\mathbf{H}\mathbf{U}^{(k+1)} - \mathbf{G}\mathbf{Q}^{(k+1)} = \mathbf{Sb}(\mathbf{U}^k)$$

and the solution of this system of linear equations yields the solutions at the times t_k.

We illustrate the method with two examples, one linear and one nonlinear. We use the linear form $f(R) = 1 + R$ in the dual reciprocity domain function approximation. In both cases we see that the coarse-grained solution 'pulls back' the fine-grained solution tracking the analytic solutions to within a satisfactory approximation.

We show that the hybrid Laplace transform/finite difference method provides a suitable approach to the solution of diffusion problems.

In this investigation we consider the approach in a sequential manner. The process is, however, inherently parallel; the fine-grained solutions could all be obtained independently. Also, there would be no inter-processor communication and the implementation would have an excellent load balance since each processor performs exactly the same program on the same amount of data.

It is important to notice that in a parallel environment we can afford to do as much work in each time slab as would be needed in a global solution with the same finite difference approach to yield a solution at least as accurate as that produced by the coarse-grained, Laplace transform, solution.

A relation between the logarithmic capacity and the condition number of the BEM-matrices

W. Dijkstra[1], R.M.M. Mattheij[2]

[1]Department of Mathematics and Computing Science, Eindhoven University of Technology, P.O. Box 513, 5600 MB Eindhoven, The Netherlands, w.dijkstra@tue.nl

[2]Department of Mathematics and Computing Science, Eindhoven University of Technology, P.O. Box 513, 5600 MB Eindhoven, The Netherlands, r.m.m.mattheij@tue.nl

Keywords: Boundary element method; logarithmic capacity; condition number; Laplace problem.

1 Abstract

We establish a relation between the logarithmic capacity of a two-dimensional domain and the solvability of the boundary integral equation for the Laplace problem on that domain. It is proved that when the called logarithmic capacity is equal to one the boundary integral equation does not have a unique solution. A similar result is derived for the linear algebraic systems that appear in the boundary element method. As these systems are based on the boundary integral equation, no unique solution exists when the logarithmic capacity is equal to one. Hence the system matrix is ill-conditioned. We give several examples to illustrate this and investigate the analogies between the Laplace problem with Dirichlet and mixed boundary conditions.

2 Introduction

Boundary integral equations (BIE) form the basis for the boundary element method (BEM), which turns the BIE into a linear system of algebraic equations. The succes of the solution process of the linear system depends to a large extent on the condition number of the corresponding system matrix. Therefore it is important to have an a priori estimate for the magnitude of the condition number. To retrieve information about this condition number we have to resort to information resulting from the boundary integral formulation. If the BIE does not have a unique solution also the system of equations in the BEM does not have a unique solution, and the corresponding system matrix is ill-conditioned.

For the uniqueness of the solution of the BIE arising from a Laplace equation some interesting results can be found in literature. In [1], [2] and [3] it is observed that the BIE for the Laplace equation with Dirichlet boundary conditions does not have a unique solution if the scaling of the domain is inappropriate. This introduces an extraordinary phenomenon: the scaling of a domain affects the uniqueness properties of the solution of the BIE. Consider the BIE on a unit square domain, for instance, and rescale the domain to an arbitrary size. For almost all scalings the problem will have a unique solution, but there is one particular scaling for which this is not true. An intriguing question is whether we can know this scaling beforehand.

The remedy is to choose a scaling such that a unique solution does exist. It turns out that this is achieved when the Euclidean diameter of the domain is smaller than one. The authors in [4] give an explanation for this, using the concept of logarithmic capacity. They prove that if the logarithmic capacity of a domain is equal to one, then the boundary integral operator is not positive definite, and consequently no unique solution exists. It is shown that this logarithmic capacity is strongly related to the Euclidean diameter, see [5] and [6]. Unfortunately, for very few

domains the logarithmic capacity can be calculated explicitly. However, upper and lower bounds exist [7], [8] and also numerically computed estimates can be found [9].

As of yet, the Laplace problem with mixed boundary conditions received little attention . In [10] and [11] it is stated that this problem may not be uniquely solvable if the logarithmic capacity is equal to one, but this statement is not clarified any further. Therefore the topic of this paper is existence of a unique solution of the BIE for the Laplace equation with mixed boundary conditions in relation with the logarithmic capacity. We are aware of several formulations of the boundary integral equations. In this paper we choose for the direct symmetric collocation formulation. The direct formulation involves functions that can be easily related to physical quantities, whereas the indirect formulation uses auxiliary functions that have no physical meaning. The symmetric formulation, involving the single and double layer potentials, is more commonly used than the asymmetric formulation, which incorporates the hypersingular operator. Moreover, the asymmetric formulation yields matrices whose condition numbers are insensible to rescaling the domain. We prefer the collocation method above the Galerkin method. Again the collocation method is more commonly used and it does not require a second integration step like Galerkin method does.

References

[1] M.A. Jaswon and G. Symm. *Integral Equation Methods in Potential Theory and Elastostatics*. Academic Press, London, 1977.

[2] G.C. Hsiao. On the stability of integral equations of the first kind with logarithmic kernels. *Arch. Ration. Mech. Anal.*, 94:179–192, 1986.

[3] I.H. Sloan and A. Spence. The Galerkin method for integral equations of the first kind with logarithmic kernel: theory. *IMA J. Numer. Anal.*, 8:105–122, 1988.

[4] Y. Yan and I.H. Sloan. On integral equations of the first kind with logarithmic kernels. *J. Integral Equations Appl.*, 1:549–579, 1988.

[5] G. Pólya and G. Szegö. *Isoperimetric Inequalities in Mathematical Physics*. Princeton University Press, Princeton, 1951.

[6] T.J. Ransford. *A lower bound for capacity, pp136-138 in Linear and complex analysis problem: Problem book 3, part II, edited by V.P. Havin and N.K. Nikolski, Lecture Notes in Math.* Springer, New York, 1994.

[7] R.W. Barnard, K. Pearce, and A.Y Solynin. Area, width, and logarithmic capacity of convex sets. *Pacific J. Math.*, 212:13–23, 2003.

[8] C. Pommerenke. *Univalent Functions*. Vandenhoeck und Ruprecht, Göttingen, 1975.

[9] J. Rostand. Computing logarithmic capacity with linear programming. *Experiment. Math.*, 6:221–238, 1997.

[10] G.C. Hsiao, E.P. Stephan, and W.L. Wendland. On the integral equation method for the plane mixed boundary problem of the laplacian. *Math. Methods Appl. Sci.*, 1:265–321, 1979.

[11] G. Schmidt and H. Strese. The convergence of a direct BEM for the plane mixed boundary value problem of the laplacian. *Numer. Math.*, 54:145–165, 1988.

An Alternative Approach to Boundary Element Methods via the Fourier Transform

Fabian M.E. Duddeck[1]

[1] Department of Engineering, London University, Queen Mary College, Mile End Road, London E1 4NS, UK, f.duddeck@qmul.ac.uk

Keywords: Boundary Element Method, Fourier Transform, Fundamental Solution, Kirchhoff Plate Equation, Anisotropic Elasticity.

Abstract. The Fourier-BEM generalizes the standard BEM approach such that it can be applied to all cases of linear partial differential operators as long as the coefficients of these operators are constant. The knowledge of a fundamental solution is crucial to solve engineering problems with boundary element methods (BEM). Although available for a large number of cases relevant in engineering, there is still a need to find fundamental solutions which can be used in BEM; e.g. in the case of general anisotropic elastic media in three dimensions, a fundamental solution is still not known analytically.

Some approaches have been developed where the fundamental solution was derived in the Fourier space (transform with respect to spatial and temporal coordinates). If the differential operator is linear and has constant coefficients, its transformed form can be easily inverted, which leads directly to the Fourier transform of the fundamental solution. Unfortunately, the inverse transform can often not be obtained analytically. Numerical approaches have been developed; but they introduce additional numerical errors. The exact behavior of the fundamental solution around its singularities should be well represented; thus the numerical effort is rather high. The numerical values are normally evaluated before the BEM computation and stored in tables. An interpolation between these values during BEM computation is adding additional numerical errors to the overall approximation. It is therefore attractive to develop an approach, where these numerical drawbacks can be avoided. This is offered by the Fourier-BEM recently developed and first presented in Duddeck [3].

The principal idea is to avoid the inverse Fourier transform of the fundamental solution and to work directly with the Fourier transformed fundamental solution. Via Parseval's theorem, which states the equivalence of energy terms (or scalar products) in both, the original space and in the Fourier space, alternative boundary integral equations (BIE) can be established in the Fourier transformed domain. They lead to matrices identical to those obtained via the standard BIE. This approach can be applied to all cases as long as the differential operator is linear and has constant coefficients. Thus, the Fourier transformed boundary element method (or Fourier-BEM) generalizes the standard BEM.

For the Fourier BEM, every term should be established in the Fourier domain. Because a Galerkin approach leads to symmetric matrices and does not require a second integration in the Fourier BEM, this approach was preferred to the conventional collocation BEM. The trial and the test functions can be easily transformed to the Fourier domain as long as they are defined on straight elements. Otherwise a numerical approach can be selected.

In this paper, the method is summarized and then applied to isotropic and anisotropic plate problems according to Kirchhoff's theory (thin plates) with and without Winkler foundations. The differential operator is of fourth order leading in a Galerkin approach to highly singular integral equations. Although these singularities are quite complex, it can be shown easily that all strong and hyper singular terms are vanishing in both, the original and the Fourier transformed domain. In the small example, all integrals were solved analytically, thus – in contrast to other publications - no numerical errors, i.e. artificial oscillations, are occurring here at the edges of a rectangular plate. As an example, a clamped square plate is regarded subjected to a uniform load. The total system of Galerkin boundary integral equations were solved leading to the results depicted in the figure below.

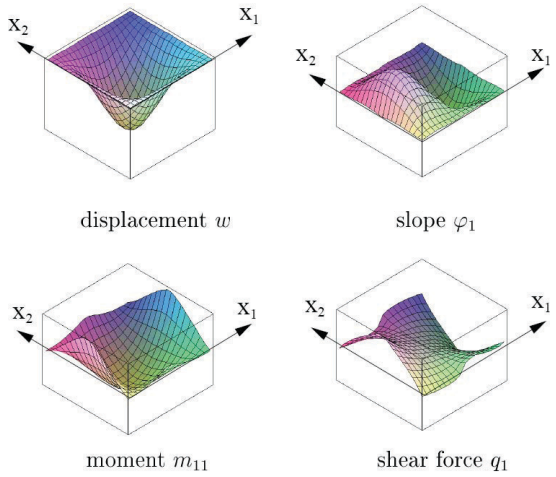

References

[1] H.Antes and P.D.Panagiotopoulos *The Boundary Integral Approach to Static and Dynamic Contact Problems*, Birkhäuser (1992).

[2] D.E.Beskos (ed.) *Boundary Element Analysis of Plates and Shells*, Springer (1991).

[3] F.M.E.Duddeck *Fourier-BEM – Generalization of Boundary Element Methods by Fourier Transform*, Springer (2002).

[4] F.M.E.Duddeck and M.Geisenhofer *A generalization of BEM by Fourier transform*, Computational Mechanics **28**, 303-310 (2002).

[5] F.M.E. Duddeck *Fourier-BEM – Or what to do if no fundamental solution is available?* Meccanica 36, 437-448 (2001).

[6] A.Frangi and M.Bonnet *A Galerkin symmetric and direct BIE method for Kirchhoff elastic plates: Formulation and implementation*, Int. J. Numer. Meth. Engrg **41**, 337-369 (1998).

[7] L.Hörmander *The Analysis of Linear Partial Differential Operators I*, 2nd edition, Springer (1990).

[8] P.Jahn *Die Randelement-Methode für elastisch gebettete Platten*, PhD thesis, University of Kassel (1998).

[9] M.Kitahara *Boundary Integral Equation Methods in Eigenvalue Problems of Elastodynamics and Thin Plates*, Elsevier (1985).

[10] S.G.Lekhnitskii *Anisotropic Plates*, Gordon & Breach (1968).

[11] A.Pomp *The Boundary-domain integral method for elliptic systems with an application to shells*, Springer (1998).

[12] L.Schwartz *Theorie des distributions*, Vol. I-II, Hermann & Cie (1950/51).

[13] M.Zhao Randelementmethode und Makroelemente für isotrope und anisotrope Kirchhoffsche Platten, PhD thesis, ETH Zurich (1995).

Fast BEM-FEM coupling for magnetostatics

A. Frangi[1], L. Ghezzi[2] and P. Faure-Ragani[2]

[1]Dept. of Structural Engineering, Politecnico of Milan, Italy, attilio.frangi@polimi.it
[2]ABB AT Italy Simulation Group, Italy

Keywords: Magnetostatics, multipole accelerators, FEM-BEM coupling

Abstract. Three dimensional magneto-mechanical problems at low frequency are addressed by means of a coupled fast Boundary Element - Finite Element approach with total scalar potential and focusing especially on the issue of global force calculation on movable ferromagnetic parts. The differentiation of coenergy in this framework and the use of Maxwell tensor are critically discussed and the intrinsic links are put in evidence. Three examples of academic and industrial applications are employed for validation.

Introduction

Several industrial relays working at low frequency display non-linear material behaviour of fixed and movable ferromagnetic parts embedded in the linear air domain. These features naturally call for the application of coupled BEM-FEM approaches which have been discussed in several contributions (e.g. [2, 4]) and take advantage of the versatility of the FEM to model material non-linearities and of the ability of integral approaches to account for infinite domains and movable structures. As often occurs in magnetostatics, the total scalar potential approach is privileged, since it is generally more robust than alternative edge element formulations [2] and avoids cancellation errors which are intrinsic in the perturbation scalar potential approach.
One of the main goals of numerical analyses is the evaluation of forces and moments which govern the mechanical response of the relay. Generally, the methods for force calculation in low frequency devices are based on one of two approaches (see e.g. [3, 6, 7, 8, 9]): the Maxwell stress tensor (MST) and the differentiation of the coenergy functional (DCF), or virtual work principle. These two approaches are usually derived from somewhat different starting points, even if in [6, 7] their strong connection has been put in evidence employing concepts of material differentiations. This common link is here re-established in the case of a general non linear material surrounded by air in the context of the coupled BEM-FEM approach. In the MST the force is computed by integrating over a surface enclosing the volume of interest provided it does not intersect other regions with surface or volume currents. Clearly, the quality of the solution strongly depends on the choice of the surface. Virtual work, on the other hand, computes the force on a body by evaluating the variation of the co-energy of the system either by sensitivity analysis, or by imposing a small physical displacement and using finite differences.

Formulation

Let us assume that the variation of currents inside the conductor is slow enough to neglect dynamic effects and justify the adoption of a magnetostatic formulation.
Let Ω_F denote the ferromagnetic domains, Ω_A the infinite "air" domain surrounding Ω_F and Γ the interface between Ω_F and Ω_A, endowed with the unit normal $\mathbf{n}$ pointing from Ω_F to Ω_A.
The field variables are assumed to satisfy the isotropic nonlinear constitutive relations:

$$\mathbf{B}_F = \mu_r(\mathbf{x}, |\mathbf{H}|)\mu_0\mathbf{H}_F \quad \text{in} \quad \Omega_F, \qquad \mathbf{B}_A = \mu_0\mathbf{H}_A \quad \text{in} \quad \Omega_A \tag{1}$$

where $\mathbf{H}$ is the magnetic field intensity and $\mathbf{B}$ the magnetic flux density. Also, the current density $\mathbf{j}$ is assumed to vanish in Ω_F while currents in Ω_A are treated as input data. Using the scalar potential

approach with ϕ total scalar magnetic potential, a Finite Element discretization is envisaged for Ω_F based on the variational equation:

$$\int_{\Omega_F} \nabla\tilde{\phi}(\mathbf{x})\mu_r(\mathbf{x},|\nabla\phi|)\nabla\phi(\mathbf{x})\mathrm{d}V = \int_{\Gamma} \tilde{\phi}(\mathbf{x})B_n(\mathbf{x})\mathrm{d}S, \quad \forall\tilde{\phi}\in H^1(\Omega_F) \tag{2}$$

where $B_n = \mathbf{B}\cdot\mathbf{n}$, while collocation BE are employed for Ω_A in view of its linear constitutive behaviour. The third Green identity written for a source point $\mathbf{y}$ lying on Γ reads:

$$k\phi^p(\mathbf{y}) = \int_{\Gamma} \left\{-G(\mathbf{y},\mathbf{x})B_n(\mathbf{x}) + \left[\nabla G(\mathbf{y},\mathbf{x})\cdot\mathbf{n}(\mathbf{x})\right]\phi^p(\mathbf{x})\right\}\mathrm{d}S \tag{3}$$

where kernel $G(\mathbf{y},\mathbf{x})$ is the potential theory Kelvin kernel. Since the perturbation potential $\phi^p = \phi - \phi^a$, where ϕ^a is the analytic potential which can be computed starting from given currents, eqns. (2) and (3) are expressed in terms of the unknown fields B_n and ϕ. For the numerical solution of the above system, Ω_F is discretized with four-node tetrahedra and the set of their facets lying on Γ represents the triangulation employed for the discretization of the BEM equation (3). The total potential ϕ is chosen in the space of continuous piece-wise linear functions as well as $\tilde{\phi}$, since a Galerkin approach is adopted for the FEM equations. The normal flux B_n is modeled as piecewise constant (constant over each BEM). Equation (3) is then collocated at the center of every triangular facet. Alternative elegant variational approaches have been proposed in the literature, but collocation is adopted here in order to privilege the crucial computing speed. The solution of the linear system is performed via an iterative GMRES solver and the matrix vector product required at each iteration is accelerated via fast multipole techniques.

In industrial applications one of the main objectives of the analysis is the computation of forces and moments acting on the movable ferromagnetic part Ω_{FM} which can be often treated as rigid. This poses severe difficulties especially when the gap between Ω_{FM} and the other fixed ferromagnetic parts Ω_{FF} is much smaller than the typical problem dimension. One of the key advantages of a coupled BEM-FEM approach is that Ω_{FM} can be freely moved without having to modify the mesh or deform it, hence it is the ideal tool for the problem at hand.

In the literature on Finite Elements several techniques are proposed resorting either to the concept of Maxwell tensor or to the differentiation of the coenergy functional. These techniques are here revisited to discuss their applicability in the present context.

Let us consider the infinite domain containing the structure of interest in which the movable part Ω_{FM} undergoes a given rigid body movement. We continuously extend the movement to the surrounding air by means of the mapping $\mathbf{y} = \mathbf{\Phi}(\mathbf{x},t)$, with initial condition $\mathbf{x} = \mathbf{\Phi}(\mathbf{x},0)$, which defines a domain transformation as a function of a parameter t (fictitious time) and initial position $\mathbf{x}$. The transformation $\mathbf{\Phi}(\mathbf{x},t)$ induces the velocity $\boldsymbol{\theta}(\mathbf{y},t) = \mathbf{\Phi}_{,t}(\mathbf{x},t)$ which, in Ω_{FM}, will necessarily have the rigid-body form $\boldsymbol{\theta}(\mathbf{y},t) = \mathbf{d}(t) + \boldsymbol{\omega}(t)\wedge(\mathbf{y}-\mathbf{x}_0)$, where $\mathbf{d}(t)$ represents the velocity of $\mathbf{x}_0$, $\boldsymbol{\omega}(t)$ the angular velocity associated to the rigid body movement and $\mathbf{x}_0$ is a fixed arbitrary point. The instant power of magnetic forces will then have the simple expression:

$$P(t) = \mathbf{F}(t)\cdot\mathbf{d}(t) + \mathbf{C}(\mathbf{x}_0,t)\cdot\boldsymbol{\omega}(t) \tag{4}$$

where $\mathbf{F}(t)$ and $\mathbf{C}(\mathbf{x}_0,t)$ are the resultant force and resultant moment with respect to $\mathbf{x}_0$, respectively, of forces acting on Ω_{FM}. Let us now focus the attention on the coenergy functional. It is well known that the instant power $P(t)$ associated to the rigid body movement of Ω_{FM} is the material derivative $\overset{\star}{\Psi}$ (see e.g. [3, 6, 7]) of Ψ when the material derivatives $\overset{\star}{\phi}$ of ϕ in the ferromagnetic parts and $\overset{\star}{\phi^p}$ of ϕ^p in air vanish. Using the formulas of material derivatives one obtains

$$\Psi = \int_{\Omega_\infty}\int_0^{\mathbf{H}} \mathbf{B}\mathrm{d}\mathbf{H}\mathrm{d}V \quad\rightarrow\quad P(t) = \int_{\Omega_\infty} \mathbf{B}\overset{\star}{\mathbf{H}}\mathrm{d}V + \int_{\Omega_\infty}\left(\int_0^{\mathbf{H}}\mathbf{B}\mathrm{d}\mathbf{H}\right)\nabla\cdot\boldsymbol{\theta}\,\mathrm{d}V \tag{5}$$

The combined use of eqns. (4) and (5) with suitable choices of $\mathbf{d}$ and $\boldsymbol{\omega}$ yields the desired values of $\mathbf{F}(t)$ and $\mathbf{C}(\mathbf{x}_0,t)$. This formula leads to the classical Maxwell tensor expression of forces and couples

Mesh	Mx	MxS	FD1	FD2
M1	332.7	332.4	342.87	343.02
M2	358.9	354.5	359.4	359.5
M3	370.9	362.8	365.6	365.7
M4	372.0	370.18	370.99	371.12
exact	372.88			

Table 1: Comparison of forces [N] on hollow sphere with different techniques

and also serves as a a basis for many FEM implementations. The approach of interest herein consists in evaluating the derivative of the coenergy functional using finite differences. This technique has been proposed several times in the literature in the context of FEM approaches, but discarded in view of possible cancellation errors, of the difficulty intrinsic in the evaluation of the coenergy of the infinite domain and of the need of multiple analyses. All these obstacles seem to play a minor role with the present BEM-FEM approach and finite differences turn out to be very competitive both in terms of accuracy, as shown in the numerical examples, and in terms of efficiency. Indeed, coenergy is a global measure and suffers marginally from the presence of local narrow gaps; moreover the analysis of industrial components is often required for a series of positions of Ω_{FM}, so that finite differences can be computed at almost zero cost. Even if a single geometric configuration is needed, the second phase, which is necessary for computing the finite difference, can be performed employing the relative permeability η_r obtained at convergence and the global cost hence gets only marginally incremented. Let us consider the coenergy of the infinite domain. It can be shown that, if Ψ^a_∞ is the coenergy in the infinite domain if $\mu_r = 1$ in Ω_F,

$$\Psi = \int_{\Omega_F} \left(\int_0^{\mathbf{H}} \mathbf{B} \mathrm{d}\mathbf{H} - \frac{\mu_0}{2} |\mathbf{H}^a|^2 \right) \mathrm{d}V + \frac{1}{2} \int_\Gamma (\phi - \phi^a)(B_n + B^a_n) \mathrm{d}S + \Psi^a_\infty \tag{6}$$

Clearly, when computing finite differences, Ψ^a_∞ cancels out since the current is assumed to be independent of Ω_{FM} movements.

Levitating sphere. Let us consider the classical benchmark of a hollow sphere with center point in $(0, 0, 0)$, outer radius 50 mm, inner radius 35 mm, $\mu_r = 500$, immersed in the magnetic field created by a circular coil of radius 70 mm and lying in a plane $x_3 = 30$ mm with given input current $I = 20000$ A. Four meshes (M1 with 1186 FE elements and 384 BE elements; M2 with 2813 FE elements and 864 BE elements; M3 with 6276 FE elements and 1536 BE elements; M4 with 29098 FE elements and 4707 BE elements) and four different techniques are employed for evaluating the global vertical force: *Mx* employs Maxwell tensor on a bounding surface S_M; *MxS* still applies Maxwell tensor but on the skin $\partial\Omega_{FM}$. *FD1* and *FD2*, on the contrary, are finite differences techniques using a vertical fictitious displacement of 0.001 mm 0.0001 mm respectively. A good convergence towards the exact value is observed, even with the first three very coarse meshes. The high accuracy of the *MxS* technique on the third and fourth meshes, however, has been obtained with an "optimal" surface S_M placed at a distance from Γ of the same order of magnitude as the typical surface element size. The finite difference technique turns out to be almost insensitive to the entity of the translation in a large range, numerical cancellations are virtually absent with the values of translations adopted and is hence a very robust approach.

Electromagnetic actuator. A second academic example is addressed in order to test the efficiency of the proposed approach in the presence of narrow gaps. It consists of an inner cylindrical core of length 100 mm and radius 20 mm, an external hollow cylinder of length 100 mm and width 5 mm, surrounded by a solenoidal winding simulated by 50 circular wires with a gap of 1 mm w.r.t. the cylinder surface and carrying an input current of $I = 2$ A each. The overlap between the two cylinders

gap	MxS	FD	Maxwell 2D
2 mm	.00192	.00222	.00223
1 mm	.00224	.00244	.00242
.5 mm	.00212	.00251	.00253
.1 mm	.00235	.00259	.00261

Table 2: Comparison of forces [N] on the inner core for different gaps between the two cylinders

is of 50 mm. The material of the cylinders is assumed linear with $\mu_r = 500$. The gap between the cylinders is decreased progressively from 2 mm to .1 mm. The results obtained are presented in Table 2 and are compared with the 2D (axysimmetric) commercial code Maxwell 2D. It is well know that 2D FEM codes can predict global forces with high precision, while this is not always the case in 3D. The accuracy of the 3D BEM-FEM code with finite differences is excellent, even if the mesh adopted is rather coarse (42291 FE elements and 11640 BE elements) and the gaps very thin. A displacement of .1 mm has been employed for computing FD, but results are almost insensitive up to 1 mm. As largely expected, the accuracy of Maxwell tensor on the skin rapidly decays even if results are still acceptable from an engineering point of view. The Mx approach has not been tested in view of the difficulty of creating a separate surface in the very thin gaps considered.

References

[1] Biro O., Preis K., Richter K.R. : On the use of the magnetic vector potential in the nodal and edge finite element analysis of 3D magnetostatic problem, *IEEE, Trans. Magn.*, 32, 651–654 (1996)

[2] Bossavit A. : *Computational elecretomagnetism*, Academic press, 1998,

[3] Coulomb J.L., Meunier G., : Finite Element implementation of virtual work principle for magnetic or electric force and torque computation, *IEEE Transaction on Magnetics*, 20, 1894–1896 (1984)

[4] Frangi A., Faure-Ragani P., Ghezzi L. : Magneto-mechanical simulations by a coupled Fast Multipole Method - Finite Element Method and multigrid solvers, *Computers and Structures*, 83, 718–726 (2005)

[5] Golia N.A., Tsiboukis T.D. : Magnetostatics with edge elements: a numerical investigation in the choice of the tree, *IEEE, Trans. Magn.*, 30, 2877–2880 (1994)

[6] Henrotte F., Vande Sande H., Delige G., Hameyer K. : Electromagnetic Force Density in a Ferromagnetic Material, *IEEE Transaction on Magnetics*, 40, 553–556 (2004)

[7] Kim D., Lowther D.A., Sykulski J.K. : Efficient Force Calculations Based on Continuum Sensitivity Analysis, *IEEE Transaction on Magnetics*, 1404, 1407–556 (2005)

[8] Ren Z. : Comparison of different force calculation methods in 3D finite element modeling, *IEEE, Trans. Magn.*, 30, 3471–3474 (1994)

[9] Vandevelde L., Melkebeek J.A.A. : A Survey of Magnetic Force Distributions Based on Different Magnetization Models and on the Virtual Work Principle, *IEEE, Trans. Magn.*, 37, 3405–3409 (2001)

Computational Modelling of Added mass effect on Hydrodynamic forces

Paola Gardano[1] and Peter Dabnichki[2]

[1] Department of Engineering, Queen Mary, University of London, Mile End Road, London, E1 4NS, UK email p.gardano@qmul.ac.uk

[2] Department of Engineering, Queen Mary, University of London, Mile End Road, London, E1 4NS, UK email p.dabnichki@qmul.ac.uk

Keywords: Boundary Element Methods; Laplace equations; added mass;

Abstract The present work utilises the Boundary Element Method to obtain the solution of the three dimensional Laplace's equation for the analysis of the flow around a moving body (human arm performing front crawl stroke) in an infinite domain. The study considers the effect of the added mass and the acceleration on the hydrodynamic forces (Drag and Lift) generated by the interaction between the flow and the body at different geometric configurations- variable elbow angle.

Introduction The dynamics of a structures surrounded by water requires special consideration in terms of induced acceleration in water and production of extra force on the structure in addition to the fluid dynamics drag force. This extra force can be modelled as the product of a hypothetical mass of water and the acceleration of the structure, the added mass. Theoretically the simplest approach for considering the flow around a structure is the potential flow idealization. The surrounding water is assumed to be incompressible and non-viscous which is very close to the actual behaviour of the fluid, and the resulting flow is assumed to be irrotational. The resulting governing equation under these assumptions is the Laplace equation. However, it is evident that the imposed flow assumptions are not entirely correct and solutions for real-life problems need to be rigorously validated. The effect of the added mass on the hydrodynamic forces during front crawl swimming is studied in this work. Front crawl is the fastest and most effective swimming style as the arm stroke is by far the major contributor to the forward movement of the swimmer and the most important part of his propulsion. Drag and Lift forces provide the majort contribution to the propulsion and the effect of the added mass can be seen on both forces. Swimming research has been until recently confined to steady analysis in both experimental and theoretical studies. However, due to the limitations of the experimental methods it is very difficult if not impossible to attribute the contribution of different factors to the propulsive force. Analytical approach is impossible due to the complex nature of the equations. Hence numerical approach becomes an invaluable tool in such simulations. The most prominent such approach is the Computational Fluid Dynamics (CFD) which is a summary name for a variety of computational methods. Although these methods are very powerful tools in studying flow type and properties, they are very intensive computationally and sometimes cumbersome for application to practical problems. The aim of this paper is to obtain an accurate representation of the grand added mass matrix in order to assess its effect on the propulsion generation during the stroke. The Boundary Element Method has been adopted to find the solution of the Laplace's equation that described our potential flow problem and to calculate the added mass matrix for a model of human arm simulating front crawl-stroke in quasi-static conditions. The hydrodynamic forces obtained in a low-speed wind tunnel on a prosthetic human arm have been corrected with the added mass effect and then compared with data obtained in a water pool on a similar model of human arm. In this way we assessed the importance of a dynamic analysis for the swimming phenomenon through the fundamental introduction of added mass and acceleration.

Method Boundary Element Method was used for the added mass calculation and was applied to the solution of the Laplace's equation that describing potential flow problem. The added mass is expressed as

$$m^k = \int_S \varphi^k n^k dS \tag{1}$$

with $k = 1,..,6$ that describes the linear and rotational motions, and where $\vec{n}$ is the unit normal vector on the body surface. The potential φ^k is the solution to the Laplace's equation $\nabla^2 \varphi^k = 0$ and the boundary condition $grad\varphi^k \cdot \vec{n} = \frac{\partial \varphi^k}{\partial n} = n^k$.

The solution to the Laplace's equation is obtained by covering the body surface with local source strength $\sigma(\xi,\eta,\zeta)$ at point $q(\xi,\eta,\zeta)$. To determine the finite number N of values $\sigma_i (i = 1,2,3...N)$ the integral equation becomes

$$\frac{\partial \varphi_i^k}{\partial n_i} = -\frac{1}{2}\sigma_i^k + \sum_{j=1}^{N} \sigma_j^k \int_{S_i} \vec{n}_i \cdot \nabla G_{ij}^k ds \qquad \begin{cases} i = 1,2,3,...,N \\ j = 1,2,3,...,N \\ k = 1,...,6 \end{cases} \tag{2}$$

After σ_i^k are determined, the velocity potential can be obtained by

$$\varphi_i^k = \sum_{j=1}^{N} \sigma_j^k \int_{S_i} G^k(x_i, y_i, z_i, \xi, \eta, \zeta) d \tag{3}$$

The each panel added mass can be get by $m_i^k = \varphi_i^k n_i^k A_i$ and the added mass of the body is

$$m^k = \sum_{i=1}^{N} m_i^k \tag{4}$$

The computational simulation was conducted on a three dimensional model of human arm performing front crawl stroke. The arm surface mesh contained 1024 six-nodded triangular rigid spherical shell elements. A single degree of freedom motion was analysed – rotation about the shoulder with variable speed. The kinematic variable was the angle of attack - the angle between plane of the arm and the flow direction. The range of motion analysed was 0^o - 130^o (slightly more than the normal stroke range) in increments of 10^o. The analysed configurations were for elbow angle of 180^o, 160^o and 135^o. The derived results were compared to the experimental ones reported by Lauder and Dabnichki (2005). This approach allows to both assessing the effect of the added mass and the suitability of the BEM for use in such problems.

Conclusion This paper assessed the suitability and reliability of the Boundary Element Method to analyse the problem of the added mass. In our specific case we calculated the added mass matrix of a human arm model performing front crawl in swimming even though this method can be extended to any other hydrodynamic case. What that makes this technique preferable to any CFD software is the avoided time-consuming. With the Boundary Element we analyzed a potential flow and the time we spent to run the program and obtain the added mass matrix was nearly 15 sec against the 3 hours of any CFD software. In this way we reached our principal aim to overcome the use of Navier-Stokes equations by using a more simple equation as Laplace's one, and at the same time we avoid the introduction the time dependency that would tend to bring in an always increased error. We show the superiority of a quasi static approach against a dynamic in terms of its effectiveness and accuracy as well.

References

1. Aliabadi, M. H. *The Boundary Element Method. Vol.2. Applications in solids and structures* 2002.
2. Gardano, P. and Dabnichki, P. *On Hydrodynamics of Drag and Lift of the Human Arm, Journal of Biomechanics* 2005; (http://www.jbiomech.com/inpress).
3. Lauder, M.A. and Dabnichki, P. *Estimating propulsive forces – Sink or swim. Journal of Biomechanics* 2005; 38: 1984-1990.

Meshless virtual boundary method and its applications to 2D elasticity problems

Sun Hai-tao[1], Wang Yuan-han[2]

[1]School of Civil Engineering and Mechanics, Huazhong University of Science and Technology, Wuhan, 430074, China, 13339838988@hb165.com

[2]School of Civil Engineering and Mechanics, Huazhong University of Science and Technology, Wuhan, 430074, China, yhwang0062@163.com

Keywords: numerical method, integral equation, interpolation scheme, radial basis function, virtual boundary, singular integral, boundary effect, singular values decomposition

Abstract. Many governing equations of engineering and scientific problems can be expressed mathematically as boundary integral equations (BIE). Since analyses of such BIE are usually hard in close form, various numerical methods have been developed for obtaining approximate solution. Conventional boundary element methods (BEM) for solving BIE numerically developed since 1960s share the same drawbacks of the other element-based numerical methods. One of them is that meshing techniques are required for generating elements. However, meshing task is a time exhausting process to the complex problem domain, especially in the case of elements being in distortion. In addition, BEM is usually required to treat singular integral arising from the fundamental solutions while source point is coincided with the field point. The boundary effects and corner problem are other troubles of BEM.

In the past decade, as a potential new generation of numerical method in computational mechanics, meshless methods have been receiving increasing attention from researchers. The manifestly characteristics of meshless methods are that mesh is not required, and the domain interested is discretized into a set of nodes instead of the collection of the elements. Furthermore, approximate solutions of the field variables are constructed based on a set of scattered nodes instead of on few elements. To take the advantage of the reduction of the problem dimension by one, the idea of meshless methods has been also used in BIE for overcoming the defect of the meshless methods in calculation efficiency. In most meshless methods for solving BIE, the field variables to be found are constructed based on moving least square (MLS) approach. Boundary node method (BNM) and meshless local boundary integral equation method (LBIE) are two major ones based on MLS approach. Since MLS approach lacks the Kronecker delta function property naturally, it is difficult to treat the boundary conditions in those numerical methods. In order to overcome the trouble resulted from the absence of the Kronecker delta function property, the other methods, such as boundary point interpolation method (BPIM), boundary radial point interpolation method (BRPIM), as well as boundary element-free method (BEFM) based on an improved moving least square method (IMLS) have been reported lately. Nevertheless, the challenge for eliminating singular integral and boundary effects resulted from the fundamental solution remains yet.

This paper proposes a novel virtual boundary method (VBM) for eliminating singular integral and boundary effect listed previous. In this work, the idea of the superposition method is introduced for establishing governing equations of the system in BIE. The core of the method is that extensional boundaries corresponding to the continuous true boundaries in coordinates, named virtual boundaries, are defined in the same space of the true domain. Over each virtual boundary, an auxiliary source function, named virtual source function, is supposed to be imposed on continuously. The sum of the effects of the virtual source functions and true source functions applied to the true domain of the problem must yield to the boundary conditions prescribed on the true boundaries while the fundamental solutions are implemented to the whole domain. As a result, the system governing equations are derived easily in weak form. Following the procedure of the numerical methods, discretization techniques are applied to the system governing equations. For this goal, an interpolation scheme based on the indirect radial basis function networks (IRBFN) is used to represent the original function for its high accuracy either in function interpolation or in function derivatives. This node-based interpolation scheme paves the way for that the elements are no more needed. In effect, Kronecker delta function property of the IRBFN can be implemented by adjusting the weighted values of the nodes. Due to this quasi-Kronecker delta function property of the interpolants, boundary conditions can be imposed as conveniently as conventional BEM. hence, virtual

source functions can be determined by solving the discretized system governing equations. Correspondingly, any field variable value desired in true domain would be evaluated according the system governing equations. Apart from virtual boundaries should be not intersection with true boundaries, no any other limit is required to the virtual boundaries. Therefore, virtual boundaries can be chosen as simple as possible. Usually a circle for 2D problems or a sphere for 3D problems is good choice for its simple. In addition, convenient numerical integral format is another important consideration. Since the virtual boundaries are always kept off the true boundaries, singular integration is not a problem at all. Boundary effects can be manipulated by adjusting the interval between the virtual boundaries and true boundaries. Outward normal of the true boundaries are not required in the calculation process, and the value of the outward normal of the virtual boundaries is determined uniquely for their smoothness and continuousness.

Several classical numerical test examples of 2D elasticity problems have been posed for verifying the performances of the method proposed. In the examples, all virtual boundaries are chosen as a circle whether for irregular shape of the problem domain or for the complex domain problems. Results show that the method has rather rapid convergence rate and higher accuracy even if the virtual boundaries and true boundaries are discretized by few nodes. Singular integration and boundary effects are avoided completely. Corner problem is nonexistent also. The algorithm of the method can be implemented simply.

References

[1] C.A.Brebbia, C.F.Telles, L.C.Wrobel *Boundary Element Techniques: Theory and Applications in Engineering*, Springer-Verlag, Berlin (1984.)

[2] P.K.Banerjee *Boundary Element Method in Engineering*, McGraw-Hill, Maindenhead, Berkshire, U.K (1994).

[3] H.C.Sun, L,H,Zhang, Q.Xu, Y.M.Zhang *Non-singularity Boundary Methods*, Dalian University of Technology Press, Dalian (1999).

[4] B.Nayroles, G.Touzot, P.Villon *Computational Mechanics*, **10**, 307-318 (1992).

[5] T.Blytschko, Y.Y.Lu, L.Gu, *International Journal for Numerical Methods in Engineering*, **37**, 229-256 (1994).

[6] W.K.Liu, S.Jun, Y,Zhang *International Journal for Numerical Methods in Fluids* **20**, 1081-1106 (1995).

[7] C.A.M.Duarte, J.T.Oden *Numerical Methods for Partial Differential Equations*, **12**, 673-705 (1996).

[8] J.T.Oden, C.A.M.Duarte, O.C.Zienkiewicz *Computer Methods in Applied Mechanics and Engineering*, **153**, 117-126 (1998).

[9] J.Braun, M.Sambridge *Nature*, **376**, 655-660 (1995).

[10] P.Lancaster, K.Salkauskas *Mathematics of Computation*, **37**, 141-158 (1981).

[11] S.Mukherjee, Y.X. Mukherjee *International Journal for Numerical Methods in Engineering*, **40**, 797-815 (1997).

[12] V.S.Kothnur, S.Mukherjee, Y.X. Mukherjee *International Journal of Solids and Structures*, **36**, 1129-1147 (1999).

[13] M.K.Chati, S.Mukherjee, Y.X. Mukherjee *International Journal for Numerical Methods in Engineering*, **46**, 1163-1184 (1999).

[14] T.Zhu, J.D.Zhang, S.N.Atluri *Computational Mechanics*, **21**, 223-235 (1998).

[15] G.R.Liu, Y.T.Gu *Engineering Analysis with Boundary Elements*, **28**, 475-487 (2004).

[16] Y.T.Gu,G.R.Liu *Structural Engineering and Mechanics*, **15(5)**, 535-550 (2003).

[17] N.Mai-Duy, T.Tran-Cong *Applied Mathematical Modeling*, **27**, 197-220 (2003).

[18] G.Burgess, E.Mahajerin *Computers and Structures*, **19**, 697-705 (1984).

[19] J.Park, I.W.Sandberg *Neural Compute*, **3**, 246-257 (1991).

[20] I.H.Guzelbey, G.Tonuc *Communications in Numerical Methods in Engineering*, **16**, 769-776 (1999).

[21] G.H.Golub,C.F.Van Loan, *Matrix Computations (Third Edition)*, Johns Hopkins University Press, Maryland, Baltimore (1996).

[22] S.P.Timoshenko, J.N.Goodier, *Theory of Elasticity (Third Edition)*, McGraw-Hill, New York (1970).

The detection of super-elliptical inclusions in infrared computerised axial tomography

N.S.Mera[1], L. Elliott[2] and D.B.Ingham[2]
[1]Centre for Computational Fluid Dynamics, University of Leeds, UK, N.S.Mera@leeds.ac.uk
[2]Department of Applied Mathematics, University of Leeds, UK,{lionel,amt6dbi}@amsta.leeds.ac.uk

Keywords: inclusion detection, superellipses, evolution strategy

Abstract: The purpose of this study is to investigate the efficiency, accuracy and rate of convergence of an evolutionary algorithm for detecting inclusions parameterised by superellipses in non-destructive evaluation and testing. The inverse problem investigated consists of identifying the geometry of discontinuities in a conductive material from Cauchy data measurements taken on the boundary. The super-elliptical form allows the parameteric model to characterise a variety of shapes whilst at the same time regularizing the problem by the function specification method. The boundary element method is employed in order to solve the direct problems. The algorithm developed by combining evolution strategies, the boundary element method and super-elliptical parameterisation is found to be fast and efficient.

Mathematical formulation

We consider the inverse conductivity problem which requires the determination of an isotropic object D, inclusion or cavity, contained in a domain Ω from measured temperature, ϕ, and heat flux, $\frac{\partial \phi}{\partial n}$, on the boundary $\partial\Omega$. We assume that the conductivity tensor K is symmetric and positive definite, whilst the medium $\Omega - D$ is isotropic with conductivity I. The refraction (transmission, conjugate) problem for the temperature ϕ is given by

$$\nabla \cdot ((I + (K - I)\chi_D)\nabla\phi) = 0, \quad \text{in } \Omega \qquad \phi = f, \quad \text{on } \partial\Omega \tag{1}$$

subject to refraction conditions related to the continuity of the temperature ϕ and its heat flux densities where χ_D is the characteristic constant function of the domain D. Assuming that K is known, the inverse conductivity problem requires the determination of D if the heat flux $\frac{\partial \phi}{\partial \boldsymbol{n}} = h$ is specified on $\partial\Omega$. The inclusion detection problem can be reformulated as an optimisation problem if for a given possible solution D for the cavity the direct problem (1) is solved to evaluate the heat flux on the outer boundary $\phi'_{calc} = \left.\frac{\partial \phi}{\partial \boldsymbol{n}}\right|_{\Gamma}$. Then the solution to the problem may be found by minimising the functional $J(D) = \|\phi'_{calc} - h\|_{L^2(\Gamma)}$ where q is the measured heat flux on the outer boundary.

Previous studies investigating the use of evolutionary algorithms for inclusions detection have only considered circular inclusions, see[1]. It is the purpose of this study to consider more a general parameterisation, namely the super-elliptical parameterisation given by

$$\left|\frac{x - x_0}{a}\right|^p + \left|\frac{y - y_0}{b}\right|^q = 1 \tag{2}$$

Thus, the problem of indentifying the inclusion D is reduced to identifying the parameters x_0, y_0, a, b, p and q. It should be noted that if $p = q = 2$ we obtain an ellipse while if $p = q = 2$ and $a = b$ we obtain the circular case. When p and q are increased the superellise is approaching a rectangular shape.

The Evolution Strategy with Covariance Matrix Adaptation (CMAES) see [2] is employed for optimisation since it is efficient for problems for which derivative based methods may fail due to a rugged search landscape

presenting multiple discontinuities, sharp bends, noise and local optima. The CMAES achieve higher rates of convergence than other evolution strategies by employing evolution paths rather that single mutation steps in the adaptation process. A detailed analysis of the advantages and limitations of the CMAES can be found in [2].

Numerical results

In order to test the efficiency of the algorithm proposed, we consider the domain $\Omega = \{(x, y) \mid (x^2+y^2 < R^2\}$, with $R = 2$, $k = 1$ with an isotropic inclusion D parameterised given by a superellipse given by eq (2). The inclusions are also allowed to be rotated at an angle θ_0 with respect to the axes of coordinates and therefore the there are seven parameters to be identified, namely x_0, y_0, a, b, p, q and θ_0.

The intermediate direct problems are solved using a Boundary Element Method (BEM). For the problem of inclusion detection, the BEM is particularly suitable since the geometry of the system changes for every possible solution tested during the optimisation process. This reduces the computational effort and eliminates the important perturbations due to changes in the mesh.

Figure 1 presents the CMAES generated solution in comparison with the exact solution for various inclusions of various sizes and locations. It should be noted that Figure 1 shows the results of several *different* problems, each consisting of the detection of a single inclusion, rather than the detection of multiple inclusions simultaneously. The numerical results have been obtained using 300 objective function evaluations and $s = 5\%$ noise added into the input data. It can be seen that the inclusions are retrieved very accurately even if only a small number of objective function evaluations are used.

Various other test examples have been considered and it was found that the algorithm proposed is very

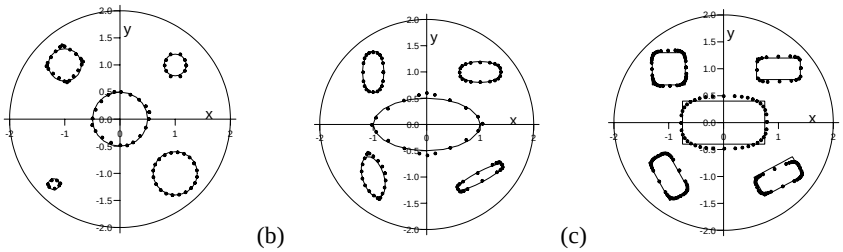

Figure 1: The numerical solution obtained by the CMAES (•) for various test examples given by (a) circular (b) elliptical and (c) rectangular inclusions of various sizes and locations in comparison with the exact solution (—). The five inclusions presented represent five single inclusion problems rather than one multi-inclusion problem.

efficient in locating an unknown inclusion even if no information about the shape of the inclusion is available. Overall, it may be concluded that the algorithm proposed is a robust, efficient and fast method for detecting the size and location of subsurface inclusions.

References

[1] N.S. Mera, L. Elliott and D.B. Ingham, Detection of subsurface cavities in IR-CAT by a real coded genetic algorithm, *Applied Soft Computing*, **2**, 129- 139 (2002).

[2] N. Hansen and A. Ostermeier Completely derandomized self-adaptation in evolution strategies, *Evolutionary computation*, **9**, 159-195 (2001).

Thermo-poro-elastostatic Green's Functions for Unsaturated Soils

Ehsan Jabbari[1] and Behrouz Gatmiri[1,2]

[1]Civil Engineering Faculty, University of Tehran, Tehran, Iran, Email: ehsan.jabbari@gmail.com

[2]Ecole Nationale des Ponts et Chaussées, Paris, France, Email: gatmiri@cermes.enpc.fr

Keywords: Boundary element method; thermal Green's function; fundamental solution; porous media; unsaturated soils.

Introduction

The study of coupled heat and moisture transfer in a deformable partly saturated porous medium is an area of research receiving considerable current attention. One reason for this interest is that the problem is of importance in the strategic, international issue of the safe disposal of high-level nuclear waste.

The Boundary Element Method (BEM), as the most efficient one among the numerical methods for solving the boundary value problems governing the various physical phenomena, is going to be employed for more complicated and coupled ones regarding the behavior and consequently the governing differential equations. As in this method, during formulating boundary integral equations, the applied mathematics concept of the Green's functions has been employed; this type of fundamental solutions for the governing partial differential equations should be first derived. Indeed, attempting to solve numerically the boundary value problems for unsaturated soils using boundary elements method leads one to search for the associated Green's functions.

The Green's functions for the governing partial differential equations of porous media have been presented in a series of papers begins with the work of Cleary and have grown with a pair of papers published by Chen as the most complete ones for saturated porous media.

For unsaturated soils the first Green's functions have been presented by the authors for isothermal static and quasi-static two and three-dimensional full and half-space problems. The present research is an effort for deriving thermo-poro-elastic full- and half-space Green's functions for two- and three-dimensional unsaturated media, for the first time, using a few necessary and sophisticated simplifications based on the previously introduced two- and three-dimensional Green's functions for the nonlinear governing differential equations of unsaturated soils for static and quasi-static poroelastic media by the authors and aims to extend the results to the thermal static problems. By employing the derived Green's functions in a proper computational model one will be able to compose a BEM model for prediction of thermoelastostatic behavior of unsaturated soils.

Governing Equations

For an unsaturated material influenced by heat effects, the governing partial differential equations consist of four main groups: equilibrium equations, air transfer equations, fluid transfer equations and heat diffusion equations. The equilibrium equations consist of static equilibrium equations based on the two independent parameters $(\sigma - p_a)$ and $(p_a - p_w)$, with linear elastic behavior and stress-strain relations including heat effects and also linear strain-displacement relations.

The air transfer equation consist of conservation law for air mass including the Darcy's law for air flow in which air coefficient of conductivity is a function of degree of saturation and consequently a function of suction. Likewise, water transfer equation employs conservation law and Darcy's law, again with the conductivity coefficient which is a function of suction, also considers vapor diffusion phenomenon based on the Philip and de Vries theory. Finally, heat equation consist of heat diffusion equation included in a conservation law applied for energy.

Green's Functions

For the Green's functions of the composed mathematical model to be derived, as the first step, the nonlinear governing differential equations should be linearized. This process should be performed so that the key features of the nonlinearity to be reserved.

For deriving the Green's functions of a linear system of partial differential equations, the classical method of Kupradze or Hörmander may be used. Based on this method, one has to search for a scalar potential function which has to be multiplied to the matrix of the cofactors of the differential operators' matrix of the governing differential equations that results in the Green's function's matrix. This procedure has been applied for both two- and three-dimensional problems and the corresponding Green's functions have been derived.

Since most of the engineering problems, especially in geomechanics and soils and foundation engineering, are of semi-infinite types in two or three-dimensional spaces, the corresponding half-space solutions are of much interest regarding computational applications. In this regard, the half-space Green's functions may be obtained applying the method of reflection or imaging which has been already used in other mathematical applications like hydrodynamics, employing the idea that on the reflection line or surface the solutions are of zero value.

Verification

Although, the final and exact verification and validation of the resulted Green's functions may be performed after preparing the computational model and employing it for comparison between physical observations and computational prediction, in this stage it is also possible to verify the results mathematically. In this regard, we have shown that, similar to the isothermal case, if the coefficients representing the thermal behavior of the phenomenon approach to zero the Green's functions will approach to the corresponding isothermal solutions exactly.

Illustration

Two of the derived Green's functions are illustrated in the following figures for a special normal type of unsaturated soil which show the expected typical behavior of a Green's function. Below the half-space two dimensional g_{11} and three-dimensional g_{12} are shown through Figs. 1-2.

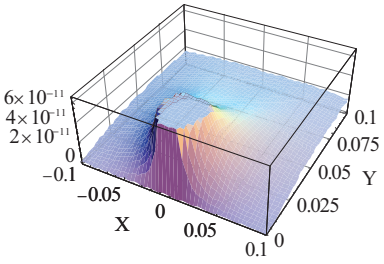

Fig. 1: 2D Half-space Green's function g_{11} solid skeleton displacement in direction one due to unit point load in direction one.

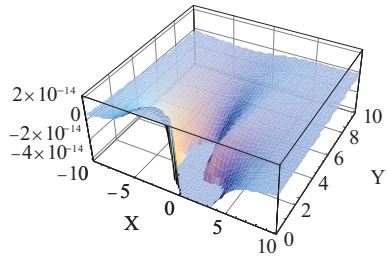

Fig. 2: 3D Half-space Green's function g_{12} solid skeleton displacement in direction one due to unit point load in direction two at $z = 0.10\,m$.

References

[1] B.Gatmiri, E.Jabbari, *5th International Conference on Boundary Element Techniques* (M.H.Aliabadi, V.M.A. Leitão), EC:, Lisbon, 217-221 (2004).

[2] B.Gatmiri, E.Jabbari, *5th International Conference on Boundary Element Techniques* (M.H.Aliabadi, V.M.A. Leitão), EC:, Lisbon, 223-227 (2004).

[3] B.Gatmiri, E.Jabbari, *International Journal of Solids and Structures*, **42**(23), 5971-5990 (2005).

[4] B.Gatmiri, E.Jabbari, *International Journal of Solids and Structures*, **42**(23), 5991-6002 (2005).

Application of the Method of the Fundamental Solutions as a Coupling Procedure to Solve Outdoor Sound Propagation

Sebastian Hampel[1], Adrián P. Cisilino[2] and Sabine Langer[3]

[1]Institute of Applied Mechanics, Technical University Braunschweig
P.O. Box 3329, D-38023 Braunschweig, Germany
E-Mail: sebastian.hampel@tu-bs.de

[2]Welding and Fracture Division, Faculty of Engineering, University of Mar del Plata
Av. Juan B. Justo 4302 - 7600 Mar del Plata, Argentina
E-Mail: cisilino@fi.mdp.edu.ar

Keywords: BEM, method of fundamental solutions, coupling, ray method, sound propagation

Introduction

In a computational model for outdoor sound propagation, the relevant propagation phenomena, among which are refraction and diffraction, must be implemented. All numerical methods applied in this field so far have disadvantages or limits. The Finite Element Method has to discretize the domain and hence is restricted to closed or at least moderate sized domains. The Boundary Element Method can hardly consider inhomogeneous domains and the computation effort increases exponentially for large systems. Geometric acoustics algorithms like ray tracing consider sound as particles and are hence not able to represent wave phenomena.

Hence, it is the intuition of these studies to combine the advantages of the BEM and of the ray method: In the near field where obstacles and complex geometries occur – and so diffraction and multiple reflection are expected - the model uses the BEM. Then, a ray model is coupled to compute the sound emission at large distances, because this model can take into account refraction resulting from wind or temperature profiles.

The ray model requires point sources as input data. However, a boundary element calculation always delivers the pressure or its normal derivative along the boundary. Hence, for the coupling of both models it is necessary to convert the BEM results into equivalent point sources. The Method of Fundamental Solutions (MFS) is found suitable for this purpose.

Problem Formulation

In outdoor acoustics, the considered domain is an infinite half space (see Figure 1). To couple the BEM and ray model, this half space is divided into a BEM domain and a ray domain by defining a virtual interface. Along this interface, the pressure is computed with the BEM (see Figure 1a). The idea behind the MFS is to place a number of sources with unknown intensities around the domain of interest. These intensities are then computed in order to fulfill prescribed boundary conditions at discrete points on the boundary of the domain (See Figure 1b). The MFS [1] can be either applied with fixed source positions or with an optimization algorithm, which finds the optimal source positions by minimizing the residual along the boundary in a least-squares sense.

Results and discussion

Two approaches are proposed for the MFS: The first one assumes fixed source positions whereas the second variant applies an optimization algorithm to find the optimal positions for the equivalent sources. With this purpose the subroutine LMDIF from MINPACK [2] was used.

Obtained results for the fixed-sources solution show that the positions of the sources have a strong influence on the matrix condition and in consequence on the quality of the MFS approximation. If the sources are too far away from the boundary points compared to the distance between two sources or two boundary points, the system will be ill-conditioned (i.e. high condition numbers). On the other hand, if the sources are too close to the boundary, the matrix entries will become infinite as the fundamental solutions are singular of $r \to 0$. In brief, the condition number of the system matrix depends on the number of sources and their relative positions with respect to the boundary points.

For an optimization algorithm it is usually very challenging to find the global minimum of a residual, if it has many local minima and maxima. The pressure field with complex pressure values and a nontrivial geometry shows to have a residual field which oscillates strongly in space. So for these cases a gradient-based optimization algorithm will fail, if the initial source positions are not chosen accidentally very close to the optimal positions. For the solution with the moving sources an approach is proposed which separates the complex pressure signal into its amplitude and phase information. It is shown that with this separation the optimization algorithm can be successfully applied to find the optimal source position. By optimizing the solution with respect to the amplitude only, the residual becomes quite smooth and therefore the problem is much easier to solve for the optimization algorithm. The time-harmonic characteristic is added and adjusted in a second step. To consider only the amplitude for optimization, the MFS algorithm was adapted, so that the fundamental solution is replaced by its absolute value and as boundary condition the pressure amplitudes are used.

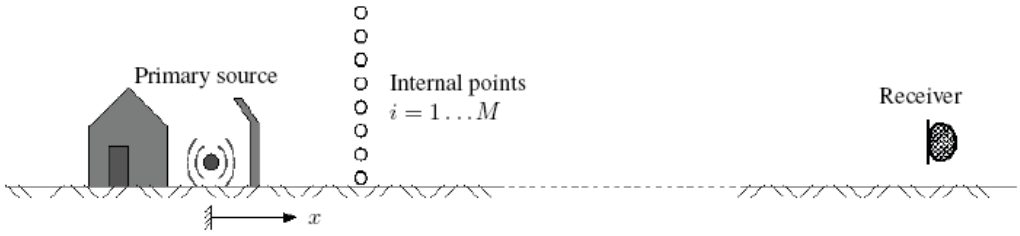

(a) BEM model configuration

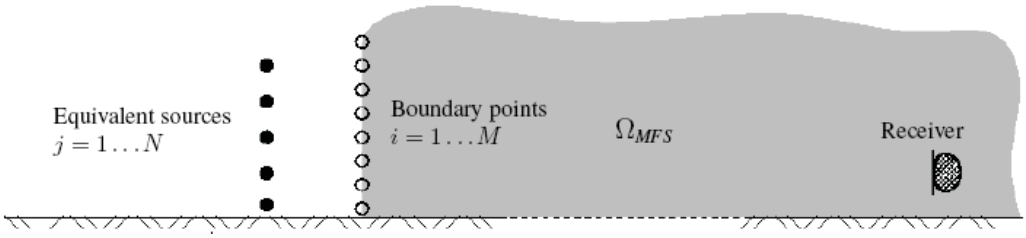

(b) MFS model configuration

Figure 1: Scheme of the hybrid model with one-way coupling at the interface

Conclusions

It is shown in this paper that the MFS can be successfully applied to couple a wave-based method and ray methods for solving outdoor sound propagation. The pressure distribution, which is a result from a wave-based method, e.g. the BEM, can be well-approached by a number of equivalent point sources, which are required as input data for most ray methods. The MFS formulation with moving sources delivers more accurate results than the one using fixed sources.

References

[1] G. Fairweather, A. Karageorghis, and P. A. Martin. The method of fundamental solutions for scattering and radiation problems. Engineering Analysis with Boundary Elements, 27, 759–769 (2003).

[2] Netlib Software library. MINPACK. URL: http://www.netlib.org/minpack/, Chicago, USA, (2005)

Local Defect Correction for the Boundary Element Method

G. Kakuba, R. M. M. Mattheij, M.J.H. Anthonissen

Eindhoven University of Technology, CASA,

P.O.Box 513, 5600MB Eindhoven, The Netherlands

g.a.kakuba@tue.nl,

Tel.: +31-40-2475546

Keywords: local activity, local defect correction, global coarse grid, local fine grid

Abstract

In the boundary element method, the solution of a function on a given domain is expressed as an integral equation in terms of its values and normal derivatives at the domain boundary. The boundary conditions are either Dirichlet or Neumann or both in the case of a mixed boundary conditions problem. Sometimes the boundary contains small regions of high activity. This paper presents an efficient way to implement the Boundary Element Method (BEM) to capture the high activity. In boundary regions where accuracy is critical, like in adaptive surface meshes, the method of choice is Local Defect Correction (LDC). We formulate the method and demonstrate its applicability and reliability by means of an example. Numerical results show that LDC and BEM together provide accurate solutions with less computational requirements like memory space and time. This is important given that BEM systems usually consist of dense matrices. With fine meshes required to capture the high activity in local boundary regions where accuracy is critical, like in adaptive surface meshes, the resulting matrices are always large and thus raising computational complexity. Applying Local

Defect Correction (LDC) to the BEM in a way of a domain decomposition algorithm can be seen as a compromise between global refinement which is very expensive in memory and work and local grid refinement at selected parts of the global grid which requires the least additional memory and may be much faster than the former. This is a very attractive factor as BEM usually results in dense systems. We show that it is at least twice less complex to incorporate LDC in BEM rather than use a composite grid and at least 40 times less complex if LDC was used instead of uniform global refinement. Already, a lot of work has been done on LDC algorithms with other numerical methods and a lot of literature on BEM is readily available. We build on this work and develop an algorithm that integrates LDC with BEM to provide a less complex option for boundary value problems with localised high activity behaviours. The problem is first solved on a global coarse grid; the computed coarse grid forms part of the boundary condition for a local problem where a more accurate solution can be computed by means of a smaller grid size. The global coarse grid solution and the local fine grid solution are combined in a special way in an iterative manner through defect correction to improve the first coarse grid approximation. The new coarse grid approximation can in turn provide a boundary condition for a new local problem. The process is repeated till convergence, which is in general very fast.

The Boundary Element Method for Solving the Laplace Equation in Two-dimensions with Oblique Derivative Boundary Conditions

D. Lesnic
University of Leeds, Department of Applied Mathematics, Leeds LS2 9JT, UK
e-mail: amt5ld@maths.leeds.ac.uk

Keywords: Boundary element method (BEM), Laplace's equation, Oblique boundary conditions.

Abstract. In this communication, we extend the Neumann boundary conditions by adding a component containing the tangential derivative, hence producing oblique derivative boundary conditions. A variant of Green's formula is employed to translate the tangential derivative to the fundamental solution in the BEM. The two-dimensional steady state heat conduction with the imposed oblique boundary conditions has been tested in a circular domain in which the Laplace equation is the governing equation producing results at the boundary in excellent agreement with the available analytical solution. Convergences of the normal and tangential derivatives at the boundary are also achieved. This means that if oblique derivative boundary conditions are prescribed, then the gradient of the solution ∇u can be accurately obtained on the boundary without the need of hypersingular analysis, or $\nabla u-$type methods [1]. The numerical boundary data is then used to calculate the values of the solution at interior points again with success. The outlined test case has been repeated with various boundary element meshes and results indicate that the accuracy of the numerical results increase with increasing the boundary discretisation.

1. Introduction

Let us consider steady-state heat conduction given by the Laplace equation inside a plane bounded domain $\Omega \subset R^2$ with a smooth boundary $\partial\Omega$, namely

$$\nabla^2 u = 0, \quad \text{in } \Omega. \tag{1}$$

which has to be solved subject to the oblique derivative boundary condition

$$b_1 \frac{\partial u}{\partial \nu} + b_2 \frac{\partial u}{\partial \tau} = g, \quad \text{on } \partial\Omega, \tag{2}$$

where $\partial/\partial\tau$ denotes the derivative in the direction tangential to $\partial\Omega$, g is a given continuous function, and b_1, b_2 are given smooth functions satisfying $(b_1, b_2) \neq (0, 0)$ on $\partial\Omega$. Boundary conditions of the type (2) arise in the study of the motion of water in a canal [2, pp.25-27]. The condition that b_1, b_2 are smooth functions satisfying $(b_1, b_2) \neq (0, 0)$ on $\partial\Omega$ ensures the ellipticity of the problem (1) and (2) and it is called the Shapiro-Lopatinskii condition [3, pp.40,61]. In the special $b_1 = 1$, $b_2 = 0$ we obtain the Neumann boundary condition

$$\frac{\partial u}{\partial \nu} = g, \quad \text{on } \partial\Omega. \tag{3}$$

In what follows, we assume that $b_1 \neq 0$ on $\partial\Omega$, such that the boundary condition (2) becomes normal [3, p.63], and then the problem (1) and (2) has a solution in $C^2(\Omega) \cap C(\overline{\Omega})$, which is unique up to a constant, if and only if

$$\int_{\partial\Omega} \frac{g - b_2 \frac{\partial u}{\partial \tau}}{b_1} ds = 0. \tag{4}$$

In the case when b_1 and b_2 are constants, then since $\partial\Omega$ is a smooth closed curve we have that $\int_{\partial\Omega} \frac{\partial u}{\partial \tau} ds = 0$, and hence condition (4) becomes

$$\int_{\partial\Omega} g \, ds = 0, \tag{5}$$

which is the well-known condition for the existence of a solution of the Neumann problem (1) and (3).

In order to make the solution of the problem (1) and (2) unique we further require that

$$\int_{\partial\Omega} u \, ds = 0. \tag{6}$$

If mixed boundary conditions are allowed, i.e. u is specified at least at one point on $\partial\Omega$, then there is no need to impose (6).

2. Green's Formula

Denoting by $G(p,p') = -\frac{1}{2\Pi} ln \mid p - p' \mid$ the fundamental solution of the Laplace eq (1) in two-dimensions, we have the Green formula [4],

$$\eta(p)u(p) = \int_{\partial\Omega} \left[G(p,p') \frac{\partial u}{\partial \nu}(p') - u(p') \frac{\partial G}{\partial \nu(p')}(p,p') ds(p') \right], \quad p \in \overline{\Omega}, \tag{7}$$

where $\eta(p) = 1$ if $p \in \Omega$ and $\eta(p) = 0.5$ if $p \in \partial\Omega$.

Since $\partial\Omega$ is a smooth closed curve the following identity

$$0 = \int_{\partial\Omega} \frac{\partial}{\partial \tau(p')} (u(p') b_1^{-1}(p') b_2(p') G(p,p')) ds(p')$$

$$= \int_{\partial\Omega} \left[b_1^{-1}(p') b_2(p') G(p,p') \frac{\partial u}{\partial \tau}(p') + u(p') \frac{\partial}{\partial \tau(p')} (b_1^{-1}(p') b_2(p') G(p,p')) \right] ds(p'), \quad p \in \overline{\Omega}. \tag{8}$$

holds. By substituting (2) into (7) and using (8) we obtain

$$\eta(p)u(p) = \int_{\partial\Omega} \left\{ \frac{g(p') G(p,p')}{b_1(p')} - u(p') \left[\frac{\partial G}{\partial \nu(p')}(p,p') - \frac{\partial}{\partial \tau(p')} (b_1^{-1}(p') b_2(p') G(p,p')) \right] \right\} ds(p'), \quad p \in \overline{\Omega}. \tag{9}$$

By using (8) we avoided the use of finite differences in implementing the oblique derivative boundary condition (2).

Applying eq (9) at $p \in \partial\Omega$ we obtain a Fredholm integral equation of the second kind which has a unique solution provided that (4) and (6) are fulfilled.

Once $u \mid_{\partial\Omega}$ has been accurately obtained, eq (9) gives the solution $u(p)$ explicitly at any interior point $p \in \Omega$. Also, the use of (7) for $p \in \partial\Omega$ gives the normal derivative $\partial u / \partial \nu$ on $\partial\Omega$, and finally, if $b_2 \neq 0$ on $\partial\Omega$, eq (2) gives the tangential derivative $\partial u / \partial \tau$ on $\partial\Omega$.

References

[1] V.Mantic, E.Graciani and F.Paris *Communications in Numerical Methods in Engineering*, **15**, 547-556 (1999).

[2] R.Dautray and J.-L.Lions *Mathematical Analysis and Numerical Methods for Science and Technology, Vol1*, Springer-Verlag (1990).

[3] V.A.Kozlov, V.G.Maz'ya and J.Rossmann *Elliptic Boundary Value Problems in Domains with Point Singularities*, Mathematical Surveys and Monographs, Vol.52, AMS, Providence (1997).

[4] G.T.Symm and R.A.Pitfield *Solution of Laplace's Equation in Two Dimensions*, NPL Report NAC44 (1974).

From damage to crack: a B.E. approach

Vincenzo Mallardo[1], Claudio Alessandri[2]

[1] Dep. Architecture – via Quartieri 8 – 44100 Ferrara (Italy) – mlv@unife.it

[2] Dep. Architecture – via Quartieri 8 – 44100 Ferrara (Italy) – ale@unife.it

Keywords: Nonlocal, damage, crack, BEM

Abstract. Following some recent results (see [1-3]), the Authors mean to present some analyses concerning the strain localisation in damage analysis by the Boundary Element Method (BEM) and the possibility to shift from the continuous damage analysis to the crack analysis. A non local approach of integral type is applied in the context of a damage model. A criterion is introduced in order to insert a crack in the damaged zone. Such macro-crack can be analysed by the Dual Buoundary Element Method (DBEM). The BEM/DBEM seems to be very suitable for such application. In consequence of the localisation, the damaged zone results to be small in comparison with the total size of the structure, i.e. the domain discretisation is limited. Furthermore, due to the special features of the DBEM, the introduction of the crack requires a minimum addition of unknowns.

Evolution from damage to crack

For a isotropic damage model, the stress-strain relation can be written in the following way:

$$\sigma = (1-d)\mathbf{C}^{el} : \varepsilon \tag{1}$$

The model is set consistently with thermodynamic principles by the introduction of a kinematic internal variable α, a energy per unit of volume Y and a force X:

$$Y := \frac{1}{2}\varepsilon : \mathbf{C}^{el} : \varepsilon \qquad \mathrm{X} := k \ln^{n} \frac{c}{1-\alpha}\,. \tag{2}$$

k, c and n are material parameters. The existence of a damage activation function $g(Y, \mathrm{X})$ is assumed. Under the hypothesis of generalised associative damage behaviour, the damage activation function and the flaw laws can be written as:

$$g(Y,\mathrm{X}) = Y - Y_0 - \mathrm{X} \le 0 \qquad \dot{d} = \dot{\lambda} = \dot{\xi} \ge 0 \qquad \text{with } \dot{\lambda} \ge 0 \text{ and } \dot{\lambda}\, g = 0 \tag{3}$$

The nonlocal version of the described model is obtained by substitution of the strain energy rate Y with its nonlocal value (see [2] for details).

The governing integral equations are given by the displacement boundary integral, by the expression of the stress state at any internal point and, on the basis of the DBEM, by the displacement boundary integral equation and the by the traction equation, both at a crack node.

Before the crack initiation, the discretised form of both the classical displacement boundary integral equation and the integral expression of the stress tensor are adopted in the iterative scheme.

Once the damage in one or some points passes a fixed threshold $\bar{d}$, a crack line is inserted and the discretised form of the dual boundary (displacement and traction) equations is added collocating at every crack node. The proposed model may furnish snap-back branches in the equilibrium path, i.e. it may be necessary to introduce an arclength constrain in the general system of equations. This is achieved by following the scheme proposed in [1].

The crack extends when the damage around the crack tip reaches a critical value $\bar{d}$. If $\bar{d}$ is set equal to the unity, the stress transfer is fully correct. This is not true if the critical value of the damage is set less than one, i.e. lines on which the stress tensor is different from zero are substituted by traction free crack lines. The drawback could be avoided if the transition between damage and traction-free crack is led by using the fictitious crack model both for the closing normal force and for the frictional force.

A numerical example

A numerical example is presented in order to assess the efficienty of the procedure

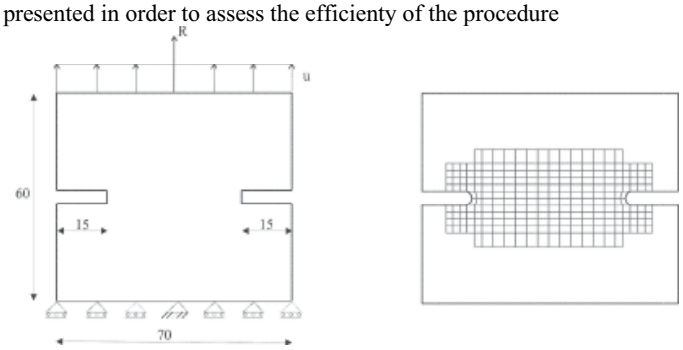

Fig. 1 - Geometry, load condition and domain discretisation. E=36000MPa and ν=0.15

It refers to the slab in Fig. 1 where a plane stress behaviour is assumed and measures are given in millimeters. An increasing displacement is applied on the top edge of the slab, the corresponding distributed reaction with resultant R is not uniform. The domain discretisation drawn in Fig. 1 is adopted.

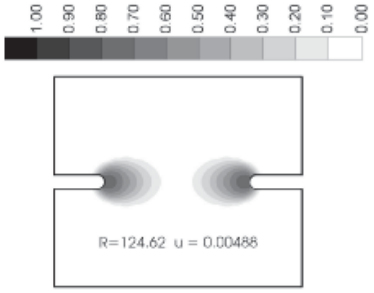

Fig. 2 - Damage contour plot at the crack initiation

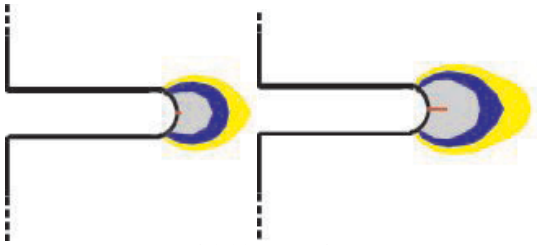

Fig. 3 – Crack initiation and propagation

Fig. 2 shows the nonlocal damage contour at the load level in which the crack occurs, i.e. the damage parameter exceeds a pre-defined critical value $\bar{d}$ =0.85. The crack starts correctly at the notches. A zoom on the left notch of the slab is given in Fig. 3. The red colour corresponds to d=0.85 whereas the remaining three colours correspond to the levels 0.8, 0.75 and 0.7.

In the left part of Fig. 3 the red point gives the point of the crack initiation. The right part describes the crack configuration some load steps further. The crack propagates in the correct direction.

Summary

A new method for the evolution from damage to crack in brittle materials with the Boundary Integral Equations has been proposed. The idea is to shift from a nonlocal damage model to a discrete crack model when the damage parameter reaches a critical value. The crack is numerically treated by the DBEM.

References

[1] V. Mallardo, C. Alessandri, *Eng. Analysis Bound. Elem.*, **28(6)**, 547-559, (2004).

[2] V. Mallardo, *Computer Modelling in Engineering & Sciences*, submitted, 2006.

[3] V. Mallardo, C. Alessandri, *Structural Durability & Health Monitoring*, accepted, 2006.

Boundary element analysis of three-dimensional exponentially graded isotropic elastic solids

R. Criado, J.E. Ortiz, V. Mantic, L.J. Gray, F. Paris

[1] School of Engineering, University of Seville, Camino de los Descubrimientos s/n, Sevilla E-41092, Spain

[2] Computer Science and Mathematics Division, Oak Ridge National Laboratory, Oak Ridge TN 37831-6367, USA

Keywords: functionally graded materials, boundary element method, three-dimensional elasticity, Somigliana identity, fundamental solution in tractions.

Introduction

Functionally Graded Materials (FGMs) [1] represent a new generation of composites, having a continuous variation of apparent material properties obtained through a progressive variation of their microstructural composition. Stress concentrations appearing at material discontinuities in various applications (for example, thermal barrier coatings) can be avoided or diminished using FGMs.

The Boundary Element Method (BEM) [2,3] is a suitable numerical technique for elastic analysis, capable of solving problems with material and geometrical discontinuities, e.g., crack growth and contact, and also very suitable for flaw detection and shape optimization. Nevertheless, an adaption of BEM to non-homogeneous media is a hard task, as fundamental solutions for such media are difficult to obtain.

Fundamental solutions for 2D and 3D elastic problems in exponentially graded isotropic materials have been deduced only recently in [4,5]. These solutions have not as yet been checked computationally, to the knowledge of the present authors, which can be due to the fact that implementing them in a BEM code is far from straightforward.

In the present work the displacement fundamental solution U_{jl} corresponding to a point force in a 3D exponentially graded elastic isotropic media, developed originally in [5] and corrected in [6], is employed in the form presented in [6]. Moreover, a new expression of the corresponding traction fundamental solution T_{jl} is presented herein, and both functions have been implemented in a 3D collocational BEM code. To check the correctness of the kernel function expressions and to prove their suitability to be implemented in a BEM code, and also to check the overall BEM implementation, two 3D problems with known analytic solutions for exponentially graded materials have been analysed by this BEM code.

Elastic Fundamental Solution in 3D Exponentially Graded Isotropic Materials

Material properties. In the case of isotropic exponentially graded materials, the Lamé constants vary according to the following law:

$$\lambda(\boldsymbol{x}) = \lambda_0 \exp(2\boldsymbol{\beta}\,\boldsymbol{x}) \text{ and } \mu(\boldsymbol{x}) = \mu_0 \exp(2\boldsymbol{\beta}\,\boldsymbol{x}), \tag{1}$$

where $\boldsymbol{x}$ is a point in the material and the vector $\boldsymbol{\beta}$ defines the direction and exponential variation of grading, $\beta = |\boldsymbol{\beta}|$, λ_0 and μ_0 are the Lamé constants on the plane that includes the origin of coordinates. It is easy to check, that the Posson ration is constant, $\nu = \lambda_0 / 2(\lambda_0 + \mu_0)$.

Displacement fundamental solution. According to [5], the displacement fundamental solution can be written as

$$\boldsymbol{U}(\boldsymbol{x}, \boldsymbol{x}') = \exp\{-\boldsymbol{\beta}.(\boldsymbol{x} + \boldsymbol{x}')\}\{\boldsymbol{U}^0(\boldsymbol{x} - \boldsymbol{x}') + \boldsymbol{U}^g(\boldsymbol{x} - \boldsymbol{x}')\}, \tag{2}$$

where $U_{jl}(\boldsymbol{x},\boldsymbol{x}')$ gives the *j*-th displacement component at $\boldsymbol{x}$ due to a unit point force acting in the *l*-direction at point $\boldsymbol{x}'$, and U^0_{jl} is the weakly singular Kelvin fundamental solution associated to a homogenous isotropic material defined by λ_0 and μ_0 (see [2,3]). The so-called grading term

$$U^g_{jl}(\boldsymbol{x}-\boldsymbol{x}') = -(4\pi\mu_0 r)^{-1}(1-e^{-\beta r})\delta_{jl} + A_{jl}(\boldsymbol{x}-\boldsymbol{x}'), \tag{3}$$

is bounded and vanishes for $\beta = 0$ and $r = |\boldsymbol{r}|$ where $\boldsymbol{r} = \boldsymbol{x}-\boldsymbol{x}'$. According to [5,6] the term A_{jl} is composed of the several single integrals involving Bessel functions and several double integrals involving hyperbolic functions.

A discussion of the properties of the fundamental solution U_{jl} together with recommendations for its numerical evaluation can be found in [6].

Traction fundamental solution. The starting point in the evaluation of tractions in an exponentially graded material due to a unit point force is the differentiation of the fundamental solution in displacements U_{jl}. These derivatives are used to determine the corresponding strains, and then, employing the constitutive law with the tensor of elastic stiffnesses given in (1), the corresponding stresses can be obtained.

Differentiation of (2) yields

$$\frac{\partial U_{jl}}{\partial x_k}(\boldsymbol{x},\boldsymbol{x}') = \exp(-\boldsymbol{\beta}(\boldsymbol{x}+\boldsymbol{x}'))\left(\frac{\partial U^0_{jl}}{\partial x_k}(\boldsymbol{x}-\boldsymbol{x}') + \frac{\partial U^g_{jl}}{\partial x_k}(\boldsymbol{x}-\boldsymbol{x}')\right) - \beta_k U_{jl}(\boldsymbol{x},\boldsymbol{x}'). \tag{4}$$

Although the derivative of U^0_{jl} is strongly singular, this term eventually produces the Kelvin traction kernel for a homogeneous material; the expressions can be found in [2,3]. The derivative of U^g_{jl} is weakly singular and can be expressed, in view of (3) as

$$\frac{\partial U^g_{jl}}{\partial x_k}(\boldsymbol{x}-\boldsymbol{x}') = -\frac{\delta_{jl}}{4\pi\mu_0}\left\{\frac{e^{-\beta r}(\beta\, r_{,k})}{r} - \frac{(1-e^{-\beta r})r_{,k}}{r^2}\right\} + \frac{\partial A_{jl}}{\partial x_k}(\boldsymbol{x}-\boldsymbol{x}'). \tag{5}$$

Note that the weakly singular character of $\partial U^g_{jl}/\partial x_k$ directly follows from the boundedness of U^g_{jl} and the Gauss divergence theorem.

The strains E_{ijl} associated with the fundamental solution in displacements U_{jl} are given by

$$E_{ijl}(\boldsymbol{x},\boldsymbol{x}') = \frac{1}{2}\left(\frac{\partial U_{il}}{\partial x_j}(\boldsymbol{x},\boldsymbol{x}') + \frac{\partial U_{jl}}{\partial x_i}(\boldsymbol{x},\boldsymbol{x}')\right). \tag{6}$$

Applying the constitutive law with the elastic stiffnesses from (1) yields the corresponding stresses:

$$\Sigma_{ijl} = 2\mu(\boldsymbol{x})E_{ijl}(\boldsymbol{x},\boldsymbol{x}') + \lambda(\boldsymbol{x})E_{kkl}(\boldsymbol{x},\boldsymbol{x}')\delta_{ij}. \tag{7}$$

Then, substituting (6) into (7) and using (4) yields

$$\Sigma_{ijl}(\boldsymbol{x}-\boldsymbol{x}') = \exp(\boldsymbol{\beta}(\boldsymbol{x}-\boldsymbol{x}'))\left(\Sigma^0_{ijl}(\boldsymbol{x}-\boldsymbol{x}') + \Sigma^g_{ijl}(\boldsymbol{x}-\boldsymbol{x}')\right), \tag{8}$$

where the strongly singular term $\Sigma^0_{ijl}(\boldsymbol{x}-\boldsymbol{x}')$ represents the stress tensor σ_{ij} at $\boldsymbol{x}$ originated by a unit point force in direction *l* at $\boldsymbol{x}'$ in the homogeneous elastic isotropic material having Lamé constants λ_0 and μ_0 (see [2,3]). The weakly singular grading term $\Sigma^g_{ijl}(\boldsymbol{x}-\boldsymbol{x}')$ is expressed as:

$$\Sigma^g_{ijl}(\boldsymbol{x}-\boldsymbol{x}') = \mu_0\left(\frac{\partial U^g_{il}}{\partial x_j} + \frac{\partial U^g_{jl}}{\partial x_i} - \beta_i\left(U^0_{jl}+U^g_{jl}\right) - \beta_j\left(U^0_{il}+U^g_{il}\right)\right) + \lambda_0\left(\frac{\partial U^g_{kl}}{\partial x_k} - \beta_k\left(U^0_{kl}+U^g_{kl}\right)\right)\delta_{ij}. \tag{9}$$

Finally the corresponding traction vector $T_{il}(\boldsymbol{x},\boldsymbol{x}')$, associated with the unit outward normal vector $\boldsymbol{n}(\boldsymbol{x})$, is obtained from $\Sigma_{ijl}(\boldsymbol{x}-\boldsymbol{x}')$ by the Cauchy lemma:

$$T_{il}(\boldsymbol{x},\boldsymbol{x}') = \Sigma_{ijl}(\boldsymbol{x}-\boldsymbol{x}')n_j(\boldsymbol{x}) = \exp(\boldsymbol{\beta}(\boldsymbol{x}-\boldsymbol{x}'))\left(T^0_{il}(\boldsymbol{x},\boldsymbol{x}') + T^g_{il}(\boldsymbol{x},\boldsymbol{x}')\right) \tag{10}$$

where, as for the stress, T^0_{il} represents the well-known strongly singular fundamental solution in tractions for a homogeneous material (parameters λ_0 and μ_0) (see [2,3]), and T^g_{il} is the weakly singular grading term obtained from $T^g_{il}(\boldsymbol{x},\boldsymbol{x}') = \Sigma^g_{ijl}(\boldsymbol{x}-\boldsymbol{x}')n_j(\boldsymbol{x})$.

Boundary Element Method

The boundary integral formulation for an isotropic, exponentially graded body Ω with (Lipschitz and piecewise smooth) boundary $\partial\Omega$ is considered. The derivation follows the standard procedures for a homogeneous material [2,3]. Starting from the 2nd Betti Theorem of reciprocity of work for a graded material, one can derive the corresponding Somigliana identity:

$$C_{il}(\boldsymbol{x}')u_i(\boldsymbol{x}') + \int_{\partial\Omega} T_{il}(\boldsymbol{x},\boldsymbol{x}')u_i(\boldsymbol{x})dS(\boldsymbol{x}) = \int_{\partial\Omega} U_{il}(\boldsymbol{x},\boldsymbol{x}')t_i(\boldsymbol{x})dS(\boldsymbol{x}). \tag{11}$$

The strongly singular traction kernel integral is evaluated in the Cauchy principal value sense. The evaluation of the coefficient tensor of the free term C_{il} is not a problem. The weakly singular grading term and the exponential coefficient in (10) will play no role in the following limit procedure, thus, the value of C_{il} coincides with its value for the homogeneous isotropic material [7] whose properties are defined by the Lamé constants λ_0 and μ_0:

$$C_{il}(\boldsymbol{x}') = \lim_{\varepsilon\to 0}\int_{S_\varepsilon(\boldsymbol{x}')\cap\Omega} T_{il}(\boldsymbol{x},\boldsymbol{x}')dS(\boldsymbol{x}) = \lim_{\varepsilon\to 0}\int_{S_\varepsilon(\boldsymbol{x}')\cap\Omega} T^0_{il}(\boldsymbol{x},\boldsymbol{x}')dS(\boldsymbol{x}), \tag{12}$$

$S_\varepsilon(\boldsymbol{x}')$ being a spherical surface of radius ε centered at $\boldsymbol{x}'$.

The numerical implementation of (11) in this work employs standard approximation techniques. A collocation approximation based upon a nine-node continuous quadrilateral quadratic isoparametric element is employed to interpolate the boundary and the boundary functions. The evaluation of regular integrals is accomplished by Gaussian quadrature with 8x8 integration points, whereas an adaptive element subdivision following the procedure developed in [8] is utilized for nearly singular integrals. A standard polar coordinate transformation [8] is employed to handle the weakly singular integrals involving the kernel U_{il} and the rigid body motion procedure is invoked for evaluating the sum of the free term coefficient tensor C_{il} and of the Cauchy principal value integral with the kernel T_{il}.

Numerical Results

A unit elastic cube $(0,1)^3$ exponentially graded in x_3-direction with grading coefficient $\beta = \ln 2$ is considered. In both test problems, symmetry boundary conditions are imposed on the three faces coincident with the coordinate planes. Elastic solutions in this cube having different loads and different Poisson ratios are studied using a very coarse mesh with one boundary element per face.

Errors in displacements and stresses, respectively, are normalized by the maximum displacement and by σ_0, a nominal stress involved in the definition of each problem.

Example 1. Let the cube with the Poisson ratio $\nu = 0$ be subjected to a constant normal traction σ_0 on its face x_3=1, the other faces, x_1=1 and x_2=1, being traction free. The exact solution of this problem can be found in [6]:

$$u_1 = 0,\quad u_2 = 0,\quad u_3 = \frac{\sigma_0}{2\beta E_0}\left(1-\exp(-2\beta\, x_3)\right) \text{ and } \sigma_{33} = \sigma_0,\ \sigma_{ij} = 0 \text{ for } (\mathrm{i},\mathrm{j}) \neq (3,3). \tag{13}$$

The maximum normalized error obtained by BEM in displacements $u_3(1,1,x_3)$ is less than 0.4% and in stresses $\sigma_3(x_1,x_2,0)$ is less than 1.1%.

Example 2. Let the cube with the Poisson ratio $\nu = 0.3$ be subjected to a constant normal displacement $\sigma_0 * 1/E_0$ on its face x_1=1, E_0 being the Young modulus defined by λ_0 and μ_0, the other faces, x_2=1 and x_3=1, being traction free. The exact solution of this problem can also be found in [6]:

$$u_1 = \frac{\sigma_0}{E_0} x_1, \; u_2 = -\frac{\nu\sigma_0}{E_0} x_2 \text{ and } u_3 = -\frac{\nu\sigma_0}{E_0} x_3, \; \sigma_{11} = \sigma_0 \exp(2\beta x_3), \; \sigma_{ij} = 0 \text{ for } (i,j) \neq (1,1). \quad (14)$$

The maximum normalized error obtained by BEM in displacements $u_1(x_1,0.5,1)$ is less than 0.17%, in displacements $u_3(1,0.5,x_3)$ is less than 0.07%, and in stresses $\sigma_{11}(0,0,x_3)$ is less than 1.1%.

Conclusions

The numerical solution of the 3D Somigliana displacement identity for isotropic elastic exponentially graded materials by a direct collocation BEM code has been successfully developed. The fundamental solution in displacements obtained in [5,6] and the new expression for fundamental solution in tractions introduced here, have been implemented in the BEM code. To the best knowledge of the authors, this is the first implementation of a 3D direct BEM code for such materials. The numerical solutions of a couple of examples with known analytic solutions have produced excellent accuracy, confirming the correctness of the kernel functions and their implementation.

Acknowledgements: The present work has been developed during the stay of R.C. at ORNL (funded by the Applied Mathematical Sciences Research Program of the Office of Mathematical, Information, and Computational Sciences, U.S. Department of Energy, contract DE-AC05-00OR22725 with UT-Battelle), and the stays of J.E.O. and L.J.G. at the University of Seville (funded by the the Spanish Ministry of Education, Culture and Sport: Juan de la Cierva Programm and SAB2003-0088, respectively). V.M. and F.P. have been supported by the Spanish Ministry of Science and Technology through project MAT2003-03315.

References

[1] S. Suresh and A. Mortensen *Fundamentals of Functionally Graded Materials*, IOM Communications (1998).

[2] F. París and J. Cañas *Boundary Element Method Fundamentals and Applications*, Oxford University Press (1997).

[3] M.H Aliabadi *The Boundary Element Method, Vol1 :Applications in Thermo-Fluids and Acoustics, Vol2: Applications in Solids and Structures,* Wiley (2002).

[4] Y. Chan, L.J. Gray, T. Kaplan and, G.H. Paulino *Proceedings Royal Society London A* **460**, 1689-1706 (2004).

[5] P.A. Martin, P. A., J.D. Richardson, L.J. Gray and J.R. Berger *Proceedings of the Royal Society of London*, **A 458**, 1931–1947 (2002).

[6] R. Criado, L.J. Gray, V. Mantic and F. París *International Journal for Numerical Methods in Engineering* (submitted).

[7] V. Mantic *Journal of Elasticity* **33**, 191-201 (1993).

[8] J.C. Lachat and J.O. Watson *International Journal for Numerical Methods in Engineering* **10**, 991-1005 (1976).

Numerically Synthesized Displacement and Stress Solutions for a 3D Viscoelastic Half Space Subjected to a Vertical Distributed Surface Stress Loading Using the Radon and Fourier Transforms

Marco Adolph[1], Edson Rodrigues Carvalho[2], Euclides Mesquita[1*]

[1] Dept. of Computational Mechanics - UNICAMP –13081-970 - Campinas, SP - Brasil
euclides@fem.unicamp.br
[2] Dept. of Exact Sciences – CEUL – UFMS, Brazil

Keywords: half space, viscoelasticity, Radon transform, Fourier transform, dynamic displacement and stresses

Abstract. In this article a numerical solution for a 3D isotropic, viscoelastic half-space subjected to vertical rectangular surface stress loading of constant amplitude is synthesized with the aid of the Radon and Fourier integral transforms. Dynamic displacement and stress fields are computed for the half-space surface as well as for points inside the domain. The analysis is performed in the frequency domain. Viscoelastic effects are incorporated by means of the elastic-viscoelastic correspondence principle. The equations of motion are solved in the Radon-Fourier transformed domain. Inverse transformations to the physical domain are accomplished numerically. The scheme used to perform the numerical inverse transformations is addressed. The solution is validated by comparison with results available in the literature. A sample of original dynamic results for displacement and stress fields for the 3D half-space are furnished.

Problem Statement. The problem to be solved consists of a 3D half space submitted to a rectangular harmonic distributed load of constant amplitude with dimensions (2a x 2b) applied on the free surface, see figure 1. The medium is considered isotropic and viscoelastic.

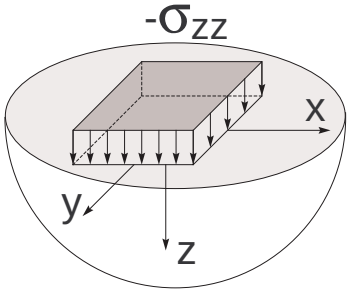

Figure 1: Half-space subjected to a rectangular surface loading

The problem is governed by the Navier equations in the frequency domain:

$$\mu \bar{U}_{i,jj} + (\lambda + \mu)\, \bar{U}_{k,ki} = -\omega^2 \rho \bar{U}_i \tag{1}$$

The vertical traction excitation $\bar{\sigma}_{zz}$ applied at the half-space surface $(z = 0)$ is incorporated in the formulation as boundary conditions:

$$\bar{\sigma}_{zz}(x, y, z = 0, \omega) = \begin{cases} -1; & |x| \le a, |y| \le b \\ 0; & |x| > a, |y| > b \end{cases} \tag{2}$$

$$\bar{\sigma}_{zy}(x, y, z = 0, \omega) = 0 \qquad \bar{\sigma}_{zx}(x, y, z = 0, \omega) = 0 \tag{3}$$

Solution strategy. The equations of motion are solved in the Radon-Fourier [1] transformed domain. Inverse transformations to the physical domain are accomplished numerically. A typical solution is given in terms of double integrals as shown in equation (4) [2]:

$$U_z = \frac{1}{2\pi}\frac{1}{\sqrt{2\pi}}\int_{-\pi/2}^{\pi/2}\int_{-\infty}^{\infty} sign(\delta\xi)\, e^{i\delta\xi(xCos\theta+ySen\theta)}\,\xi\delta\left\{A\cdot e^{-\delta\cdot\alpha_1\cdot z}+C\cdot e^{-\delta\cdot\alpha_2\cdot z}\right\}d\xi\, d\theta \qquad (4)$$

Numerical results. The dynamic displacement component $U_z(x)$ inside the half-space for the line with coordinates $y=0$ [m], $z=1$ [m] is given in figure 2. These results are compared with a solution based on the double Fourier integral [2]. Figure 3 shows the dynamic stress components σ_{xz} for the line with coordinates y=0, z=0.5. The parameters used in this calculations are: μ=1N/m^2, ρ=1kg/m^3, ν=0.4, ω=2rad/s, η=0.1.

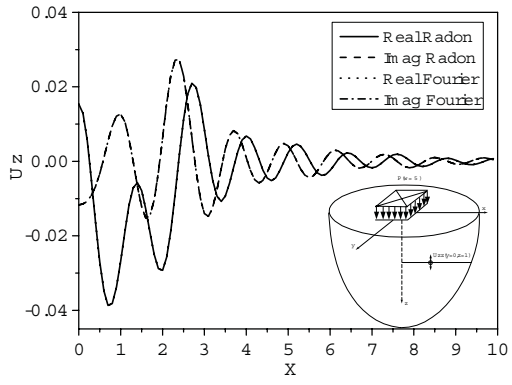

Figure 2: Dynamic displacement component $U_z(x, y=0, z=1)$

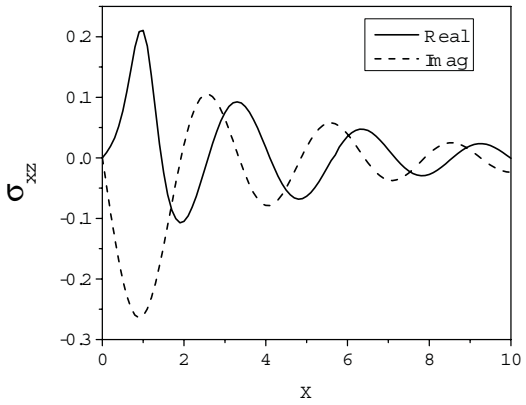

Figure 3: Dynamic stress component $\sigma_{xz}(x, y=0, z=0.5)$

Acknowledgments

The research leading to this article has been supported by Fapesp, CNPq, Capes and FUNDECT-UFMS. This is gratefully acknowledged.

References

[1] Deans SR. The *Radon Transform and Some of Its Applications*. Krieger Publishing Company: Malabar, Florida, 1993.

[2] Adolph M. *Synthesis of 3D Green's functions and auxiliary viscoelastic states using the Radon transform*. PhD Thesis, FEM/Unicamp, 2006 (in Portuguese).

Isoparametric FEM vs. BEM for Elastic Functionally Graded Materials

Vincenzo Minutolo[1] ,Eugenio Ruocco[2] ,Tommaso Colella[3]

Dipartimento di Ing. Civile, Seconda Università di Napoli, via Roma 29 81031 Aversa, Italy

[1]vincenzo.minutolo@unina2.it

[2]eugenio.ruocco@unina2.it

[3]tommaso.colella@unina2.it

Keywords: Functionally Graded Materials (FGM), Isoparametric Finite Element Method (FEM), Domain Boundary Element Method (FGM DBEM), Boundary Element Method (BEM).

Abstract The Domain Boundary Element Method (DBEM) for Functionally Graded Materials is presented. The proposed formulation uses classical Kelvin s fundamental solution able to handle any gradation even if analytical solution does not exist. The method is compared with isoparametric FGM Finite Element Method. It is shown that DBEM gives more accurate results when mesh re nement is required due to stress gradients and distorted elements.

Introduction

Functionally Graded Materials (FGM) are the class of materials whose relevant properties vary continuously within the body. The variability depends, in the majority of practical situations, on the microstructure made of different component phases arranged in suitable pattern to ful ll compound requirements. Wide literature has been published dealing with technological, mechanical and theoretical aspects of FGM and references can be found in many edited books [1, 2, 3]. From the computational point of view, recently generalized isoparametric formulation of Finite Element Method (FEM) has been proposed by Paulino and coathors. [4, 5, 6] dealing with isotropic and anisotropic FGM. In these works, the material properties are mapped onto the nodes of nite element description and the values are interpolated at the Gauss point level by isoparametric shape functions.

Several authors develop application of FGM Boundary Element Method too; it is noticeably that, unlike FEM, BEM requires the knowledge of analytical or mixed numerical-analytical Fundamental Solution (FS) for the FGM [7, 8, 9, 10].

Since the properties of FGM, a great effort is devoted to fracture mechanics of FGM, in [11] where elastostatic analysis of antiplane crack in FGM is proposed, exponential variability is assumed and Galerkin hyper-singular BEM is adopted.

In many practical applications of the FGM modeling and numerical simulations, the evaluation of the constitutive law is made starting from observation of the material micro-mechanics and of the constituent special pattern. Consequently it is only possible to acquire point-wise value of the constitutive parameters rather than the analytical expression of their variation and, to evaluate FS, the acquired point-wise values of the constitutive law have to be interpolated analytically. Once the FS is obtained, it possible to apply the BEM to perform calculations on the actual problem.

With respect to BEM, isoparametric FEM only requires to interpolate the constitutive law at the element level using simple serendipity polynomial, consequently no analytical solution over the domain has to be evaluated.

The above considerations seem to discourage the use of BEM for FGM simulation; anyway there are some situations for the BEM to be competitive with respect to the FEM, especially when high stress gradient occurs like in fracture mechanics or models with highly distorted mesh.

In the paper,a comparison between the FEM isoparametric formulation for FGM [4] and a DBEM formulation is proposed where DBEM is obtained by applying the FS for homogeneous isotropic reference material.

DBEM formulation

The governing equation of the DBEM model is here after,

$$\begin{aligned}[\kappa_{lh}(\xi) - A_{lh}(\xi)]\, u_h(\xi) = \int_{\partial\Omega} G_{lj}(x,\xi)\, p_j(x)\, dS - \int_{\partial\Omega} F_{lj}(x,\xi)\, u_j(x)\, dS + \\ + \int_{\Omega} G_{lj}(x,\xi)\, b_j(x)\, dV + \int_{\partial\Omega} \hat{F}_{lj}(x,\xi)\, u_j(x)\, dS + \int_{\Omega} \hat{b}_{lj}(x,\xi)\, u_j(x)\, dV\end{aligned} \tag{1}$$

The reference material for the unbounded space is linearly elastic isotropic and homogeneous with elastic tensor C°_{ijhk}, the actual material is made of heterogeneous linear elastic material with variable and anisotropic $C_{ijhk}(x)$.

In the Eq. (1), two new kernels occur, the first is a traction-like term:

$$\hat{F}_{lj}(x,\xi) = L_{ijhk} B_{lhk} n_i = \hat{T}_{lij}(x,\xi)\, n_i(x) \tag{2}$$

the second a body force-like term

$$\hat{b}_{lj}(x,\xi) = \frac{\partial}{\partial x_i}\left[\hat{T}_{lij}(x,\xi)\right] \tag{3}$$

By defining the elastic difference tensor as follws

$$L_{ijhk}(x) = C^{\circ}_{ijhk} - C_{ijhk}(x) \tag{4}$$

it can be seen that the term $B_{lij}(x,\xi)$ is the strain of the fundamental solution, hence the terms in Eqs (2) and (3) depend on the variability of the material. Moreover the coefficient matrix $A_{lh}(\xi)$ on the left hand side of Eq (1), can be calculated and reported in the fullpaper [15]

$$\lim_{\delta \to 0} \int_S B_{lij}(x,\xi)\, n_k(x)\, dS = J_{lijk}(\xi) \tag{5}$$

notice that Eq.(1) holds for purely anisotropic material as well, provided to assume the operator (4) to be constant.

Results

Results concerning plates with crack and circular hole are reported. The results show that DBEM attain the same result than FEM but with coarse meshes. The reported results are parametrised with respect to the number n of the division of the mesh on the shorter side of the plate, n represents a measure of the mesh refinement

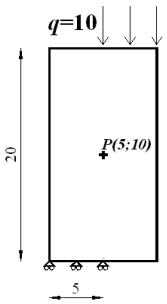

$E(x) = \gamma(y)\, E^0 \qquad \gamma(x) = ke^{\beta y},$
$E^0 = 2.1 \cdot 10^5 N/mm^2 \quad \nu = 0.3, \gamma(0) = 1$

	FEM		BEM	
n	$u_y(P)10^3$	W	$u_y(P)10^3$	W
2	-.91432	.099863	-.92419	.10063
4	-1.0049	.10540	-1.0270	.10624
6	-1.0438	.10733	-1.0629	.10816
8	-1.0645	.10830	-1.0803	.10881
10	-1.0774	.10888	-1.0911	.10931
12	-1.0863	.10928	-1.0982	.10973
14	-1.0927	.10956	-1.1040	.10002
16	-1.0976	.10977	-1.1075	.11023
18	-1.1015	.10994	-1.1112	.11044

Vertical displacement, u_y,
Strain energy W.

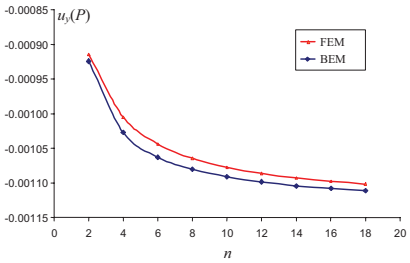

Displacement vs
division number

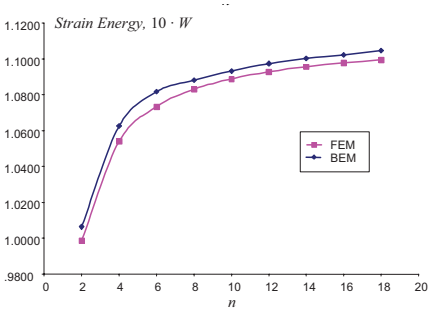

Strain Energy vs
division number

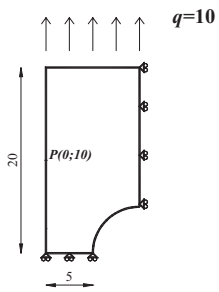

Plate with hole

	FEM		BEM	
n	$\sigma_{yy}(P)$	$u_y(P)$	$\sigma_{yy}(P)$	$u_y(P)$
2	1.5565E+01	1.1438E-03	1.5690E+01	1.1474E-03
4	1.5741E+01	1.1446E-03	1.5757E+01	1.1454E-03
8	1.5782E+01	1.1447E-03	1.5786E+01	1.1449E-03

Vertical Stress σ_{yy}
Vertical displacement, u_y

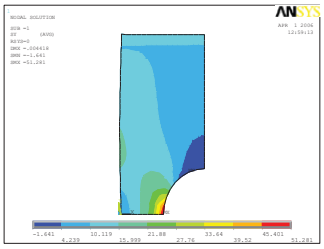

FEM Stress: n = 8

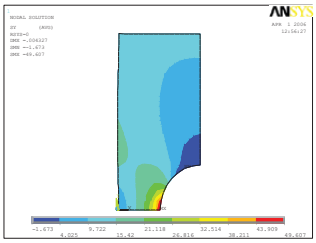

DBEM Stress: n = 8

References

[1] Ichikawa, K. (Ed) (2001); Functionally graded materials in the 21st century, Kluwer Academic Publishers: Norwell, Ma.

[2] Watanabe, K.; Ziegler, F. (Ed) (2003); Dynamics of Advanced Materials and Smart Structures, Proc. IUTAM Symposium 20-24 May 2002, Kluwer Academic Publishers: Dordrecht.

[3] Pan, W.; Gong, J.; Zhang, L.; Chen, L. (Ed) (2003); Functionally Graded Materials VII, Proc. Of the VII int. Symposium (FGM2002), Beijing 15-18 October, 2002, Trans Tech Publication Ltd.: En eld NH.

[4] Kim, JH.; Paulino, G.H. (2002): Isoparametric Graded Finite Elements for nonhomogeneous isotropic and orthotropic materials, J. of App. Mech., vol. 69, pp. 502-511.

[5] Kim, JH.; Paulino, G.H. (2001): Finite Element evaluation of mixed mode stress intensity factors in functionally graded materials, International J. Num. Meth. Engng, vol. 53, pp. 1903-1935.

[6] Wang, B.L.; Tian, Z.H. (2005) Application of nite element- nite difference method to the determination of transient temperature eld in functionally graded materials, FE Anal. Des., vol. 41 pp. 335-349.

[7] Sutradhar, A.; Paulino, G.H. (2004): The simple boundary element method for transient heat conduction in functionally graded materials. Comp. Meth. App. Mech. Engng, vol. 193, pp. 4511-4539.

[8] Sutradhar, A.; Paulino, G.H.; Gray, L.J. (2005): On hypersingular surface integrals in the symmetric Galerkin boundary element method: application to heat conduction in exponentially graded materials. Int. J. Num. Meth. Engng, vol. 62, pp. 122 157.

[9] Ang, W-T.; Clements, D.L.; Vahdati, N. (2003): A dual reciprocity boundary element method for a class of elliptic boundary value problems for non-homogeneous anisotropic media, Engng. Anal. B E, vol. 27 pp. 49-55.

[10] Ang, W-T.; Kusuma, J.; Clements, D.L. (1996): A boundary element method for a second order elliptic partial differential equation with variable coefficients. Engng Anal.BE, vol. 18, pp. 311-316.

[11] Zhang, CZ.; Sladek, J.; Sladek, V. (2005): Antiplane crack analysis of a functionally graded material by a BIEM. Comp. Mat.Sci., vol. 32 pp. 611-619.

[12] Aliabadi M.H.; Wrobel, L.C. (2002): Boundary Element Method, Wiley, New York.

[13] Banerjee P.K. (1993): The Boundary element method in Engineering Science, Mc Graw Hill, London.

[14] Guiggiani, M. (1994): Hypersingular formulation for boundary stress evaluation. Engng. Anal. BE, Vol. 13, pp. 169-179

[15] Minutolo, V.; Ruocco, E.; Colella, T. (2006): Isoparametric FEM vs. BEM for Elastic Functionally Graded Materials, CMES, (submitted 2006).

A new high-order time-kernel BIEM for the Burgers equation

N. Mai-Duy[1a], T. Tran-Cong[1b], R.I. Tanner[2]

[1a] maiduy@usq.edu.au and [1b] trancong@usq.edu.au

Faculty of Engineering and Surveying

The University of Southern Queensland, QLD 4350, Australia

[2] rit@aeromech.usyd.edu.au

School of AMME

The University of Sydney, NSW 2006, Australia

Keywords: Burgers equation, radial-basis-function networks, transient problems, time-dependent fundamental solutions, boundary-integral-equation methods

In this paper, a high-order interpolation scheme, namely integrated radial-basis-function networks (IRBFNs), is introduced into the time-kernel boundary-integral-equation method (BIEM) to approximate the unknown functions in boundary and volume integrals for the solution of the Burgers equation. All relevant integrals are written in terms of nodal variable values. Solutions over the temporal domain can be obtained at once rather than step by step as in the case of conventional BIEMs.

Parabolic differential equations have been employed in a variety of engineering problems. Solutions to these equations can be found by means of numerical discretization methods such as BIEMs, finite-difference (FDMs), finite-element (FEMs) and finite-volume (FVMs) methods. For BIEMs (e.g. [1,2]), there are several approaches proposed to deal with a time-derivative term. Based on the criterion of fundamental solutions used, they can be classified into two groups. The first group employs time-dependent fundamental solutions, i.e. time derivatives enter the integral representation through the kernel functions, which allows the process of discretization in time and space to be conducted in a similar fashion. The second group employs stationary fundamental solutions. Some additional treatments for time derivatives are thus required; they generally fall into one of two categories: Laplace transforms and finite-difference schemes.

In the context of time-kernel BIEMs, there are relatively few papers on using high-order interpolation schemes to approximate the unknown functions with respect to time. The case of using quadratic functional variation was reported in [2]. Recently, Grigoriev and Dargush [3] employed quartic interpolation functions, and their obtained results indicated a significant improvement in accuracy, convergence rate and error distribution.

Radial-basis-function networks have found a wide range of applications in the field of numerical analysis. These networks exhibit good approximation properties. For example, it has been proved that RBFNs are capable of representing any continuous function to a desired level of accuracy by increasing the number of hidden neurons (universal approximation) [4]. Madych and Nelson [5] showed that the multiquadric (MQ) interpolation scheme converges exponentially with respect to the number of data points used. It was found that IRBFNs have higher approximation power than differentiated RBFNs [6].

In the present work, instead of using high-order Lagrange polynomials such as quadratic and quartic interpolation functions, the proposed method employs MQ-IRBFNs to represent the unknown functions in boundary and volume integrals. Numerical implementations of ordinary and double integrals involving time in the presence of IRBFNs are presented in detail. All relevant integrals are written in terms of nodal variable values. The proposed method is verified through the solution of diffusion and convection-diffusion problems. Numerical results obtained show that the IRBFN-BIEM attains a significant improvement in accuracy over low-order time-kernel BIEMs and FDMs (Tables 1 & 2).

	u (error %)				
t	FDM-CN	FDM-PI	FDM-WT	Present	Exact
0.025	0.5637(12.35)	0.6888(7.09)	0.6807(5.84)	0.6432(0.00)	0.6432
0.050	0.5440(9.69)	0.5330(7.47)	0.5286(6.58)	0.4959(0.01)	0.4959
0.075	0.3493(9.68)	0.4226(9.27)	0.4188(8.29)	0.3867(0.01)	0.3868
0.100	0.3313(9.66)	0.3376(11.76)	0.3341(10.58)	0.3021(0.01)	0.3021
0.125	0.2117(10.31)	0.2705(14.58)	0.2671(13.14)	0.2360(0.01)	0.2360
0.150	0.2038(10.50)	0.2169(17.60)	0.2137(15.86)	0.1844(0.01)	0.1844
0.175	0.1270(11.84)	0.1740(20.74)	0.1710(18.67)	0.1441(0.01)	0.1441
0.200	0.1262(12.10)	0.1396(20.99)	0.1369(21.57)	0.1126(0.01)	0.1126
0.225	0.0756(14.12)	0.1120(27.33)	0.1096(24.54)	0.0880(0.01)	0.0880
0.250	0.0787(14.47)	0.0899(30.76)	0.0877(27.58)	0.0687(0.01)	0.0687

Table 1. Diffusion problem, $0 \le x \le 1,\ 0 \le t \le 0.25,\ \Delta x = 0.1,\ \Delta t = 0.025$: Temperature at the centre of the slab obtained by the present method and various FDMs. The latter which use the same time step and finer spatial discretization ($\Delta x = 0.05$) are extracted from the paper of Haberland and Lahrmann [7] in which CN stands for Crank-Nicolson, PI: pure implicit and WT: weighted time step. The maximum error is 0.01% for IRBFN-BIEM while they are 14.47%, 30.76% and 27.58% for FDM-CN, FDM-PI and FDM-WI, respectively.

	u (error %)					
	$t = 1.2$			$t = 3$		
x	GBIEM	Present	Exact	GBIEM	Present	Exact
0.20	0.13173(0.62)	0.13092(0.00)	0.13092	0.06036(0.44)	0.06010(0.01)	0.06009
0.40	0.26285(0.60)	0.26127(0.01)	0.26128	0.12068(0.43)	0.12015(0.00)	0.12016
0.60	0.39264(0.56)	0.39043(0.00)	0.39044	0.18095(0.43)	0.18018(0.00)	0.18018
0.80	0.52012(0.50)	0.51756(0.01)	0.51753	0.23906(0.18)	0.23861(0.00)	0.23863
0.90	0.57950(0.29)	0.57780(0.00)	0.57781	0.23766(1.63)	0.24158(0.00)	0.24159
0.92	0.58466(0.01)	0.58482(0.02)	0.58472	0.22050(2.48)	0.22616(0.00)	0.22612
0.94	0.57336(0.77)	0.57760(0.03)	0.57779	0.18997(3.51)	0.19696(0.01)	0.19690
0.96	0.51253(2.42)	0.52551(0.05)	0.52524	0.14228(4.58)	0.14915(0.01)	0.14911
0.98	0.33294(5.04)	0.35023(0.11)	0.35060	0.07698(5.41)	0.08140(0.01)	0.08139

Table 2. Convection-diffusion problem, $\mathrm{Re} = 100,\ 0 \le t \le 3,\ 0 \le x \le 1,\ \Delta x = 0.02,\ \Delta t = 0.1$: Solution profiles at some time levels. Results by the generalized BIEM (GBIEM) using linear and constant elements, $\Delta x = 0.01$ and $\Delta t = 0.01$ [8] are also included. The proposed method yields a very high level of accuracy and its errors do not accumulate in time.

References

[1] P.K. Banerjee and R. Butterfield *Boundary Element Methods in Engineering Science,* McGraw-Hill (1981).

[2] C.A. Brebbia, J.C.F. Telles and L.C. Wrobel *Boundary Element Techniques Theory and Applications in Engineering*, Springer-Velag (1984).

[3] M.M. Grigoriev and G.F. Dargush *International Journal for Numerical Methods in Engineering*, **55**, 1-40 (2002).

[4] J. Park and I.W. Sandberg *Neural Computation*, **3**, 246-257 (1991).

[5] W.R. Madych and S.A. Nelson *Mathematics of Computation*, **54**, 211-230 (1990).

[6] N. Mai-Duy and T. Tran-Cong *Applied Mathematical Modelling*, **27**, 197-220 (2003).

[7] C. Haberland and A. Lahrmann *International Journal for Numerical Methods in Engineering,* **25,** 593-609 (1988).

[8] K. Kakuda and N. Tosaka *International Journal for Numerical Methods in Engineering,* **29,** 245-261 (1990).

The Use of the Tangential Differential Operator in the Boundary Integral Equation for Stresses and the Dual Boundary Element Method

L Palermo Jr[1], LPCPF Almeida[1], PC Gonçalves[1]

[1] Universidade Estadual de Campinas, Faculdade de Engenharia Civil, Arquitetura e Urbanismo, Brazil, leandro@fec.unicamp.br.

Keywords: Tangential Differential Operator, Dual Boundary Element Method, Stress Intensity Factor

Abstract. Accurate values for stresses at the boundary may be evaluated with the stress boundary integral equation (BIE) [1]. Nevertheless, the differentiation of the kernels of integrals in the displacement equation to obtain a BIE for stresses increases the order of the kernel singularity and an additional care is necessary to treat the improper integrals. The use of the tangential differential operator (TDO) in the stress BIE is an interesting procedure when Kelvin type fundamental solutions are employed. The order of the kernel singularity is reduced with this strategy [2, 3, 4] and the Cauchy principal value sense or the first order regularization can be used in the resultant BIE.

Several strategies have been employed to analyze crack problems such as the displacement discontinuity method [5, 6], the crack Green's function method [7, 8], the subregion (or subdomain) method [9] and the dual boundary element method (DBEM) [10, 11, 12]. The dual equations of the method are the displacement and the traction BIEs. When the displacement BIE is applied to one of the crack surfaces and the traction equation to the other, general mixed-mode crack problems can be solved with a single domain formulation. Although the integration path is still the same for coincident points on the crack surfaces, the respective boundary integral equations are now distinct. The collocation point position to perform the traction boundary integral equation and the strategy used to treat improper integrals are the essential features of the formulation.

Plane problems containing an internal or an edge crack are studied in this paper. Linear shape functions were employed to approximate displacements and efforts in the boundary elements. The same shape function was used for conformal and non-conformal interpolations with nodal parameters positioned at the ends of the elements. The collocation points were shifted to the interior of the element at a distance of a six part of its length from the end. The number of collocation points in the element was defined by the computer code according to the condition of the last node, which means that elements with the discontinuity at the first node had one collocation point. The present numerical implementation was studied in [13] for the dual formulation with traction BIE containing a hypersingularity of order r^{-2}. The main feature shown in that study was the use of conformal interpolations along the crack surfaces without losing the accuracy of the dual formulation.

The dual formulation with TDO in the traction BIE is analyzed in the present study. The derivatives of the adopted shape function for displacements (linear functions) are used in the traction equation as required for the TDO. The use of non-conformal interpolations required that the effect of the ends was introduced in the integration by parts to obtain the TDO. The near-tip displacement extrapolation was used to obtain stress intensity factors as explained in [10, 13].

The numerical results obtained were close to literature values. A minimum difference was noted in the results presented in [10, 13] and those obtained using the TDO, which have the benefit of the reduction of the order of the singularity. The use of derivatives of the adopted shape function for displacement without using other interpolation for TDO was an interesting alternative. It is important to note that constant values were obtained as derivatives of the linear shape function and the results were not degraded. Regarding the present numerical implementation, a conformal interpolation on the crack surface can be used without losing the accuracy of the dual formulation even when the BIE for tractions employs the TDO on low order elements.

References

[1] Guiggiani, M., Hypersingular formulation for boundary stresses evaluation. Eng. Anal. Bound. Elem., 14, 169-179, 1994.

[2] Bonnet, M, Boundary Integral Equation Methods for Solids and Fluids, John Wiley & Sons Ltd., 1999.

[3] Kupradze, VD, Three-dimensional problems of the mathematical theory of elasticity and thermoelasticity. North Holand, 1979.

[4] Sladek, J, Sladek, V, Three-dimensional curved crack in an elastic body, Int. J. Solids Struct., 19, 425-436, 1983.

[5] Crouch, SL, Solution of plane elasticity problems by the displacement discontinuity method, International Journal of Numerical Methods in Engineering, 10, 301-342, 1976.

[6] Wen, PH, Dynamic fracture mechanics: displacement discontinuity method, Computational Mechanics Publications, 1996.

[7] Snyder, MD, Cruse, TA, Boundary integral equation analysis of cracked anisotropic plates, International Journal of Fracture, 11, 315-342, 1975.

[8] Telles, JCF, Castor, GS, Guimarães, S, Hypersingular Green´s function generation and fracture mechanics problems, Boundary Element Method XVI, Brebbia, CA, Computational Mechanics Publications, 443-453, 1994.

[9] Blandford, GE, Ingraffea, TA, Liggett, JA, Two-dimensional stress intensity factor computations using the boundary element method, International Journal of Numerical Methods in Engineering, 17, 387-404, 1976.

[10] Portela, A, Aliabadi, MH, Rooke, DP, The dual boundary element method: Effective implementation for crack problems, International Journal of Numerical Methods in Engineering, 33, 1269-1287, 1992.

[11] Hong, H & Chen, J, 1988, Derivations of integral equations of elasticity, Journal of Engineering Mechanics ASCE, 114, pp. 1028-1044.

[12] Chen, WH, Chen, TC, An efficient dual boundary element technique for a two-dimensional fracture problem with multiple cracks. International Journal of Numerical Methods in Engineering, 38, 1739-1756, 1995.

[13] Almeida, LPCPF, Palermo Jr., L, On the Implementation of the Two Dimensional Dual Boundary Element Method for Crack Problems, “5th International Conference on Boundary Elements Techniques”Lisboa, Portugal, 2004.

[14] Civelek, M. B. & Erdogan, F., 1982, Crack problems for a rectangular sheet and an infinite strip, International Journal of Fracture, vol.19, pp.139-159.

[15] Murakami, Y., 1987, Stress Intensity Factors Handbook, Pergamon Press, Oxford.

A MLPG(LBIE) numerical method for solving 2D incompressible and nearly incompressible elastostatic problems

V. Vavourakis, D. Polyzos

Department of Mechanical Engineering and Aeronautics, University of Patras, Greece
Institute of Chemical Engineering and High Temperature Process ICETH-FORTH, Rio, Greece

A new Meshless Local Petrov-Galerkin (MLPG) method, based on Local Boundary Integral Equation (LBIE) considerations, is proposed here for the solution of two-dimensional, incompressible and nearly incompressible elastostatic problems. Such continuum linear elastic media with Poisson ratio being equal to 0.5 are called incompressible since they deform without volume changes. Typical examples of materials with incompressible elastic behaviour are rubber-like and undrained saturated porous solids. The classical stress tensor defined in the compressible elastic theory, as the Poisson ratio approaches 0.5, is no longer valid since the Lamè constant λ tends to infinity, thus, a new constitutive equation is needed to be determined. This is accomplished by considering the stress tensor as a function of displacements and hydrostatic pressure, while displacements satisfy an extra condition known as additional condition of incompressibility [Hughes TJR. The finite element method: Linear elastic and dynamic finite element analysis. Prentice-Hall International (1987)].

Although the Finite Element Method (FEM) is a powerful and robust numerical tool widely used for solving linear and non-linear elastic problems, in its conventional form it suffers by severe locking and matrix ill-conditioning problems when incompressible or nearly incompressible materials are considered. After the pioneering work of Herrmann [Herrmann LR. Elasticity equations for incompressible and nearly incompressible materials by a variational theorem. AIAA Journal (1965)] who first developed a mixed FEM formulation of compressible elasticity capable of considering incompressibility, a plethora of special FEM formulations working in incompressible and nearly incompressible regime have been appeared in the literature.

On the other hand, the Boundary Element Method (BEM), as it is presented in the work of Polyzos et al. [Polyzos D, Tsinopoulos SV, Beskos DE. Static and dynamic boundary element analysis in incompressible linear elasticity. European Journal of Mechanics, A/Solids (1998)], has the distinct advantage over the FEM of working without any problem for both compressible and incompressible linear elastic materials, providing results of high accuracy by discretizing only the boundary of the analyzed structure and not the whole domain as in the FEM. Nevertheless, the requirement of using the fundamental solution of the differential equation or system of equations that describe the problem of interest renders the BEM less attractive than FEM when non-linear, non-homogeneous and anisotropic compressible and incompressible elastic problems are considered. Also, the final system of linear equations taken by a BEM formulation leads to unsymmetric and full-populated matrices the numerical treatment of which is in general computationally expensive.

The meshless LBIE method was first proposed by Zhu et al. [Zhu T, Zhang JD, Atluri SN. A local boundary integral equation (LBIE) method in computational mechanics and a meshless discretization approach. Computational Mechanics (1998)] for potential problems as an alternative to the BEM. After their pioneering work, several papers dealing with LBIE formulations have been appeared in the literature.

The proposed here method utilizes, for its meshless implementation, nodal points spread over the analyzed domain and employs the Moving Least Squares (MLS) approximation for the interpolation of the interior and boundary variables. On the local and global boundaries, traction vectors are treated in a way so that no derivatives of the utilized MLS shape functions are required. The displacements, stresses and hydrostatic pressure field, at all the considered nodal points, are evaluated with the aid of their corresponding local integral representations valid for incompressible and nearly incompressible solids. Since displacements and stresses are treated as independed variables, the boundary conditions are imposed directly without any problem via the integrals defined on the global boundary of the analyzed body. The evaluation of the singular and hypersingular boundary integrals is performed directly with high accuracy through advanced integration techniques. A representative numerical example illustrates the proposed methodology and demonstrates its accuracy.

A STRAIN ENERGY DENSITY RATE APPROACH TO THE BEM ANALYSIS OF CREEP FRACTURE PROBLEMS

C. P. Providakis and S.G. Kourtakis
Department of Applied Sciences
Technical University of Crete, GR-73100 Chania, Greece

Keywords: Fracture, Creep, Strain energy density rate, boundary element method

Abstract

Cracks can degrade the integrity of structural components. This is a particular concern in the design of aircraft engines and steam turbines where the high temperature prevails and failure by creep components deformation is a concern. In these high level of temperatures the time-dependent creep fracture phenomenon can be considered as of multi-scale nature, particularly when physical size is scaled down to the dimensions of the material microstructure. For a dominant crack in metallic components that undergo creep deformation, the creation of macrocrack surface along the main crack (Mode I) path should be distinguished from the creation of microcrack surfaces off to the side of main crack where the creep enclaves are located. In this sense, creep fracture could be also considered as a multiscale process.

More than two decades ago, the strain energy density criterion was proposed [1] as a fracture criterion in contrast to the conventional theory of G and K of the Griffith's energy release rate assumptions in elastic fracture mechanics. This provided an alternative approach to failure prediction for the same stress solution. The distinctions were empasized in the works of Sih[2]. The strain energy density criterion gained momentum and credibility in engineering. A review on the use of this criterion can be found in [3-4].

It is well known that for cases of realistic and practical problems in time-dependent fracture analysis of creeping cracked components the use of numerical solutions such as finite element method (FEM) and boundary element method (BEM) become imperative. For a review on the subject on can consult Beskos [5].

In the search for an accurate, yet generalized, computational method for evaluating singular crack tip stress and strain fields, the singular element approach in conjunction with boundary element method (BEM) has been properly used in various fracture mechanics applications. Several researchers have contributed to this field: Blandford et al[6] was the first who introduced the traction singular quarter-point boundary element approach in combination with a multi-domain formulation to the solution of both symmetrical and non-symmetrical crack problems. Thereafter, this approach has been extensively used in the application of the boundary element method to two- and three- dimensional crack problems. An extension of the quarter-point element technique was used by Hantschel et al[7] who made an attempt to model crack tip fields arising in two-dimensional elastoplastic cracked panels by introducing some special singular boundary elements which took into account the HRR singularity field (Hutchnison[8]; Rice and Rosengren, [9]) near the crack tip.

In connection with the boundary element determination of near crack tip stress and strain fields in cracked structural components undergoing two-dimensional inelastic deformation one should mention the works of Professor Mukherjee and his co-

workers for Mode I and II [10, 11] and Mode III [12]. A more comprehensive review in BEM solutions of inelastic could be found in the review article of Aliabadi[13].
In the present paper, the strain energy density rate concept is applied as a fracture criterion in association with the use of a previously developed, by the present authors, creep strain-traction singular element (CR-STSE) to determine the crack initiation involved in creeping cracked structural components. The creep constitutive model used in the numerical calculations is the Norton power law creep model (Nortan [14]) but any other creep constitutive model having similar mathematical structure can be easily implemented in the proposed algorithm. The strain energy density rate theory is also applied to determine the direction of the crack initiation for a center cracked plate in tension which is subjected to Mode I loading conditions.

References

[1] Sih, G.C., (1973), Some basic problems in fracture mechanics and new concepts, *J. Eng. Fract. Mech*., 365-377.
[2] Sih, G.C., (1991), *Mechanics of Fracture Initiation and Propagation*, Kluwer Academic Publishers, Dordrecht.
[3] Gdoutos, E.E., (1984), Problems of mixed mode crack propagation, In: Engineering Applications of Fracture Mechanics, vol. II, Martinus Nijhof, Netherlands.
[4] Carpinteri, A., (1986), Crack growth and material damage in concrete: plastic collapse and brittle fracture, In: Engineering Applications of Fracture Mechanics, vol. V, Martinus Nijhof, Netherlands.
[5] Beskos, D.E. (1987), *Numerical methods in dynamic fracture mechanics*, EUR-11300 EN, Joint Research Center of EC Ispra Establishment, Ispra, Italy.
[6] Blandford, G.E., Ingraffea, A.R., Ligget J.A., (1981), Two dimensional stress intensity factor computations using the boundary element method, *Int. J. Num. Meth Engng*, **17**, 387-404.
[7] Hantschel, T., Busch, M., Kuna M., Maschke, H.G., (1990), Solution of elastic-plastic crack problems by an advanced boundary element method. In Numerical Methods in Fracture Mechanics, pp. 29-40, A.R. Luxmoore and D.R.J. Owen (Eds.), Pineridge Press, Swansea.
[8] Hutchinson, J.W., (1968), Singular behavior at the end of a tensile crack in a hardening material, *J. Mech Phys Solids*, **16**, 13-31.
[9] Rice, J.R. and Rosengren, G.F., (1968), Plane strain deformation near a crack tip in a power-law hardening material, *J. Mech Phys Solids*, **16**, 1-12.
[10] Mukherjee, S., Morjaria, M. (1981), A boundary element formulation for planar time-dependent inelastic deformation of plates with cutouts, *Int. J. Solids and Structures*, **17**, 115-126.
[11] Morjaria, M., Mukherjee, S., (1981), Numerical analysis of planar, time-dependent inelastic deformation of plates with cracks by the boundary element method, *Int. J. Solids and Structures*, **17**, 127-143.
[12] Morjaria, M., Mukherjee, S., (1982), Numerical solution of stresses near crack tips in time-dependent inelastic fracture mechanics, *Int. J. Fracture,* **18** (4), 293-310.
[13] Aliabadi, M.H., (1977), Boundary element formulations in fracture mechanics, *Appl Mech Rev*, **50**(2), 83-96.
[14] Nortran, F.H., (1929),*The Creep of Steel at High Temperatures*, McGraw-Hill, New York.

An Efficient Green's Function for Acoustic Waveguide Problems

J. A. F. Santiago[1] and L. C. Wrobel[2]

[1] COPPE/UFRJ – Programa de Engenharia Civil, Caixa Postal 68506

21945-970 Rio de Janeiro, Brazil; E-mail: Santiago@coc.ufrj.br

[2] Brunel University – School of Engineering and Design, Uxbridge,

Middlesex UB8 3PH, England; E-mail: Luiz.Wrobel@brunel.ac.uk

Keywords: Shallow Water Acoustics, Wave Propagation, Ewald's Method.

Abstract. Efficient implementations of the boundary element method for underwater acoustics should employ Green's functions which directly satisfy the boundary conditions on the free surface and the horizontal parts of the bottom boundary. In the present work, these Green's functions are constructed by using either eigenfunction expansions or Ewald's method. This method is discussed in detail, including an attempt to optimise the value of the parameter *b*, which splitting the integral employed in Ewald's representation.

Introduction

Recent papers by Linton [1] and Papanicolaou [2] discuss numerous mathematical techniques for accelerating slowly convergent series. They show that one powerful technique is the method of Ewald [3], which is capable of providing dramatic improvements in the speed of convergence. This method has been successfully implemented in the BEM context by Venakides *et al.* [4], for the calculation of electromagnetic scattering of photonic crystals.

In the present article, a two-dimensional model is studied as representative of coastal regions, which have little variation in the long shore direction. The Ewald's method was derived and implemented for speeding-up the calculations of the eigenfunction expansion of the Green's function. The accuracy of both forms of the Green's function obtained by the techniques above mentioned are compared with respect to the number of iterations, particularly close to singularities.

Consider the problem of acoustic wave propagation in a region of infinite extent, considering sections with constant depth and sections with irregular seabed topography [5].

If the medium in the absence of perturbations is quiescent, the velocity of sound is constant and the source of acoustic disturbance is time-harmonic, the problem is governed by the Helmholtz equation [6]. The problem is subject to the Dirichlet condition at free surface, the Neumann boundary condition at bottom and Sommerfeld radiation condition at infinity. According to Green's second identity, the Helmholtz equation, can be transformed into the boundary integral equation, conform reference [7].

Function for the parameter *b* used in the Ewald's Method

The underlying idea of Ewald's Method is to split the integral in equation obtained by means of Eigenfunction Expansion into two parts [8]. The parameter *b*, which divides this integral, is chosen appropriately taking account of the position of the source and field points and should vary between 0 and 1 ($0 < b < 1$) to accelerate the decay of the term containing b^{2n}. For the variation of the field point **X**, with coordinates (x,y), in a vertical line containing the source point **S**, with coordinates (u,v), the parameter b can be defined as $b(\beta) = \alpha\left[\cos(\beta\pi)+1\right]/2 + \gamma$, in which $\beta(y)$ is a y-dependent function defined as ($Y_B \le y \le Y_F$):

$$\beta = \begin{cases} 1 + r/\beta_0 & \text{for } v-\beta_0 \le y \le v+\beta_0 \\ 1 + a_2/\beta_0 & \text{for } Y_F - v - 2\sqrt{\beta_0} \le y \le Y_F - v + 2\sqrt{\beta_0} \\ 0 & \text{for y beyond of that intervals} \end{cases} \quad , where \quad \begin{array}{c} r = |y-v| \\ \beta_0 = H/\theta \\ a_2 = (v+y-Y_F)^2/4 \end{array} \tag{1}$$

where H is the depth of the free surface; Y_F is the y co-ordinate of the free surface and α, γ and θ are constants. In the present paper α, γ and θ are taken to be 0.1, 0.000001 and 20, respectively.

Example

A problem of acoustic wave propagation from a region of depth h = 10.0 m was studied in order to verify the performance of the function $b(r)$ in the Ewald series. Different situations were considered, in which the position of the source point **S** was fixed and the field point **X** varied along a vertical and a horizontal line. The sound velocity and frequency are taken to be 1500 m/s and 1000 Hz, respectively [8].

For all case analysed, the real part of the functions $G_M(\mathbf{S},\mathbf{X})$ and $G_E(\mathbf{S},\mathbf{X})$ produced virtually the same results, confirming the validity of Ewald's representation.

Figure 1 presents the number of iterations necessary for the functions G_M (NiGM) and G_E (NiGE) to converge, for a source point **S** located at the position (1.0,1.0) m, and a field point **X** moving along the same vertical line in which the source point is located, from y = 0.0 to y = 10.0 m. It can be seen that a much faster convergence is produced by the function G_E (number of iterations around 60).

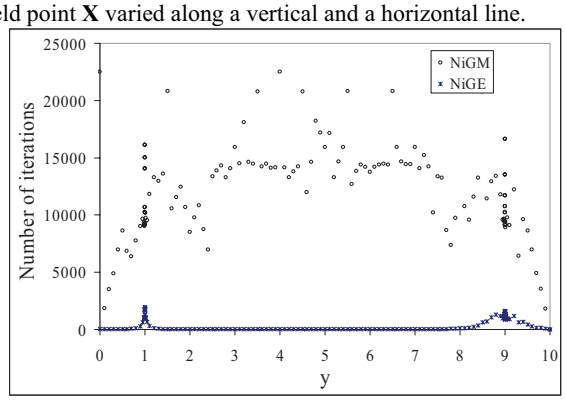

Figure 1: Number of iterations of the functions along of a vertical line

Conclusions

The Ewald's method was derived in this paper for speeding-up the calculations of the eigenfunction expansion of the Green's function for underwater acoustic analysis by the BEM. It was shown that Ewald's representation is an accurate and efficient method when the source and field points are located along the same vertical line or otherwise. The influence of the parameter b used to split the infinite integral was investigated, as well as the singular integral generated by the infinite series obtained by the Ewald's method.

According to this preliminary study, the proposed function $b(\beta)$ employed as parameter in the Ewald's method presented a good performance. Higher values of b improve the speed of convergence of the series for source and field points placed along the same vertical line, while the accuracy near singularities is improved by using lower values of b.

References

[1] C.M. Linton, *The Green's function for the two-dimensional Helmholtz equation in periodic domains*, Journal of Engineering Mathematics, **33**, 377-402, 1998.

[2] V. Papanicolaou, *Ewald's method revisited: Rapidly convergent series representation of certain Green's functions*, J. Comput. Anal. Appl., **1**, 105-114, 1999.

[3] P.P. Ewald, *Die Berechnung optischer and elektrostatischen Gitterpotentiale*, Ann. Phys., **64**, 253-268, 1921.

[4] S. Venakides, M.A. Haider and V. Papanicolaou, *Boundary integral calculations of two-dimensional electromagnetic scattering by photonic crystal Fabry-Perot structures*, SIAM J. Appl. Math., **60**, 1686-1706, 2000.

[5] J.A.F. Santiago and L.C. Wrobel, *A boundary element model for underwater acoustics in shallow waters*, Computer Modeling in Engineering & Science, **1**, 73-80, 2000.

[6] L.E. Kinsler, A.R. Frey, A.B. Coppens and J.V. Sanders, *Fundamentals of Acoustics*, 3rd edition, Wiley, New York, 1982.

[7] L.C. Wrobel and M.H. Aliabadi, *The Boundary Element Method*, Wiley, Chichester, 2002.

[8] J.A.F. Santiago and L.C. Wrobel, *Modified Green's functions for shallow water acoustic wave propagation*, Engineering Analysis with Boundary Elements, 28, 1375-1385, 2004.

GREEN FUNCTIONS FOR A CONTINUOUSLY NON-HOMOGENEOUS SATURATED MEDIA

Sarang Seyrafian[1], Behrouz Gatmiri[2] and Asadollah Nourzad[3]

[1]Department of Civil Engineering, University of Tehran, Tehran, Iran, sseyraf@ut.ac.ir
[2]Department of Civil Engineering, University of Tehran, Tehran, Iran and
Ecole Nationale des ponts et Chaussées, Paris, France, gatmiri@cermes.enpc.fr
[3]Department of Civil Engineering, University of Tehran, Tehran, Iran, noorzad@ut.ac.ir

Keywords: Boundary element method, Green function, depth non-homogeneity, saturated media, soil-structure interaction

In this paper, as shown in Fig. 1, an unbounded saturated media subjected to normal point load at the surface is considered. The mass density, porosity and permeability of the media are constant but the shear modulus varies solely with depth.

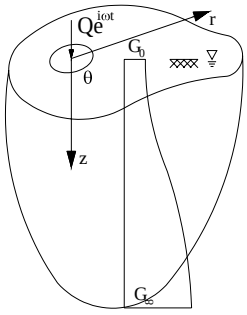

Figure1. Non-homogeneous saturated half space subjected to periodic normal point load

The variation of shear modulus is described by an exponential function as follows [Vrettos (1991)].

$$G\ (z) = G_\infty - (G_\infty - G_0)e^{-\alpha z} \tag{1}$$

Where G_0 and G_∞ are the shear modulus at the surface and infinite depth respectively and a is a constant with the dimension of inverse length, called coefficient of depth non-homogeneity or non-homogeneity parameter. By varying the parameters a, G_0 and G_∞, a wide range of real soil strata can be approximately described by Eq.1.

Firstly the system of governing differential equations, for the above media, obeying Biot's poro-elastic theory is derived [Biot 1956 and Gatmiri 1990]. The system of equations, formed by four coupled partial differential equations, is converted to ordinary differential equations' system by means of Hankel integral transforms. Then the system of equations is solved by use of generalized power series (Frobenius method) and the expressions for displacements in the interior of the media or in the other words, the Green functions for the media are derived by avoiding to introduction of any potential functions. The results of the research can be approximately used to analyze the dynamic response of a multi-layer media and B.E.M. formulation for soil- structure

interaction problems if the variation of shear modulus in different layers is estimated by an appropriate continuous function in the whole media.

As a result of this study, the effect of depth non-homogeneity on the response of the media, the variation of dimensionless real parts of vertical and radial displacements versus dimensionless frequency are illustrated in figures 2 for different values of G_0/G_8 ratio and different values of depth non-homogeneity parameter.

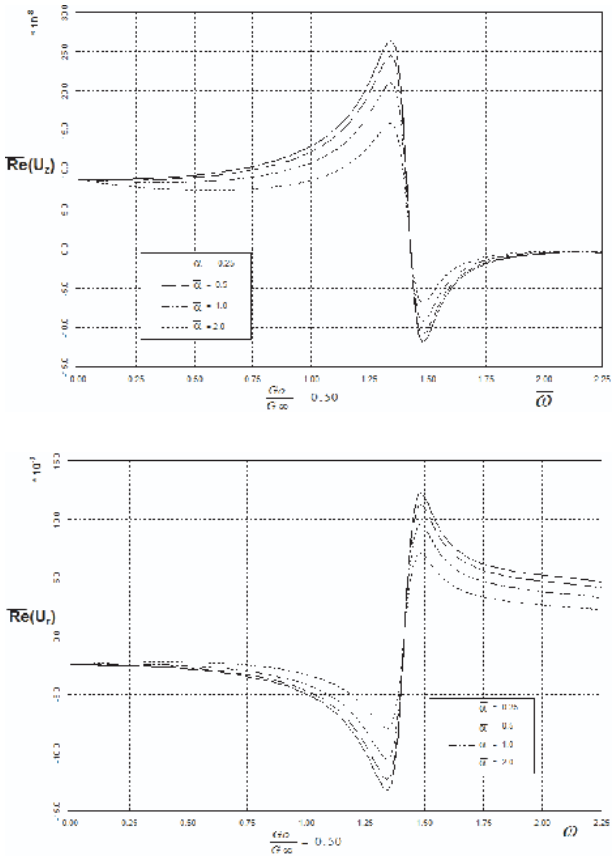

Figure2. Variation of vertical and radial displacements versus frequency for different depth non-homogeneity parameters $(\frac{G_0}{G_\infty} = 0.5)$

References

[1] M.A. Biot, Theory of Propagation of Elastic Waves in a Fluid Saturated Porous Solid: I. Low Frequency Range, *The Journal of Acoustical Society of America*, **28**,168-178 (1956).
[2] B. Gatmiri, A simplified finite element analysis of wave induced effective stress and pore pressures in permeable sea beds, *Géotechnique* **40,** 15-30 (1990).
[3] C. Vrettos, Time-harmonic Boussinesq problem for a continuously non-homogeneous soil, *Earthquake Engineering and Earthquake Engineering*. **20,** 961-977 (1991).

Sedimentation of a solid particle immersed in a thin fluid film

A. Sellier[1], L. Pasol[2]
[1] LadHyx. Ecole polytechnique, 91128 Palaiseau Cédex, France
e-mail: sellier@ladhyx.polytechnique.fr
[2] LPT, Escpci, Paris, France
e-mail: laurentiu.pasol@espci.fr

Keywords: Boundary-integral equations, sedimentation, fluid film, wall-particle interactions, free surface-particle interactions.

Abstract. The gravity-driven rigid-body motion of a 3D and arbitrarily-shaped solid particle in a fluid film bounded by two parallel plane solid wall and free surface is determined by using a boundary element approach. For such a purpose the Green tensor that complies with all the boundary conditions is analytically obtained and numerical results are given for a spherical particle.

Introduction and motivations

The motion of solid particles in a thin film fluid bounded by a plane solid wall and a free surface admits many industrial applications such as photographic coating. Hence, [1] recently addressed the two-dimensional gravity-driven film flow of a suspension of 2D solid particles. The present work introduces a new approach to cope with the gravity-driven rigid-body motion of a 3D solid particle with arbitrary shape in a fluid film. It is therefore the first step towards modelling the rheology of fully three-dimensional suspension-film flows.

Governing problem

We consider, as sketched in figure 1, a solid particle $\mathcal{P}$ immersed in a Newtonian viscous fluid with uniform density ρ and viscosity μ. Both the fluid, here confined between the plane solid wall $\Sigma_1(x_3 = 0)$ and the undisturbed plane free surface $\Sigma_2(x_3 = H)$, and the particle are subject to a uniform gravity field $\mathbf{g}$. Morevover, $\mathcal{P}$ is homogeneous with volume $\mathcal{V}$, mass $\mathcal{M}$ and center of mass O'.

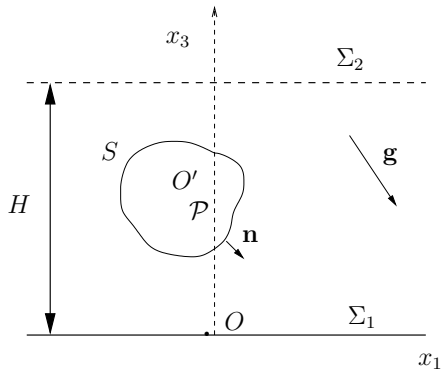

Figure 1. Case of a solid particle immersed in a fluid film and subject to the uniform gravity field $\mathbf{g}$.

The action of gravity induces a rigid-body motion of $\mathcal{P}$ with unknown translational velocity $\mathbf{U}$ (the velocity of O') and angular velocity $\mathbf{\Omega}$ with respect to Σ_1 and a low-Reynolds-number quasi-static fluid flow. At any point M in the fluid domain Ω, the fluid has velocity $\mathbf{u}$, pressure $p + \rho\mathbf{g}.\mathbf{OM}$ and stress tensor $\boldsymbol{\sigma}$. If $\mathcal{P}$ has a smooth boundary S with unit outward normal $\mathbf{n}$ and a negligible inertia, one arrives at the following problem

$$\mu\nabla^2\mathbf{u} = \nabla p \text{ and } \nabla.\mathbf{u} = 0 \text{ in } \Omega, \ (\mathbf{u}, p) \to (\mathbf{0}, 0) \text{ as } |\mathbf{OM}| \to \infty, \tag{1}$$

$$\mathbf{u} = \mathbf{0} \text{ on } \Sigma_1, \quad \mathbf{u}.\mathbf{e}_3 = \mathbf{e}_1.\boldsymbol{\sigma}.\mathbf{n} = \mathbf{e}_2.\boldsymbol{\sigma}.\mathbf{n} = 0 \text{ on } \Sigma_2, \tag{2}$$

$$\mathbf{u} = \mathbf{U} + \boldsymbol{\Omega} \wedge \mathbf{O'M} \text{ on } S, \tag{3}$$

$$\int_S \boldsymbol{\sigma}.\mathbf{n} dS = (\rho\mathcal{V} - \mathcal{M})\mathbf{g}, \quad \int_S \mathbf{O'M} \wedge \boldsymbol{\sigma}.\mathbf{n} dS = \mathbf{0}. \tag{4}$$

Advocated steps

Omitting details for a sake of conciseness, we here only briefly describe the required steps as follows:

i) We first analytically obtain the Green's function that satisfies (1) and the specific mixed boundary conditions (2). This is here achieved by extending the approach employed in [2] for the case of two solid and parallel plane boundaries. This key step makes it possible to express each Cartesian component of the Green's tensor in closed form.

ii) We then introduce 6 auxiliary steady Stokes flow induced in the liquid by three pure translations and three pure rotations of the particle. Exploiting those flows and the reciprocal identity yields 6 Fredholm boundary-integral equations of the first kind on S that are sufficient to calculate $(\mathbf{U}, \boldsymbol{\Omega})$ without computing the fluid flow $(\mathbf{u}, p)$ subject to (1)-(4). By the way, we also derive a basic integral representation for the velocity field $\mathbf{u}$ in the entire fluid domain.

iii) The numerical implementation resorts to 6-node curvilinear and triangular boundary elements [3,4] on the particle's surface S. This choice makes it possible to accurately compute the particle's rigid-body motion at a reasonable cpu time cost.

Preliminary numerical results

Although the proposed procedure (theory and numerical implementation) is valid for arbitrarily-shaped particles preliminary results will be presented at the talk for a spherical body. The migration of the sphere is found to deeply depend upon its location, the gravity field and the film thickness. It will be shown that the sphere may then either move faster, slower or at the same speed as if isolated in an unbounded fluid.

Conclusions

A new approach is presented to determine the settling motion of a solid and arbitrarily-shaped particle immersed in a liquid film of a Newtonian fluid. The Green's tensor associated to this geometry is analytically obtained and its use makes it possible to reduce the problem to the treatment of 6 boundary-integral equations of the first kind on the particle's surface.

References

[1] X. Li and C. Pozrikidis. Film flow of a suspension down an inclined plane. *Phil. Trans. R. Soc. Lond. A* **361,** pp. 847-869 (2003).

[2] R. B. Jones. Spherical particle in Poiseuille flow between planar walls. *Journal of Chemical Physics,* **121,** number 1 pp. 483-500 (2004).

[3] M. Bonnet *Boundary Integral Equation Methods for Solids and Fluids*, John Wiley & Sons Ltd, (1999).

[4] C. Pozrikidis *Boundary integral and singularity methods for linearized viscous flow*, Cambridge University Press, (1992).

The Application of a Hybrid Inverse Boundary Element Problem Engine for the Solution of Potential Problems

S. Noroozi[1], P. Sewell[1] and J. Vinney[1]
[1]Faculty of Computing, Engineering and Mathematical Sciences,
University of the West of England (UWE),
Bristol, BS16 1QY, UK.
Email: siamak.noroozi@uwe.ac.uk

Keywords: Boundary Element Modelling, Artificial Neural Network, Back Propagation, Linear Extrapolation, Weight Updating.

Introduction

Boundary Element Analysis (BEA) is now an established techinique widely used in many industries. In terms of structural analysis, the technique is almost exclusively used for discrete event simulation. In practice BEA of a large structure involves the discrete solution for a single time-step. If the effect of changing loads or other boundary conditions is required, this will usually involve expensive and often time consuming remodelling and/or re-runs of the solution software.

Researchers at the University of the West of England (UWE) have been investigating and developing hybrid solution schemes for solving inverse problems. This paper discusses the application of this research to develop an inverse problem engine to solve an inverse Boundary Element problem utilising a modified Trefftz method. The inverse methodology is based on the combined application of Artificial Neural Networks (ANN) and BEA. The proposed solution strategem has been compiled into an automated inverse Boundary Element problem solver with a powerful Graphical User Interface (GUI). It is assumed that the reader is familiar with BEA and its application to both potental and elastostatic problems.

Artificial Intelligence - Inverse Problem Analysis

An Artificial Intelligence approach, specifically an ANN, as an Inverse Problem Solver can be utilised for predicting the potential (external temperatures on a body) from the known internal temperatures as has been shown from preliminary evaluation of the inverse technique detailed elsewhere [1,2,3]. In general, ANNs were established from the study of the biological nervous system. In other words Neural Networks are an attempt at creating machines to behave like the human brain by using components that behave like biological 'neurons'. These elements are all interconnected and work in conjunction with each other, hence the development of the name 'Neural Network'. An ANN can often be thought of as a black box device for information processing that accepts inputs and produces outputs. Inverse problems are classed as problems where the responses (i.e. internal temperatures on a body) are known however the external temperatures, which generated them, are not.

Hybrid Inverse Boundary Element Problem Engine Design

Developing an Inverse Problem Engine, utilising an ANN, that is capable of determining the loads on a complex component requires four main areas to be considered:

1. *Acquisition of training data* – this should allow the reliable capture and generation of training data (i.e. external temperatures and the internal temperature responses).
2. *ANN architecture* – this should determine an accurate mathematical relationship (function) for the training data in as short a time period as possible (i.e. minimisation of the error function to an acceptable accuracy in the minimum number of loops).
3. *ANN software* – this should enable all the tasks required for network training, utilisation and data analysis to be accessed and performed within a simple and logical GUI.
4. *Acquisition of problem data* – this should allow the reliable capture of problem data (i.e. internal temperatures due to real external temperatures).

The developments in each of these areas have been discussed in the paper and the resultant system is presented through a case study.

Hybrid Inverse Boundary Element Problem Engine Case Study

A study was performed to assess the developed system. The problem chosen for the case study was a rectangular plate heated to 1000^{o}C on the left edge, -500^{o}C on the right edge and insulated on the other two sides. The aim of the case study was to determine the usability and accuracy of the Inverse Problem Engine by comparing the actual temperatures on the left and right edge found using direct analysis with the predicted temperatures found using the Inverse Problem Solver.

To validate the trained ANN eight problem patterns were generated from applying eight sets of four external temperatures (Actual Temperatures) to the model and collecting the internal temperature data. The problem patterns were then introduced to the network and the predicted external temperatures that caused them found (ANN Temperatures). The comparison of the Actual and ANN predicted temperatures for four of the eight problem patterns can be found in Fig. 1. The results in clearly shown that the ANN can predict four external temperatures caused by eighteen internal temperatures with a high level of accuracy within the specified temperature range.

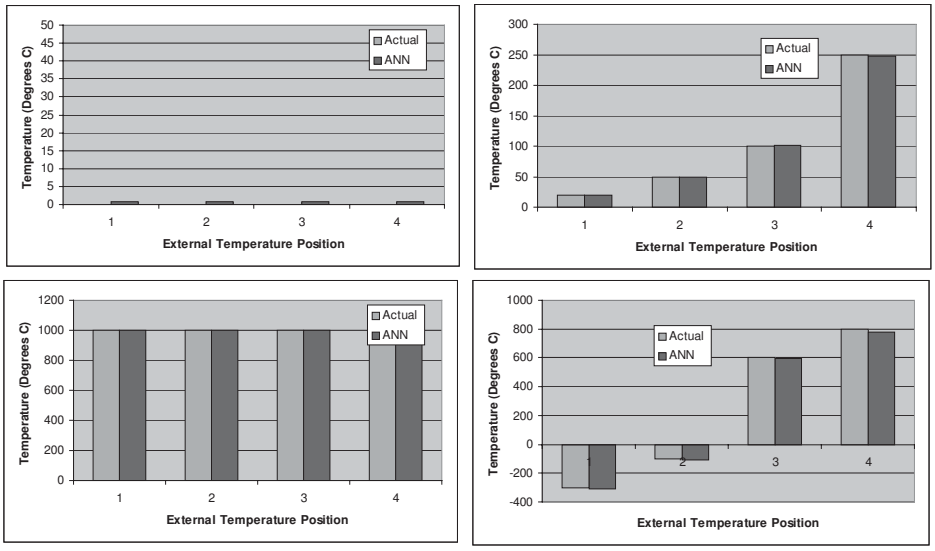

Figure 1: Comparison of actual and predicted external temperatures for four problem patterns.

Conclusion

A tool has been developed and tested through a case study that enables the user to can solve both direct and the inverse Boundary Element problems with ease. The software developed provides a simple to use interface, which allows simple analysis of the obtained results. A summary of the main development and achievements to date are detailed below, the developments are:

- an easy to use Graphical User Interface (GUI).
- a training methodology.
- a Boundary Element specific Inverse Problem Engine.

A critical appraisal of the system has highlighted several areas that require future investigation, which include:

- the development of a thermocouple data acquisition collection interface.
- investigation of the technique utilising time dependent parameters.
- the assessment of the potential of the tool for investigation of complex problems.

If these recommendations for further investigation can be achieved a complete and fully robust system could be developed.

References

[1] S.Noroozi, R. Amali, J. Vinney *The application of combined Artificial Neural Network and Boundary Element for potential problems*, Joint Meeting of the International Conference on Boundary Element Techniques and International Association for Boundary Element Methods, Rutgers University, NJ, USA, 16-18 July, 47-56, (2001).

[2] S.Noroozi, R. Amali, J. Vinney *Development of a generalized inverse problem engine for boundary element analysis of potential problems*, 3rd International Conference on Boundary Element Techniques and International Association for Boundary Element Methods (BETEQ2002), Beijing, China, 10-12 September, 169-175, (2002).

[3] S.Noroozi, R. Amali. J. Vinney *Combined BEA and ANN for the analysis of 3D inverse boundary domain problems*. 4th International Conference on Boundary Element Techniques and International Association for Boundary Element Methods (BETEQ2003), University of Granada, Spain, 15-17 July, 439-444, (2003).

Analyzing Production-Induced Subsidence Using Coupled Displacement Discontinuity and Finite Element Methods

Shunde Yin[1], Leo Rothenburg[1] and Maurice B. Dusseault[2]

[1] *Department of Civil Engineering, University of Waterloo, Waterloo, ON N2L 3G1, Canada.*

[2]*Department of Earth Sciences, University of Waterloo, Waterloo, ON N2L 3G1, Canada.*

ABSTRACT

In this paper, we apply a Displacement Discontinuity-FEM coupling method to a classic petroleum engineering problem: the evaluation of subsidence over a compacting oil reservoir. We use displacement discontinuity methods to account for the reservoir surrounding area, and finite element methods in the fully coupled simulation of the reservoir itself. This approach greatly reduces the number of degrees of freedom compared to an analyzing fully coupled problem using only a finite element or finite difference discretization.

Key words: Poroelasticity; subsidence; half space; displacement discontinuity method; finite element method

1. Introduction

Conventional reservoir simulator treats only the transport problem in the reservoir. This is analogous to assuming that the overburden has no stiffness and the total vertical stress on the upper surface of the reservoir is unaffected by pressure changes in the reservoir; i.e., it is assumed that $\Delta p = \Delta\sigma'_v$. This is clearly inadequate, as any change in pressure must be accompanied by a change in volume ($\Delta V/V = C\cdot\Delta\sigma'$, where C is compressibility); therefore, for any non-uniform pressure change in the reservoir, $\Delta p \neq \Delta\sigma'_v$, because of the stiffness of the overburden. An analytical solution presented by Rothenburg, Bratli and Dusseault(1996) for transient two-dimensional radial flow of a compressible fluid into a vertical penetrating well shows clearly that the stiffness of the strata, both reservoir and overburden, is an essential coupling element which must be taken into account. In the limit, for full coupling of flow and stress in the reservoir zone, the complete mechanical response of the overburden must be accounted for, even factors such as stratification and anisotropic properties.

In this paper, to achieve coupling in an efficient manner, we attempt to exploit the advantages of the displacement discontinuity method in solving the stress-strain problem in infinite and semi-infinite domains, combined with finite element methods for solving the flow-deformation system in the reservoir.

2. Subsidence Analysis by Hybrid DDFEM Model

2.1Displacement Discontinuity Method (DDM)

The Displacement Discontinuity method is a boundary element method for solving problems in solid mechanics. In geomechanics, it is usually used for analyzing large scale mining layouts in infinite or semi-infinite media(Salamon 1963), and it is useful in cases involving displacements along faults or joints, in fracture mechanics, and for simulating mining in tabular ore bodies (which extend at most a

few meters in one direction and hundreds or thousands of meters in the other two). An advantage of the displacement discontinuity method for problems in geomechanics, like any boundary method, is that boundary conditions at infinity are automatically satisfied. Hence, full domain discretization and stipulation of boundary conditions on non-infinite boundaries can be avoided. Inspired by the similarities between a tabular ore body and the typical tabular reservoir in an oil field, we may consider applying this highly efficient method to the area outside the reservoir.

2.2 Coupling of Displacement Discontinuity and Finite Element Methods

We combine a FEM method for the reservoir with a DD formulation for the surrounding strata, to address the compaction induced surface subsidence problem numerically in a half-space domain.

The exchange of the information between the reservoir model and the DD model is performed. The information that the FEM model provides is the deformation of the reservoir, which is then converted into displacement discontinuity provided to the DD model; the information that the DD model provides is the stress state of the reservoir, which is then converted into overburdens provided to the FEM model.

3. Verification and Conclusions

Verification through the comparison with Geertsma's solution(Geertsma 1966) shows that the DDFEM method leads to correct solutions. Conclusions are made:

1. The present method has advantages over the FEM method alone which must introduce proximal boundaries (not a true half-space) and leads to a much larger number of degrees of freedom for the discretization of the surrounding strata.

2. It has the advantage of higher accuracy with a reduced number of degrees of freedom through considering the reservoir compaction as one part of the problem, and its influence on the surrounding impermeable half-space domain as the second part of the problem. This seems to be a relatively natural way of addressing a large number of realistic problems.

4. References

1. Rothenburg L, Bratli RK, Dusseault MB. A poroelastic solution for transient fluid flow into a well. PMRI Publications, University of Waterloo, Canada, 1994.

2. Salamon MDG. Elastic analysis of displacements and stresses induced by the mining of seam or reef deposits, Part I, Journal of the South African Institute of Mining and Metallurgy 1963; **64**, 128-149.

3. Geertsma J. Problems of rock mechanics in petroleum production engineering. In Proceedings of the First Congress of International Society of Rock Mechanics, Lisbon, 585-594. 1966.

Analysis of thick functionally graded plates by local integral equation method

J. Sladek [1] , V. Sladek [1] , Ch. Hellmich[2] and J. Eberhardsteiner[2]

[1] Institute of Construction and Architecture, Slovak Academy of Sciences, 845 03 Bratislava, Slovakia, sladek@savba.sk

[2] Institute for Mechanics of Materials and Structures, Vienna University of Technology, Karlsplatz 13/202, 1040 Wien, Austria, Christian.Hellmich@tuwien.ac.at

Keywords: Functionally graded material, plate bending problem, orthotropic material, local boundary integral equations, static and impact load, Laplace-transform, Meshless approximation

Abstract. Functionally graded materials are multi-phase materials with the phase volume fractions varying gradually in space, in a pre-determined profile. Often, these spatial gradients in material behaviour render FGMs as superior to conventional composites. FGMs posses some advantages over conventional composites because of their continuously graded structures and properties [1]. Due to the high mathematical complexity of the initial-boundary value problems, analytical approaches for the FGMs are restricted to simple geometry and boundary conditions. Thus, analyses in FGM demand accurate and efficient numerical methods. The finite element method can be successfully applied to problems with an arbitrary variation of material properties by using special graded elements [2]. In commercial computer codes, however, material properties are considered to be uniform on each element. The boundary element method (BEM) is a suitable numerical tool for this purpose, too. However, for a general continuously nonhomogeneous body the fundamental solution for many governing equations are not yet known in literature. One possibility to obtain a BEM formulation is based on the use of fundamental solutions for a fictitious homogeneous medium.

During the last several decades, laminated composite plates have been widely used in engineering structures. It is well known that the classical thin plate theory of Kirchhoff gives rise to certain non-physical simplifications mainly related to the omission of the shear deformation and the rotary inertia, which become more significant for increasing thickness of the plate. The effects of shear deformation and rotary inertia are taken into account in the Reissner-Mindlin plate bending theory. The first application of the boundary integral equation method to Reissner's plate model was given by Van der Ween [3]. Number of applications to analyze functionally graded plates is very limited. Only Reddy [4] applied the FEM to FGM plates using the third-order shear deformation plate bending theory.

In the present paper, the authors have developed a meshless method based on the local Petrov-Galerkin weak-form to solve static and dynamic problems for orthotropic thick plates with material properties continuously varying through the plate thickness. The Reissner-Mindlin theory reduces the original 3-d thick plate problem to a 2-d problem. It is assumed that the material properties are graded along the plate thickness, and the profile for volume fraction variation is represented by

$$P(x_3) = P_b + (P_t - P_b)V \quad \text{with} \quad V = \left(\frac{x_3}{h} + \frac{1}{2}\right)^n \ , \tag{1}$$

where P denotes a generic property like modulus, P_t and P_b denote the property of the top and bottom faces of the plate, respectively, and n is a parameter that dictates the material variation profile. Poisson ratios are assumed to be uniform.

The bending moments $M_{\alpha\beta}$ and the shear forces Q_α are defined as

$$\begin{bmatrix} M_{11} \\ M_{22} \\ M_{12} \end{bmatrix} = \int_{-h/2}^{h/2} \begin{bmatrix} \sigma_{11} \\ \sigma_{22} \\ \sigma_{12} \end{bmatrix} x_3 dx_3 \qquad \text{and} \qquad \begin{bmatrix} Q_1 \\ Q_2 \end{bmatrix} = \kappa \int_{-h/2}^{h/2} \begin{bmatrix} \sigma_{13} \\ \sigma_{23} \end{bmatrix} dx_3 \ , \tag{2}$$

where $\kappa = 5/6$ in the Reissner plate theory.

One obtains expressions for bending moments $M_{\alpha\beta}$ and of the shear forces Q_α

$$M_{\alpha\beta} = D_{\alpha\beta}\left(w_{\alpha,\beta} + w_{\beta,\alpha}\right) + C_{\alpha\beta}w_{\gamma,\gamma}$$
$$Q_\alpha = C_\alpha\left(w_\alpha + w_{3,\alpha}\right) \quad , \tag{3}$$

where for linear gradation of material properties ($n = 1$)

$$D_{11} = \frac{D_1}{2}\left(1-\nu_{21}\right), \qquad D_{22} = \frac{D_2}{2}\left(1-\nu_{12}\right), \qquad D_{12} = D_{21} = \frac{G_{12t}h^3}{12},$$
$$C_{11} = D_1\nu_{21}, \qquad C_{22} = D_2\nu_{12}, \qquad C_{12} = C_{21} = 0,$$
$$D_\alpha = \frac{(E_{\alpha t} + E_{\alpha b})h^3}{24(1-\nu_{12}\nu_{21})}, \quad D_{12} = D_{21} = \frac{(G_{12t} + G_{12b})h^3}{24}, \quad D_1\nu_{21} = D_2\nu_{12},$$
$$C_\alpha = \frac{(G_{\alpha 3t} + G_{\alpha 3b})}{2}\kappa h, \tag{4}$$

and for a quadratic gradation:

$$D_\alpha = \frac{E_{\alpha b}h^3}{12(1-\nu_{12}\nu_{21})} + \frac{(E_{\alpha t} - E_{\alpha b})h^3}{30(1-\nu_{12}\nu_{21})}, \quad D_{12} = D_{21} = \frac{G_{12b}h^3}{12} + \frac{(G_{12t} - G_{12b})h^3}{30},$$
$$C_\alpha = G_{\alpha 3b}\kappa h + \frac{(G_{\alpha 3t} - G_{\alpha 3b})}{3}\kappa h. \tag{5}$$

In the Reissner-Mindlin plate bending theory the governing equations (equations of motion) have the form

$$M_{\alpha\beta,\beta}(\mathbf{x},t) - Q_\alpha(\mathbf{x},t) = \frac{\rho h^3}{12}\ddot{w}_\alpha(\mathbf{x},t),$$
$$Q_{\alpha,\alpha}(\mathbf{x},t) + q(\mathbf{x},t) = \rho h\ddot{w}_3(\mathbf{x},t) \qquad \mathbf{x}\in\Omega \quad , \tag{6}$$

where ρ is the mass density. The Greek indices vary from 1 to 2. The dots indicate differentiations with respect to time *t*.

According to the meshless local Petrov-Galerkin (MLPG) method, we construct a weak-form for Laplace transforms of governing equations over the local subdomains Ω_s^i around each node $\mathbf{x}^i$ inside the global domain Ω . If unit step functions are chosen for the test functions in local weak forms the following local boundary integral equations can be derived

$$\int_{\partial\Omega_s^i}\bar{M}_\alpha(\mathbf{x},s)d\Gamma - \int_{\Omega_s^i}\bar{Q}_\alpha(\mathbf{x},s)d\Omega - \int_{\Omega_s^i}\frac{\rho h^3}{12}s^2\bar{w}_\alpha(\mathbf{x},s)d\Omega + \int_{\Omega_s^i}\bar{R}_\alpha(\mathbf{x},s)d\Omega = 0 \quad , \tag{7}$$

$$\int_{\partial\Omega_s^i}\bar{Q}_\alpha(\mathbf{x},s)n_\alpha(\mathbf{x})d\Gamma - \int_{\Omega_s^i}\rho hs^2\bar{w}_3(\mathbf{x},s)d\Omega + \int_{\Omega_s^i}\bar{R}_3(\mathbf{x},s)d\Omega = 0 \ . \tag{8}$$

Meshless approximation of the generalized displacements on a simple domain, based on the Moving Least-Squares (MLS) method, allows for elegant and efficient numerical integration of domain-integrals in eqs (7) and (8). The Stehfest's inversion method is applied to obtain the time-dependent solution. Numerical results for isotropic and orthotropic square plates with various boundary conditions and subjected to static and impulse loadings are presented to illustrate the applicability of the proposed method.

References

[1] Suresh S., Mortensen A. *Fundamentals of Functionally Graded Materials.* Institute of Materials, London (1998).

[2] Kim J.H., Paulino G.H. Isoparametric graded finite elements for nonhomogeneous isotropic and orthotropic materials. *Journal of Applied Mechanics ASME*, **69**, 502-514 (2002).

[3] Van der Ween F. Application of the boundary integral equation method to Reissner's plate model. *International Journal for Numerical Methods in Engineering*, **18**, 1-10 (1982).

[4] Reddy J.N. Analysis of functionally graded plates. *International Journal for Numerical Methods in Engineering* , **47**, 663-684 (2000).

Shear Deformation Effect in Second-Order Analysis of Composite Frames Subjected in Variable Axial Loading by BEM

E.J. Sapountzakis and V.G. Mokos
School of Civil Engineering, National Technical University,
Zografou Campus, GR-157 80 Athens, Greece, cvsapoun@central.ntua.gr

Keywords: Transverse shear stresses; Shear center; Shear deformation coefficients; Beam; Frame; Second Order Analysis; Nonlinear analysis; Boundary element method.

Abstract. In this paper a boundary element method is developed for the second-order analysis of frames consisting of composite beams of arbitrary doubly symmetric constant cross section, taking into account shear deformation effect. Each composite beam consists of materials in contact each of which can surround a finite number of inclusions (Fig.1). Moreover, it is subjected in an arbitrarily concentrated or distributed variable axial loading. To account for shear deformations, the concept of shear deformation coefficients is used [1]. The analysis of the plane frame leads to the construction of the 6x6 local stiffness matrix for each beam component, relating the nodal displacement vector in the local coordinate system, with the respective nodal load vector. The elements of this matrix are evaluated from the solution of the following boundary value problem

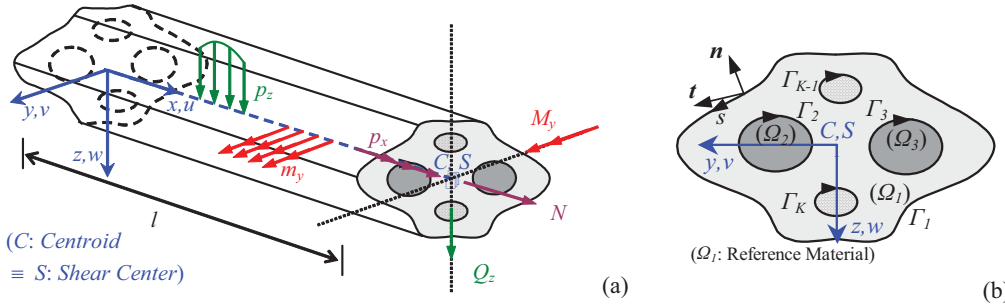

Fig.1. Prismatic beam in torsionless bending (a) with an arbitrary doubly symmetric composite cross-section (b).

$$E_1 I_y \left(1+\frac{N}{G_1 A_z}\right)\frac{d^4 w}{dx^4} = p_z - p_x \frac{dw}{dx} + N\frac{d^2 w}{dx^2} + \frac{dm_y}{dx} - \frac{E_1 I_y}{G_1 A_z}\left(\frac{d^2 p_z}{dx^2} - 3p_x \frac{d^3 w}{dx^3} - 3\frac{dp_x}{dx}\frac{d^2 w}{dx^2} - \frac{d^2 p_x}{dx^2}\frac{dw}{dx}\right)$$

inside the beam (1)

$$\alpha_1 w(x) + \alpha_2 R_z(x) = \alpha_3 \quad (2a)$$

$$\beta_1 \frac{dw(x)}{dx} + \beta_2 M_y(x) = \beta_3 \quad \text{at the beam ends } x = 0,1 \quad (2b)$$

where

$$I_y = \sum_{j=1}^{K} \frac{E_j}{E_1} \int_{\Omega_j} z^2 d\Omega_j \ , \qquad A_z = \kappa_z A = \frac{1}{a_z} A \ , \qquad A = \sum_{j=1}^{K} \frac{G_j}{G_1} \int_{\Omega_j} d\Omega_j \quad (3a,b,c)$$

are the moment of inertia, the shear area and the area of the composite cross section, κ_z is the shear correction factor, a_z the shear deformation coefficient of the Timoshenko's beam theory, $w = w(x)$ is the beam deflection, $N = N(x)$ is the beam axial force, R_z, M_y are the stress resultants at the beam ends, p_x,

p_z, m_y are the arbitrarily distributed axial, transverse loading and bending moment, respectively and α_i, β_i $(i=1,2,3)$ are given constants. Eqns. (2a,b) describe the most general boundary conditions associated with the problem at hand and can include elastic support or restrain. It is apparent that all types of the conventional boundary conditions (clamped, simply supported, free or guided edge) can be derived form these equations by specifying appropriately the functions α_i and β_i (e.g. for a clamped edge it is $\alpha_1 = \beta_1 = 1$, $\alpha_2 = \alpha_3 = \beta_2 = \beta_3 = 0$).

In the aforementioned boundary value problem the axial force inside the beam or at its boundary can be evaluated from the solution of the following boundary value problem

$$E_1 A \frac{d^2 u}{dx^2} = -p_x \qquad \text{inside the beam} \qquad (4)$$

$$c_1 u(x) + c_2 N(x) = c_3 \qquad \text{at the beam ends } x = 0, l \qquad (5)$$

where $u = u(x)$ is the beam axial displacement and c_i $(i=1,2,3)$ given constants.

The aforementioned two boundary value problems together with a third one concerning a stress function are solved employing a pure BEM approach, that is only boundary discretization is used. The evaluation of the shear deformation coefficients is accomplished from the aforementioned stress function using only boundary integration [2]. The essential features and novel aspects of the present formulation compared with previous ones are summarized as follows.

i. The composite beam is subjected in an arbitrarily concentrated or distributed variable axial loading.
ii. The composite beam is supported by the most general boundary conditions including elastic support or restrain.
iii. Shear deformation effect is taken into account.
iv. The shear deformation coefficients are evaluated using an energy approach, instead of Timoshenko's [1] and Cowper's [3] definitions, for which several authors have pointed out that one obtains unsatisfactory results or definitions given by other researchers, for which these factors take negative values.
v. The effect of the material's Poisson ratio ν is taken into account.
vi. The proposed method employs a pure BEM approach (requiring only boundary discretization) resulting in line or parabolic elements instead of area elements of the FEM solutions (requiring the whole cross section to be discretized into triangular or quadrilateral area elements), while a small number of line elements are required to achieve high accuracy.

It is worth here noting that the reduction of eqns.(1), (3), (4) using the modulus of elasticity E_1 and the shear modulus G_1 of the first material, could be achieved using any other material, considering it as reference material.

Numerical examples with great practical interest are worked out to illustrate the efficiency, the accuracy and the range of applications of the developed method. The influence of both the shear deformation effect and the variableness of the axial loading are remarkable. The analysis of plane frames consisting of homogeneous beams of arbitrary doubly symmetric simply or multiply connected constant cross section is treated as a special case.

References

[1] S.P.Timoshenko and J.N.Goodier, *Theory of Elasticity,* 3rd edn, McGraw-Hill, New York, (1984).
[2] V.G.Mokos and E.J.Sapountzakis A BEM Solution to Transverse Shear Loading of Composite Beams, *International Journal of Solids and Structures*, **42**, 3261-3287 (2005).
[3] G.R. Cowper The Shear Coefficient in Timoshenko's Beam Theory, *Journal of Applied Mechanics*, ASME, **33**(2), 335-340 (1966).

How EADS uses the Fast Multipole Method to boost its simulation in electromagnetism and acoustics

G. Sylvand (EADS-CRC F)
I. Terrasse (EADS-CRC F)

We are interested in the numerical simulation of waves propagations in electromagnetism and acoustics governed by the Maxwell and Helmholtz equations. We have to solve this kind of problem in fields such as furtivity, antenna design and placement, etc. More precisely, we choose to solve these equations in the frequency domain and in integral form, which results in having to solve a full complex linear system. When the characteristic size of the objects considered grows compared to the wavelength, the traditional methods to solve this system (standard Cholesky) become unsuited because of a prohibitory cost in term of storage and computing time. In the Eighties, these methods are used on workstations and are limited to problems involving a few thousands of unknowns, and objects whose diameter does not exceed a few wavelengths. In the Nineties, the use of parallel machines makes it possible to handle cases with up to 100.000 unknowns however with exactly the same methodology.

We implemented in EADS simulation software family ASERIS an algorithm called fast method multipôle allowing to solve the same equations in a much more economic manner. With the FMM, and in conjunction with an iterative solver (such as GMRES), one can solve the linear system interesting us in much more reasonable times and for much more significant problem sizes. These methods were implemented and validated both in electromagnetism and acoustics simulation softwares on distributed memory parallel machine. Thanks to all this research, we could carry out simulations of size without precedent on industrial cases in electromagnetism and acoustics.

For example, the image below is the result of a calculation of interaction between a simplified missile (seen in section here) comprising an air intake and an incidental plane wave (source : JINA Workshop 2004). The object measures 1,2 m, the frequency of the wave is 17 GHz, the mesh comprises 1,2 million unknowns. The presence of the cavity makes this kind of computation generally very difficult. Here, simulation took only 3 hours on 4 Opteron processors. On the image, one sees very well that the phenomena of multiple reflexions inside the cavity was well taken into account. The same case solved by a Cholesky method would have required 20.000 hours of computation (estimated, of course!) on the same machine. Without the Fast Multipole Method, this type of simulation is very difficult if not impossible to carry out.

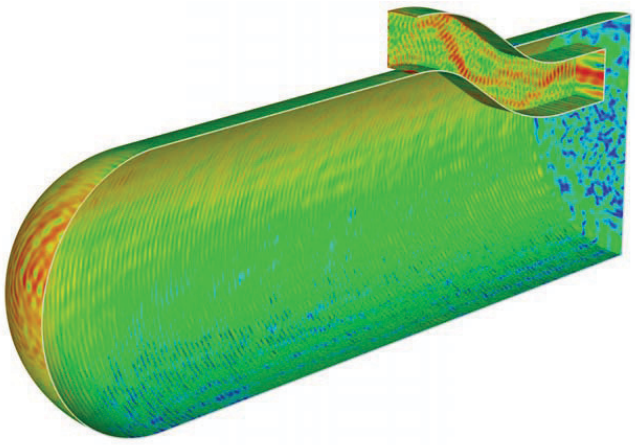

Boundary Element Stress Analysis of Thin, Layered Anisotropic Bodies

Y.C. Shiah[1], Y.C. Lin[1], and C. L. Tan[2)*]

[1] Dept. of Aerospace Engng. and Systems Engng., Feng Chia University
100 Wenhwa Road, Seatwen 40, Taichung, Taiwan
[2] Dept. of Mechanical & Aerospace Engng., Carleton University,
Ottawa, Canada K1S 5B6

Abstract

In the stress analysis of thin, slender bodies using the conventional Boundary Element Method (BEM), the integrals in the boundary integral equation (BIE) becomes nearly singular. This is because of the singular nature of the fundamental solutions to the governing equations of the problem which form the integrands. As a result, the accurate numerical evaluation of these integrals using quadrature rules that are based on simple polynomial representations poses some difficulties even though the integrands are regular in the strict mathematical sense within the limits of integration. Over the years, many different schemes have been proposed by various researchers to "regularize" nearly singular integrals which arise in various BEM formulations. They include the special weighted Gauss method, the Taylor series expansion and singularity subtraction method, the variable/coordinate transformation method, the projection transformation method, the auxiliary surface method, schemes to analytically regularize the BIE formulations to obviate computing the nearly singular integrals, and a few others. For various reasons, no one particular scheme among them has been widely adopted in BEM formulations.

Thin, layered, anisotropic material systems occur in many important applications in engineering. Examples include structural laminated composites, bi-crystals and thin film-substrate systems in solid state electronic devices, and single crystal alloy turbine blades with thermal barrier coatings. Failure due to debonding at the interfaces and excessive stresses in the layers when under mechanical and thermal loads are important design considerations. In this paper, regularization using integration by parts is carried out on the weakly singular integral in the BIE for two-dimensional anisotropic elasticity to reduce the order of the singularity of the integrand. Following this, the integral containing the traction fundamental solution is analytically integrated to give the exact formulation for a general element of n-th order interpolation of the variables. This allows the integrals to be very accurately evaluated even for very thin bodies and without the need for excessively refined meshes. The effectiveness and applicability of the proposed scheme are demonstrated by example problems in which the BEM results are compared with those obtained using the commercial FEM software ANSYS.

* Corresponding Author: Tel. 1-613-520-2600 ext. 5699
Fax. 1-613-520-5715; Email: ctan@mae.carleton.ca

On The NGF Procedure for LBIE Elastostatic Fracture Mechanics

L. S. Miers[1] and J. C. F. Telles[2]

Federal University of Rio de Janeiro – COPPE/UFRJ – Programa de Engenharia Civil, Caixa Postal 68506, Cep 21945-970, Rio de Janeiro , RJ, Brasil

[1] lsmiers@coc.ufrj.br [2] telles@coc.ufrj.br

Keywords: LBIE, meshless methods, numerical Green's function, fracture mechanics.

Abstract. This work aims at extending the concept of the Numerical Green's Function (NGF), well known from boundary element applications to fracture mechanics, to the Local Boundary Integral Equation (LBIE) context. As a "companion" solution, the NGF is used to remove the integrals over the crack boundary and is introduced only for source points whose support touches or contains the crack. The results obtained with the coupling of NGF-LBIE in previous potential discontinuity Laplace's equation problems and the authors' experience in NGF-BEM fracture mechanics were the motivation for this development.

Introduction

Meshless methods are increasingly proving to be quite accurate in the analysis of the most common problems found in engineering applications. They can be very efficient, in terms of computer time, in solving problems that need a great number of node repositioning during the analysis, which can be more expensive than the analysis itself when using mesh-based methods.

Normally, a meshless method is a mesh-free counterpart of a well-established mesh-based method [1,2] and because of this, there is no reason to believe that the improvements made for the mesh-based procedures cannot be implemented in their mesh-free versions.

In this work, the concept of the numerical Green's function (NGF) for 2-D elastostatic fracture mechanics is introduced in the local boundary integral equation (LBIE) method, which has been brought into existence from the boundary integral equation, basic to the boundary element method (BEM). The NGF for fracture mechanics was first used in a BEM approach [3] during the last decade and has recently been used for potential discontinuity simulations, already applied to the LBIE, generating very good results [4].

The approximation scheme for the trial function used here is the well-known moving least squares (MLS) method, which is the most common alternative in the bibliography. The singular integrals are computed using Kutt's quadrature [5] procedure, well-known from previous BEM implementations.

Numerical Green's Function

Consider an infinite elastic plane with an unloaded crack inside under the action of a unit point load applied at $\boldsymbol{\xi}$. The fundamental displacements and tractions for this case can be calculated by superposition [8], which mathematically reads

$$u_{ij}^{G}(\boldsymbol{\xi},\mathbf{x}) = u_{ij}^{*}(\boldsymbol{\xi},\mathbf{x}) + u_{ij}^{c}(\boldsymbol{\xi},\mathbf{x}) \qquad p_{ij}^{G}(\boldsymbol{\xi},\mathbf{x}) = p_{ij}^{*}(\boldsymbol{\xi},\mathbf{x}) + p_{ij}^{c}(\boldsymbol{\xi},\mathbf{x}) \tag{1}$$

where ( )* refers to Kelvin's fundamental solution and ( )c indicates the complementary part .
According to [3], the complementary part of the solution can be calculated as follows

$$u_{ij}^{c}(\boldsymbol{\xi},\mathbf{x}) = \int_{\Gamma_i} p_{jk}^{*}(\mathbf{x},\boldsymbol{\zeta}) \cdot c_{ik}(\boldsymbol{\xi},\boldsymbol{\zeta}) d\Gamma(\boldsymbol{\zeta}) \qquad p_{ij}^{c}(\boldsymbol{\xi},\mathbf{x}) = \int_{\Gamma_i} P_{jk}^{*}(\mathbf{x},\boldsymbol{\zeta}) \cdot c_{ik}(\boldsymbol{\xi},\boldsymbol{\zeta}) d\Gamma(\boldsymbol{\zeta}) \tag{2}$$

where $\boldsymbol{\zeta}$ is a point on Γ_i and $c_{ik}(\boldsymbol{\xi},\boldsymbol{\zeta})$ are the crack openings

$$c_{ik}(\boldsymbol{\xi},\boldsymbol{\zeta}) = u_{ik}^{c}(\boldsymbol{\xi},\boldsymbol{\zeta}^{s}) - u_{ik}^{c}(\boldsymbol{\xi},\boldsymbol{\zeta}^{i}) \tag{3}$$

which can be calculated by solving the following system of equations

$$\mathbf{S}\mathbf{c}_{ij}(\boldsymbol{\xi},\boldsymbol{\zeta}) = \mathbf{p}_{ij}^{*}(\boldsymbol{\xi},\boldsymbol{\zeta}) \tag{4}$$

Matrix S is square of dimension 2N (N is the number of points on Γ_i) that depends only of the crack's geometry. This complete formulation can be seen in [3] and is herein implemented for the LBIE method [4].

Example

This example is depicted in Figure 1. The results are compared with the ones presented in [3]. For this example it is considered: $E = 50000$, $\nu = 0.2$, number of nodes $N = 210$.

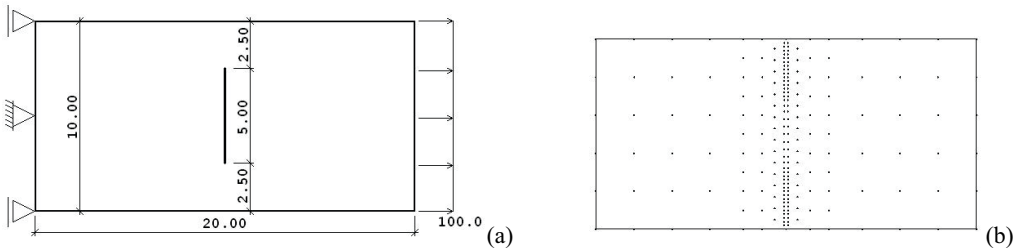

Figure 1 – (a) geometry and (b) node cloud of the example

The stress intensity factor K_I is obtained here using a relation presented in [8]. The comparison of the results obtained with this technique and those found with NGF-BEM (numerical Green's function with BEM) and AGF-BEM (analytical Green's function with BEM) are presented in Table 1.

Table 1 – comparison of results

Method	K_1/K_0	Error (%)
NGF-LBIE	1.182	0.51
NGF-BEM	1.1877	0.99
AGF-BEM	1.1871	0.94
estimated	1,176 ± 1%	-

Conclusion

This work aimed at introducing the concept of the NGF for fracture mechanics into the context of the LBIE method. Here the LBIE formulation was presented for the elastostatic problem, as well as the procedure for obtaining the NGF for fracture mechanics and the MLS approximation scheme used to interpolate the trial function.

The result produced illustrates the accuracy of the NGF-LBIE procedure and encourage new developments in this area of research.

References

[1] S.N. Atluri and S.Shen *Computer Modeling in Engineering & Sciences,* **3**(1): 11-51 (2002).
[2] S.N. Atluri, J. Sladek, V. Sladek and T. Zhu *Computational Mechanics,* **25**: 180-198 (2000).
[3] J.C.F. Telles, G.S. Castor and S. Guimarães *International Journal for Numerical Methods in Engineering,* **38**:3259-3274 (1995).
[4] L.S. Miers and J.C.F. Telles *Structural Integrity & Durability,* **1**(3): 225-232 (2005).
[5] C.A. Brebbia, J.C.F. Telles and L.C. Wrobel *Boundary Element Techniques: Theory and Application in Engineering*, Springer (1984).
[6] Y. Chen, A. Eskandarian, M. Oskard and J.D. Lee *Theoretical and Applied Fracture Mechanics,* **41**: 83-94 (2004).
[7] V. Sladek, J. Sladek, S.N. Atluri and R. van Keer *Computational Mechanics,* **25**: 394-403 (2000).
[8] L.P.S. Barra and J.C.F. Telles *Engineering Analysis with Boundary Elements,* **23**(1): 77-87 (1999).

Fast Multipole Boundary Element Analysis of Two-Dimensional Elastoplastic Problems

P. B. Wang[1] and Z. H. Yao[2]

[1] Department of Automotive Engineering, Tsinghua University, Beijing 100084, China, wangpengbo01@mails.thu.edu.cn

[2] Department of Engineering Mechanics, Tsinghua University, Beijing 100084, China, demyzh@tsinghua.edu.cn

Keywords: fast multipole, boundary element method, elastoplastic, nonlinear analysis

Abstract: This paper presents a fast multipole BEM for the analysis of two-dimensional elastoplastic problems. Both of the boundary integrals and domain integrals are calculated by recursive operations on a quad-tree structure without explicitly forming the coefficient matrix. Combining multipole expansions with local expansions, computational complexity and memory requirement of the matrix-vector multiplication are both reduced to $O(N)$, where N is the number of DOFs (degrees of freedom).

BEM Formulation of Elastoplasticity

Considering a homogeneous solid of domain Ω bounded by a boundary Γ, the following integral equation can be written for the displacement rate at a boundary source point x [1].

$$c_{\alpha\beta}(x)\dot{u}_\beta(x) = \int_\Gamma u^*_{\alpha\beta}(x,y)\dot{t}_\beta(y)d\Gamma(y) - \int_\Gamma t^*_{\alpha\beta}(x,y)\dot{u}_\beta(y)d\Gamma(y) + \int_\Omega \hat{\sigma}^*_{\alpha\beta\gamma}(x,Y)\dot{\varepsilon}^p_{\beta\gamma}(Y)d\Omega(Y) \tag{1}$$

And the following integral equation can be obtained for the stress rate at an internal point X

$$\dot{\sigma}_{\alpha\beta}(X) = \int_\Gamma u^*_{\alpha\beta\gamma}(X,y)\dot{t}_\gamma(q)d\Gamma(y) - \int_\Gamma t^*_{\alpha\beta\gamma}(X,y)\dot{u}_\gamma(y)d\Gamma(y) + \int_\Omega \tilde{\sigma}^*_{\alpha\beta\gamma\zeta}(X,Y)\dot{\varepsilon}^p_{\gamma\zeta}(Y)d\Omega(Y) + f_{\alpha\beta}(\dot{\varepsilon}^p_{\gamma\zeta}(X)) \tag{2}$$

Implementation of the Fast Multipole Method

The fast multipole BEM uses the same discretization as the conventional BEM. The boundaries of the model are discretized using boundary elements and the internal domain where local yielding is expected to occur are discretized using internal cells. Then an adaptive quad-tree structure is constructed [2]. The boundary and domain elements are both allocated into the leaves of the tree. An example is shown in Fig.1, where each leaf contains at most six boundary elements or internal cells. Both of the boundary integrals and domain integrals are calculated by recursive operations on the quad-tree structure without explicitly forming the coefficient matrix. Combining multipole expansions with local expansions [3], computational complexity and memory requirement of the matrix-vector multiplication are both reduced to $O(N)$, where N is the number of DOFs (degrees of freedom).

In order to solve the system equations of elastoplastic problems, an incremental iterative algorithm is employed, which follows the loading history accurately. In each loading step, an iterative procedure is executed to determine the plastic strains at the interior nodes where the material is possibly yielded. In each iteration step to obtain the new plastic strains, the equation system is solved by the generalized minimum residual method (GMRES), which uses the sparse approximate inverse type as the preconditioner.

Numerical Example

This example considered a square plate with 16×16 periodically distributed circular holes as shown in Fig. 2. The outer boundary of the plate is subjected to uniform normal displacement $\overline{u}_n = 0.04\text{mm}$ under plain strain conditions. Ideal plasticity is assumed with the following material properties:

Young's modulus $E = 42000\,\text{MPa}$, Yield stress σ_0=105MPa, Poisson ratio ν=0.33.

The boundaries and expected yielding areas were discretized by quadratic elements and constant cells, respectively. The whole model has 107,520 boundary DOFs and 645,120 internal DOFs.

In the fast multipole BEM analysis, the order of the finite series was set as 25; the loading process was divided into 6 increments, and 10 iterations were employed in each increment. The analysis was done on a desktop PC and the total CPU time was 9.77 hours. Fig.3 shows the distribution of the equivalent von Mises stress in a unit square, where only the expected yielding area is plotted. To verify the BEM results, a unit square was isolated and analyzed using a commercial FEM software MSC/Marc, and the corresponding results are shown in Fig.4.

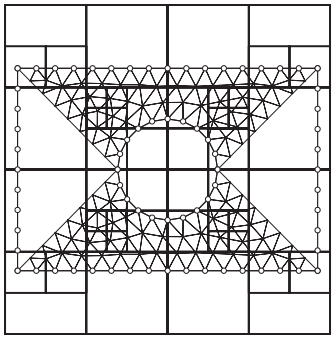

Fig. 1 A quad-tree

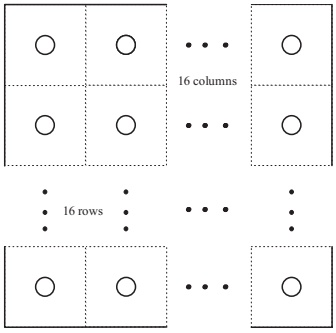

Fig. 2 A square plate with 16×16 circular holes

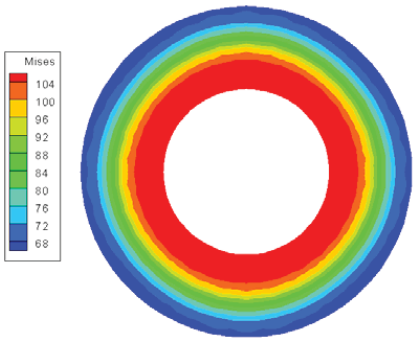

Fig.3 Distribution of the von Mises stress (BEM)

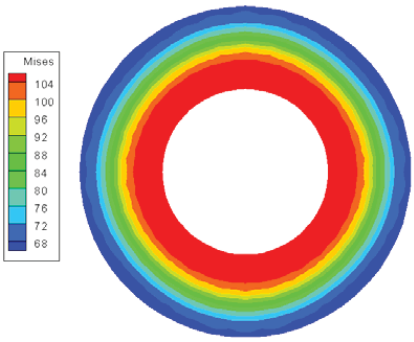

Fig.3 Distribution of the von Mises stress (BEM)

References

[1] J.C.F. Telles *The Boundary Element Method Applied to Inelastic Problems.* Springer-Verlag (1983).

[2] N. Nishimura *Appl. Mech. Rev.*, **55**, 299-324 (2002).

[3] L. Greengard and V.Rokhlin J. *Comput. Phys.*, **135**, 280-292 (1997)

Quasi-static 3D Rolling-Contact

R. Abascal and L. Rodríguez-Tembleque
Escuela Superior de Ingenieros
Camino de los descubrimientos s/n
E-41092 Seville, SPAIN
E-mail: abascal@us.es

The solution of 3D Rolling-Contact problems involves the solution of the frictional contact problem using directional derivatives depending on the rolling velocity.

Elastic equations are computed by BEM and solved satisfying the non-linear boundary conditions. In this process the number of equations corresponding to each node in possible contact is usually duplicated to include the contact equations, which change from each solution step to the next, and the static condensation of the non-contacting degrees of freedom is often used to reduce the size of the non-linear problem solved each iteration, but this process is highly expensive for 3D problems.

If the BEM is used together with advanced non-linear solution methods, i.e., Augmented Lagrangian with Generalized Newton Method (GNM), the complementarity between unknowns and some relationships between the contact restrictions with friction can be used to simplify and accelerate the solution of contact problems.

In this work a new algorithm that takes advantage of these relationships to solve the problem, without using the static condensation and making use of an iterative equation system solution method, will be presented. The new algorithm solves in each iteration a different equation system, of the same size that the one derived from the elastic equations, using as starting solution the one obtained during the previous iteration.

The methodology developed starts from a representation of the contact equations by a new projection function of the augmented tractions, and using an approximation of the rolling derivative. This function, when included in the GNM, produces a very simple jacobian, maintaining a good convergence ratio.

From the eulerian perspective, the directional derivative can be viewed as a flux of material on the body surface in the rolling direction. In this work, we use a balance law on the body surface to ensure that all material that comes into a patch of boundary elements also go out, both in the correct direction, independent of the mesh, regular or irregular, and the relative alignment with the rolling direction.

For each step, the directional derivative is estimated using previous values, included as a constant in the solving process, and corrected. This process permits the use of fast algorithms developed previously by the authors for contact problems without rolling, avoiding the condensation process and reducing the number of unknowns.

To illustrate the capabilities of this algorithm, several examples will be solved showing the accurate results obtained, and the necessary computational effort.

High order boundary integral methods for Maxwell's equations: coupling of Microlocal Discretization and Fast Multipole Methods

L. Gatard[1,2], **A. Bachelot**[1], **K. Mer-Nkonga**[2],
[1] MAB, Université Bordeaux 1, 351 cours de la Libération, 33405 Talence cedex
[2] Commissariat l'Energie Atomique-Centre Etude Scientifique et Technique d'Aquitaine, BP2, 33114 Le Barp, France
e-mail: Ludovic.Gatard@math.u-bordeaux1.fr

ABSTRACT

An efficient method to solve time harmonic Maxwell's equations in unbounded exterior domain for high frequencies is obtained by using the integral formulation of Després mixed up with a coupling method based on the Microlocal Discretization Method (MDM) and the Fast Multipole Method (FMM) [1]. However, some aspects of this method still remain to study. One of these aspects is the use of curved microlocal finite elements of higher order, in order to satisfy the error's estimations of the MDM.
The integral formulation of Després [2], for Leontovicth's type impedance boundary conditions, results in a linear system with good properties which allow us to solve the system with an efficient iterative method.
After discretization, we have to solve a dense linear system with a size N proportionnal to the free wave number $k = 2\pi f/c$ where f is the frequency of the incident wave and c the speed of light. By using the multi-level FMM (MLFMM) [3] which is based on the reduction of the interactions generated by the Green kernel between multipole boxes, we can reduce the complexity of the matrix-vector calculation of the iterative solution to $O(NlnN)$. Currently, the implementation of curved finite elements of order 2 was done in a code coupling integral equations of Després and MLFMM. We obtain good results in the cases of sphere and almond by using curved finite elements of order 2.
Another strategy to solve Maxwell's equations is to reduce the size of the linear system. We reduce the size of the system by the use of MDM introduced by Abboud, Nédélec and Zhou [4]. In MDM, when we discretize the unknown, we give some information on the oscillatory behaviour of the solution by the approximation of the phase function of the unknown. Then, we have a new unkown (less oscillatory) that we can approximate with a number of degrees of freedom of order $k^{\frac{2}{3}}$ instead of k^2. However, it's still necessary to approximate the surface of the objet by a mesh with a number of elements in k^2. Then, the MLFMM is used to speed up the calculation of the system [1]. In order to achieve a high level of accuracy, in the case of perfectly absorbing objects, we consider the use of curved finite elements of higher order.

REFERENCES

[1] E. Darrigrand "Coupling of Fast Multipole Method and Microlocal Discretization for the 3-D Helmholtz Equation", J. Comput. Phys., (2002).

[2] F. Collino and B. Després "Integral equations via saddle point problems for time-harmonic Maxwell's equations", J. of Comput. and Applied Math., Vol. 150, pp. 157–192, (2003).

[3] W.C. Chew, J.M. Jin, E. Michielssen, and J.M. Song "Fast and Efficient Algorithms in Computational Electromagnetics", Artech House, Boston, MA, (2001).

[4] T. Abboud, J.-C. Nédélec and B. Zhou "Improvement of the Integral Equation Method for High Frequency Problems", Third international conference on mathematical aspects of wave propagation phenomena, SIAM, pp. 178–187, (1995).

TIME DOMAIN 3D FUNDAMENTAL SOLUTIONS FOR SATURATED POROELASTIC MEDIA WITH INCOMPRESSIBLE CONSTITUENTS

Mohsen Kamalian[1], Behrouz Gatmiri[2], Morteza Jiryaei Sharahi[3]

[1]International Institute of Earthquake Engineering and Seismology (IIEES), Tehran, Iran, kamalian@iiees.ac.ir
[2]University of Tehran and Ecole Nationale des ponts et Chaussees, Paris, France, gatmiri@cermes.enpc.fr
[3]International Institute of Earthquake Engineering and Seismology (IIEES), Tehran,Iran, jiryaei@iiees.ac.ir

Keywords: boundary element, dynamic poroelasticity, incompressible, time domain, fundamental solution

1. Introduction

Transient poroelastodynamic fundamental solutions are some of the key ingredients required for solving wave propagation problems in saturated porous media. These solutions involve the responses of the medium to suddenly apllied point forces and a supplementary scalar source with Heaviside step functions in time. Considering the practical variables of solid skeleton displacement and fluid pressure, Gatmiri and Kamalian [1], among others, derived an approximate transient 2D fundamental solutions for the u-p formulation which can be used in BE algorithms. Later Gatmiri and Nguyen [2] proposed much less complicated transient 2D fundamental solutions for the u-p formulation of saturated porous media consisted of incompressible constituents.

Presentation of time-domain fundamental solutions for the u-p formulation of 3D saturated porous media with incompressible constituents constitutes the main purpose of this paper. Some numerical results are plotted that show the accuracy of the proposed solutions.

2. Governing Equations

Equations of dynamic poroelasticity expressing, respectively, the conservation of total momentum, the flow conservation for the fluid phase, the constitutive equation of a poroelastic solid and the generalized Darcy's law in the frame of Biot theory have been considered.

The u-p governing equations for poroelastic media with incompressible solid particles and fluid could be obtained in the Laplace transform domain as follows [1and 2]:

$$\mu\tilde{u}_{i,jj} + (\lambda+\mu)\tilde{u}_{j,ji} - \rho s^2\tilde{u}_i - \alpha\tilde{p}_{,i} + f_i = 0 \tag{1}$$

$$k\tilde{p}_{,ii} - \alpha\tilde{u}_{i,i} + \tilde{\gamma} = 0 \tag{2}$$

Where the tilde denotes a Laplace transform and s is the Laplace transform parameter.

3. Laplace Transform and Time Domain Fundamental Solutions

The explicit three dimensional Laplace transform domain fundamental solutions for equations (1) and (2), which involves the response to suddenly applied three point forces and a supplementary scalar source with Heaviside step function in time, have been obtained by employing directly the Kuperadze method [3]. Returning to the real time domain requires inverting the exponential functions of equations in Laplace transform domain as well as their coefficients by employing the convolution theorem. Using the simplified assumptions of u-p formulation as well as solid grain and fluid incompressibilities, enables one to obtain the inverse Laplace transforms of the exponential functions in an exact and much less complicated manner compared to the extremely difficult case of complete dynamic formulation of poroelastic media.

The explicit and simple closed form expressions of the time domain fundamental solutions could be obtained as follows:

$$G_{ij}=\left(\int_{1/v_d}\left(\left(\frac{A_{ij}}{2\beta\rho}(t-\tau)-\frac{A_{ij}}{(2\beta)^2\rho}(1-\exp(-2\beta(t-\tau)))+\frac{C_{ij}}{\rho v_d^2}\right)g_1(\tau)+\frac{B_{ij}}{\rho v_d}g_2(\tau)\right)d\tau\right)H(t-\frac{r}{v_d})$$
$$+\frac{A_{ij}}{\rho(2\beta)^2}\left(1-\exp(-2\beta t)-2\beta t+2\beta^2t^2\right)$$
$$+\left(-\frac{A_{ij}}{2\rho}\left(t-\frac{r}{v_s}\right)^2-\frac{B_{ij}}{\rho v_s}\left(t-\frac{r}{v_s}\right)+\left(D_{ij}-\frac{C_{ij}}{\rho v_s^2}\right)\right)H\left(t-\frac{r}{v_s}\right) \quad (3)$$

$$G_{4i}=\left[-\frac{r_{,i}}{4\pi\alpha r^2}\left(\int_{1/v_d}(1-\exp(-2\beta(t-\tau)))g_1(\tau)d\right)-\frac{2\beta r_{,i}}{4\pi v_d\alpha r}g_2(t)\right]H\left(t-\frac{r}{v_d}\right)$$
$$+\frac{r_{,i}}{4\pi\alpha r^2}(1-\exp(-2\beta t)) \quad (4)$$

$$G_{44}=\frac{1}{4\pi kr}\left[\int_{1/v_d}(1-\exp(-2\beta(t-\tau)))g_1(\tau)H\left(t-\frac{r}{v_d}\right)+\exp(-2\beta t)\right] \quad (5)$$

where I_0, I_1, $H(t)$ and $\delta(t)$ denote the modified Bessel functions of the first kind of orders zero and one, and the Heaviside step and Dirac delta functions, respectively.

3. NUMERICAL RESULTS

A set of numerical results and comparisons are presented in this paper to demonstrate the accuracy of the proposed analytical time-domain fundamental solutions. A saturated soft soil with incompressible solid grains and pore water is considered in which the material properties are defined in the metric system as follows: λ=12.5 MPa, μ=8.33 MPa, ρ =2120 kg/m^3, $\alpha=1$, $\kappa=1\times10^{-7}$ m^4/Ns. The applied force (or fluid source) point is located at coordinate (0,0,0) and the receiver is located at coordinate (0.01,0.02,0.03). Figures 1 shows the accuracy of the presented analytical closed form solution for G_{44} components as an example.

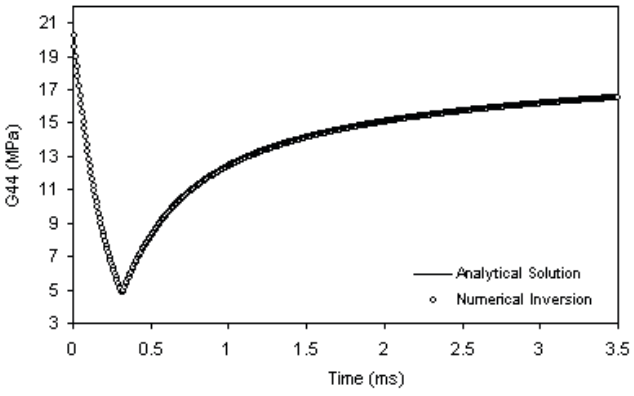

Figure 3. Three-dimensional pressure time history at (0.01,0.02,0.03) due to fluid injection at (0,0,0)

References

[1]B.Gatmiri and M. Kamalian, On the Fundamental Solution of Dynamic Poroelastic Boundary Integral Equations in Time Domain, *ASCE; The International Journal of Geomechanics*, Vol. 2, No.4, 381-398, 2002.

[2]B.Gatmiri and K.V.Nguyen, Time 2D fundamental solutions for saturated porous media with incompressible fluid*, Commun. Numer. Meth. Engng.,* **21**(3), 119-132, 2004.

[3]V. D. Kupradze, *Three dimensional problems of the mathematical theory of elasticity and thermoelasticity*, North-Holland, Amsterdam, 1979.

Correction of the crack extension direction in the Dual Boundary Element Method

T. Lucht[1], F. Aliabadi[2]

[1] Department of Mechanical Engineering, Solid Mechanics, Technical University of Denmark, 2800 Lyngby, Denmark, trl@mek.dtu.dk

[2] Department of Engineering, Imperial College, University of London, UK. M.H.Aliabadi@imperial.ac.uk

Keywords: Boundary element method, crack, propagation, direction, correction

Abstract.
In this paper a new procedure to correct the crack extension direction is proposed in connection with crack growth analyzed by the Dual Boundary Element Method (DBEM). The proposed correction procedure and an existing correction procedure are evaluated by solving three different computational crack growth examples. In all the three examples it is found that analyses of the crack path performed with big crack extensions and the proposed crack correction procedure is in excellent agreement with analysis of the crack path performed with very small crack extensions. Furthermore it is shown that the existing correction procedure has a tendency to overcorrect the crack growth direction if the stop criterion for the iterative correction procedure is not specified for each new crack growth analysis.

The DBEM is well suited to study crack propagation because discretization only occurs at the boundary and therefore the remeshing task is greatly reduced [1] when compared to other computational methods such as the finite element method. In the DBEM the crack growth process is simulated by an incremental crack-extension analysis. Each crack increment is in general modeled with a straight extension which results in a curved crack path formed by a piece-wise straight crack. For each increment the direction of the crack extension needs to be found from the stress intensity factors. Several theories have been proposed to describe the direction of mixed-mode crack growth and one of the most commonly used is the maximum principal stress criterion [2]. The criterion prescribes that the crack will grow perpendicular to the direction of the maximum principal stress. In order to avoid introduction of an error when the maximum principal stress criterion is used with an incremental formulation, each straight crack extension would have to be infinitesimal as the crack growth direction changes when the crack grows. A correction procedure to correct the extension direction of the increment can however be applied to ensure that a unique crack path is achieved with different analyses of the same problem performed with different size of the crack-extension increments.

A. Portela, M. H. Aliabadi and D. P. Rooke [1] presented a simple procedure to correct the direction of the crack-extension increment. In this procedure the error introduced by extending the crack perpendicular to the maximum principal stress evaluated only at the old crack tip is corrected in several iterations by the direction of the maximum principal stress found at the new crack tip. For each iteration the direction of the crack extension is corrected so that the crack increment leads towards the crack path calculated with an infinitesimal crack extension size. However as will be shown in the paper this correction procedure has a tendency to overcorrect the direction of the crack extension, as it is difficult to find a general stop criterion for the iterative procedure.

Another crack correction procedure is proposed in the present paper. In this procedure it is assumed that the crack increment has a continuous deflection and therefore it can be approximated with a second order polynomial. The direction of the maximum principal stress at the old crack tip is at first used to place a new crack increment. From the extension direction found at both the old and the new crack tip it is possible to calculate the corrected crack tip position, since the direction must change linearly when a second polynomial is used. As piece-wise straight elements are most general in the Dual Boundary Element Method the second order crack path that connects the old and new crack tip is replaced by a straight crack increment. A similar approximation of the shape of the crack increment is used in the predictor-corrector method [3] which is based on an incremental parabolic approximation of the crack path together with the modified virtual crack closure integral method.

References

[1] A. Portela, M. H. Aliabadi and D. P. Rooke, *Computers and Structures*, **46**, 237-247 (1993)

[2] F. Erdogan and G. C. Sih, *J. Basic Engng*, **85**, 519-527 (1963)

[3] H. Thielig and M. Wünsche, *Advances in Fracture and Damage Mechanics*, **IV**, 287-293 (2005)

Propagation of seismic P and SV waves in alluvial valleys with vertical gradient of velocity

Francisco Luzón[1], Francisco J. Sánchez-Sesma[2] , J. Alfonso Pérez-Ruiz[1], Leonardo Ramírez-Guzmán[3] and Andrés Pech[4]

[1] Departamento de Física Aplicada and Instituto Andaluz de Geofísica, Universidad de Almería. Cañada de S. Urbano s/n. 04120-Almería.Spain. fluzon@ual.es

[2] Instituto de Ingeniería, UNAM. Ciudad Universitaria, Coyoacán 04510, México DF, México. sesma@servidor.unam.mx

[3] Department of Civil and Environmental Engineering, Carnegie Mellon University, Forbes 5000, Pittsburgh PA 15217. USA. lramirez@andrew.cmu.edu

[4] Contro Interdisciplinario de Investigación para el DEsarrollo Integral Regional, CIIDIR-Oaxaca, Instituto Politécnico Nacional. México. apech@ipn.mx

Keywords: Boundary element method, Green function, vertical heterogeneity, sedimentary basins soil dynamics, seismology.

Abstract. The propagation of seismic *P* and *SV* waves within inhomogeneous alluvial valleys has been computed using the Indirect Boundary Element Method (IBEM). We used the approximate analytical expressions of the Green´s functions for a medium with constant vertical-gradient of velocity to compute the response of various inhomogeneous soft deposits. These simulations provided interesting results that displayed complex amplification patterns in a rich spectrum of frequencies and locations. We compared these results with the calculated using homogeneous material within the alluvial basins. The impedance contrast (relative to half-space) is not constant in all sediments of the valley (i. e. is dependent upon depth). Indeed, the lowest wave velocities are on the free surface of our model. This induces significant lateral reflections of surface waves that have great influence on the free-surface displacements, in comparison with the homogeneous models. The heterogeneity completely modifies the response and produces a complex behavior due to body and surface waves that have a tendency to trapping energy at the shallowest region.

The Green functions. Consider an elastic isotropic medium with wave velocity varying linearly with depth. Under the assumptions of constant ratio of *P*- to *S*-wave velocities the "radial" and "transverse" components of the approximate analytic 2D Green´s functions for an unit line force in the *z* or *x* directions can be expressed (see Reference [1]) as,

$$G_{R_w z} \approx P\cos j_0, \quad (1), \qquad G_{j_0 z} \approx Q\sin j_0 \quad (2)$$

or

$$G_{R_w x} \approx P\sin j_0, \quad (3) \qquad G_{j_0 x} \approx -Q\cos j_0, \quad (4)$$

respectively, where

$$P = \Lambda\frac{i}{8\rho_0}\left(A-B\right), \quad (5) \qquad Q = \Lambda\frac{-i}{8\rho_0}\left(A+B\right). \quad (6)$$

Here $i=\sqrt{-1}$,

$$A = \frac{H_0^{(1)}(\omega\tau_\alpha)}{\alpha_0^2} + \frac{H_0^{(1)}(\omega\tau_\beta)}{\beta_0^2}, \quad (7) \qquad B = \frac{H_2^{(1)}(\omega\tau_\alpha)}{\alpha_0^2} - \frac{H_2^{(1)}(\omega\tau_\beta)}{\beta_0^2}, \quad (8)$$

and where the frequency independent factor Λ can be expressed as (see [2])

$$\Lambda = \left(\frac{1+\gamma z_0}{1+\gamma z}\right)^{\frac{n+2}{2}} \sqrt{2\ln\left(\frac{R_2+R_1}{R_2-R_1}\right)\frac{(z_0+h)(z+h)}{R_1R_2}}. \quad (9)$$

In these equations $H_m^{(1)}$ is the Hankel´s function of the first kind and *m* order, ω = circular frequency, τ_α and τ_β are the travel times of *P* and *S* waves, respectively, $R_1=\sqrt{(x-x_0)^2+(z-z_0)^2}$ and $R_2=\sqrt{(x-x_0)^2+(z+z_0+2h)^2}$. In the expressions of the Green functions the explicit time dependence $e^{-i\omega t}$ has been omitted. The time displacements on 50 receivers at the free surface of the models used here (see fig. 1) are shown. A remarkable characteristic of the heterogeneous models is that they exhibit a tendency to amplify the level of surface motion because the velocity gradient makes them more likely to become energy traps, as compared with their homogeneous counterparts.

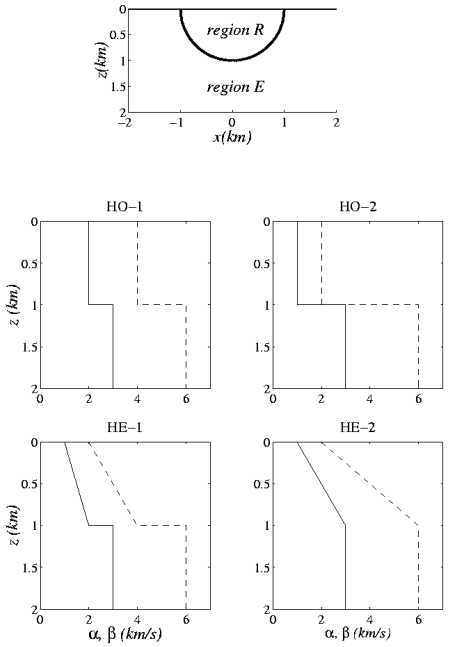

Figure 1. a) Semi-circular sedimentary basin (region *R*) underlying a half-space (region *E*). b) Wave velocity profiles (dotted line for *P* waves, and continuous line for *S* waves) in depth at $x = 0$ for four semi-circular sedimentary basins of radius $a = 1$ km. These models correspond to homogeneous (HO-1 and HO-2) and heterogeneous basins (HE-1 and HE-2). All models have the same geometry and the same *P* and *S* wave velocity for the halfspace $\alpha_E = 6$ km/s *and* $\beta_E = 3$ km/s, respectively.

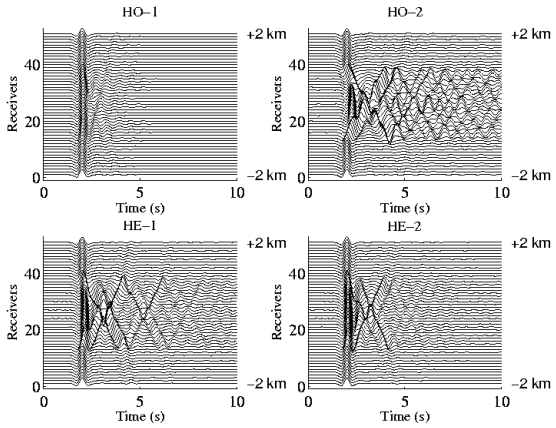

Figure 2. Synthetic seismograms for the vertical displacements produced at the free surface of the four models (see figure 1b) considered in the present study, under vertical incidence of *P* waves. The incident time signal is a Ricker pulse with a characteristic period of $t_p = 0.75$ s

References

[1] Sánchez-Sesma FJ, Madariaga R, Irikura K. An Approximate Elastic 2D Green's Function for a Constant-Gradient Medium. *Geophysical Journal International*; **146**: 237-248, (2001)

[2] Ramírez-Guzmán L, Sánchez-Sesma FJ, Luzón F. Funciones de Green 2D y 3D para un medio heterogéneo, derivación y aplicaciones. *Memorias técnicas del XIV Congreso Nacional de Ingeniería Sísmica*. (México): 142-156. *In Spanish*, (2003)

Recursive Evaluation of Time Convolution Integrals in the Spectral Boundary Integral Method for Mode III Dynamic Fracture Problems

H. Zafarani[1], As. Noorzad[2], Kh. Bargi and A. Ansari[3]

School of Civil Engineering, University of Tehran, Tehran 11365-4563, I.R. Iran

[1] zaferani@ut.ac.ir

[2] noorzad@ut.ac.ir

[3] aansary@ut.ac.ir

Keywords: Boundary Integral Method; Spectral Method; Recursive Method; Dynamic Fracture Mechanics; Anti-plane Shear; Elastodynamics

The analysis of the spontaneous growth of a shear crack can help us to investigate the entire rupture process of a natural earthquake. However, the corresponding boundary value problems are quite challenging in terms of required memory and processor power. In order to reduce computational cost, recently a spectral method has proposed [1-3] which adopts Fourier series representations for the spatial dependence of stress and slip along the interface, with the (time-dependent) coefficients in the Fourier series (also referred to as modes) being related to one another in a way which obtains from exact solution to the equations of elastodynamics. This allows an efficient numerical method, based on the use of the Fast Fourier Transform in each time step to convert between spectral and spatial domains.

The spectral method does add a lot of efficiency in problems that have translational invariance, as it diagonalizes the matrix that relates stresses to slips (or slip velocities). Hence, even though one still needs to compute convolutions, there are much fewer of them to compute. However, the evaluation of these convolutions is still the most time consuming stage of the elastodynamic analysis [2] and thus several "tricks" must be used to reduce it [4]. This reduction implies a lower total CPU time and a larger range of application of the spectral method. On the other hand, a significant effort has been made in linear system theory and dynamic soil-structure interaction analysis to reduce the computational cost associated with the evaluation of the convolution integrals, and several efficient schemes have been developed [5, 6].

In this study, for the first time, a recursive method proposed by Wolf and Motosaka [5] has been implemented for the evaluation of the time convolution integrals for some of the lower Fourier modes in 2D anti-plane crack propagation problem. The kernel of integral for the lower modes don't decay as rapid as higher modes, so the truncation procedure proposed by Lapusta et al. [4] is less effective for them. In this recursive evaluation of the convolution integrals in the time domain the output at any time step is computed from the input at this time and a few of the most recent past values of the output and input. This highly accurate scheme dose not corresponds to a truncation of the convolution integral that only retains recent past input values [5]. It is shown that analysis of a 2D anti-plane crack propagation problem involving N_t time steps based on the recursive evaluation of convolution integrals, requires $O(\alpha N_t)$ computational resources for each Fourier mode (as opposed to $O(N^2{}_t)$ for a classical algorithm), where α is a constant depending on the implementation of the method with typical values much less than N_t. The practical

implementation of the method has been elucidated, and examples illustrating its accuracy have been presented. Figure 1 compares the numerical and analytical solutions of a planar crack, which begins to break at its midpoint at the initial time step and propagates bilaterally at a fixed speed of 0.9 times the Rayleigh wave speed which is $c_R = 0.919\beta$. The slip is shown at several positions along the z-axis as a function of time. The continuous lines show the exact analytical solutions, while the dots represent the numerical ones. The numerical results follow the analytical solution very closely.

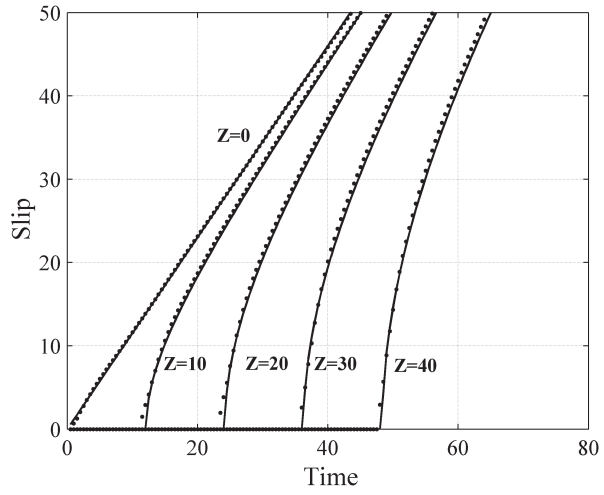

Figure 1. Comparison of the numerical and analytical solutions for the self-similar dynamic crack growth problem with fixed speed of 0.9 times the Rayleigh wave speed which is $c_R = 0.919\beta$. The dots denote the numerical results and the solid lines represent the analytical.

The results obtained with the recursive algorithm show that it is very precise and it reduces significantly the computation effort needed to solve 2D anti-plane crack propagation problem.
The computation methodology implemented here can be extended easily to 3D cases where it can be employed for the simulation of complex spontaneously fault rupture problems which carry a high computational cost.

References

1. Geubelle PH, Rice JR. A spectral method for three-dimensional elastodynamic fracture problems. *Journal of Mechanics and Physics of Solids* 1995; **43**:1791–1824.
2. Perrin G, Rice JR, Zheng G. Self-healing slip pulse on a frictional surface. *Journal of Mechanics and Physics of Solids* 1995; **43**:1461–1495.
3. Morrissey JW, Geubelle PH. A numerical scheme for mode III dynamic fracture problems. *International Journal for Numerical Methods in Engineering* 1997; **40**:1181–1196.
4. Lapusta N, Rice JR, Ben-Zion Y, Zheng G. Elastodynamic analysis for slow tectonic loading with spontaneous rupture episodes on faults with rate- and state-dependent friction. *Journal of Geophysical Research* 2000; **105**:23765–23789.
5. Wolf JP, Motosaka M. Recursive evaluation of interaction forces of unbounded soil in time domain. *Earthquake Engineering and Structural Dynamics* 1989; **18**:345–363.
6. Wolf JP, Motosaka M. Recursive evaluation of interaction forces of unbounded soil in time domain from dynamic-stiffness coefficients in frequency domain. *Earthquake Engineering and Structural Dynamics* 1989; **18**:364–376.

Amplification Pattern of 2D Semi-Sine Shaped Valleys Subjected to Vertically Propagating Incident Waves

Mohsen Kamalian[1], Behrouz Gatmiri[2], Abdollah Sohrabi-Bidar[3,] Ali Khalaj[1]

[1]Geotechnical Engineering Research Center, International Institute of Earthquake Engineering and Seismology, 26 Arghavan St., North Dibajee, Farmanieh, Tehran, I.R.Iran.
[2]University of Tehran, Enghelab Ave., Tehran, Islamic Republic of IRAN and Research Director and Lecturer, Ecole Nationale des Ponts et Chaussees, Paris, France
[3]Seismology Research Center, International Institute of Earthquake Engineering and Seismology, 26 Arghavan St., North Dibajee, Farmanieh, Tehran, I.R.Iran.

Keywords: Semi-sine Shaped Valley, Amplification, Site Effect, Topography Effect, BEM and Time Domain.

Abstract

Nowadays it is well established that the seismic ground response of surface topographies could be different compared to those of the free field motion during earthquakes. Although the topography effect on ground response could be very important when the wavelength is comparable to irregularity dimensions [1], but there are only few building codes which have considered this issue. This is due to complex nature of the seismic wave scattering by topographical structures which can only be solved accurately and economically by advanced numerical methods under realistic conditions. Recent compilation of works on the numerical modeling of seismic propagation have been presented by Beskos [2] and Sanches-Sesma et al. [3].

Bouchon [1] was the first who investigated the seismic response of 2D semi-sine shaped valleys. He carried out an interesting parametric study, including valleys with different shape ratios (ratio of height to half width of the valley) of 0.2 to 0.8, subjected to incident SH waves with wave lengths of 5.0 times the height of the valley. The most important result achieved was that in valleys with shape ratios of more than 0.33, a zone of de-amplification takes place at the center, which extends to the lower parts of the slopes, whereas in valleys with smaller shape ratios, de-amplification takes place at the edges instead of the center. Review of the literature shows that perfect parametric studies on seismic behavior of 2D semi-sine shaped valleys subjected to incident P and SV waves have been seldom published. The published works were restricted to either the simple case of incident SH waves or to some specific values of shape ratio and dimensionless frequency (ratio of the incident's wave length to the width of the valley).

This paper presents the most important results of an extensive numerical parametric study carried out by time-domain BEM [4] on amplification patterns of 2D homogenous semi-sine shaped valleys subjected to vertically propagating incident P and SV waves. All amplification factors were defined with respect to the free field motion (twice the incident motion) and were calculated as the ratio of the Fourier amplitude of the horizontal (or vertical) motion to the Fourier amplitude of the free field motion. All results have been presented in dimensionless forms, using the well known dimensionless frequency (or its inverse: the dimensionless period). The parametric study included seven different shape ratios, ranging from 0.1 to 2.0 and assumed a linear elastic behavior for the media with four different Poisson's ratios of 0.1, 0.2, 0.33 and 0.4. Based on engineering interests, a dimensionless period interval of 0.25 to 8.33 was considered, which corresponds to incident waves with wave lengths of 0.25 to 8.33 times the valley's width.

The most important results achieved were that:

1. At any point along the ground surface, irrespective of being inside or outside the valley, the free field motion would be either amplified or de-amplified and both components of motion exist.
2. The amplification pattern of the valley is strongly influenced by its shape ratio, the wave length of the incident wave, the wave type and to a less extent by the Poisson's ratio of the media.
3. Two distinct zones along the valley could be distinguished: The center zone in which the motion is mostly de-amplified, irrespective of its shape ratio and the wave length of the incident motion; The edge zone in which the ground motion is considerably amplified in broad frequency bands, especially if impinged by incident waves possessing wave lengths of equal to or twice the width of the valley.
4. The edge zone of the valley experience higher amplification potential in the case of incident P waves, whereas its center zone experiences higher de-amplification potential in the case of incident SV waves.

5. The high spatial variation of the motion amplitude along the ground surface inside and outside the valley could result in considerable relative displacements, which should be taken into consideration in seismic design of line structures such as life lines, bridges and dams founded across the valley.
6. If the valley has a shape ratio of less than 0.1 or is impinged by incident waves with lengths of much greater than that of the valley's dimension, the ground surface response would be approximately the same as the well known free field motion and the topography effect could be ignored..

References

[1] M. Bouchon *Effect of Topography on Surface Motion, Bull. Seism. Soc. Am.,* **63**, 615–632, (1973).
[2] D.E. Beskos *Boundary element methods in dynamic analysis: Pt. II (1986-1996), App. Mech. Rev,* **50**, 149-197, (1997).
[3] F.J. Sánchez-Sesma, V.J. Palencia and F. Luzón *Estimation of local site effects during earthquakes: an overview, ISET Journal of Earthquake Technology,* **39**, 167-193, (2002).
[4] Kamalian M., Gatmiri B. & Sohrabi A.; *On Time-Domain Two-Dimensional Site Response Analysis of Topographic Structures by BEM*; *Journal of Seismology and Earthquake Engineering (JSEE)*; Vol. 5(2); pp. 35-45; (2003).

Infinite Boundary Elements In 2D Elasticity

Alberto Salvadori
DICATA, University of Brescia, via Branze 38, 25123 Brescia, Italy
alberto.salvadori@ing.unibs.it

Keywords: Boundary elements, infinite domains, analytical integrations.

Modeling unbounded domains is an important issue in engineering: electro-magnetism, fluid dynamics, soil and soil-structure mechanics are but a few areas in which unbounded domains are of usual concern [1, 2]. The unbounded nature of the domain can be reproduced in two ways: i) by selecting a fictitious truncated domain, the so called *finite domain technique*; ii) via *infinite domain techniques*, the topic the present note dals with.

In the first class, the most challenging task is enforcing the appropriate boundary conditions along the artificial boundaries that give rise from the domain truncation, especially in dynamics. In the *infinite domain techniques* the numerical solution can be achieved by several methods: in the finite element method (FEM), the use of suitable infinite elements is required; in the boundary element method (BEM), the fundamental solutions for a half-space [3] can be considered to solve the problem along the boundary. Such an approach reveals to be quite time consuming, even by a factor of 300 [3], due to the complexity of the involved kernels. To avoid such a drawback, infinite elements have been implemented in the framework of the boundary element method as well adopting the fullspace solution.

The success of formulation of any infinite element is contingent on satisfying some requirements [4]: in particular the shape function behavior at infinity should reproduce the asymptotic behavior of the problem solution. In the context of linear elasticity, a reciprocal - with respect to the distance from a reference point - decaying shape function was proposed in [5] in order to model the unknown displacement field along the boundary: such a formulation was further developed by several authors (see [6] for a review) also by means of the analytical integration of the strongly singular elasticity kernel.

All aforementioned works have two distinct peculiarities. They: i) deal with infinite boundary elements for three dimensional problems; ii) lie in the framework of the collocation scheme.

About the first point, it might be seen as "a consequence of the impossibility of having truly two-dimensional unbounded problem domains" (taken from [2], page 40). Nevertheless, many two-dimensional problems have well known closed form solutions; moreover, two-dimensional numerical simulations are of usual concern for engineering problems with unbounded domains. To this aim, two-dimensional infinite elements have been widely proposed in the framework of linear elastic problems: a deep review, up to 1992, can be found in [2]. In two-dimensional problems "it is easy to see that in general stresses vary as $1/r$ and thus so will strains. On integration the displacement field will have a logarithmic form. Since $\log r$ increases with r this gives the paradoxical result that the displacements at an infinite radius will, themselves, be infinite." (taken from [2], page 13). Such a paradox led to seek infinite elements with displacement approximation behavior of the form $1/r$ even in two-dimensional problems, starting from the pioneering works up to the most recent ones about FEM as well as about BEM; infinite elements with reciprocal decaying shape functions are currently implemented in many commercial codes [7]. An insight on the asymptotical behavior of the displacement field is here provided: by comparing the half plane solution and the asymptotic behavior of a half space solution, an attempt is made to give a rationale to the use of reciprocal decaying shape functions to model the displacement field at infinity. A boundary infinite element is thereafter proposed and implemented by means of analytical integrations. On the other hand, "It might be possible to devise an infinite element which incorporated a logarithmic behavior. This has not yet been tried." (taken from [2], page 42). An infinite element with constant and logarithmic shape functions is here proposed - which to the best of our knowledge, has not been considered so far - and once again implemented by means of analytical and numerical integration schemes.

As a second characteristic of all cited works, numerical analysis refer to the boundary element collocation method. As a main consequence, the Somigliana identity is invoked in the solution process on the boundary, thus merely involving strong singularities in the formulation. The symmetric Galerkin boundary element (SGBEM) scheme, makes use of the boundary integral representation of tractions, that involves a hypersingular Green's function (here collected in matrix $\mathbf{G}_{pp}$). Integration of the hypersingular kernel is never a trivial task, and in the presence of reciprocal as well as logarithmic decay functions and unbounded domains it seems to be not yet investigated. In the present note, three boundary infinite elements are proposed and implemented: one of them in the hypersingular collocation framework, the remaining in the SGBEM as well. Apparently, unsurmountable difficulties come into play in the formulation of a SGBEM scheme for general shape functions on 2D unbounded elements. Such difficulties are rooted in the variational formulation of the elastic problem in 2D half-plane, because the total potential energy of the solution of the elastic problem is itself unbounded. From the computational side, this fact led to using weighted functional spaces that give rise to the Petrov-Galerkin method. A further publication will be devoted to the afore sketched issues.

In the present note, three different elements have been proposed: a *polynomial decaying element*, where the displacement field is approximated by high order lagrangian polynomials truncated "suitably" far away from the loaded zone; a *reciprocal* $1/r$ *decaying element*, analogous to [2]; a *constant and logarithmic decaying element*. In all three cases, analytical integrations for the hypersingular kernel have been produced. The polynomial decaying element has a usual finite domain: accordingly, making use of analytical integrations that apply to standard polynomial boundary elements [8] is allowable. For the *reciprocal* $1/r$ *decaying element* analytical integrations have been performed in the general case. For the *constant and logarithmic decaying element* analytical integrations have been performed in the easy case of field point collinear or inside the unbounded element, whereas for the general case suitable numerical schemes [9] are considered.

The proposed elements have been compared in a benchmark application in terms of accuracy. The constant logarithmic element shown to be the most accurate and effective.

References

[1] D. Givoli. *Numerical methods for problems in infinite domains*. Elsevier, 1992.

[2] P. Bettess. *Infinite elements*. Penshaw Press, UK, 1992.

[3] L. Pan, F. Rizzo, and P.A. Martin. Some efficient boundary integral strategies for time-harmonic wave problems in an elastic halfspace. *Comput. Methods Appl. Mech. Engrg.*, 164:207–221, 1998.

[4] T.T. Abdel-Fattah, H.A. Hodhod, and A.Y. Akl. A novel formulation of infinite elements for static analysis. *Computers and Structures*, 77:371–379, 2000.

[5] J.O. Watson. Advanced implementation of the boundary element method for two and three dimensional elastostatics. In P.K. Banerjee and R. Butterfield, editors, *Developments in Boundary Element Methods - I*, pages 31–63. Elsevier Applied Science Publishers, 1979.

[6] A. Salvadori, A. Feriani, and A. Aliprandi. Formulation and implementation of hypersingular infinite boundary elements for soil-structure interaction problems. Technical Report 15, University of Brescia, 2004.

[7] Hibbitt, Karlsson, and Sorensen. *ABAQUS/Standard Theory Manual*, volume 6.4. 2004.

[8] A. Salvadori. Analytical integrations in 2D BEM elasticity. *Int. J. Numer. Methods Eng.*, 53(7):1695–1719, 2002.

[9] G. Monegato and L. Scuderi. Numerical integration of functions with boundary singularities. *J. Comput. Appl. Math.*, 112:201–214, 1999.

Index

R. Abascal 297
K.Abe 211
K. Adamiak 173
M. Adolph 261
E.L.Albuquerque 109
C.Alessandri 255
S.Alestra 179
J. Alfonso Pérez-Ruiz 305
M.H.Aliabadi 1, 39
139, 303
G.Alléon 213
L.P.C.P.F Almeida 269
A. Ansari 307
M.J.H.Anthonissen 251

A.Bachelot 299
P.M.Baiz 39
M. Badaoui 215
G.Baker 51
Kh. Bargi 307
M.H. Bazyar 217
A.A.Becker 197
M.K. Berrah 215
A. Benallal 7
I. Benedetti 191
K. Bertoldi 63
S. Beyer 23
D. Bigoni 63
A. Blázquez 45
M. Bonnet 29
A.S. Botta 7
R.W.Bowtell 197
M. Brun 63

B.Carpentieri 219
J. A. M. Carrer 67
E.R Carvalho 261
A.P. Cisilino 221, 249
C.Cobos Sanchez 197
T. Colella 263
F.Collino 153
D. Crann 231
R. Criado 257

P. Dabnichki 91, 229

	241
G. Davì	223
A. J. Davies	231
W.Dijkstra	233
F.M.E. Duddeck	235
R. Duraiswami	79
M.B. Dusseault	283
G. Dziatkiewicz	121
J. Eberhardsteiner	285
L.Elliott	245
A. Elvin	203
P.Faure-Ragani	237
P. Fedelinski	33, 121
A.Frangi	237
J.M. Floryan	173
F. García-Sánchez	165
P. Gardano	241
C. Gáspár	73
L.Gatard	299
B. Gatmiri	247, 277 301, 309
L.Ghezzi	237
L. Giraudba	213
P.Gloverand	197
N.A.Gumerov	79
P.C Gonçalves	269
R. Gorski	33
L.J. Gray	257
F. García-Sánchez	153
S. Hampel	249
Ch. Hellmich	285
S. Hirose	23
D.B.Ingham	245
E. Jabbari	247
M. Jiryaei Sharahi	301
T.Johansson	85
I.A.Jones	197

G.Kakuba 251
A. Kalaj 309
M. Kamalian 301, 309
G.F. Karlis 145
S. J. Kane 231
S.Kazama 211
K.Koro 211
S.G. Kourtakis 273

C-H. Lai 231
M. La Mantia 91
S. Langer 249
L.G. S. Leite 57
D.Lesnic 25, 85
Y.C. Lin 291
T. Lucht 303
F. Luzón 305

N. Mai-Duy 267
V.Mallardo 255
V. Mantič 45, 257
W. J. Mansur 67
L.Marin 197
A. Mebarki 215
R.M.M.Mattheij 233, 251
N.S.Mera 245
K.Mer-Nkonga 299
E. Mesquita 261
S.E.Mikhailov 15
A. Milazzo 191, 223
V. Minutolo 263
L. S. Miers 293
F.Millot 153
M. N. Mohamad Ibrahim 97
V.G. Mokos 2

I.V.Namestnikova 15
S. Noroozi 281
As. Noorzad 307
A. Nourzad 277

Y. Ochiai 103
C. Orlando 191
J.E. Ortiz 257

J.B. de Paiva 185
L. Palermo Jr 269
F. Paris 45, 257
L.Pasol 279
A. Pech 305
S.Pernet 153
D. Polyzo 271
C. P. Providakis 273
H.Power 197
D. Polyzos 145

L. Ramírez-Guzmán 305
L. Rodríguez-Tembleque 297
R. Rojas-Díaz 153
L. Rothenburg 283
E. Ruocco 263

A. Sáez, 153, 165
F. J. Sánchez-Sesma 305
J. A. F. Santiago 275
E.J. Sapountzakis 287
B. Šarler 127
A.Sellier 279
P. Sewell 281
S. Seyrafian 277
G.K.Sfantos 1
Y.C. Shiah 291
S. Shuib 97
K.M.Singh 133
J. Sladek 23, 139
285
V. Sladek 23, 139
285
A. Sohrabi-bidar 309
Sollero, P 109
G.Sylvanda 213
C. Song 217
Sun Hai-tao 243
G. Sylvand 289

C. L. Tan 291
A. E. Taigbenu 203
M.Tanaka 133
R.I. Tanner 267
J. C. F. Telles 293
I. Terrasse 179, 289
T. Tran-Cong 267
B.Troclet 179
S. V. Tsinopoulos 145

V. Vavourakis 271
W.S. Venturini 7, 57
J. Vinney 281
M. Wünsch 23

Useche, J 109

P. B. Wang 295
Wang Yuan-han 243
P.H.Wen 139
L. C. Wrobel 275
W.W. Wutzow 7, 185

Z. H. Yao 295
Shunde Yin 283

H. Zafarani 307
Ch. Zhang 23,153
65
A.Zhivkov 229